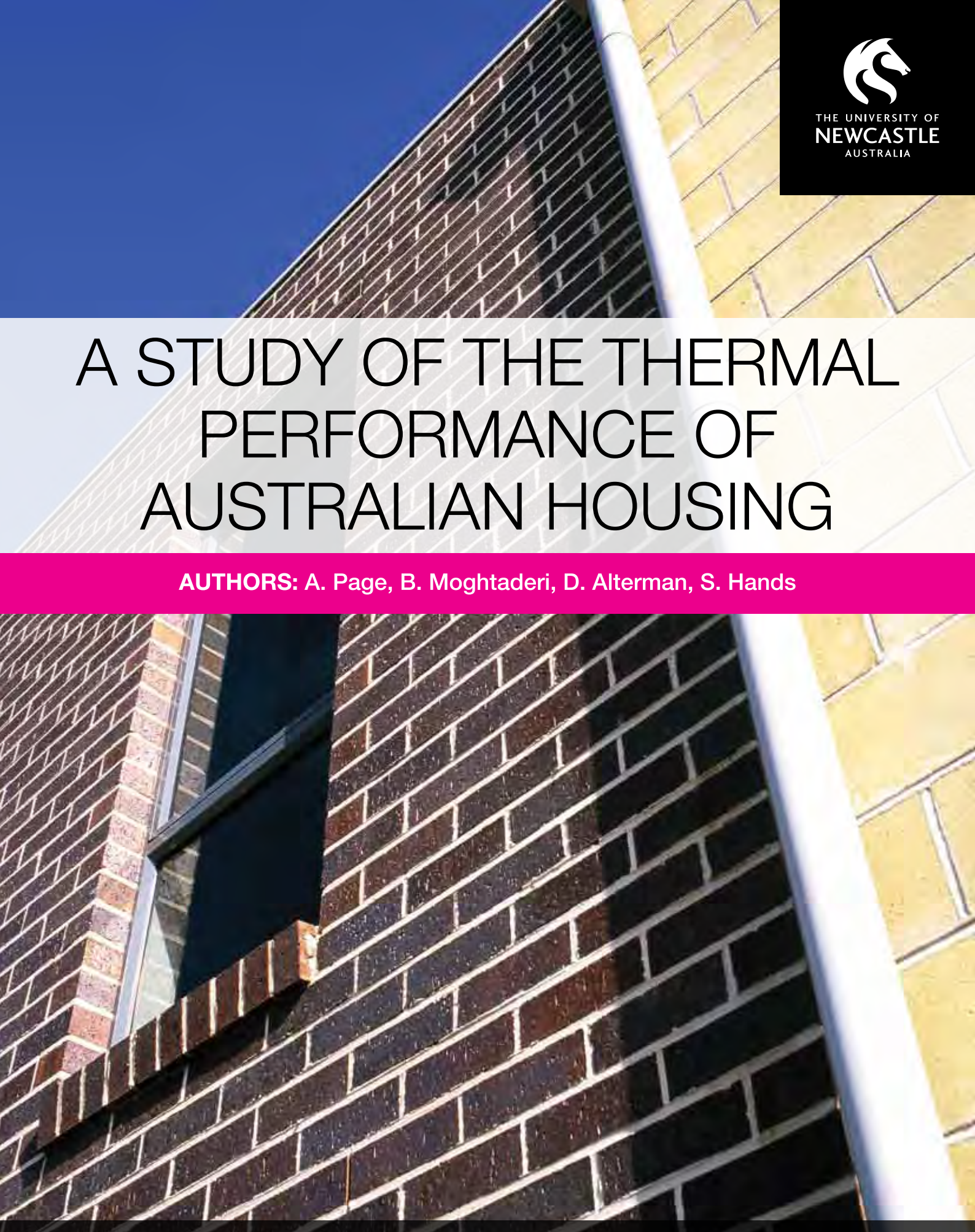

THE UNIVERSITY OF NEWCASTLE AUSTRALIA

A STUDY OF THE THERMAL PERFORMANCE OF AUSTRALIAN HOUSING

AUTHORS: A. Page, B. Moghtaderi, D. Alterman, S. Hands

Priority Research Centre for Energy
The University of Newcastle

A Study of the Thermal Performance of Australian Housing

by

Priority Research Centre for Energy
Disciplines of Chemical and Civil Engineering, School of Engineering
Faculty of Engineering & Built Environment
The University of Newcastle
Callaghan, NSW 2308
Australia

Thermal Research Group
(Present and past members)

Prof. Behdad Moghtaderi
Emeritus Prof. Adrian Page
Dr Dariusz Alterman
Dr Caimao Luo
Dr Trevor Moffiet
Mr Stuart Hands
Dr Haitham A. M. Alasha'ary
Dr Katherine Gregory
Dr Heber Sugo

Authors:

A. Page, B. Moghtaderi, D. Alterman, S. Hands

ISBN 978-0-9807618-9-4

The University of Newcastle

Deputy Director (Prof. Behdad Moghtaderi)
Priority Research Centre for Energy
The University of Newcastle
Callaghan, NSW 2308
Australia

This publication is also available on the Internet at the following address:
www.thinkbrick.com.au

Acknowledgements

Over the duration of the project assistance with the experimental program was regularly provided by the technical staff of the Disciplines of Civil and Chemical Engineering and their support is gratefully acknowledged. Particularly, the contribution of Roger Reece, John Noonan, Ian Jeans, Michael Goodwin, Ian Clarke, Ron Roberts and Neil Gardner is much appreciated. Gratitude and acknowledgement should also be given to all current and past members of the Thermal Research Group from the University of Newcastle's, Priority Research Centre for Energy for the extensive collaboration required for the successful completion of this section of the project. The financial support of the Australian Research Council and Think Brick Australia is also gratefully acknowledged. Particularly, we would like recognise the input of Cathy Inglis, Linda Ginger, Ross Maher and Elizabeth McIntyre from Think Brick Australia over the course of the project. Finally, the authors wish to acknowledge the financial and in-kind support provided to them by the University of Newcastle, particularly through the Office of the Deputy Vice Chancellor (Research).

Executive Summary

There is a growing world-wide concern for energy conservation, the reduction of greenhouse gas emissions, and the sustainability of our current living standards. The Australian Greenhouse Office estimates that a significant proportion of the end energy usage in domestic buildings is used for space heating and cooling [Australian Greenhouse Office]. The effective use of materials and design concepts to improve the inherent thermal performance of buildings will enhance both energy efficiency and thermal comfort, with obvious compounding environmental benefits.

The current building regulations and particularly the Building Code of Australia (where energy efficiency was introduced in 2003) do not fully capture all of the factors which contribute to the thermal performance of a building, particularly in relation to "Deemed-to-Satisfy" rules for walls.

In 2001 with a view to overcoming these shortcomings, Think Brick Australia in partnership with the University of Newcastle commenced an 8 year theoretical and experimental study on the thermal performance of housing systems. The project has involved the collaboration of research groups in Civil and Chemical Engineering and is based in the Priority Research Centre for Energy at the University. To date funding for the project has been in excess of $1.5M in cash from Think Brick Australia and the Australian Research Council (through three linkage grants), together with substantial in-kind support from staff of the School of Engineering in the Faculty of Engineering and Built Environment. The first phase of the project (Phase 1) has involved data collection and analytical modelling. The second phase of the project, involving the systematic analysis and interpretation of the large body of data collected, commenced in late 2009. This report describes Phase 1 of the project and presents some key findings. The outcomes of Phase 2 with detailed results and analysis will be reported on completion as a separate document.

This Phase I report provides detailed descriptions of the development and application of a "guarded hot box" apparatus for studying the thermal performance of individual walling systems, the development and detailed observation of the thermal performance of four full scale housing modules, the development of two thermal simulation software programs and a study of the smart use of thermal mass in walling systems using a hybrid wall approach.

The project consists of four main strands as follows:

(1) Strand 1 – Laboratory Testing:

A *guarded hot box* apparatus (in accordance with ASTM C1363 Standards) was developed to study the thermal properties of individual walls. These studies included the measurement of the thermal resistance (*R-value*) of wall assemblies as well as the wall behaviour under controlled temperature cycles representative of typical Newcastle summer and winter conditions. Bench scale studies were also performed for various walling systems in a conventional and/or hybrid arrangement to simulate the expected performance in full scale module tests.

(2) Strand 2 – Full Scale Housing Module Tests:

This involved the construction and monitoring of the behaviour of four full scale housing modules (6m x 6m in plane) under a range of seasonal conditions. The construction systems for the modules covered the common forms of domestic construction in Australia (brick veneer, cavity brick and lightweight constructions) as well as the more novel reverse brick veneer. The modules were constructed with an independent roof system which allowed the easy installation and modification of various walling

systems. The influence of factors such as wall insulation, windows, roof type, curtains, carpet, room ventilation and internal walls were also studied. The interior of the modules could either exist in a free floating state or be artificially controlled to maintain the temperature within a set range with the heating/ cooling requirements being measured. A total of 105 sensors were installed in each module to monitor internal and external conditions as well as temperature and heat flux gradients through each wall, roof and floor. These were recorded every 5 minutes for 24 hours per day over the testing period. This large database of all measurements has been consolidated into a form which facilitates further systematic statistical analysis.

(3) Strand 3 – The Development of Thermal Modelling Software:

Two software packages have been developed: a comprehensive modelling package based on first principles, **NUMBERS** (Newcastle University Modelling and Building Energy Rating Software); and a predictive software tool based on a fuzzy neural network approach useful for preliminary design to provide quick comparisons of several possible solutions before more detailed thermal modelling is carried out. In both cases, advantage has been taken of the availability of a large body of real data on thermal performance from the module tests to assist in verifying the computer simulations. **NUMBERS** was also verified using the ASHRAE "BESTTEST" procedures.

(4) ***Strand 4 – Smart Use of Thermal Mass:***

An investigation into the potential improvement of the overall thermal performance of a building by the use of a varying distribution of thermal mass across the external envelope (that is, a "hybrid" walling approach) was undertaken. The study included an analysis of the thermal performance of the modules as well as an actual house. In both studies a range of hybrid walling systems was investigated using simulation packages (AccuRate and NUMBERS), with the results being supplemented by experimental studies at model scale. The main outcome of this strand were recommendations for the optimum properties and arrangement of external walls in housing to maximise the advantages of thermal mass.

Since the experimental study of the full scale housing modules over a period of more than seven years has resulted in an extremely large body of data with a wide range of variables, a systematic approach is being taken in the consolidation and analysis of the data using the JMP statistical software. This work is still in progress, and when complete, detailed results will be produced as part of the Phase II report. However, from some preliminary analyses of the results, a number of general conclusions can already be drawn:

(1) For housing modules containing no major openings, wall thermal mass and accompanying thermal lag played a key role in restricting the magnitude and timing of the maximum and minimum internal temperatures. The effects of high (and low) external temperatures were ameliorated and the magnitude of the diurnal swings reduced. Cavity brickwork, brick veneer and insulated cavity brickwork modules attenuated the effect of solar radiation to varying degrees by releasing the stored heat back to the outside environment, thereby reducing the net flux entering through the wall. This was not case for the insulated lightweight walls which had higher thermal resistance but no thermal mass. As a result, there was a greater variation in internal temperatures and little thermal lag exhibited by the insulated light weight module. Additionally, the insulated lightweight system had an internal temperature diurnal swing of more than twice the insulated cavity brick module during hot conditions. Differing behavioural characteristics were observed for the insulated cavity brick, insulated brick veneer and insulated light weight modules, even though their R-values were similar. It is clear that the thermal response of a building is influenced by both the thermal resistance of the walls and their thermal mass.

(2) The presence of a north facing window became the dominant driving factor influencing the thermal behaviour of the module, with the changing solar altitude with season altering the magnitudes of heat gain. This was the case for all of the modules. The thermal mass of the slab also had some influence, particularly in removing heat from the modules as the link with the ground acted as a 'sink'. However, this impact was not a significant as the vertical thermal mass in the walling system.

(3) The performance of the modules with a north facing window under free floating conditions demonstrated that thermal mass was an effective form of heat storage to lessen the impact of internal temperatures and temperature fluctuations and improve thermal comfort. This was particularly the case for walls with internal thermal mass, whose performance was also markedly enhanced by the inclusion of cavity insulation.

The insulated lightweight construction had much less capacity for dampening the internal temperature variations and consistently had the highest diurnal swing. The brick veneer constructions had a slightly lower diurnal swing than the light weight, and the insulated cavity brick and cavity brick modules exhibited the best dampening ability. The lightweight and brick veneer constructions consistently peaked to higher internal temperatures than the insulated cavity brick and cavity brick modules. The insulated internal skin essentially 'traps' heat in the module space, and the insulated cavity brick and cavity brick modules both absorb heat from the room which helps to counter the effect of the solar gain. The insulated cavity brick module provided the most consistent and predictable behaviour across all time periods with heat absorption during day and heat release and night.

(4) For the windowless modules, the insulated lightweight module responded directly to the external environment with a rapid increase and reduction in temperature rates for this system due to its low internal thermal mass. The lightweight walls immediately transmitted heat into the module when solar radiation was incident on the external surface. Overall, for all testing periods, the insulated lightweight module exhibited no properties which had the potential to assist in maintaining adequate thermal comfort. Temperatures were consistently the highest during the day and the diurnal swing was also consistently the highest. While the high daytime temperature for the lightweight module did drop rapidly at the night, the magnitude of the temperature differences between the lightweight and heavy weight modules at night was less significant than for the daytime. Energy consumption was also high in order to counter the large diurnal swing.

(5) For controlled internal conditions, the insulated cavity brick module always consumed less energy than the other forms of construction, with the cavity insulation and the thermal mass of the internal skin playing a key role (the external skin also had a minor effect). The insulated light weight and brick veneer modules required more heating and cooling cycles as a result of their larger diurnal swings.

(6) Major benefits in thermal performance can be gained by including wall elements containing thermal mass on the interior side of the wall insulation (as in insulated cavity brick and reverse brick veneer construction). The presence of this internal thermal mass resulted in vastly improved performance in all seasons compared to both insulated brick veneer and lightweight construction.

(7) The conversion of the insulated lightweight module to insulated reverse brick veneer considerably improved the performance over the original construction due to the presence of the internal brickwork skin providing thermal mass. The lack of thermal mass in the external skin meant that its performance was marginally inferior overall to that of the insulated cavity brick system (despite the fact that the exterior skin was located outside of the insulating layer, it still had a minor influence). Overall, the insulated reverse brick veneer and insulated cavity brick performed similarly but the insulated cavity brick required less energy consumption under controlled conditions.

(8) The results clearly showed that the thermal resistance (R-value) of the walls is not the sole predictor of the thermal performance of a building. No correlation between R-Value and energy usage or free floating performance was found in any results. Similar internal conditions were achieved in modules with significantly differing R-values, indicating that there were also other factors at play (in this context factors such as curtains, carpet and controlled ventilation were all shown to have an influence on the observed thermal performance).

(9) The use of the hybrid walling concept in the design of a house has the potential to significantly improve its thermal performance. This was shown initially in relation to the performance of a series of hypothetical modules, and then illustrated by the application of the concept to a typical house.

It is clear from the above that to obtain a true indication of thermal performance, account must be taken of the performance of the building as a complete system rather than considering the thermal resistance of the walls alone. In particular, thermal mass in various parts of the building will exert a major influence and such factors need to be considered in the development of future "*Deemed to Satisfy*" rules in building regulations.

Table of Contents

1. INTRODUCTION

In recent years there has been growing world-wide concern regarding energy conservation, the reduction of greenhouse gases and sustainability. In Australia, a significant proportion of the end energy usage in domestic buildings is used for space heating and cooling (Australian Greenhouse Office, 2004). Therefore, achieving better energy efficiency in buildings has become one of the major challenges for architects and builders. These concerns have been reflected at several levels within Australia with the establishment of responsible government agencies at both the Federal and State Government levels. Several new measures have been introduced to the building industry including an energy star rating system for all new residential developments prior to building approval. This rating system involves the estimation of the energy required to maintain the interior of the building within a set temperature range taking account of the building fabric, insulation, design, orientation and locality. A star rating is obtained by comparing the energy estimate against set values for the relevant climate zone. Failure to meet minimum criteria requires changes to the building design or fabric. Several packages such as NatHERS (NatHERS), AccuRATE (AccuRATE Manual) and FirstRate (FirstRate) are available to simulate building performance. Other models such as BASIX (BASIX and Building Code of Australia) also consider broader environmental issues such as water efficiency.

The accuracy of any thermal simulation will therefore have direct implications on the prediction of the thermal performance of the building and hence the operational energy costs for the life of the structure. Obviously, the output of any simulation should reflect the actual performance of the structure. However, there is very little real data on the performance of masonry housing under Australian climatic conditions to use as input in the development of simulation models and for verification of existing packages.

Considerable improvements in thermal performance can be obtained by taking into account a range of factors in design, some of which relate to site characteristics and others which relate to the inherent properties of the construction materials. This particularly applies to the use of heavy walling such as masonry, which has inherent benefits from its thermal mass. It is important that building regulations recognise the contribution of all the properties which influence thermal performance.

With a view to overcoming the shortage of real data, Think Brick Australia, in partnership with the University of Newcastle, has undertaken an 8 year theoretical and experimental study of the thermal performance of housing systems. The project has involved the collaboration of research groups in Civil and Chemical engineering and is based in the Priority Research Centre for Energy at the University. To date funding for the project has been in excess of $1.5M in cash from Think Brick Australia and the Australian Research Council (through three linkage grants), together with substantial in-kind support from staff of the School of Engineering in the Faculty of Engineering and Built Environment. The first phase of the project (Phase I) involved data collection and analytical modelling, and was completed at the end of 2009. Phase 2 of the project, involving the systematic analysis and interpretation of the huge body of data collected, commenced thereafter. This report describes Phase I of the project and presents key results. The outcomes of Phase II with detailed results and analysis will be reported at a later date.

1.1. Project Overview

The thermal performance of typical Australian housing systems has been investigated at both a fundamental and applied level using experimental and first principles techniques. A schematic arrangement of the nature and strategy for the investigation is shown in Figure 1.1. A key feature of the study is that the theoretical

simulation models were directly informed by the data collected from the experimental strand for the different walling systems. This allowed the analytical models to be verified and then used to predict the behaviour of more elaborate structures.

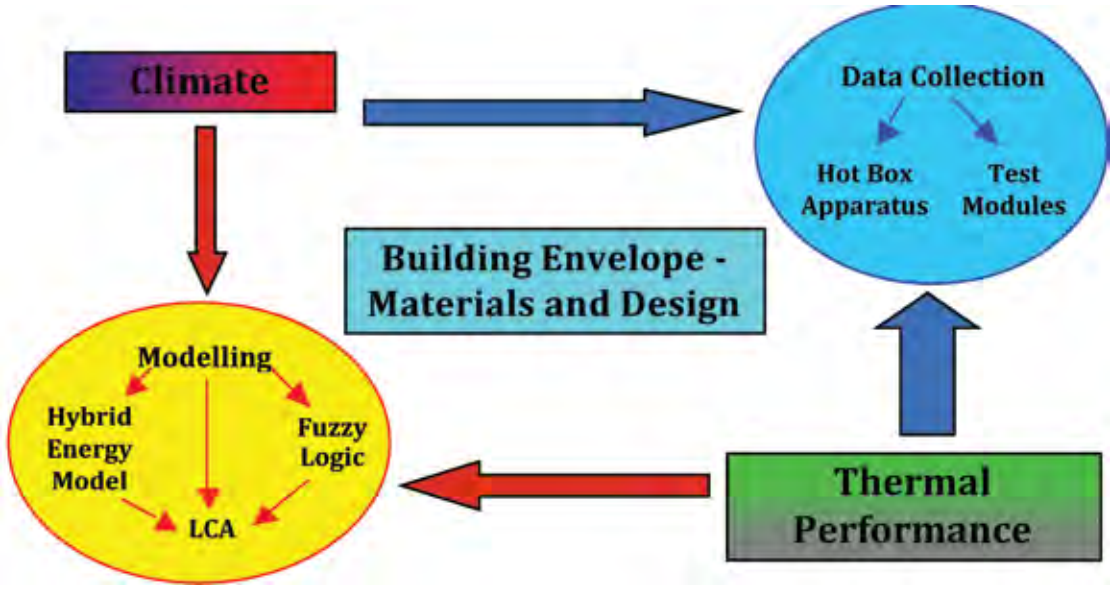

Figure 1.1 Overview of Thermal Research

The four main strands of the study were as follows:

(1) The development of a "*guarded hot box*" apparatus conforming to ASTM C1363 (American Society for Testing Materials, 1997), and the subsequent measurement of the thermal resistance of full scale housing wall assemblies either proposed or in common use

.

(2) Detailed observation of the thermal performance of four, 6m x 6m housing test modules under real weather conditions in all seasons. Initially two modules were constructed in 2003. As the program expanded, subsequent modules were constructed in 2004 and 2005 to allow a wider range of variables to be studied in parallel. The construction systems for the modules covered the common forms of domestic construction in Australia – brick veneer, cavity brick and lightweight as well as the more novel reverse brick veneer. The modules were constructed with an independent roof structure which allowed the easy replacement of the walling system. The influence of wall insulation, windows, roof characteristics, curtains, carpet, room ventilation and the influence of internal walls were also studied. The interiors of the modules were allowed to either "*free float*" with the external weather conditions, or were "controlled" by a heating/cooling system with the consumed energy being measured. A total of 105 sensors were installed in each module to monitor internal and external conditions, and temperature and heat flux gradients through each wall, roof and floor. These were monitored every 5 minutes, 24 hours a day, 7 days per week for the duration of the investigation.

(3) The development of two software modelling tools to simulate the thermal performance of buildings: a "first principles" hybrid model using computational fluid dynamics combined with zonal modelling; and a "fuzzy logic" neural network approach using the data from the test modules to "educate" a

predictive model for thermal performance.

The first approach resulted in the development of the NUMBERS software package (*Newcastle University Modelling and Building Energy Rating Software*). This comprehensive package was verified using measured data from the various housing test modules. External verification was also carried out using the ASHRAE "BESTTEST" Procedure (ASHRAE Standard, 2007 and Olsen, Brager, 2004). The second approach, apart from being novel in this field because of the availability of a large volume of educative data, resulted in computationally efficient software useful for preliminary design. This part of the study formed part of a PhD program (Alasha'ary, 2010). Although not as powerful or comprehensive as NUMBERS, the software has the potential to be used effectively at the conceptual design stage to quickly compare the thermal performance of several possible solutions before more detailed thermal modelling is carried out.

(4) A study on the "smart" use of thermal mass, taking into account the characteristics of heavy walling such as masonry which can be used to advantage in this context. The study formed part of a PhD program (Gregory K. E., 2010) having a major analytical strand using several thermal performance modelling packages (including AccuRate and NUMBERS), and was supplemented by experimental studies with a bench-scale setup that represented an exact 1/8 replica of the University of Newcastle full-scale thermal test modules. The study was also informed by the experimental and analytical studies of Strands (1) to (3) above. The main outcome of this strand was recommendations for the optimum properties and arrangement of external walls in housing to maximise the advantages of thermal mass.

All of the above studies were inter-related, with the overall aim being to identify and maximise the use of the favourable characteristics of brick masonry walling for improving the thermal performance of residential construction.

This Phase 1 report provides detailed descriptions of the development of each of the above strands together with appropriate verification of the developed software and the presentation of key outcomes. Since the experimental study of the full scale housing modules over a number of years resulted in an extremely large body of data with a wide range of variables, a systematic approach has been taken in the consolidation of the data using the JMP statistical software to analyse and interrogate the data. This work is still in progress, and complete detailed results of the study will be produced as a Phase 2 report.

2. LABORATORY TESTING

2.1. Guarded Hot Box

2.1.1. Overview

The guarded hot box is designed to evaluate the steady-state thermal performance of wall assemblies. The hot box facility measures the thermal resistance (R-value) or the conductance of walling elements by establishing a steady-state temperature gradient across the wall whilst measuring the energy to maintain a constant heat flow. This involves the use of two separate insulated chambers, hot and cold, to provide the temperature gradient together with specialised instrumentation for temperature control, temperature measurement and power. The dimensions of the walls which can be tested are 2.4 m (high) by 2.4 m (wide). The facility is shown in Figure 2.1.

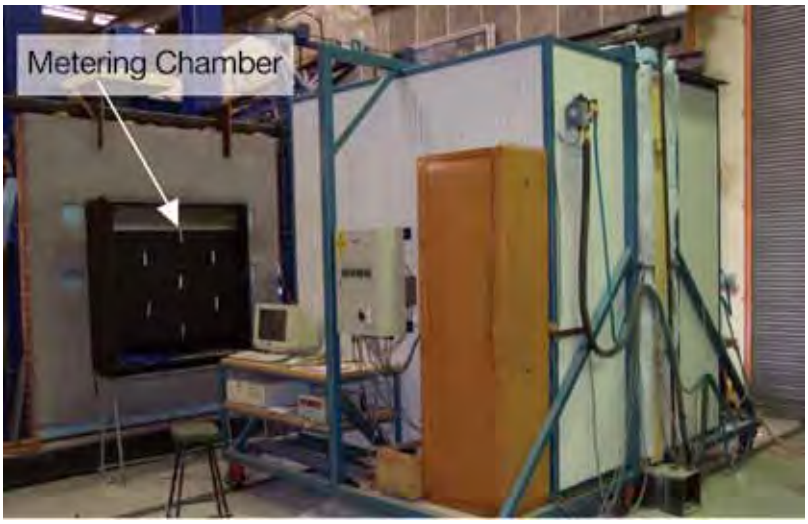

Figure 2.1 Guarded Hot Box Apparatus

The hot box facility utilises the Guarded Hot Box (GHB) principle whereby a metering chamber is incorporated on the hot side of the apparatus. This chamber measuring 1200mm x 1200mm can be observed on the left hand side of Figure 2.1. This metering chamber, or meter box, is maintained at the same temperature as the outer hot (guard) chamber thus minimising any potential flanking loss along the specimen edge and heat loss via the meter box walls. A schematic diagram of this arrangement is shown in Figure 2.2.

The apparatus was designed using the guidelines given in ASTM C236–89 '*Standard Method for Steady-State Thermal Performance of Building Assemblies by Means of a Guarded Hot Box*' (American Society for Testing Materials, 1989). ASTM C236 has since been discontinued and replaced by ASTM C1363–97 '*Standard Method for Steady-State Thermal Performance of Building Assemblies by Means of a Hot Box*' (American Society for Testing Materials, 1997). This test method encompasses both guarded and non-guarded hot box facilities.

The GHB apparatus enables close examination of the thermal properties of a variety of wall assemblies. Steady-state tests are used to obtain heat transmission coefficients (such as thermal resistance (R-value)) of wall assemblies and/or their components, solid membranes and air film resistances.

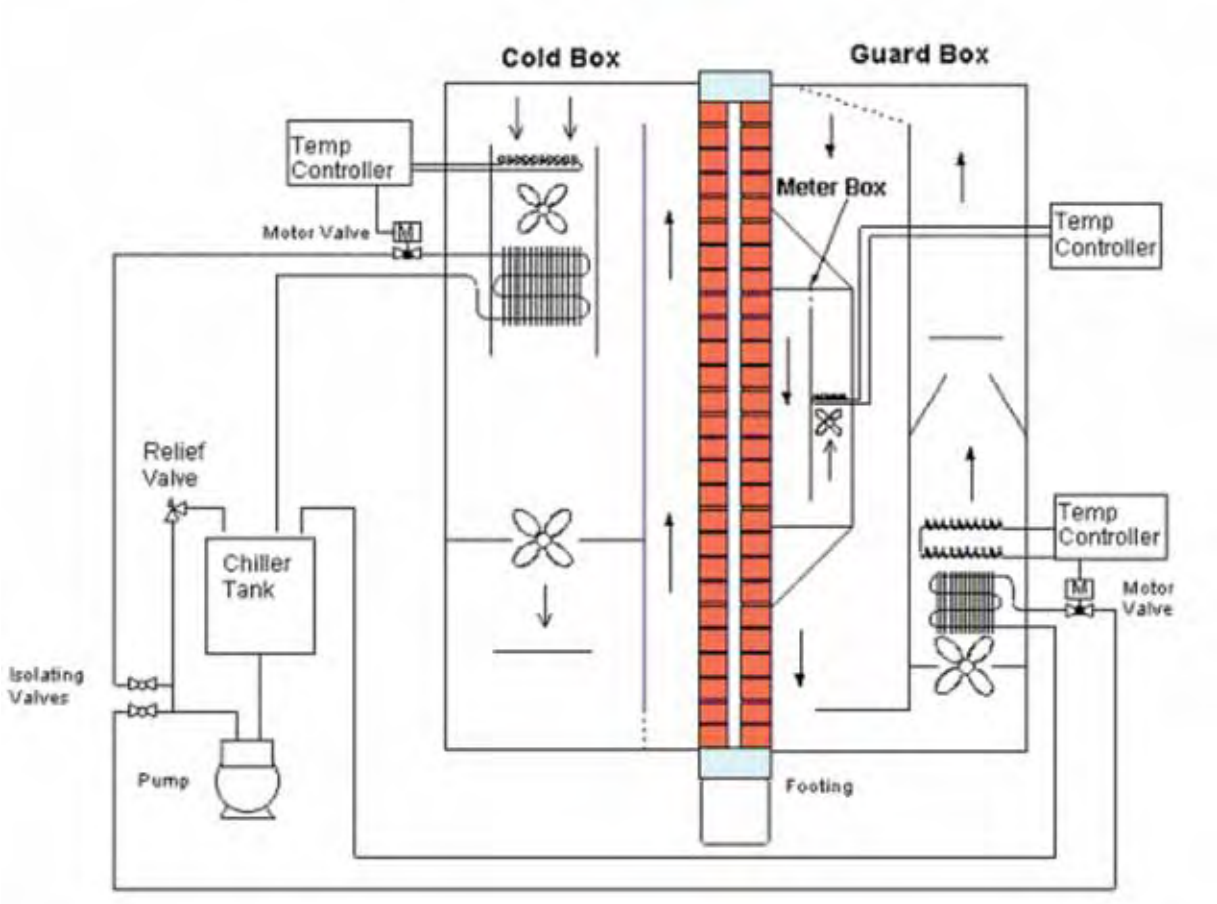

Figure 2.2 Schematic of the Guarded Hot Box Apparatus.

ASTM C236 specifies the direction of the convective air currents to maintain an equivalent temperature differential across the sample and also requires that several surface temperatures be measured with a weighted area value being used in the calculation process. Initially, an array of 7 surface thermocouples was used on each face of the sample (see Fig. 2.3). This was later revised to 6 in order to optimise the logging channel list on the precision thermometer (Prema), with the centre thermocouple still being logged by the datataker to obtain the mid-height temperature profiles.

$$\text{Weighting} = \frac{\text{total metering area}}{\text{tributary area for each thermocouple}}$$

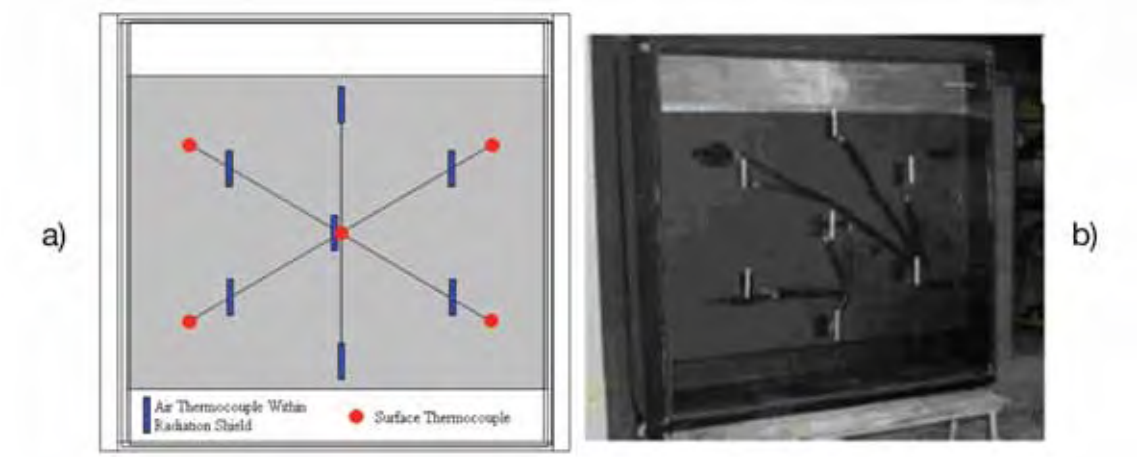

Figure 2.3. (a) Surface mounted thermocouple layout in Meter Box area and (b) Interior view of Meter Box with thermocouples

As part of the commissioning phase, R-value results obtained from the Guarded Hot Box apparatus for a polystyrene sheet were compared to those determined for a sample of the same sheet using the Heat Flow Meter Apparatus at the CSIRO Melbourne Laboratory. Polystyrene is a homogeneous material with known thermal properties. The R-value tests, carried out as part of the commissioning phase, were performed using adjacent sheets (25mm thick) which had been cut from the same expanded polystyrene block. This was to minimise any material differences (density) between the two samples. The surfaces of the sheets were painted black to increase the radiation heat transfer between the sample surface and those of the GHB apparatus.

In the CSIRO Heat Flow Meter (Clarke R. E., 2002) apparatus, a temperature differential across the sample is established via hot and cold plates at uniform temperatures in contact with the sample. The heat (flux) flowing through the sample is measured directly using calibrated thermopiles. In the Guarded Hot Box, the temperature differential is attained using a convective (air) process with a smaller (resultant) radiation component. The heat flowing through the sample (meter area) is derived from the electrical energy used by the meter box fans and by the resistive heating element. The convective nature of the heat transfer process also results in a small non-uniformity in the surface temperatures between the top and bottom of the sample. The polystyrene was tested at temperature differentials of Δ20°C, Δ18°C and Δ12°C. The GHB results are summarised in Table 2.1.

The CSIRO heat flow meter results (Clarke R. E., 2002) gave the thermal conductivity of the polystyrene sample to be 0.0366 ± 8%. Considering the differences in the two test methods, including the differing size of the samples, variations in the sample material and the inherent test differences, the 6.5% variation between the GHB and the CSIRO Heat Flow Meter was considered to be acceptable in verifying the effectiveness of the GHB apparatus. The obtained results were also consistent with literary sources.

Table 2.1 Polystyrene Calibration GHB Results

Air-to-Air Temperature Difference	R_u (m^2 K/W)	R_s (m^2 K/W)	k (W/m K)
ΔT = 20	0.979 (±0.013)	0.677 (±0.015)	0.039 (±0.002)
ΔT = 18	0.982 (±0.014)	0.678 (±0.016)	0.039 (±0.002)
ΔT = 12	0.988 (±0.017)	0.681 (±0.020)	0.038 (±0.002)
Average	0.983 (±0.015)	0.679 (±0.016)	0.039 (±0.002)

Where: R_u – air to air thermal resistance
R_s – surface to surface thermal resistance
k – thermal conductivity

For the calibration of a GHB apparatus, ASTM C236 and C1363 suggest the use of a reference sample with a known R-value. However, no tolerances are specified in the test method. ASTM C236 and C1363 comment on the results from round-robin tests carried out in the USA of 21 laboratories with a hot box apparatus. The results from the round-robin test showed measurements from two laboratories could differ by up to ±7.8% on the same specimen. The difference between the University of Newcastle GHB test result and the CSIRO Heat Flow Meter R-value for the polystyrene is well within this range given the nature of the different test arrangements and possible sample variations.

After the satisfactory verification of the GHB apparatus, two series of tests were carried out: standard steady state temperature tests to determine the R-value for a range of walling systems, and (non-standard) cyclic tests simulating day-night temperature cycles. The walling systems tested included those used in the housing module tests which formed part of Strand 2 of the investigation.

A recalibration of the GHB using the same polystyrene sheet was conducted during August 2009 to confirm the long term consistency of the apparatus which had been in use for approximately 7 years. Tests on the same sheet of polystyrene were performed again for Δ18°C and Δ12°C temperature differentials. The results showed no change from the initial calibration outside of experimental error.

2.1.2. Steady State Temperature Tests for R-Value Determination

Steady-state tests were conducted on a series of brick masonry walls using different forms of construction and masonry unit types that reflected current practice (see Table 2.3). The masonry walls were constructed from typical extruded clay bricks using a mortar mix of proportion 1:1:6 (cement:lime:sand by volume) without air-entraining plasticisers. Nominal 10mm mortar joints were used and all perpends were filled. A different mix (1:0:4) was used for any rendering, with approximately 0.3 fireclay (by volume) and some air-entraining agent added. The walls were air cured in the laboratory.

All walls were tested at least 6 weeks after construction to allow them to reach equilibrium moisture content with the laboratory air. Some walls were subsequently re-tested after different finishes had been applied. For example, the extruded brick cavity wall which was initially tested as bare brickwork, was subsequently tested with plasterboard finish and finally with cement render. The brick veneer wall was constructed using low glare reflective foil, with the reflective surface orientated towards the plasterboard cavity (consistent with standard practice). This wall was tested in both orientations under ‘heat flow in’ and ‘heat flow out’ conditions. The masonry skin of the brick veneer wall was also re-used for the ‘reverse brick veneer’ wall.

Four different masonry units were used to construct the various wall types. These are shown in Figure 2.4 and consist of a 110mm wide solid dry-pressed unit (a), a 90mm wide horizontally cored Western Australia unit (b) and two 110mm wide extruded units containing 10 core holes (c, d). The densities of the masonry walls were obtained by weighing with a crane mounted scale and subtracting the mass of the steel support frame.

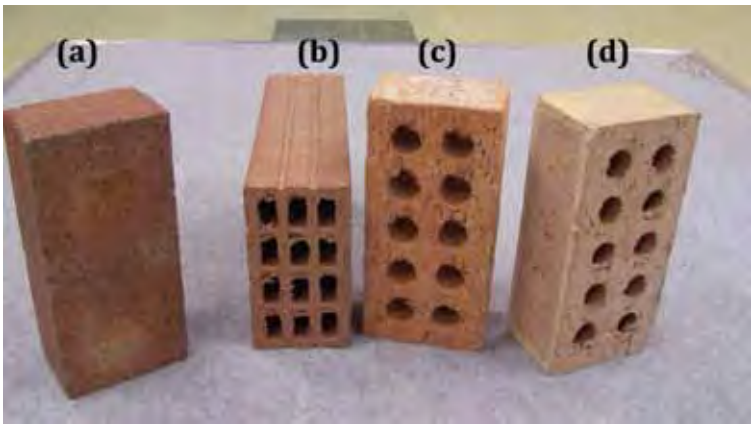

Figure 2.4 Masonry Units used in Wall Construction.

2.1.3. Results

2.1.3.1. R-value tests

The R-value tests were conducted by maintaining a constant temperature differential between the two chambers. In the tests, temperatures were appropriately set in each chamber to provide a constant rate of heat flow through the test specimen. Energy and temperature measurements from sequential four hour periods were used to calculate average thermal properties. Testing was performed for two temperature differentials, 18°C and 12°C (air-to-air). In both cases the mean wall temperatures were adjusted to 23°C in accordance with AS/NZS4859.1. A summary of the R values obtained is given in Table 2.2. Since the test walls were constructed over a considerable period of time by different brick layers, one potential source of minor inconsistencies between the results could stem from small variations in construction methods and practices.

Table 2.2 R-Values, Thermal Conductivities, U-Values and Wall Densities

Summary of R-value, Thermal Conductivity and U-values Determined using GHB Tests, November 2009							
Wall Type	Wall Density (kg/m^2)	Wall Element	Element Thickness (m)	R-value ($m^2.K/W$) $\Delta T=18^oC$	Thermal Conductivity of Element, $k_{element}$ (W/m.K)	Apparent Thermal[1] Conductivity of Wall, k_{wall} (W/m.K)	U-value[2] ($W/m^2.K$)
Esky Calibration		r_c		0.16			
25mm thick Polystyrene	0.606	$r_{polystyrene}$	0.025	0.678	0.037		
		r_h		0.17			
		$R_{s\ (surface-to-surface)}$		**0.68**		0.037	**n/a**
Single Skin		r_c		0.16			
110 mm dry-pressed (single skin)	210	r_{wall}	0.11	0.12	0.917		
		r_h		0.17			
		$R_{s\ (surface-to-surface)}$		**0.12**		0.917	8.33
		$R_{u\ (air-to-air)}$		**0.46**			**2.17**
Cavity Wall		r_c		0.15			
2 x 110 mm dry-pressed with 50mm air cavity	420	$r_{110\ pressed}$	0.11	0.12	0.917		
		r_{cavity}	0.05	0.14	0.357		
		$r_{110\ pressed}$	0.11	0.12	0.917		
		r_h		0.16			
		$R_{s\ (surface-to-surface)}$		**0.37**		0.730	2.70
		$R_{u\ (air-to-air)}$		**0.68**			**1.47**
WA Cavity Wall		r_c		0.16			
110 mm extruded + 50mm air cavity + 90mm WA unit (horizontal cored)+ 12mm render	320	$r_{90\ WA}$	0.09	0.2	0.450		
		r_{cav}	0.05	0.14	0.357		
		$r_{110\ ext}$	0.11	0.15	0.733		
		r_h		0.17			
		$R_{s\ (surface-to-surface)}$		**0.49**		0.510	2.04
		$R_{u\ (air-to-air)}$		**0.82**			**1.22**
Brick Veneer (heat flow in)		r_c		0.14			
110 mm extruded units+ 50mm air cavity reflective foil insulation +70mm pine studs + 10mm plasterboard	210	$r_{plaster-timber-foil}$	0.08	0.56	0.143		
		r_{cav}	0.05	0.14	0.357		
		$r_{110\ ext}$	0.11	0.13	0.846		
		r_h		0.16			
		$R_{s\ (surface-to-surface)}$		**0.83**		0.289	1.20
		$R_{u\ (air-to-air)}$		**1.14**			**0.877**
Brick Veneer (heat flow out)		r_c		0.17			
10mm plasterboard + 70mm pine studs + reflective foil insulation + 50mm air cavity + 110 mm extruded units	210	$r_{110\ ext}$	0.11	0.14	0.786		
		r_{cav}	0.05	0.16	0.313		
		$r_{plaster-timber-foil}$	0.08	0.6	0.133		
		r_h		0.18			
		$R_{s\ (surface-to-surface)}$		**0.90**		0.267	1.11
		$R_{u\ (air-to-air)}$		**1.26**			**0.794**
East Coast Extruded Cavity Wall		r_c		0.17			
110 mm extruded + 50mm air cavity + 110mm extruded	380	$r_{cw\ 110\ ext}$	0.11	0.14	0.786		
		r_{cav}	0.05	0.14	0.357		
		$r_{hw\ 110\ ext}$	0.11	0.15	0.733		
		r_h		0.17			
		$R_{s\ (surface-to-surface)}$		**0.43**		0.628	2.33
		$R_{u\ (air-to-air)}$		**0.77**			**1.30**
East Coast Extruded Cavity Wall (plasterboard)		r_c		0.16			
110 mm extruded + 50mm air cavity + 110mm extruded with 10mm plasterboard glued @ 600 centres	385	$r_{cw\ 110\ ext\ +\ plasterboard}$	0.12	0.26	0.462		
		r_{cav}	0.05	0.14	0.357		
		$r_{hw\ 110\ ext}$	0.11	0.15	0.733		
		r_h		0.18			
		$R_{s\ (surface-to-surface)}$		**0.55**		0.509	1.82
		$R_{u\ (air-to-air)}$		**0.89**			**1.12**
East Coast Extruded Cavity Wall (render)		r_c		0.17			
110 mm extruded + 50mm air cavity + 110mm extruded with 10mm render	400	$r_{cw\ 110\ ext\ +\ render}$	0.12	0.14	0.829		
		r_{cav}	0.05	0.14	0.351		
		$r_{hw\ 110\ ext}$	0.11	0.15	0.732		
		r_h		0.17			
		$R_{s\ (surface-to-surface)}$		**0.44**		0.640	2.28
		$R_{u\ (air-to-air)}$		**0.77**			**1.29**
Reverse Brick Veneer (Granosite)		r_c		0.19			
Granoskin finish on 7mm blueboard + 90mm pine studs @ 600 centres with R1.5 glass wool insulation in frame cavity + 110mm extruded bricks + 10mm render	210	$r_{cw\ 110\ extruded\ bricks}$	0.11	0.13	0.846		
		$r_{90mm\ insulation}$	0.09	1.42	0.063		
		$r_{hw\ 7mm\ blueboard}$	0.007	0.02	0.350		
		r_h		0.17			
		$R_{s\ (surface-to-surface)}$		**1.57**		0.132	0.64
		$R_{u\ (air-to-air)}$		**1.93**			**0.518**
Insulated Extruded Cavity Wall + Render		r_c		0.17			
110mm extruded + 50mm air cavity + 30mm extruded polystyrene sheets glued to 110mm extruded units with 10mm render	401	$r_{cw\ 110\ extruded\ bricks}$	0.11	0.14	0.785		
		r_{ca}	0.05	0.18	0.274		
		r_{poly}	0.03	0.76	0.039		
		$r_{ca+poly}$	0.08	1.04	0.077		
		$r_{hw\ 110\ extruded\ bricks}$	0.11	0.11	0.957		
		r_h		0.15			
		$R_{s\ (surface-to-surface)}$		**1.30**		0.232	0.77
		$R_{u\ (air-to-air)}$		**1.62**			**0.617**
Light-Weight Wall		r_c		0.18			
2-3mm granoskin + 7mm blueboard on 90x35mm pine studs at 600mm centres + R1.5 fibreglass batts in frame cavity + 10mm plasterboard lining	25	$r_{cw\ plasterboard}$	0.01	0.06	0.173		
		r_{ins}	0.09	1.43	0.063		
		$r_{hw\ granoskin+blueboard}$	0.01	0.02	0.404		
		r_h		0.17			
		$R_{s\ (surface-to-surface)}$		**1.51**		0.073	0.66
		$R_{u\ (air-to-air)}$		**1.86**			**0.539**
Insulated Brick Veneer		r_c		0.13			
110mm East coast extruded brick + 50mm air cavity with 90mm pines studs at 600mm sentres with low glare wall wrap + R1.5 glass wool insulation in frame cavity + 10mm plasterboard	217	$r_{cw\ 90mm\ insulation}$	0.09	1.32	0.068		
		r_{ca}	0.05	0.13	0.376		
		$r_{hw\ 110\ extruded\ bricks}$	0.11	0.13	0.862		
		r_h		0.16			
		$R_{s\ (surface-to-surface)}$		**1.58**		0.158	0.63
		$R_{u\ (air-to-air)}$		**1.87**			**0.536**

Where: r_c - cold air film resistance,
r_h - hot air film resistance,
r_{cav} – cavity resistance
$R_{u(air\text{-}to\text{-}air)}$ - total thermal resistance including air films
$R_{s(surface\text{-}to\text{-}surface)}$ - total thermal resistance excluding the external air films – these values have the greatest accuracy as temperatures were measured using the Prema precision thermometer.

Note: 1. The apparent thermal conductivity represents an average k value for the wall system. The k for individual elements in the wall may be different and caution should be used to extrapolate values for walls with different thicknesses.

2. U-values represent the reciprocal of the R-values and are usually used to express the overall heat transfer coefficient for the wall system, including inside and out side air film resistances. The U-values for surface-to-surface have been included only to highlight the contribution of air film resistances. Under steady-state conditions, the U-value is a direct measure of the rate of heat transfer (in Watts) through a $1m^2$ area of the building element when it is subjected to a temperature difference of 1°C.
3. "WA cavity wall" was constructed from 90mm horizontally cored units (Fig. 2.4(b))
4. "East coast walls" were constructed from 110mm conventional extruded units (Fig. 2.4 (c) and 2.4 (d))

2.1.3.2. Temperature Gradients – Selected Results

The following plots represent the measured temperature gradients across various wall assemblies with an 18ºC temperature differential (air-to-air). Note that these temperatures may not be the same values used for the R-value calculation but from a separate set of data logged during the test. In some plots the cavity air temperature may not be consistent as the result of a thermocouple positioning error. This sensor was inserted into the cavity after construction on a long rod, and was not always located in the centre of cavity. All other thermocouples were physically fixed to solid surfaces at the time of construction. It is of interest to study the temperature gradients at various locations through the thickness for wall assemblages. Figures 2.5 to 2.9 show the temperature profiles for a range of walls with an 18°C temperature differential (air-to-air). Note that these temperatures are a snapshot of the test data, not the averaged results used for the R-value calculation. The difference in behaviour for the different forms of construction is readily apparent, with the foil insulation in the brick veneer wall clearly playing a significant role for that system. Similar data has been collected for the other forms of wall construction listed in Table 2.2.

From the data in Table 2.2, it can be seen that the air film resistance values r_h and r_c range from 0.14-0.19. These values affect the total thermal resistance ($R_{u\,(air\text{-}to\text{-}air)}$) and are influenced by the speed of the air moving past the surface of the wall. In the Newcastle GHB, the circulation fans have been set to produce air speeds in the range of 0.2-0.3$m.s^{-1}$. (This air speed is often used as the assumed value for natural air movement along interior walls.) The interior air film resistance used in AS/NZ4859.1 is $0.04m^2.K/W$ which is lower than these measured values ($r_{interior}$ = 0.12).

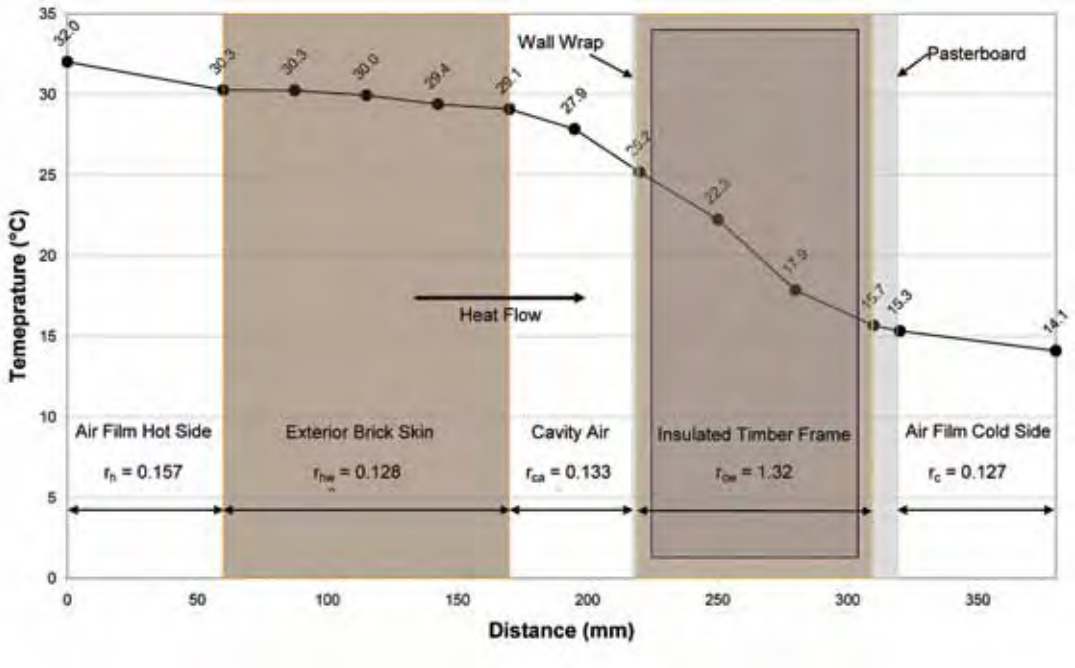

Figure 2.5 Temperature and R-value profile for Insulated Brick Veneer Wall

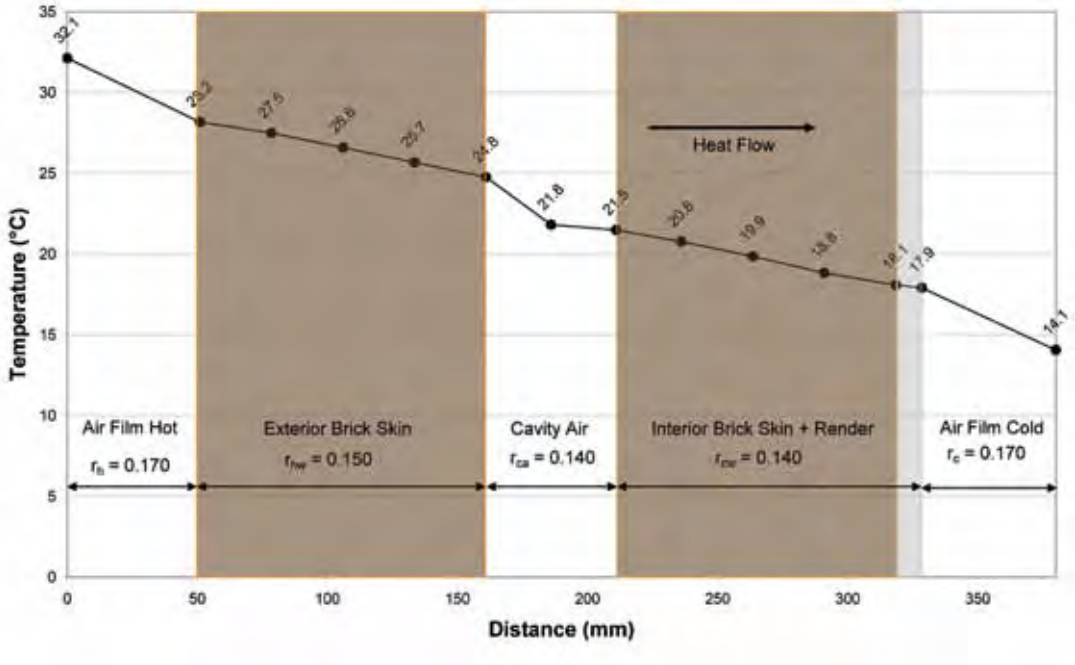

Figure 2.6 Temperature and R-value profile for Cavity Brick + Render wall

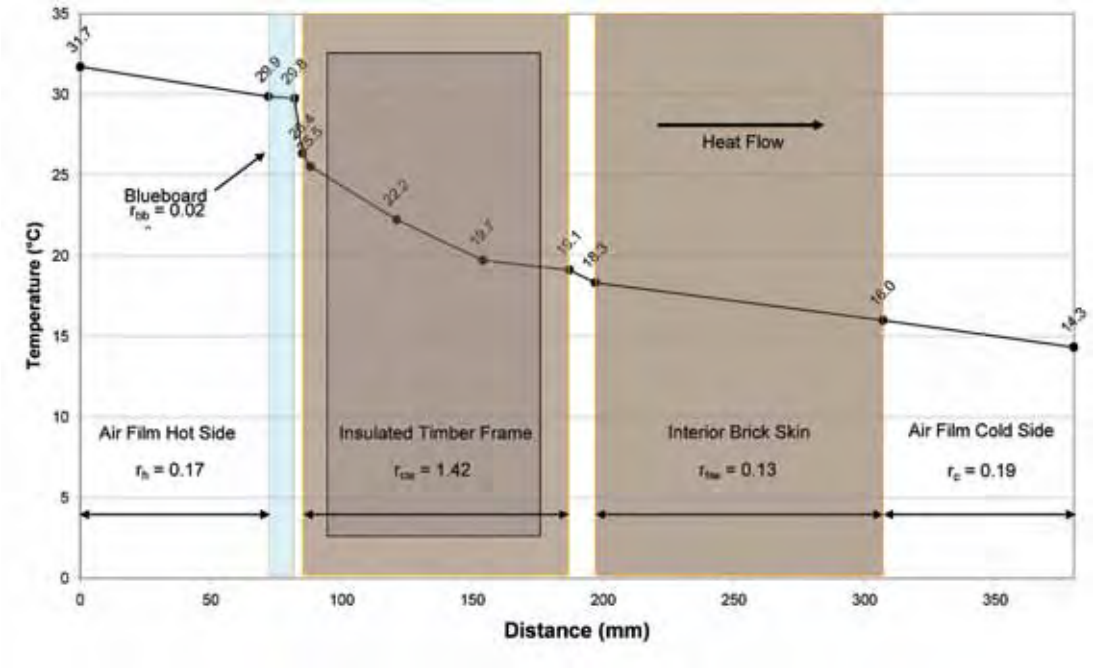

Figure 2.7 Temperature and R-value profile for Insulated Reverse Brick Veneer wall

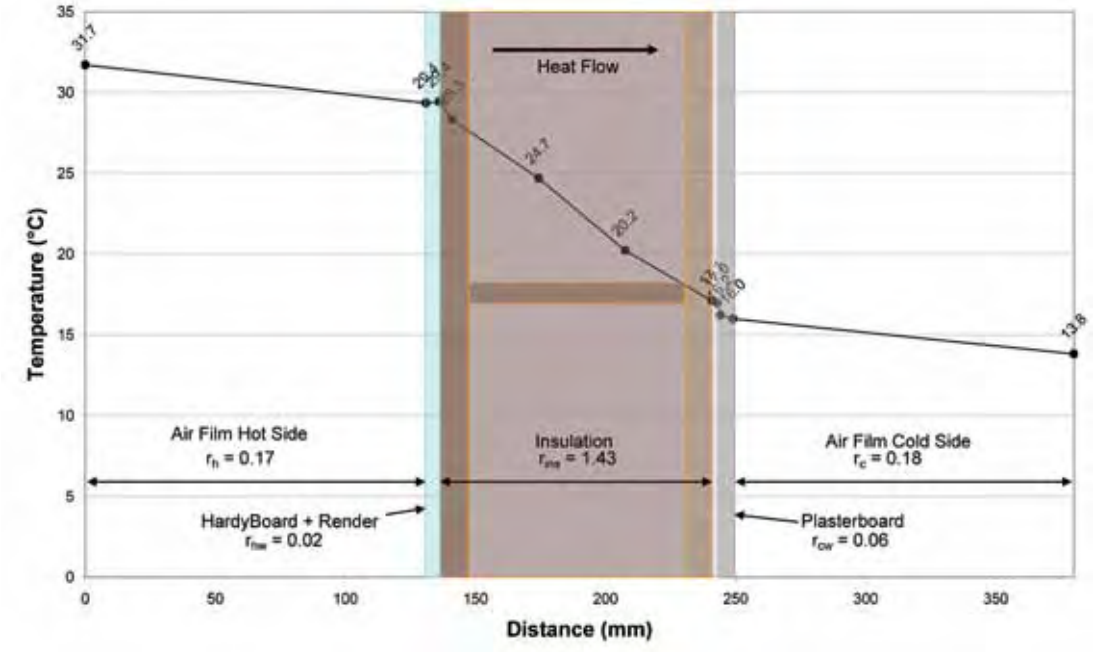

Figure 2.8 Temperature and R-value profile for Insulated Lightweight wall

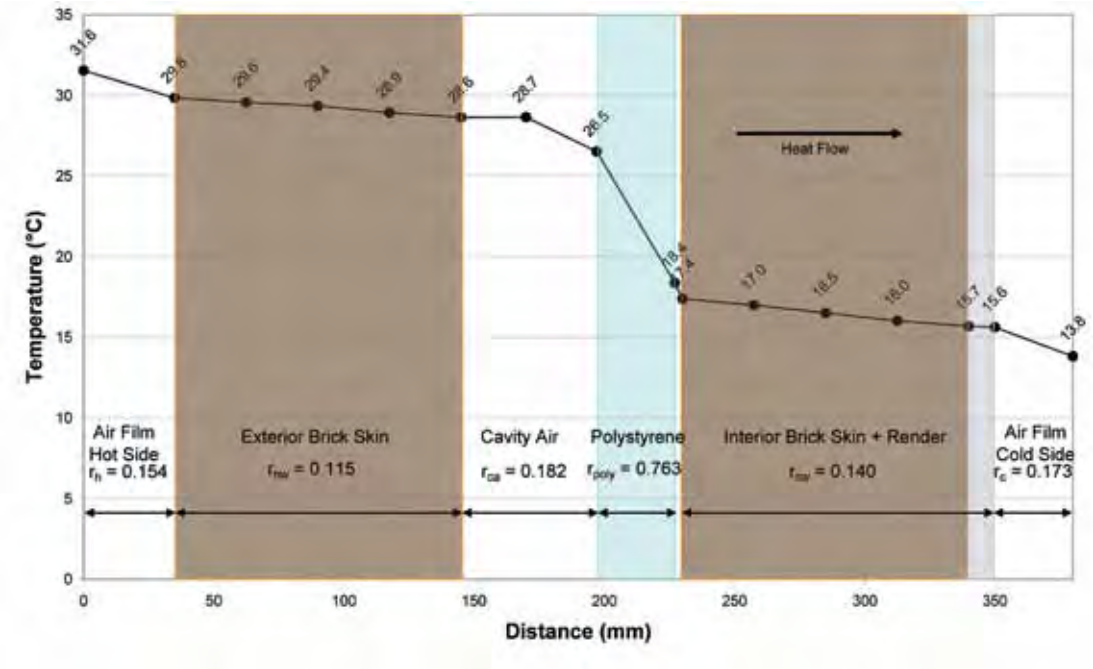

Figure 2.9 Temperature and R-value profile for Insulated Cavity Brick + Render wall

2.1.4. Cyclic Tests

A limited number of cyclic tests were also performed using the GHB apparatus to simulate typical day-night cycles, although in this case the effects of direct or indirect solar radiation are obviously not included. Typical winter and summer temperature cycles were selected from the NATHERS weather data (NatHERS) and were simulated in the GHB. Since these tests were not steady state, the meter box was removed and all temperature and heat flux profiles measured.

Tests were conducted by maintaining a set temperature on the cold side of the GHB. These temperatures were 22°C and 20°C for summer and winter respectively. The guard side was programmed with the appropriate weather temperature cycle (shown in Figures 2.10 and 2.11). The test cycles were repeated typically over a period of several days. The results provide a more 'realistic' indication of how a wall system behaves under dynamic conditions in contrast to the steady state R-value tests.

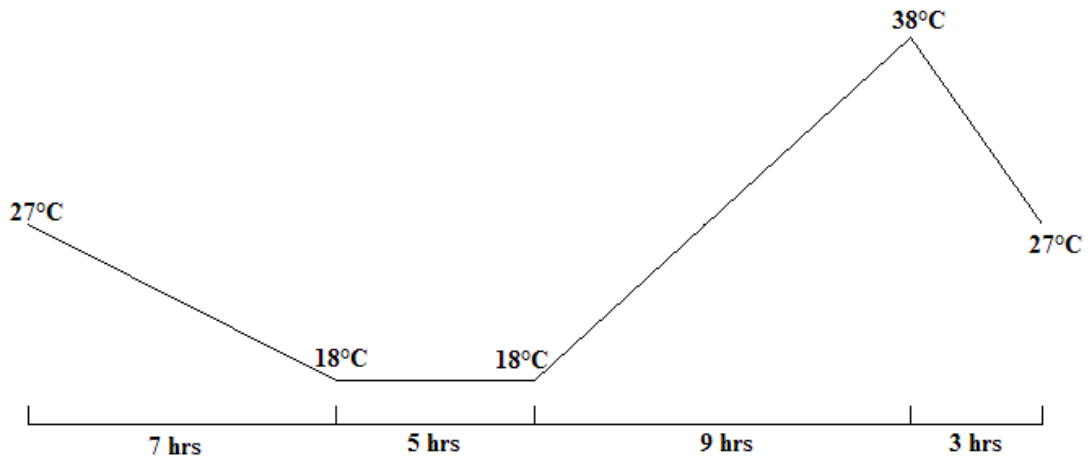

Figure 2.10 Guard side temperature cycle – summer

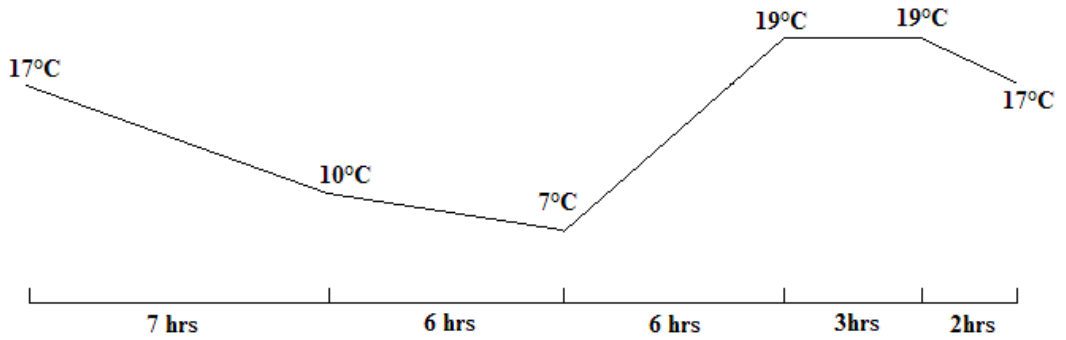

Figure 2.11 Guard side temperature cycle – winter

The cyclic results provide useful information on the heat flow attenuation and thermal lag of each individual wall element on a comparative basis for each wall type. The results illustrate the ability of a wall to attenuate heat flow and provide information on the nature of the temperature gradients established within each wall. Figures 2.12 to 2.15 show the temperature and heat flux profiles for insulated cavity brick and insulated lightweight walls. These results illustrate the mechanisms of thermal mass and thermal resistance, demonstrating how the systems perform under the influence of a dynamic input. It is important to note that the results do not entirely reflect the wall system performance in an actual dwelling as the internal air remains constant, no solar radiation is present and there is no influence from other wall surfaces. The results solely demonstrate the one dimensional heat flow mechanisms.

Figures 2.12 and 2.14 show that when the exterior surface temperature dropped below the temperature within the wall the temperature gradient through a wall section underwent a reversal. This corresponds to heat flowing out from the exterior masonry skin back to the external air. This can be observed in the heat flux profiles shown in Figures 2.13 and 2.15, with negative external surface values being recorded from approximately 6pm until 7am. Also note the reduction in peak heat flux values through the wall profile in Figures 2.13 and 2.15, and the reduction in the maxima and time delay (lag) of the profile temperatures shown in Figures 2.12 and 2.14. The temperature gradients are non-linear with the cavity forming a noticeable barrier to the transport of heat. Similar attenuations of temperature and heat flux profiles have been observed in the test modules under real weather conditions.

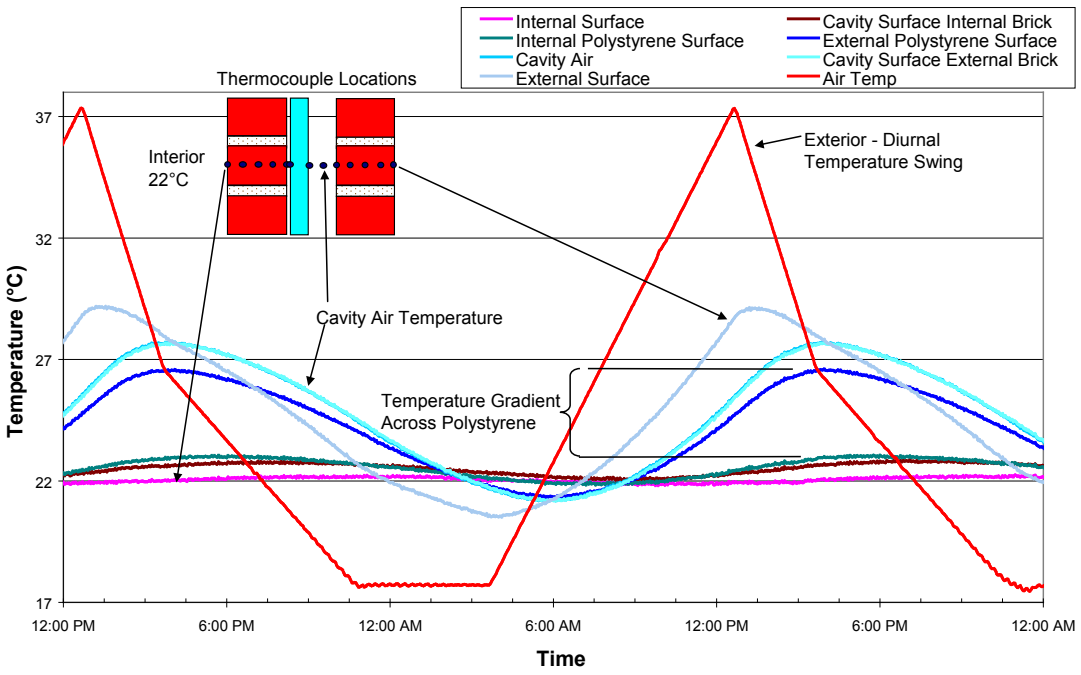

Figure 2.12 Insulated Cavity Brick Summer Cycle Temperature Profile

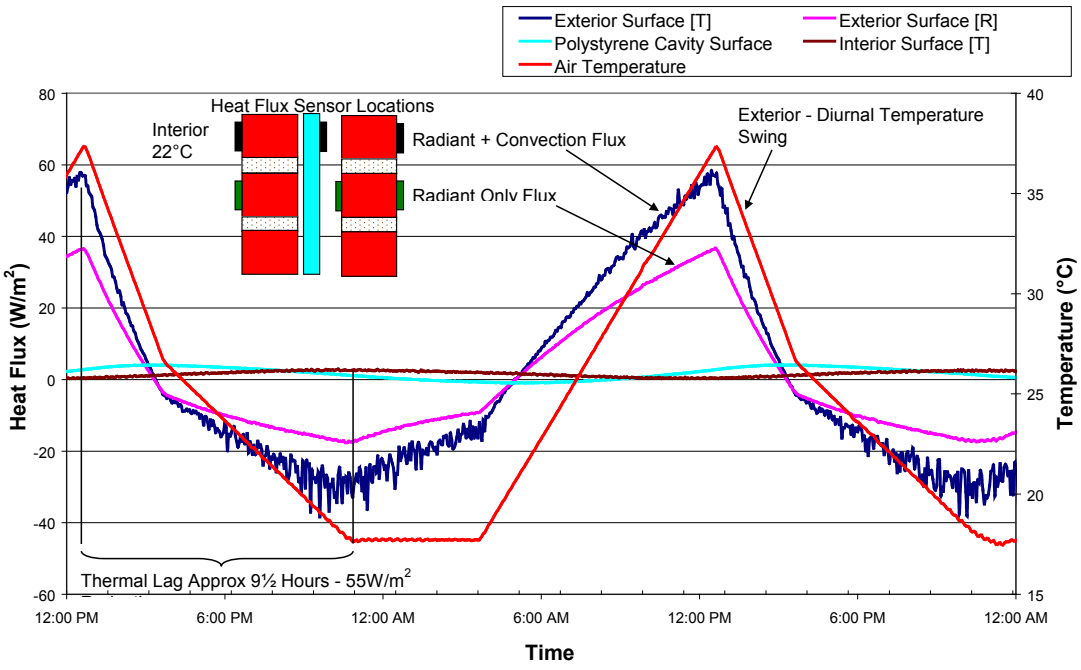

Figure 2.13 Insulated Cavity Brick Summer Cycle Heat Flux Profile

From the heat flux trend of the insulated cavity brick wall (Figure 2.13), it can be seen that a large quantity of heat is absorbed by the exterior surface. However not all absorbed heat is transferred to the interior space due to the thermal lag of approximately 9.5 hours. As a result of this lag, heat begins to flow back outwards as the external temperature drops. In contrast to this behaviour, an R-value test maintains steady state temperatures and nearly all heat absorbed from the external surface passes through the wall.

For the insulated cavity brick wall, there is a small continual flow of heat into the interior space for the cyclic test. However over 24 hours the total amount of heat/energy flow inwards is lower for the insulated

cavity brick system compared to the lightweight system (Figure 2.15). The peak flow through the insulated cavity brick wall into the cold chamber occurs at approximately 22:20 with 3 W/m^2. This occurs 9.5 hours after the peak flow into the external surface of 58 W/m^2 (Figure 2.13).

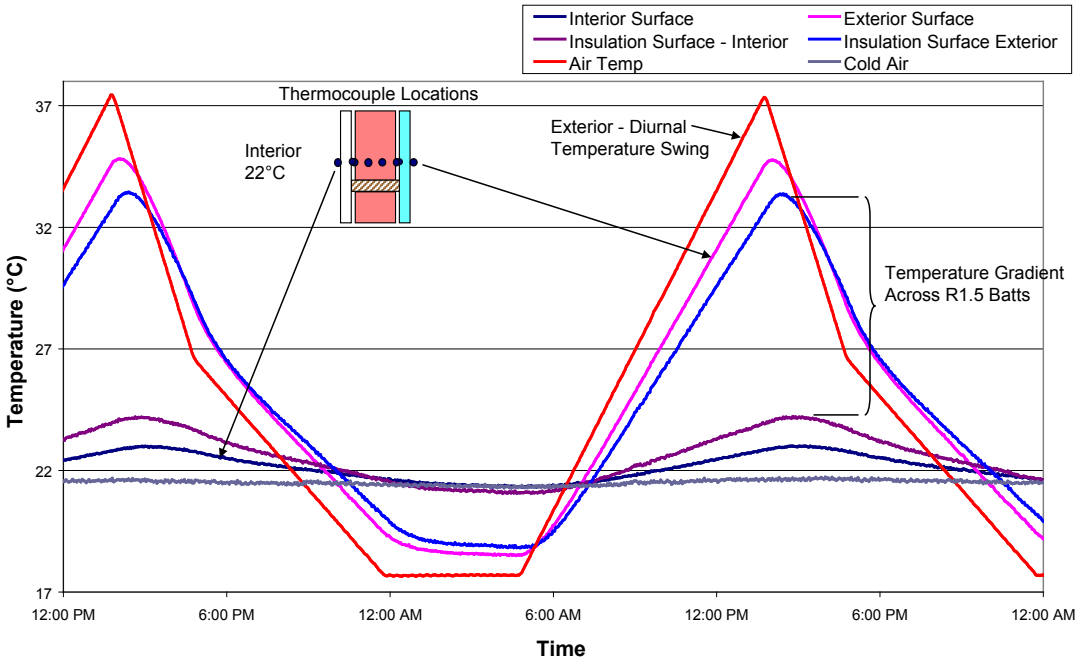

Figure 2.14 Insulated Lightweight Summer Cycle Temperature Profile

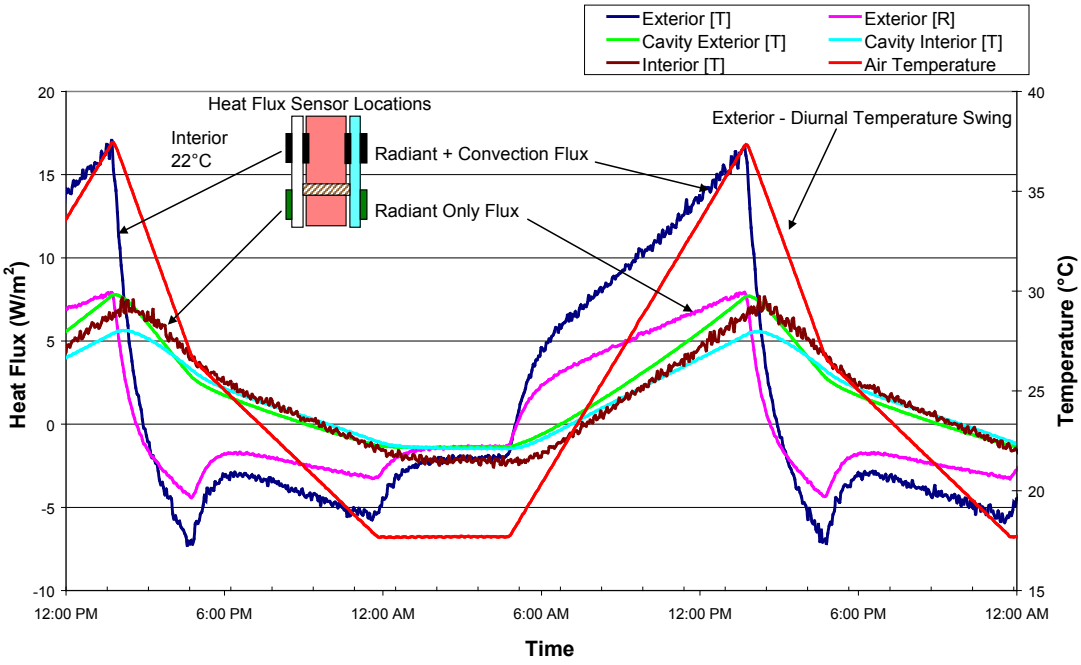

Figure 2.15 Insulated Lightweight Summer Cycle Heat Flux Profile

From Figures 2.14 and 2.15 it can be seen that for the lightweight construction the maximum temperature gradient occurred over a very short span of time. The heat flow into the interior was reduced but not delayed due to the short thermal lag. The direction of the heat flow was determined solely by the difference in temperature between the interior and exterior air. Heat flowed in when the exterior air was higher than the

interior and heat flowed out when the exterior temperature dropped below the interior. There was virtually no thermal mass within the system to produce any perceived differential between air temperatures due to the wall components. From Figure 2.15, the peak external surface inward flow was only approximately 17 W/m^2 however the peak interior flow of 7.4 W/m^2 was only 30 mins later due to the short thermal lag. Similar behaviour in regards to the heat flow was also observed in the corresponding insulated lightweight test module.

These results indicate that insulation alone has limited capacity to provide thermoregulation but can certainly provide benefits when used appropriately in conjunction with thermal mass. Insulation simply reduces the peak instantaneous heat flow with virtually no thermal lag. The temperature gradient for the insulated cavity brick showed both the time lag of the external mass and the temperature drop across the insulation within the cavity. Insulation certainly provided a benefit when placed external to the internal thermal mass, reducing the heat absorbed by the cavity surface of the thermal mass. This increases the isolation of the internal skin to the external environment allowing improved response to the internal space.

Although limited in extent, the cyclic tests illustrate well the complex nature of heat flow through all elements of a walling system. They also demonstrate the unsuitability of R-Value as a sole descriptor of wall performance as other mechanisms are taking place.

2.2. Bench Scale Study – hybrid walls study

As part of the study related to the smart use of thermal mass described in chapter 7, a small laboratory test rig was developed to allow a series of comparative studies of wall thermal performance at 1/8 scale. This section provides an overview of that study. More complete details are given in the relevant PhD thesis (Gregory K. E., 2010).

2.2.1. Bench-scale setup

The bench-scale setup (Figure 2.16) was designed and constructed to study the behaviour of different walling systems in a rapid, reproducible manner under controlled laboratory conditions.

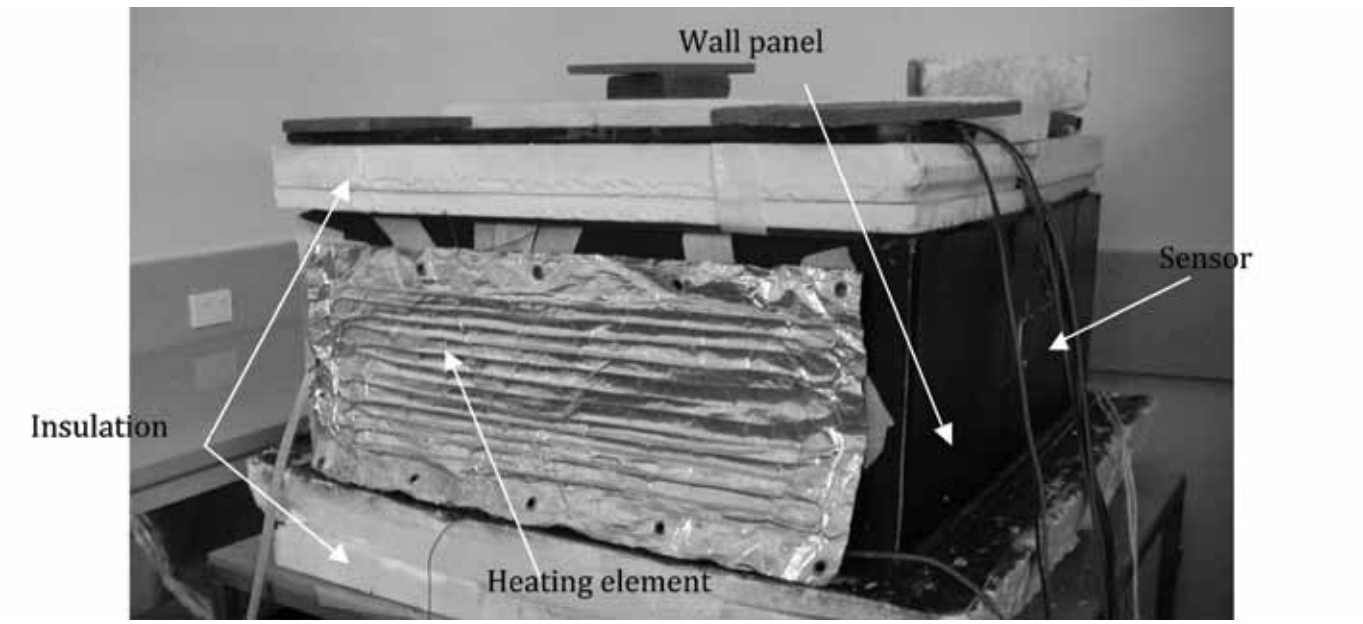

Figure 2.16 Bench-Scale Setup

The physical dimensions and configuration of the bench-scale setup were carefully selected to ensure that the setup represented an exact 1/8 replica of the full-scale thermal test house modules described in Chapter 3.

The setup consisted of a 25 mm thick reinforced concrete square slab (750 mm x 750 mm) on which four side wall panels were mounted (Figures 2.17 and 2.18). The roof was constructed from several layers of blue board insulation. The wall panels were independently mounted so that identical (i.e. conventional approach) or dissimilar constructions (i.e. hybrid wall concept) could be employed.

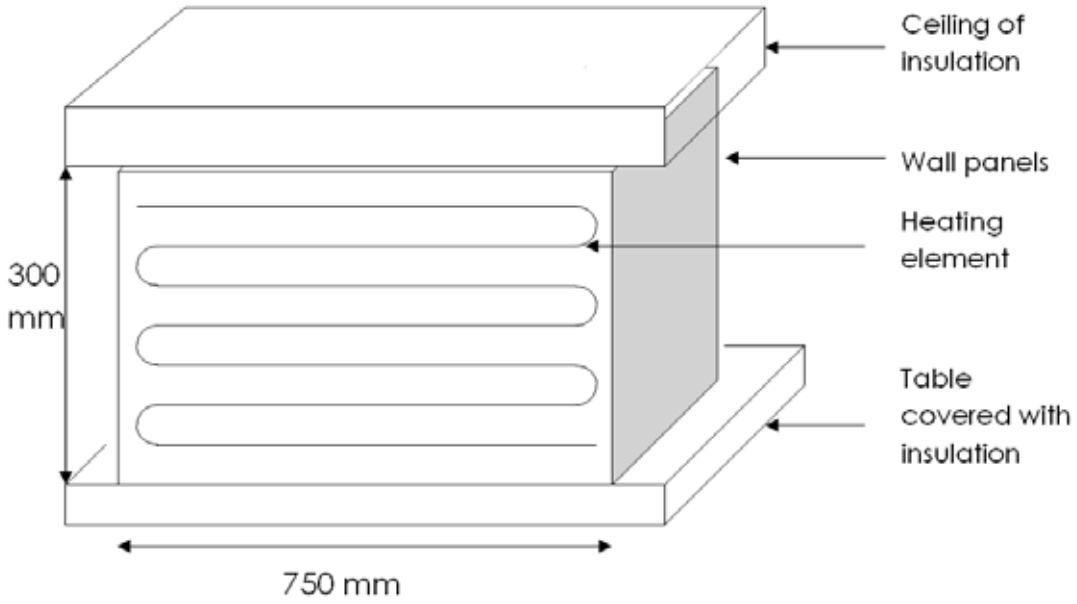

Figure 2.17 Schematic representation of the Bench-Scale setup

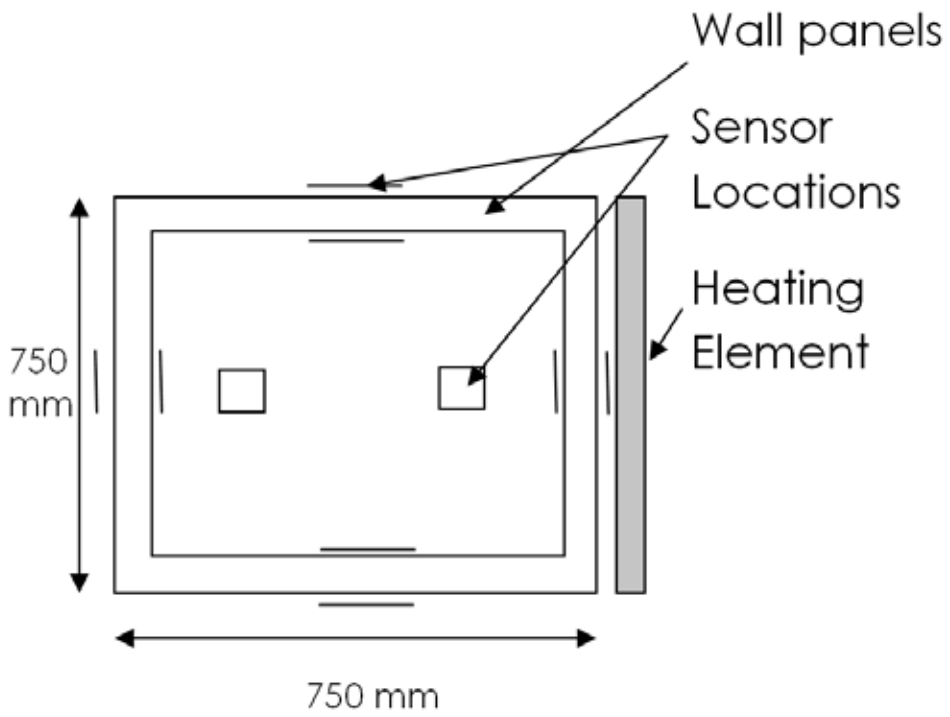

Figure 2.18 Schematic representation of the Bench-Scale setup, plan view with roof removed

Special attention was given to the construction of the wall panels to ensure that the thermal characteristics of their full-scale counterparts were accurately represented. This was achieved by maintaining the thermal conductivity (k) and thermal mass (ρC_p) of the bench-scale setup at levels similar to those used in the full-scale modules. The wall panels were fitted with electrical elements to mimic the external heat flux received by the external walls of the full-scale test house modules. The wall panels, slab, roof and cavity space were fully instrumented with thermocouples and heat flux sensors. Data was collected every minute over weekly cycles. The ambient temperature in the laboratory was maintained at 25°C throughout the experiments.

2.2.2. Rig Calibration and Operation

The heating element was programmed to activate and maintain set power until the temperatures reached steady state. The model was then allowed to cool and its performance monitored.

Data was recorded using a Datataker DT600 data logger. All temperatures were measured using type T thermocouples connected to a 30 channel expansion module housed in a thick walled aluminium box to correct for cold junction offsets. The corresponding temperature offsets were adjusted in the logging process. The heating element had to be operated at a setting that provided repeatable, safe and accurate results. An electrical resistance box was added to the heating element to control the amount of heat that was applied to the model. To find the correct setting, the heating element was operated on the cavity brick construction, firstly at only 15.50% of its capacity. At this setting the model exhibited a change in temperature of only 3.5°C (see Figure 2.19).

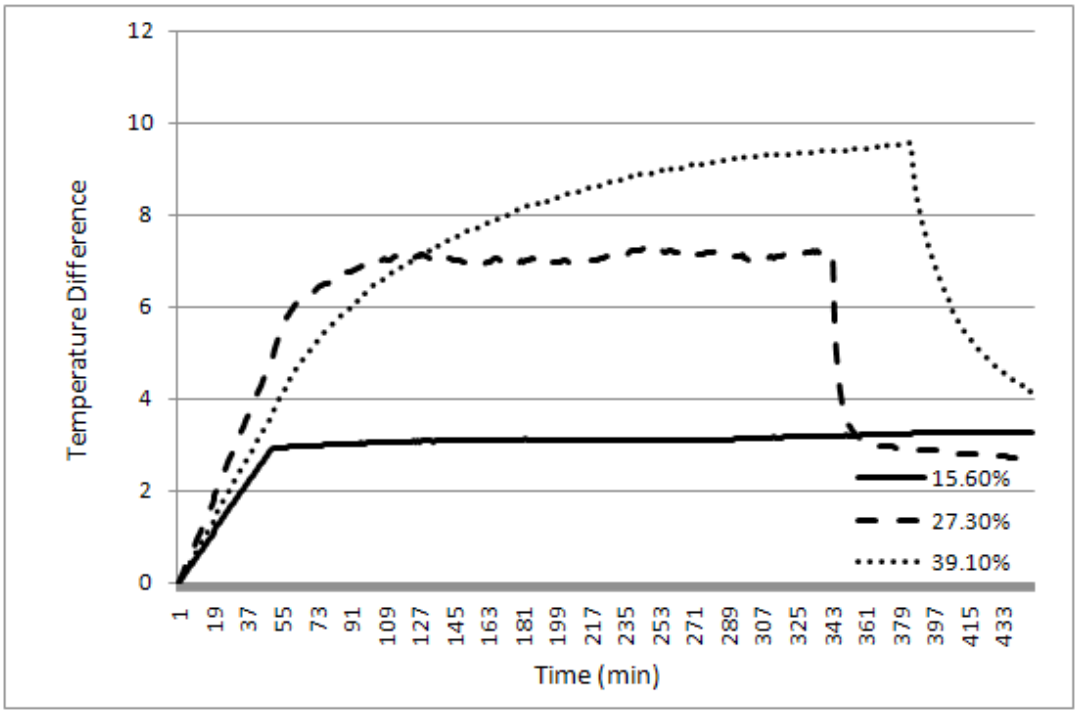

Figure 2.19 Change in internal temperature for different heating rates.

The heating element was then operated at 27.3% capacity and it was found that after a steady temperature climb for 60 minutes the temperature plateaued. This was a reasonable amount of time to operate the experiment with an internal temperature change of approximately 7°C obtained (Figure 2.19).

The heating element was then increased to 39.1% and it was found that a stable internal temperature was not reached within a 300 minute period, consequently, the heating element switched off for safety reasons.

Each heating rate was then examined using the assessment factors for cavity brick, temperature difference ratio (*TDR*) and thermal lag (*Lag*), as shown in Table 2.3. A decrement factor and lag result similar to the performance in an actual cavity brick house was required. At 15.5% the decrement factor was quite high and the time lag relatively short. The decrement factor and time lag for the 27.3% and 39.1% heating rate were much closer to what would be expected in a real structure.

Table 2.3 TDR and Lag for cavity brick for different inputs

Input	TDR	Lag (hrs)
39.1%	0.32943	5.2
27.3%	0.396985	4.1
15.5%	0.541667	2.8

Note: Temperature Difference Ratio (TDR) was derived as the decrement factor from the following equation:

$$TDR = \frac{T_{inside}^{max} - T_{inside}^{min}}{T_{outside}^{max} - T_{outside}^{min}}$$

At 39.1% heating element capacity, the cavity brick model reached quite high temperatures and operated at a similar level at which the Light Weight construction was considered to be a potential fire hazard. Therefore due to safety and time constraints the heating element was operated at 27.3% capacity. To make certain this was the correct setting for the heating element; all walling systems were then run to ensure comparable results were achieved. The heating rates of five different walling systems can be seen in Figure 2.20.

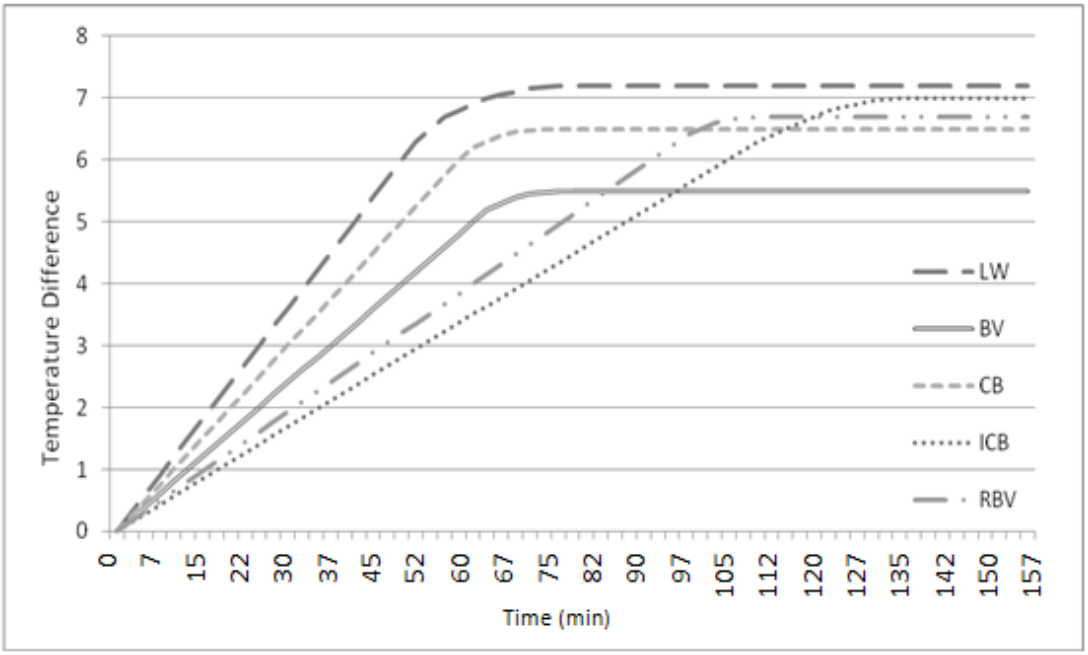

Figure 2.20 Heating rates for all walling systems at 27.3% of capacity.

The average internal and external temperature difference of the modules was 6.54 degrees, with lightweight and brick veneer at the extremities of the range. The lightweight, cavity brick and brick veneer constructions reached equilibrium at an approximately similar time of 60 minutes, whereas heavier and well insulated thermal mass constructions such as insulated reverse brick veneer and insulated cavity brick, reached equilibrium at 100 and 130 minutes respectively. Operating the heating element at 27.3% of its capacity offered a rapid simulation within the model of the performances of walling systems, with a simulation being completed in approximately 24 hours (1440 minutes). It is thus a useful method of modelling novel walling systems.

There were several variables which may influence the accuracy of the results for this experimental setup. These include:

- Warm-up time for the heating element
- Raw material changes

These were overcome by repeat experiments to reduce experimental error. To ensure the difference was detected in the thermal performance of each walling system, each of the above variables were kept as constant as possible.

The results of the experiments, together with various numerical simulations are presented as a part of Chapter 7, “Smart Utilisation of Thermal Mass”.

2.3. Summary

This chapter has described the laboratory based aspects of the testing program: full scale wall tests using the Guarded Hot Box Apparatus under both steady state and cyclic conditions; and 1/8 bench scale study of the housing module behaviour.

The ‘guarded hot box’ was used to determine the thermal resistance, or R-value, of various wall systems and their constitute components in accordance with ASTM C236-89. The GHB was also used to evaluate the dynamic wall behaviour in dynamic tests to provide a more accurate representation of the thermal performance of walling systems.

The bench scale study performed for lightweight, brick veneer, cavity brick, insulated cavity brick and reverse brick veneer walling systems in a conventional or hybrid arrangement correctly simulated the expected performance in the full scale module tests.

3. FULL SCALE IN SITU TESTS

3.1. Overview

The second strand of the project involved the construction and monitoring of the behaviour of four full scale housing modules under a range of climatic conditions over all seasons. The construction systems for the modules covered the common forms of domestic construction in Australia (brick veneer, cavity brick and lightweight construction) as well as reverse brick veneer. The modules were constructed with an independent roof which allowed easy installation and modification of walling systems. The influence of factors such as wall insulation, windows and roof type, curtains, carpet, room ventilation and internal walls was also studied. The first two modules were constructed in 2003, and additional modules built in 2004 and 2005 as the program expanded. Details of the walls and roof systems used are summarised in Table 3.1. The modules were initially built with no window openings in order to study the characteristics of each individual wall system. A major window opening was later incorporated in each northern wall.

Table 3.1 Summary of Wall and Roofing Systems

Building Element	Material(s)	Insulation	Remarks
Cavity brick wall (+Insulated cavity brick wall)	2x110 mm brickwork skins with 50mm cavity; 10mm internal render	Standard 50mm cavity or 50mm cavity with R1 polystyrene insulation fixed to cavity side of interior brick skin	Walls with & without insulation were tested
Brick veneer wall (+Insulated brick veneer wall)	110 mm external brickwork skin; 50mm cavity; internal timber frame; 10mm plasterboard	Low glare reflective foil on timber frame with or without R1.5 glasswool batts	Walls with and without insulation were tested
Lightweight wall	2-3mm acrylic render on 7mm fibro-cement sheets on a timber stud frame; 10mm internal plasterboard	R1.5 glasswool batts	
Insulated reverse brick veneer wall	2-3mm acrylic render on 7mm fibro-cement sheets on timber stud frame; internal 110mm brick skin; 10mm internal render	R1.5 glasswool batts	
Glass sliding door	Clear, 6.38 mm laminated glass set in a light coloured aluminium frame	N/A	3 panel sliding door assembly, 2050 high x 2840 wide
Ceiling	10mm plasterboard	R3.5 glasswool batts between rafters	
Tiled roof	Clay and concrete	Sarking	
Metal roof	Coated corrugated steel	Sarking	

3.2. Module Construction and Details

The modules were constructed on the campus of the University of Newcastle (latitude 33ºS) (see Figure 3.1) with a square floor plan of 6m x 6m and spaced 7m apart to avoid shading and minimise wind obstruction. With the exception of the walls and roofing material, the buildings were of identical construction, built on a concrete slab and aligned in a manner so that the northern wall of the buildings was perpendicular to astronomical north. All four buildings had a ceiling height of 2450mm. The modules were comparable in size to other buildings used in similar studies carried out in the 1980's at Maryland, USA and Canada, (Burch et.al., 1982, Dale et.al., 1985).

Figure 3.1 Module Construction

For each structure the roof was supported by an independent steel frame located just inside the walls which allowed the walling systems to be modified or changed if desired. In each case, a typical slab-on-ground footing system was used, with the wall and roof framing systems reflecting typical practice. For the modules with a tiled roof, timber trusses were used in conjunction with fired clay roof tiles over a layer of foil sarking. For the lightweight module, timber trusses were used in conjunction with a steel colorbond roof, also over a layer of foil sarking. As this study concentrated on the thermal performance of the wall systems, the ceilings were heavily insulated with R3.5 glass wool batts to minimise the "through ceiling" heat flow. To assess the impact of windows on heat flow characteristics, a major glazed opening was later included in the northern wall of the modules. The typical modules are shown in Figures 3.2 and 3.3.

Figure 3.2 Brick Veneer and Two Cavity Brick Masonry Modules

Figure 3.3 Insulated Lightweight Module

Extruded brick masonry units with light brown to pink colourations were used in the construction. For the cavity brick modules, the inside wall surfaces were rendered using a cement/sand render with a nominal thickness of 10mm. After drying, the rendered walls were painted white.

Entry to each building was via a standard solid timber door located on the southern face of the building. To minimise the flow of heat through the door, a 75mm thick layer of polystyrene foam was attached to the rear face of the door. The door was well fitting and normally kept shut making the building as air-tight as possible, only being opened to allow necessary access,.

3.3. Instrumentation of Modules

Each module was instrumented with temperature, humidity and heat flux sensors which were continuously monitored. The thermal response was assessed in two ways; a 'free-floating' state, where the temperature in the building was determined solely by the influence of the external weather conditions or, in a 'controlled' state, where the internal temperature was preset using a cooling/heating system with the required energy usage to maintain the set comfort level measured.

The instrumentation recorded the external weather conditions, ground temperature, wind speed and direction, air temperature, relative humidity, as well as the incident solar radiation on each wall surface (vertical plane) and roof (horizontal plane). For each module, temperature and heat flux profiles through the walls, slab and ceiling were recorded in conjunction with the internal air temperature and relative humidity. Typical sensor arrangements are shown schematically in Figures 3.4 to 3.8 for each of the wall types.

In total, 105 data channels were scanned and logged every 5 minutes for each of the modules all year round. The data was recorded using Datataker DT600 data loggers located in each building. All temperatures were read using Type T thermocouples connected to three, 30 channel expansion modules. To minimise any cold junction compensation errors, all the thermocouple inputs were maintained at uniform temperature through the use of a thick wall aluminium box as shown in Figure 3.9. The thermocouples recording air temperatures were placed inside shields to reduce the influence of radiation effects. All other thermocouples were glued onto the solid surface and profile thermocouples were drilled into the masonry units. The temperature recording system (thermocouple wire characteristics, cold junction compensation etc.) was calibrated using a Prema Precision Thermometer within the controlled space of the guarded hot box and the corresponding temperature offsets were programmed for automatic adjustment during the logging process.

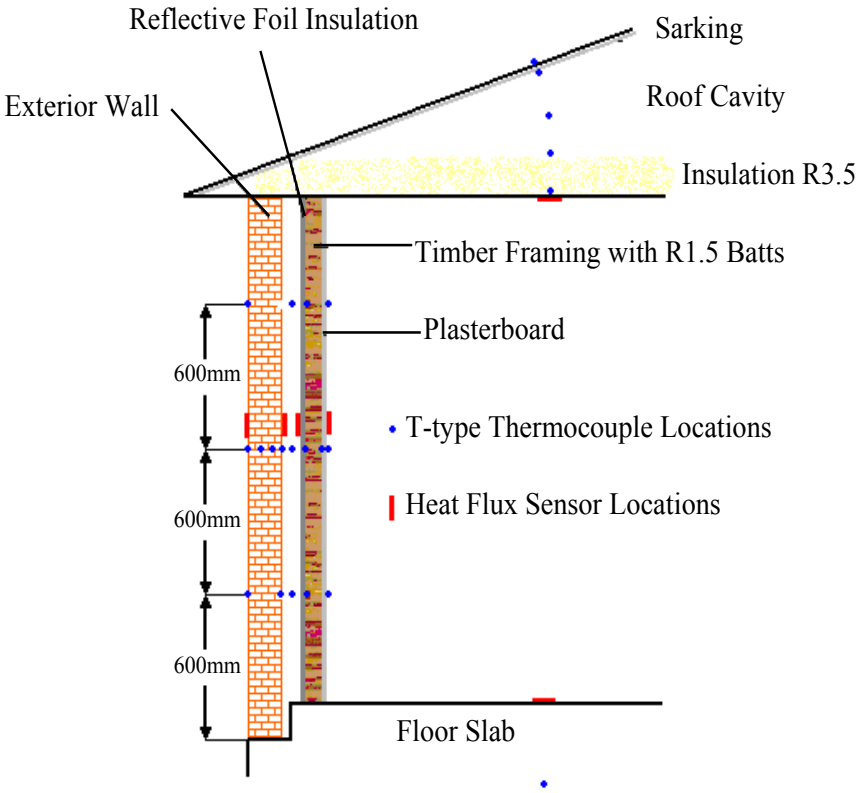

Figure 3.4 Thermocouple and Heat Flux Layout for Insulated Brick Veneer Module.

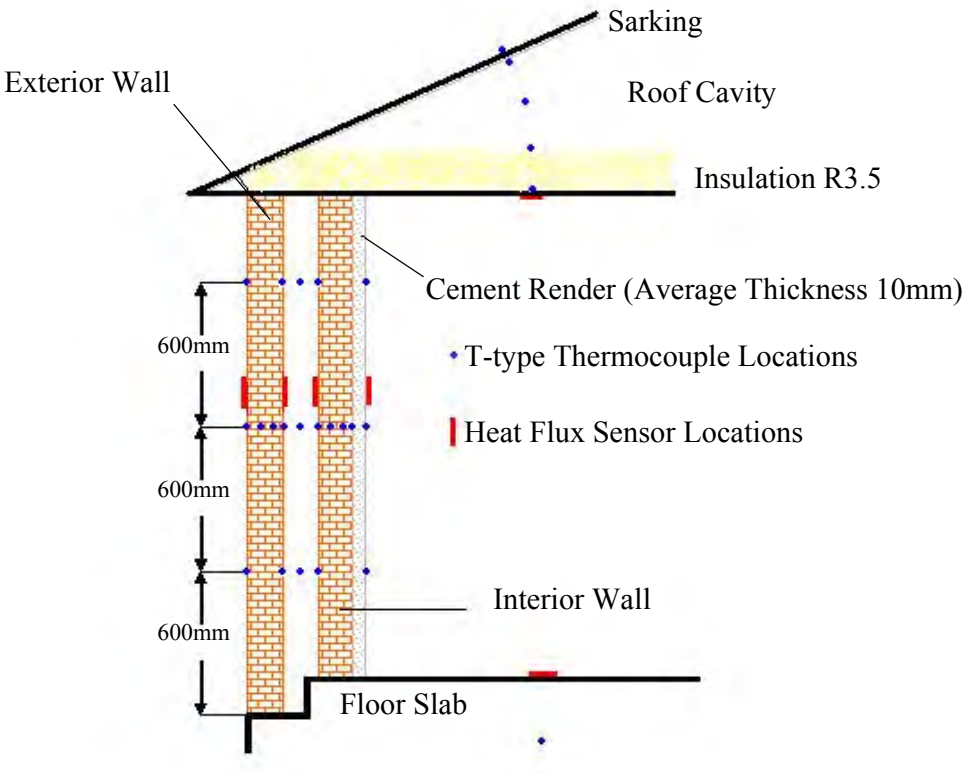

Figure 3.5 Thermocouple and Heat Flux Layout for Cavity Brick Module.

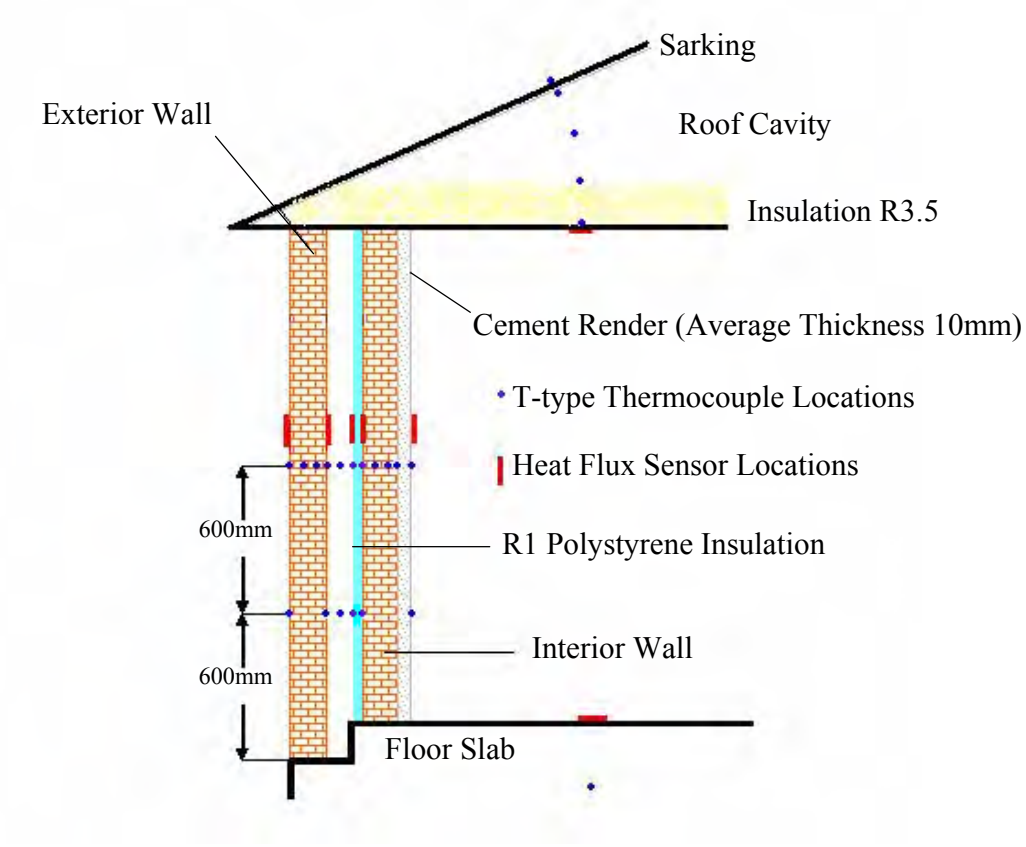

Figure 3.6 Thermocouple and Heat Flux Layout for Insulated Cavity Brick Module.

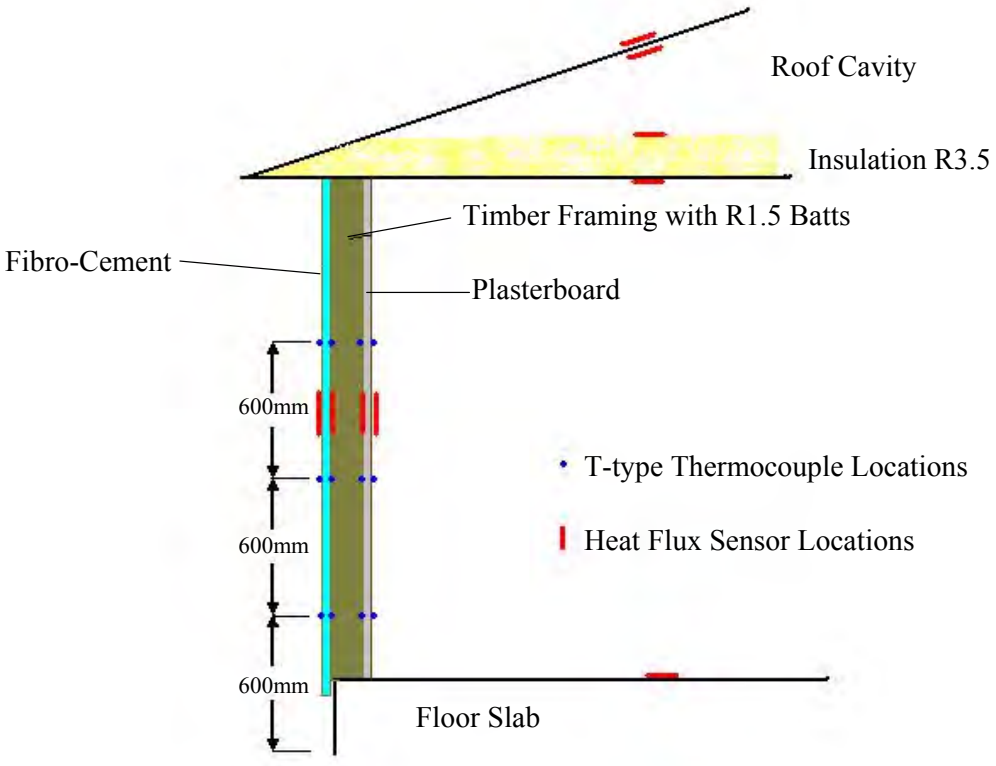

Figure 3.7 Thermocouple and Heat Flux Layout for Insulated Lightweight Module.

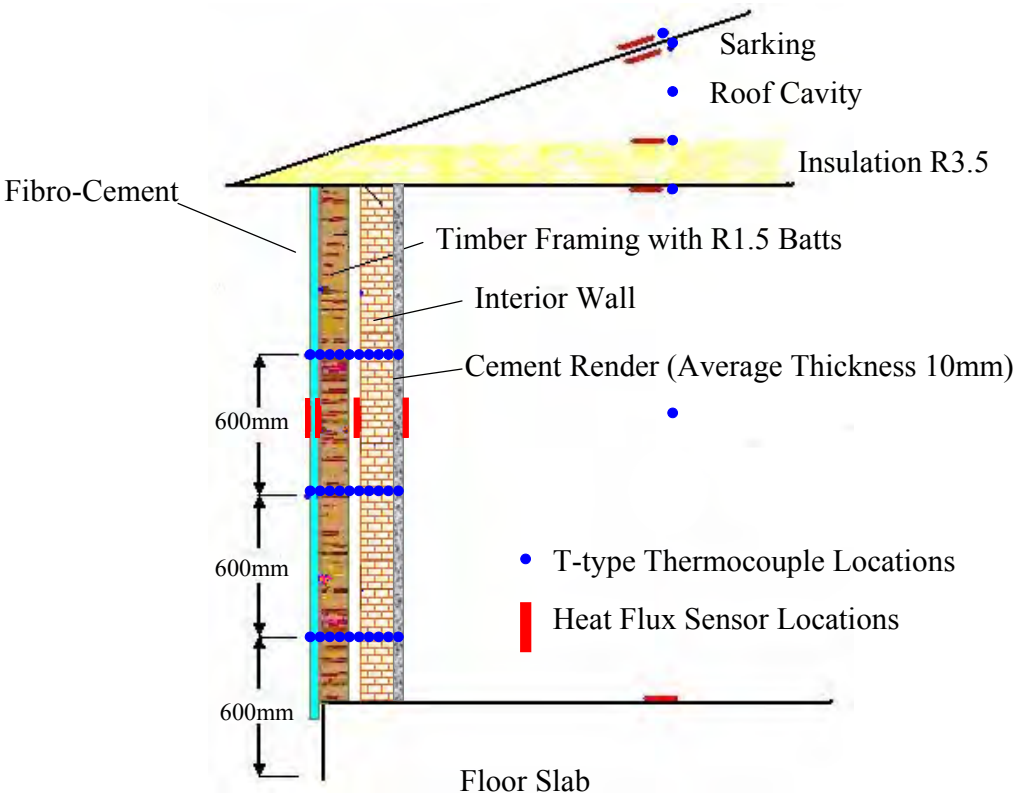

Figure 3.8 Thermocouple and Heat Flux Layout for Insulated Reverse Brick Veneer Module.

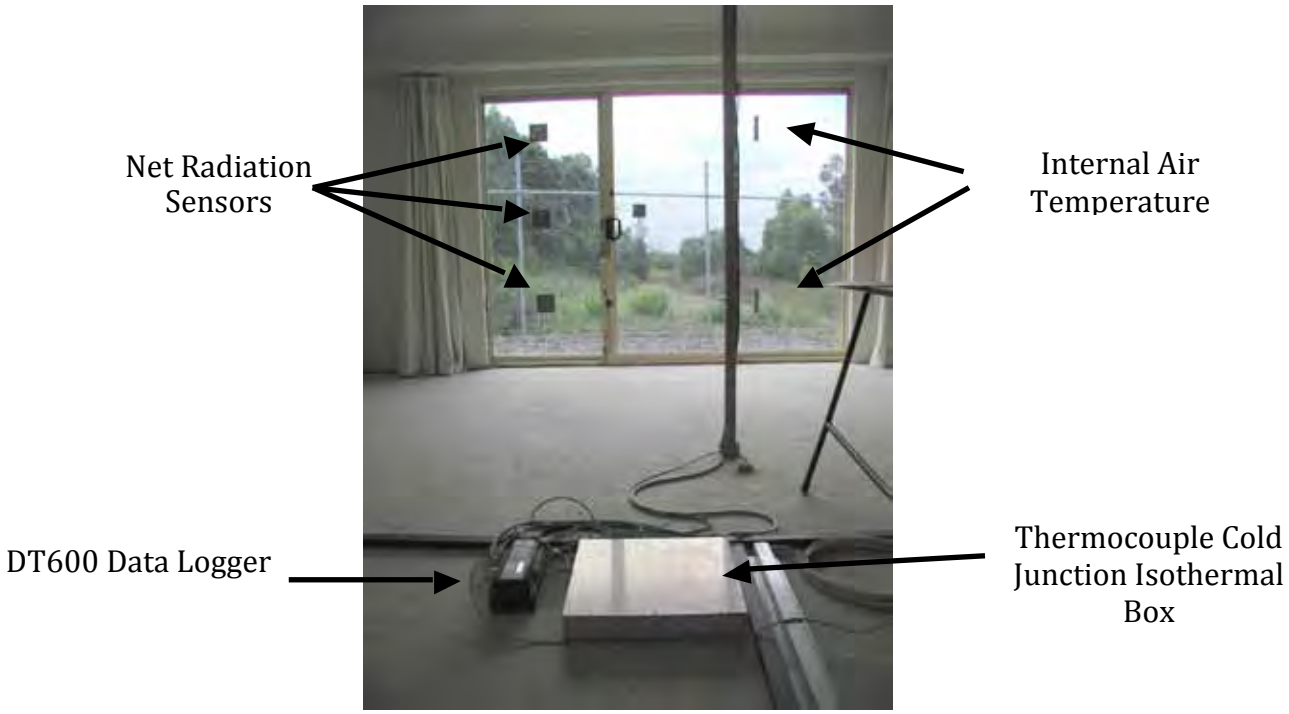

Figure 3.9 Data Logging System, Internal Air and Window Radiation Sensors

Heat flux profiles across each wall were measured using 100x100mm ultra-thin sensors with typical sensitivities in the order of 25µV/W/m^2. The heat flux sensors were placed on the wall in such a manner that the proportion of masonry unit/mortar ratio being measured was representative of that in the masonry wall. An attempt was made to match the absorbance and emissivity of the heat flux sensors to that of the masonry

units by painting and finishing the exterior sensors a similar colour to that of the bricks. The interior sensors were painted white, to match the walls, whilst the sensors located in the cavity were painted black to allow radiative heat transfer. Some of these details are shown in Figures 3.10 and 3.11. Throughout the project it has been customary to describe all heat fluxes as being positive when heat is flowing into the internal space and negative when flowing outwards.

Figure 3.10 External Wall Sensors and Internal Sensors – Brick Veneer

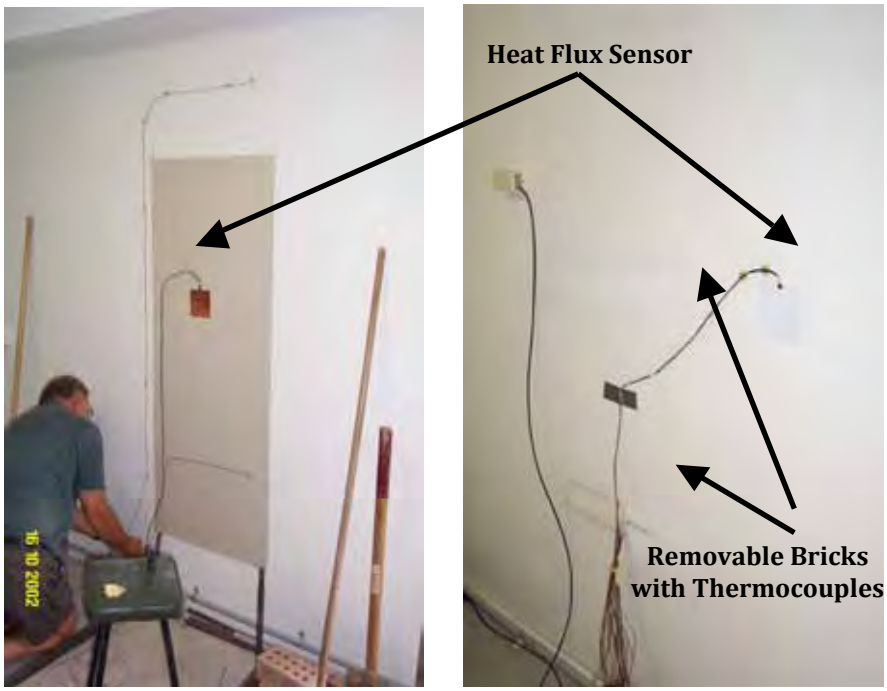

Figure 3.11 Interior of Brick Veneer and Cavity Brick Modules Showing Wall Sensors.

In conjunction with the major opening in the northern wall, heat flux sensors were also located on the concrete slab adjacent to the window (in direct sunlight) and at the rear south-east corner. Thermocouples were placed on the surface of the slab at various locations between the window and the centre of the room. Three net radiation sensors were placed at different heights along the glass panel to assess the incoming/outgoing radiation (refer to Figure 3.9 above). These sensors were suspended 100mm away from the glass surface and had a spectral range between 0.3 and 20μm. The surface temperature of the glass was recorded and additional heat flux sensors were placed on the aluminium frame.

A heating/cooling fan coil unit was installed in each of the building modules where the energy usage in maintaining a set comfort level was measured. For heating, the electrical energy consumed by the heater element was measured together with the power usage of the air circulation fan. Under cooling conditions, chilled water was introduced into the building and the flow rate and temperature rise through the heat exchanger coil measured. The amount of energy (heat) removed was then calculated from these parameters with the fan power being subtracted from the total energy. To accommodate this, a water chiller and storage tank were installed on the southern side of the building complex. The water chiller and fan coil arrangements are shown in Figure 3.12.

Figure 3.12 Water Chiller and Fan Coil Unit

3.4. Test Variables Investigated

As previously described, each module was designed to allow the selective replacement of walling systems without disturbing the roof structure. This has allowed a range of wall types and opening conditions to be considered. Since the modules were constructed progressively, (Modules I and II in 2003, Module III in 2004, and Module IV in late 2005), an increasing number of variables were considered.

A summary of the testing schedule is given in Table 3.2. Testing commenced in February 2003 and was completed in 2009. For the initial tests of Modules I and II which were brick veneer and cavity brick respectively, in each of years 2003 and 2004 the internal conditions were held constant for approximately 12 months to cover all four seasons. As can be seen from Table 3.2, because of the large number of walling systems to be considered, the length of subsequent tests for other walling combinations was reduced, but in all cases the testing period has included both hot and cold conditions.

Table 3.2 Testing schedule

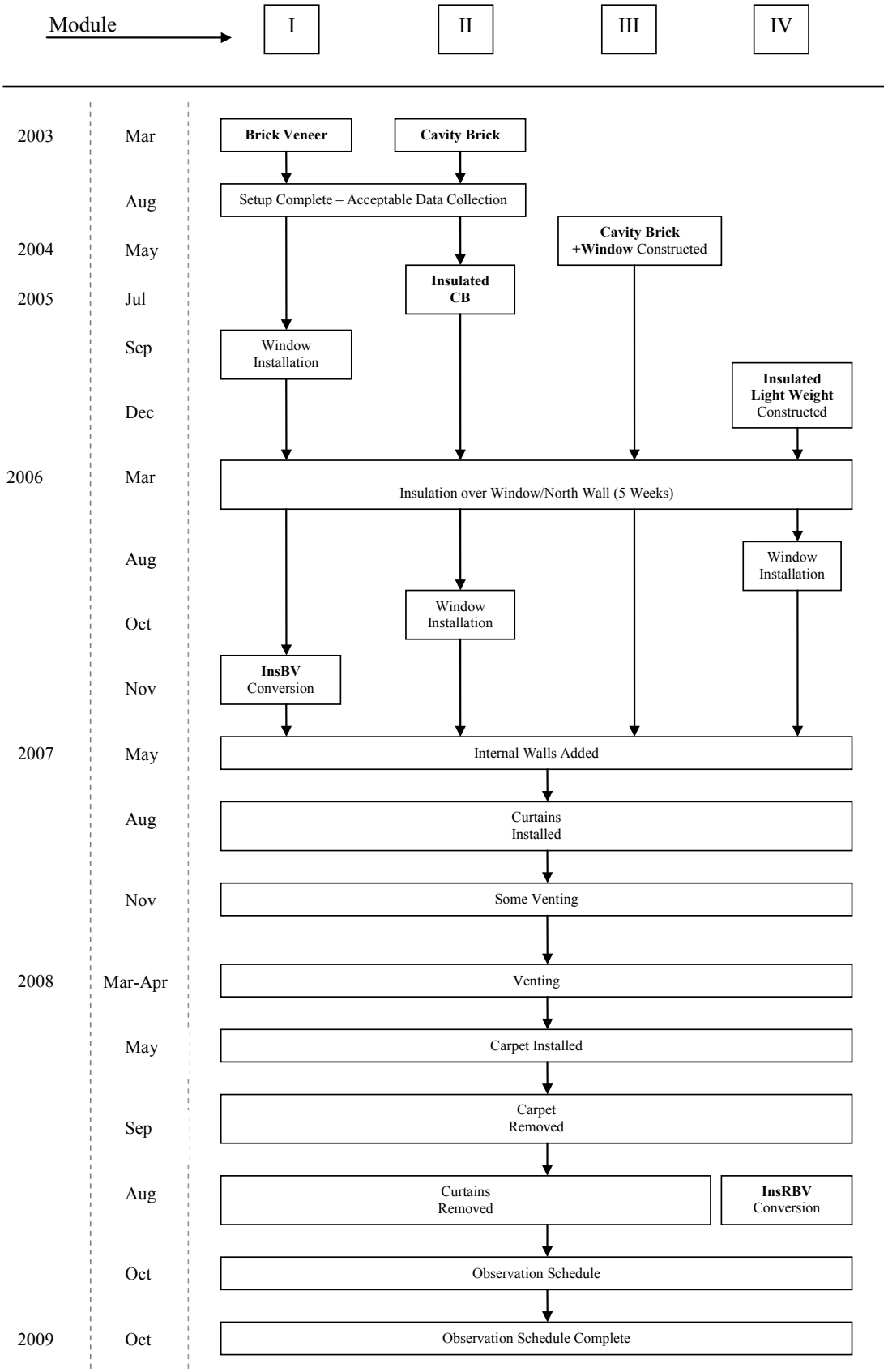

To provide some initial data on wall performance, the testing of the modules in 2003 was performed with solid walls without window openings included. This allowed data to be collected without any additional influences or variables in order to analyse the behaviour of the walling systems alone. As can be seen from Table 3.2, the brick veneer and cavity brick modules were first built, followed by the conversion of cavity brick to insulated cavity brick and the construction of an additional cavity brick module with a window. Windows were added over time to the other modules and a fourth module with a lightweight walling system was built in 2005. Insulation was added to the brick veneer timber frame during November 2006. Due to the progressive expansion of the experimental program and the staggered construction of the modules, it was not until late 2006 that all four modules had the same characteristics (with the exception of wall type) and as a result, subjected to identical weather conditions.

During 2008 the insulated lightweight module was converted to the novel insulated reverse brick veneer construction. The decision to convert this module was based on the results which showed that of all the existing modules, insulated lightweight was the worst performing, with the most undesirable thermal characteristics and the least effective in adhering to solar-passive design principles. The insulated lightweight module had the least desirable characteristics during free floating conditions with the highest temperatures during the day and the largest diurnal swing. Air conditioning results also showed high energy consumption.

The following summarises the major changes and experimental variables which were progressively made and assessed. Not all variables are reported in detail in this Phase I report.

It should be noted that judging the performance of a construction based solely on mean temperatures is inadequate and can be misleading. Therefore throughout this report the range or standard deviation is often used in conjunction with temperature to provide a clear picture.

3.4.1. Major Window Openings

To more realistically reflect the contribution of the various walling systems to solar passive behaviour, as previously mentioned a major opening was installed in the northern wall of each module. This took the form of a 3-panel sliding glass door assembly, 2050 mm high x 2840 mm wide, representing approximately 20% of the floor area (a typical living room / floor area ratio). The sliding door assembly consisted of clear, 6.38mm laminated glass, set in a light coloured aluminium frame.

3.4.2. Internal Walls

Internal walls were added to examine any effect of additional internal thermal mass on the room temperature. Heavy brick partition walls were installed within the cavity brick and insulated cavity brick modules, with light timber stud and plasterboard partitions placed in the insulated brick veneer and light weight modules (simulating the expected type of internal walls that would be built with each construction type in a typical home). Each partition wall was 2m x 1m in plan with a height of 2m and located as in Figure 3.13. The brick walls were 110mm thick; the timber stud wall had a thickness of 95-100mm. A heat flux sensor was placed 1200 mm from floor level as indicated in Figure 3.13 to measure both the heat flow into and out of the wall as well as the surface temperature.

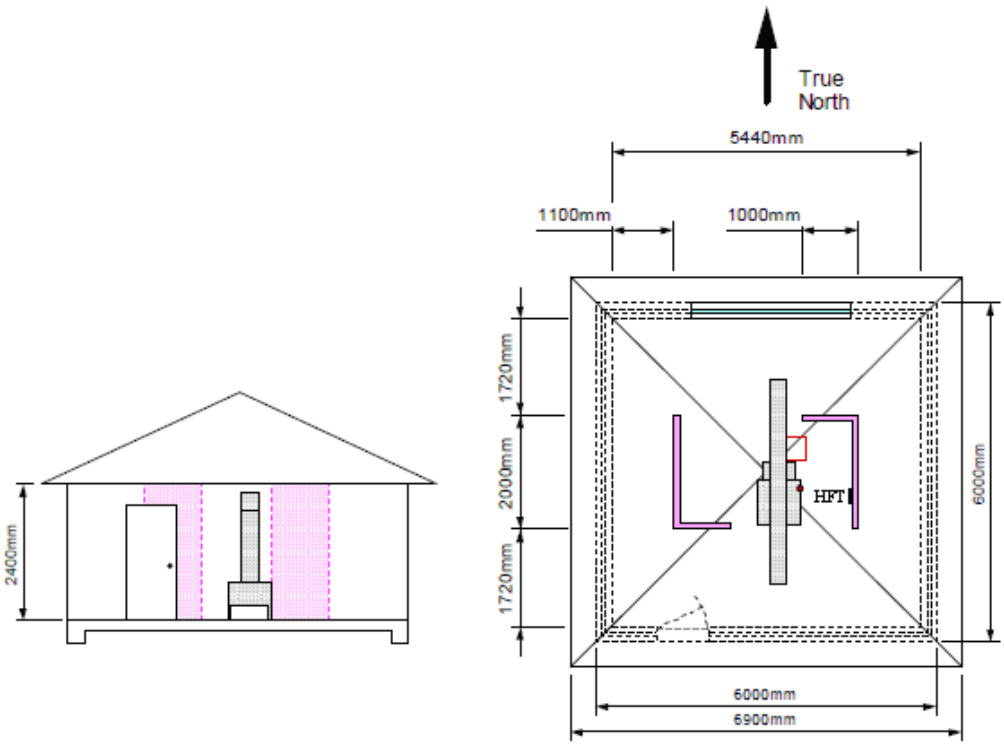

Figure 3.13 Arrangement of Internal Partition walls

3.4.3. Curtains

Curtains were installed on the window openings in late 2007 to investigate their influence on both day and night performance. A range of opened/closed scenarios was performed. The system was automated to operate from the datataker with the curtains typically opening at 6am and closing at 5pm. The curtains were also permanently closed for a period of 3 months. The curtain scenarios were intended to restrict the heat loss through the window at night as would be expected in a real home.

3.4.4. Venting

To effectively utilise thermal mass under solar-passive design principles, venting in the evenings is occasionally beneficial to allow any stored heat in the heavy walls to be removed. Some controlled venting experiments were performed to simulate this scenario. Venting was operated in varying arrangements; day venting, night venting, and permanent venting for a period of time. Venting was also conducted in combination with the use of other variables such as the operation of curtains and air conditioning.

3.4.5. Air Conditioning

As described previously, air conditioning (heating/cooling) was operated at various times throughout the entire project to measure the energy consumption required to maintain the internal temperature within a range of 18°C to 24°C. It is recognised that thermal comfort is influenced by a range of factors such as humidity, radiant energy, air speed and individual preferences etc. (Olesen B.W., Brager G.S, 2004); for simplicity in this comparative study, the internal air space temperature was used as the sole variable.

3.4.6. Carpet

The concrete floor slab in each module made a significant contribution to the total internal thermal mass. As part of the study, to assess the influence of this effect, carpet combined with a standard underlay was placed over the slab within all modules for a period of 4 months.

3.4.7. Annual Observations

The 12 month observation schedule from October 2008 to October 2009 was introduced to provide consistent experimental results under all seasonal conditions for both free floating and air conditioned states of the modules with no alteration of the module variables during that period (see Table 3.2). Table 3.3 shows the time and dates that testing took place for each period. To obtain a representative operational period under either free-floating or controlled internal conditions, a testing schedule was prepared which allowed conditions to stabilise followed by a reasonable observation period for each case (typically 6 weeks overall). Prior to the observation schedule commencing all carpet and underlay was removed, as well as the screen doors on the north facing window assembly as these created added shading within the modules reducing solar ingress. The internal partition walls still remained.

Table 3.3 12 Month Observation Schedule October 2008-October 2009

Start Date	Weeks	End Date	State of Module	
23/10/2008	1	30/10/2008	AC - Settling	
30/10/2008	4	27/11/2008	AC - Data Collection	AC - Spring
27/11/2008	1	4/12/2008	Free Floating - Settling	
4/12/2008	5	8/01/2009	Free Floating - Data Collection	Free Floating - Summer
8/01/2009	2	22/01/2009	AC - Settling	
22/01/2009	5	26/02/2009	AC - Data Collection	AC - Summer
26/02/2009	1	5/03/2009	Free Floating - Settling	
5/03/2009	4	2/04/2009	Free Floating - Data Collection	Free Floating - Autumn
2/04/2009	2	16/04/2009	AC - Settling	
16/04/2009	4	14/05/2009	AC - Data Collection	AC - Autumn
14/05/2009	1	21/05/2009	Free Floating - Settling	
21/05/2009	5	25/06/2009	Free Floating - Data Collection	Free Floating Winter
25/06/2009	2	9/07/2009	AC - Settling	
9/07/2009	5	13/08/2009	AC - Data Collection	AC - Winter
13/08/2009	2	27/08/2009	Free Floating - Settling	
27/08/2009	5	1/10/2009	Free Floating - Data Collection	Free Floating - Spring

3.5. Data Processing

The information collected over the 8 years of observations from the experimental modules formed a massive data set. It was therefore necessary to consolidate the data into a more easily accessible form for analysis. This constructed database consists of a collection of excel files linked to a collection of tables via a "*Master Control File*". This master file with the separate tables forms the effective, consolidated database. Statistical and or graphical analyses can be performed using the *Master Control File* to export data selections to subsequent specialised analysis software. To facilitate analyses across different wall systems, codes were developed that systematically named sensors according to their positions within the walls and building space. The database has enabled full utilisation of the experimental data for further research.

The JMP statistical package (SAS Institute Inc., 2000) was selected to systematically interrogate and interpret the data, given its ability to link the statistics of the data with graphics to explore, understand and

visualise the data. For example, graphical exploration and analyses can be made of the different patterns in heat flows and temperatures that occur through wall systems across different seasons.

Detailed analysis is still in progress and the results will be presented as a part of the Phase II report. A typical study using this approach is presented in Section 4.7.

3.6. Statistical Analysis

Generalised Linear Modelling was used for the statistical modelling/analysis. This method explores the relationships between variables by multiple variable techniques and correlation analysis using the JMP statistical software.

The applied statistical methods predict the average internal module air temperatures using an imprecise set of meaningful predictor variables. For some statistical prediction models, the interest is not always concerning the magnitudes of coefficients and/or variables but in the sole relationships between the variables.

Statistical methods are of particular importance given that various modules for particular wall types were not necessarily operated in the same time periods (due to progressive expansion of the testing program). Using these techniques, comparisons of the behaviour of wall systems that did not exist in the same time period can be made.

3.7. Summary

Chapters 2 and 3 have given an overview of an experimental study of the thermal performance of various walling systems both in isolation and incorporated into full scale housing modules. As indicated, the detailed analysis and interpretation of this data is still in progress, but sufficient analysis has been completed with some results and conclusions presented in Chapters 4 and 5.

4. THERMAL TEST MODULES - WITHOUT A WINDOW

4.1. Introduction

The initial module testing was aimed at studying the thermal behaviour of the wall systems alone without the added influence of solar gain through major openings such as windows. In 2003, the first modules were constructed with no major openings and their behaviour studied under the range of natural weather conditions. As shown in Table 3.2, the windowless brick veneer and cavity brick modules were constructed and tested for a 12 month period. The cavity brick module was then converted to insulated cavity brick in mid-2005 and an additional lightweight module also constructed in late 2005.

This chapter presents the results of this initial phase of the investigation which only involved windowless modules and concentrated on a study of the performance of each individual wall type rather than the building system as a whole. Subsequently, major openings and a range of other effects related to solar-passive design were also implemented. These tests are described in Chapter 5.

4.2. Comparison of Brick Veneer and Cavity Brick Modules

4.2.1. Overview

The first two modules constructed were brick veneer and cavity brick, each without any form of walling insulation. Neither module had the later installed north facing window. Therefore a comparison of the thermal behaviour of the walling systems can be made without the influence of additional variables.

For the cavity brick module the walls were constructed from extruded clay bricks with light brown to pink colourations. The inside wall surfaces were rendered using a cement/sand render with a nominal thickness of 10mm and painted white after drying. The R-Value of the cavity brick wall was measured in the guarded hot box and determined to be 0.43 m^2K/W. Full details of the module construction have been given in Chapter 3.

The walls for the brick veneer module were built from the same masonry units as for the cavity brick. The inside leaf was timber stud finished with plasterboard and painted white. The R-Value of the brick veneer wall was measured to be 0.83 m^2K/W, nearly double that of the cavity brick (0.43 m^2K/W). The following is a direct comparison of the behaviour of two windowless modules under identical weather conditions.

4.2.2. Hot Weather Conditions

4.2.2.1. Temperature Variations and Thermal Lag

The modules were exposed to very hot weather conditions from late January to early February 2003 which consisted of days above 40°C to those with less extreme conditions where temperatures were in the low thirties. Night time minimum external temperatures ranged between 19°C and 24°C (Sugo et al., 2004).

Comparisons of indoor and outdoor temperatures for one of three consecutive weeks are shown in Figure 4.1. The internal temperature of the modules fluctuates in response to the continually changing external

conditions primarily due to the movement of heat via the four external walls, in an attempt to reach thermal equilibrium. Both buildings demonstrate the ability of masonry walls to attenuate the day-night temperature variations, with the peak temperatures and their time of occurrence being later than the external peak temperatures. The attenuation is a result of the varying degrees of thermal mass present in the walling systems.

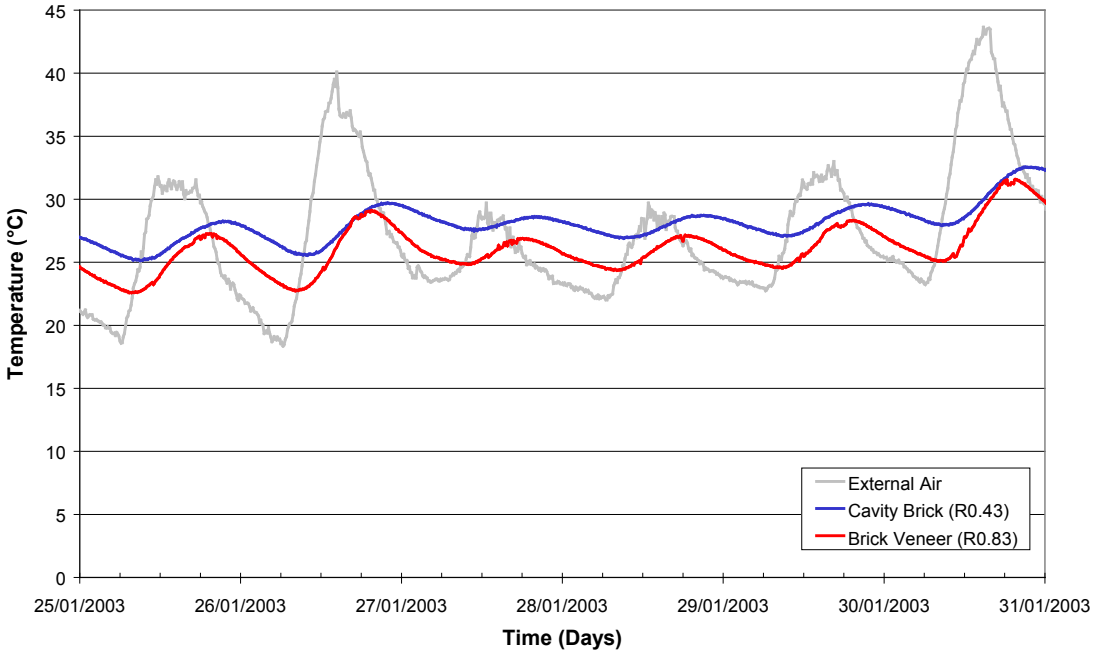

Figure 4.1 Internal and external temperature for Cavity Brick and Brick Veneer Modules (January 2003)

Generally, the internal air variations were in the order of 2.5-3.5ºC for the Cavity Brick module and 3-5ºC for the Brick Veneer with corresponding external air variations of up to 20ºC at the extreme. The smaller temperature swing of the cavity brick module was a consistent trend despite the walling system having a smaller R-value than the brick veneer construction. This can be attributed to the higher thermal mass which produces an increased thermal lag which delays heat transfer. A longer period of time was needed for the heat to be transmitted through the cavity brick walls and therefore decreased its rate of response to the external conditions. Generally the peak internal temperature of the cavity brick module lagged approximately 2 hours behind the peak internal temperature of the brick veneer module.

A change in weather occurred towards mid February significantly reducing the maximum external and internal air temperatures. In this case, since the outside air temperature was at most 5ºC cooler than the modules, there was a potential to cool the buildings down between 7pm and 7am. Cooler weather conditions also produced a steady decline in the internal temperatures of the buildings but with the internal temperatures in both modules remaining warmer than the external air conditions for several days.

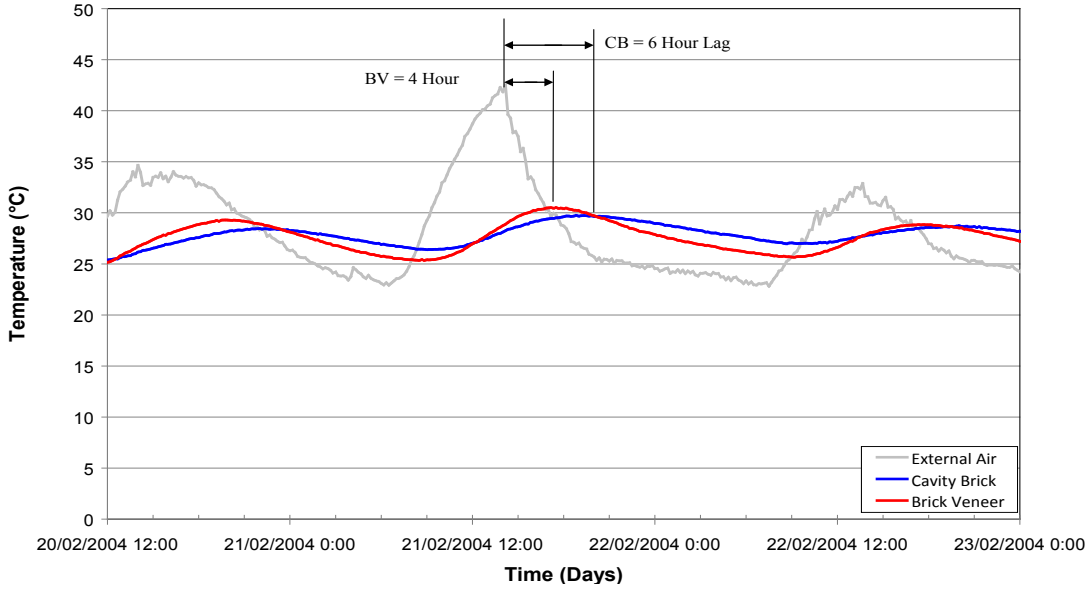

Figure 4.2 External and Internal Air Temperature Variations for the CB and BV Test Modules (February, 2004)

A further illustration of the significance of thermal mass and the accompanying thermal lag is shown in Figure 4.2. Newcastle experienced heat wave conditions during early 2004 with a maximum external air temperature on one day of 43ºC. At the time of this external temperature peak, the internal air readings were 28.5ºC and 28.7ºC for the cavity brick and brick veneer modules respectively. However these readings did not correspond to the peak internal air temperatures of the modules which occurred sometime later that day due to the delayed heat flow through both building envelopes. The maximum internal air temperature for the cavity brick occurred at 8:00pm and was 29.7ºC. For the brick veneer module, the maximum internal temperature of 30.5°C occurred at 5.30 pm, which was two and a half hours earlier than the cavity brick, reflecting the different levels of thermal mass.

These results highlight the general behaviour observed within the modules. The internal temperature was always '*chasing*' the external driving conditions and lagged it in its attempt to reach an equilibrium state due to both the response time of the walling system and the continually changing weather conditions. Both buildings demonstrated the ability of masonry walls to attenuate the day-night temperature variations. The effects were more pronounced in the cavity brick module due to the increased presence of thermal mass. These also meant that an amount of residual heat was retained internally, but this was predominately a result of the modules being a closed system.

4.2.2.2. Through-Wall Heat Flux

The behaviour of the modules was driven by the weather conditions, primarily the solar radiation and external air temperature. Changes in the solar radiation throughout the day had a direct influence on the thermal behaviour of the walling systems. Under summer conditions a high solar altitude created high external surface temperatures on the eastern and western walls. The southern wall only received diffused solar radiation while the solar incidence on the north facing wall was limited. The western wall under these conditions in February 2004 typically recorded the hottest external surface temperature, ranging between 40-52°C in the afternoon. The eastern wall surface temperature occasionally peaked at approximately 50°C but generally ranged from the mid 30s to just over 40°C. The roof tiles reached surface temperatures of approximately 70°C. Once the direct solar radiation had passed the external surface of the walls began to

cool.

Figure 4.3 shows the solar radiation received by the various walls on the 20th February, 2004. All solar radiation sensors were placed at mid height on the external surfaces parallel to the wall. The roof radiation sensor was on the horizontal plane.

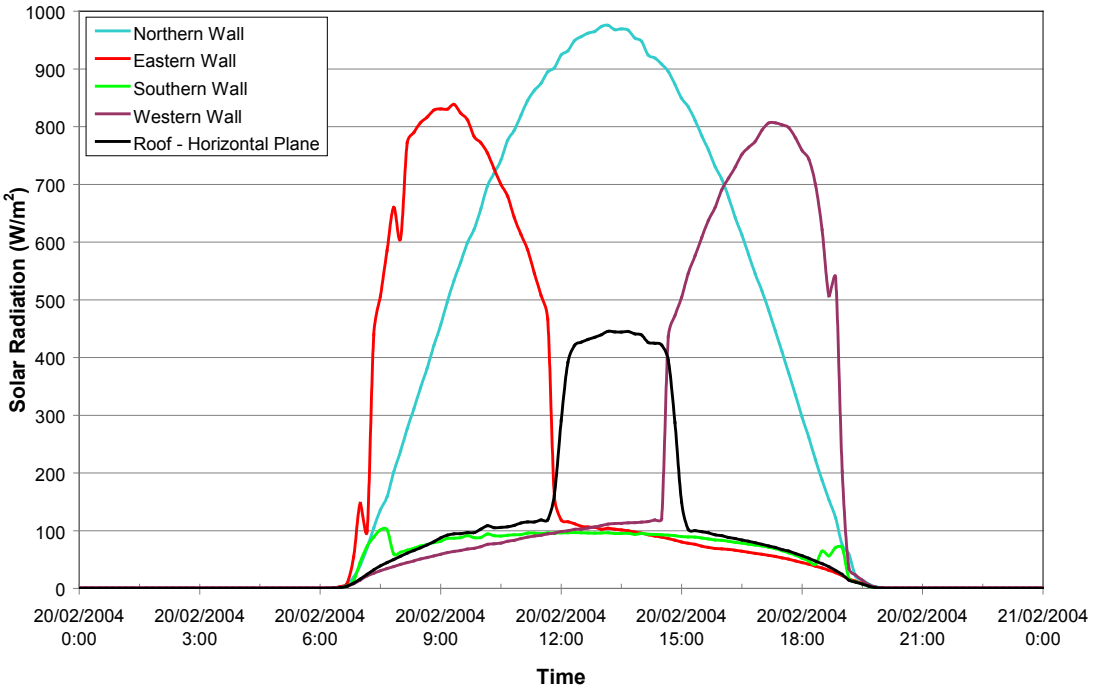

Figure 4.3 Incident Solar Radiation on Modules External Surfaces on the 20th February 2004

Not all solar radiation that was incident on the external walls was transmitted through into the building. The maximum heat flux entering the external brickwork on the western wall as shown in Figure 4.4 was approximately 200W/m^2; this is despite the peak incident solar radiation on the same surface being of a magnitude within 700-900 W/m^2. A large quantity of the heat was reflected and/or radiated back to the external environment by the brickwork. It was also observed that significant amounts of the heat stored in the wall was released back to the exterior environment at night. This behaviour was typical of all the external surfaces except the southern wall as it was only exposed to diffused radiation during the day. The absorption characteristics were nearly identical for both the cavity brick and brick veneer modules as the exterior skin was constructed from the same brick masonry. However variation was observed between the two modules for the southern wall due to the dominance of diffused solar radiation allowing increased influence from the internal wall surface and room space, particularly for the brick veneer.

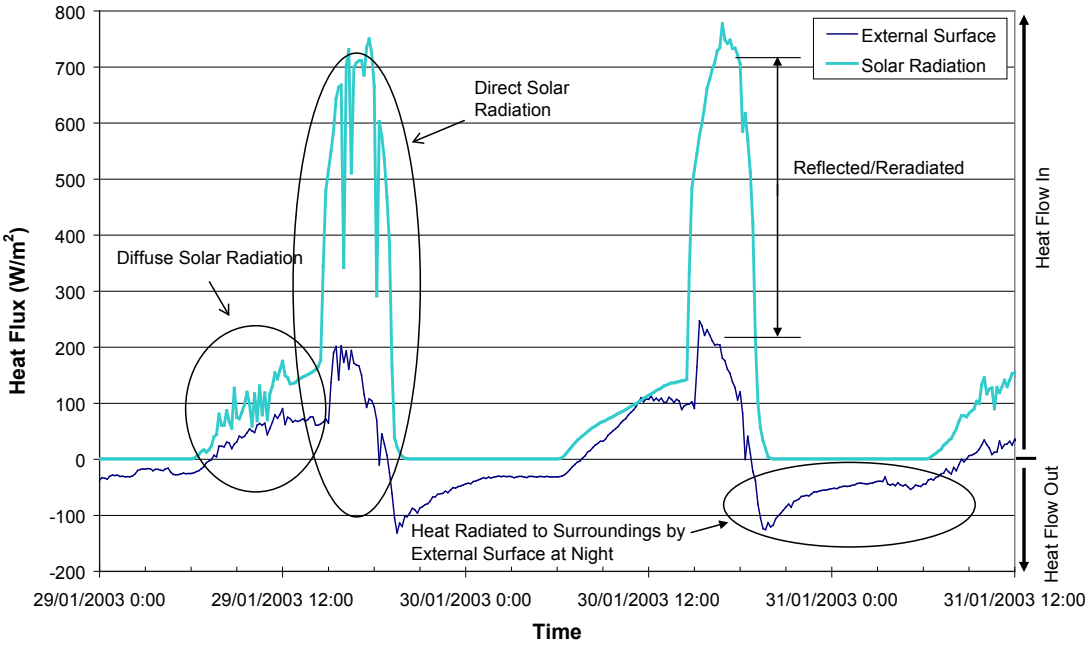

Figure 4.4 Western Wall Incident Solar Radiation and External Surface Heat Flux

The entire behaviour of each module can be explained by analysis of the heat flux profiles through the walling envelope as they provide information on the attenuation and direction of heat flow in and out of the modules for all conditions (Note that heat flux sensors were located on both the internal and external surfaces of all perimeter walls as well as in cavity air/brick interfaces). The complete heat flux profile of the western wall of the cavity brick module for the 20th and 21st of February 2004 is shown in Figure 4.5 as an example. This corresponds to the extreme temperature of over 40°C as illustrated previously (Figure 4.2).

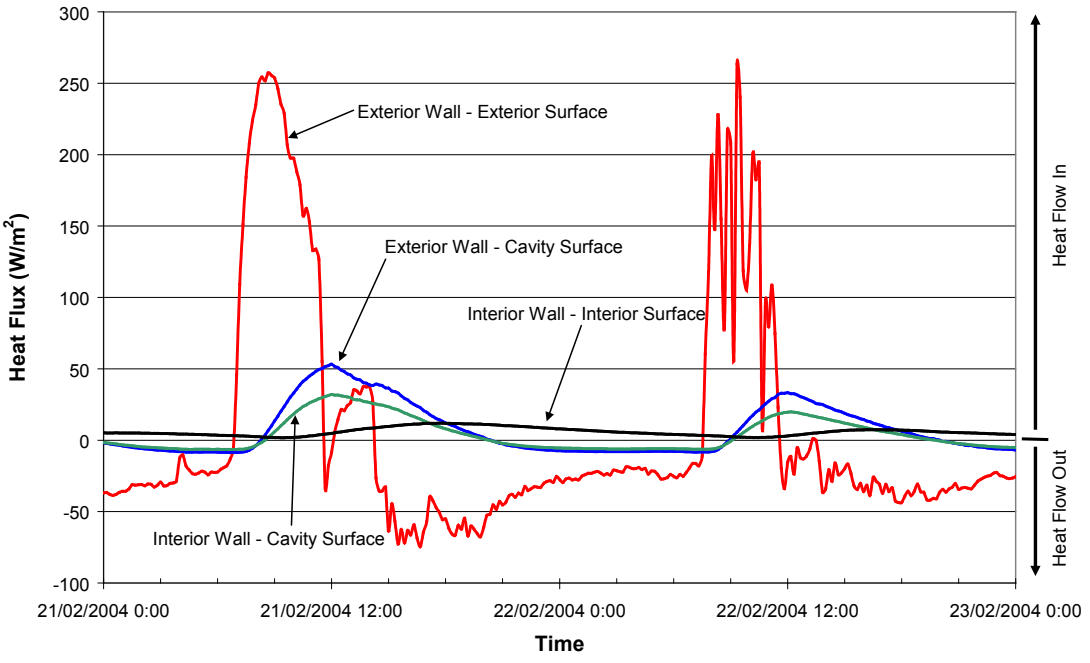

Figure 4.5 West Wall Heat Flux Profile for the CB Test Module, February 2004

It can be seen from Figure 4.5 that there is a dramatic difference in heat flux levels between the exterior and interior surfaces due to heat absorption by the wall material and the effects of the cavity. The decrease in heat flux occurs progressively through the wall with approximately 50 W/m^2 passing across the cavity surfaces. The interior masonry skin continues to attenuate the flux down to 5-6 W/m^2. A flow reversal also occurred through both masonry skins and reduces the net flux entering the building. This reversal was driven by the day-night temperature swing with cooler night time temperatures increasing the radiation and convective heat transfer rate from the masonry wall to the outside environment.

Further examination of the summer heat flux readings on the interior room surfaces indicated that heat predominately entered by the eastern and western walls, with most heat loss occurring through the southern wall. The behaviour of the heat flow for both the brick veneer and cavity brick modules is shown in Figure 4.6. The peak flux entering through the western walls is in the order of 12-13W/m^2 for both buildings. The lag for both the entering and exiting heat is also evident between the two constructions. Peak solar radiation on the western wall was at 5:30pm however, the peak internal heat flux occurred around 8pm for the brick veneer and 10pm for the Cavity Brick module, which was consistent with the peak module temperature.

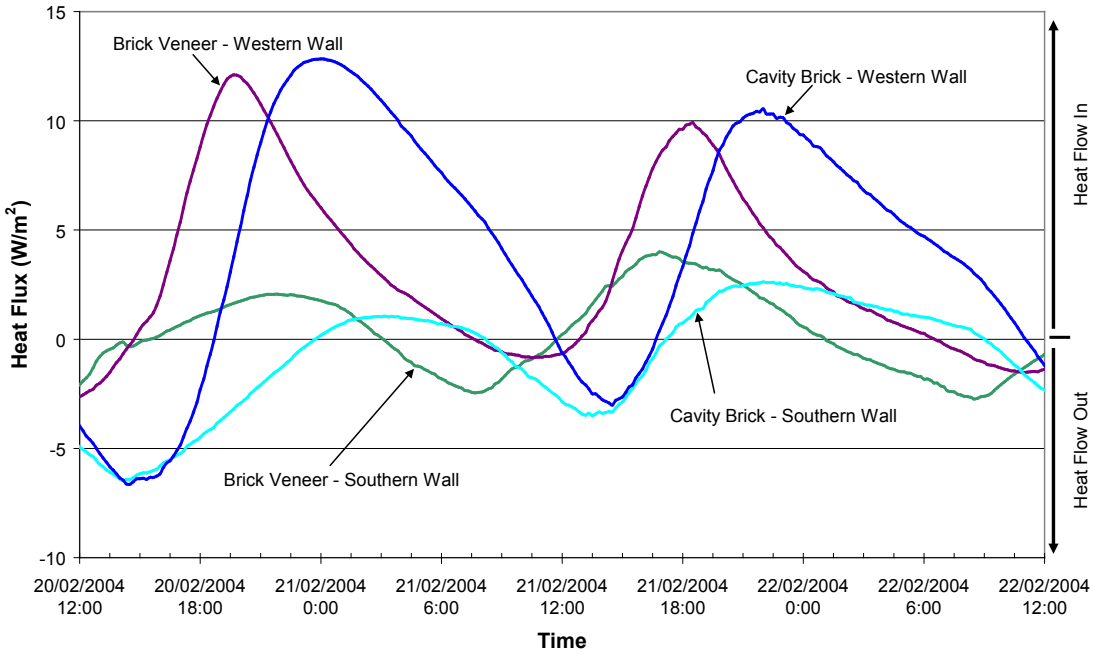

Figure 4.6 Heat Flux Measurements on the Interior Western and Southern walls of the Cavity and Brick Veneer Modules, February 2004

The energy movements for each building module depended upon the nature of the module, the seasons and the weather conditions. It is useful to study the magnitude and direction of energy flows for each component surface of a module, as it gives a good indication of the heat transfer mechanisms which are taking place. The total energy envelopes for the heat entering and leaving through the internal module surfaces for all wall orientations of the CB and BV modules in February 2004 are shown in Figure 4.7. The values correspond to the total energy exchange calculated from the heat flux measurements over three weeks of data from late January to mid February. Heat transfer predominantly occurred through the perimeter walls and varied with both the wall orientation and the driving conditions. Both the southern and northern walls of the CB and BV modules behaved in a similar fashion. Differences arose in the eastern and western wall where greater gain occurred in the cavity brick module.

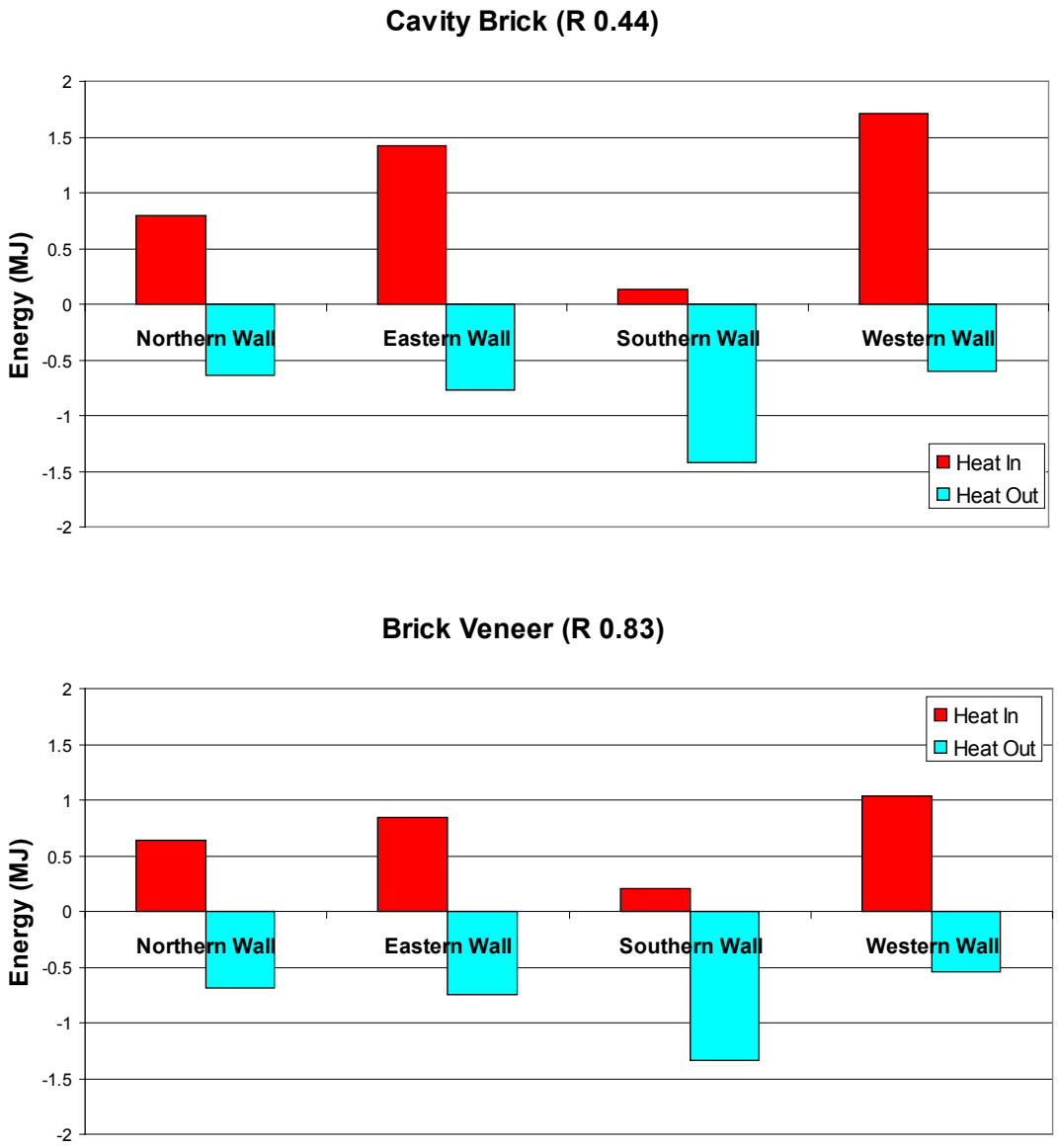

Figure 4.7 Total Energy Envelopes of the Internal Surfaces for Three Weeks, February 2004

4.2.3. Cold Weather Conditions

4.2.3.1. Temperature Variations and Thermal Lag

The external air temperature in May and June 2004 typically ranged between 10 to 22°C and gradually reduced as the season moved into winter. The Brick Veneer module (*BV*) exhibited a greater increase in temperature during the day and peaked earlier to a higher temperature than the Cavity Brick module (*CB*). The BV module had a much greater temperature swing than the CB module. The peak daily temperatures of the BV module occurred at approximately 6pm, with the peaks of the CB module occurring about 2 hours later as shown in Figure 4.8. The minimum temperatures for both modules were similar, but the BV module reached its lowest temperature earlier. The more rapid temperature drop coincided with the greater rate of heat loss from the BV module. Similarly, in the mornings, the internal temperature of the BV module increased at a greater rate than for the CB module. The dampening effect of the thermal mass of the CB module is also evident from Figure 4.8 with reduced internal temperature swings and evidence of thermal

lag. In contrast to the results for February 2004, under these cool conditions, the heat was predominately flowing out of the modules since the external air temperature was lower than the internal.

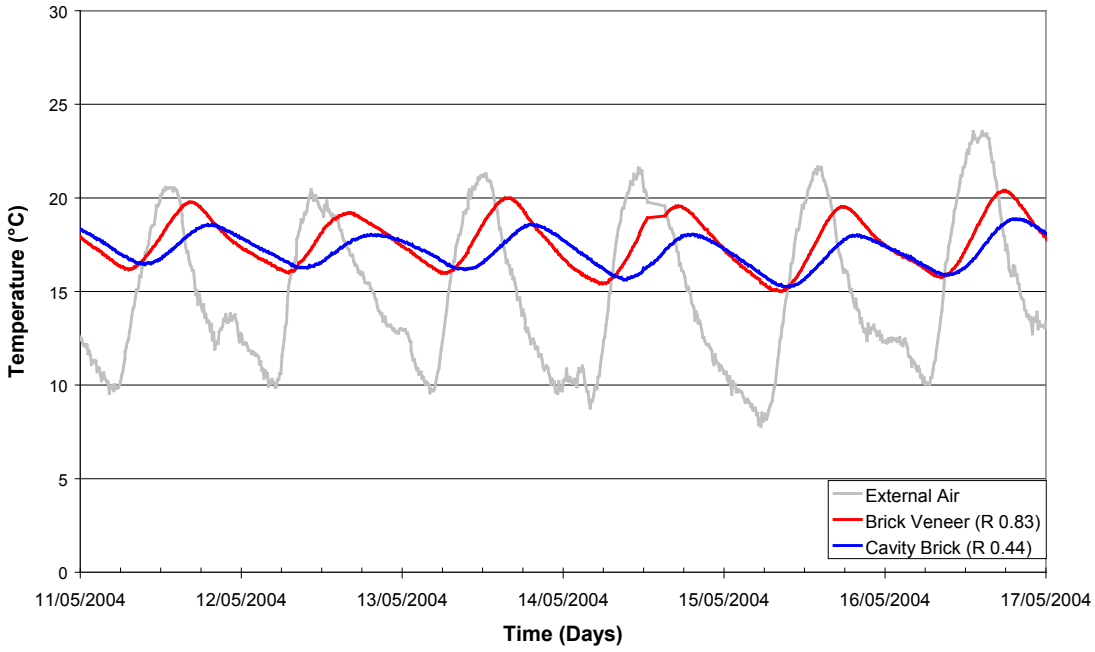

Figure 4.8 Internal and external temperature for Cavity Brick and Brick Veneer Modules, (May, 2004)

Further insight into the behaviour of modules under cold weather conditions can be obtained from Figure 4.9 which shows external and internal temperature variations for a 4 day period in June, 2004. It can be seen that the daily air temperature in the CB module oscillated between 13-16ºC giving a swing of about 2-3ºC. The mean internal air temperature for this module was 15.6ºC. The BV module had a similar behaviour but was more responsive to the driving conditions, with temperatures climbing slightly higher, up to 17-18ºC and then dropping to just above those of the CB module, resulting in a swing of about 3-4ºC. The mean temperature for the BV module was 16.2ºC though it exhibited a higher rate of heat loss in the evening with the temperature consistently decreasing below the CB module at approximately 10 p.m. The minimum temperatures also occurred earlier for the BV module than the CB module by 1-2 hours.

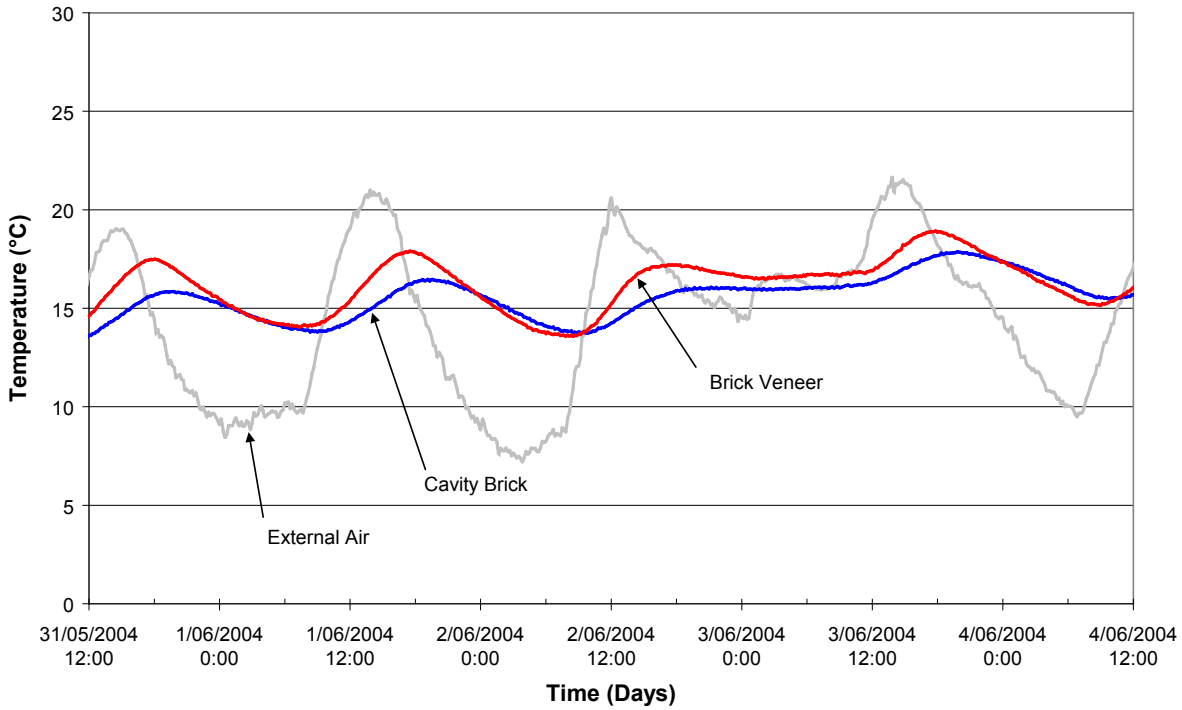

Figure 4.9 Internal and external temperature for Cavity Brick and Brick Veneer Modules for 1st week of June 2004

It should also noted that for this period, the night sky radiation effect on the roof tiles was more pronounced with a significant drop in temperature of up to 10ºC below external air temperature being observed, with the surface temperature dropping to a minimum of -2ºC. This phenomenon influenced the roof tile temperature from about 4pm until just after sunrise, with the minimum temperature being developed in the early hours of the morning. After sunrise, the roof tile temperature rose at a similar rate to the surface of the brick walls and reached a maximum temperature of about 40ºC. The very large temperature oscillations (in the order of 40ºC) and the very low temperatures experienced by the roofing material, highlights the need for adequate ceiling/roof insulation to minimise these effects.

4.2.3.2. Through-Wall Heat Flux

The incident solar radiation on the exterior surfaces of the modules for the 16th of May 2004 is shown in Figure 4.10. The maximum solar radiation received by the horizontal plane on the roof was in the order of 630W/m^2, which is less than the approximately 1000W/m^2 for the hot weather conditions in February 2004 (Figure 4.3). The magnitudes on the eastern and western walls were also reduced. However, the most significant difference was the increased solar radiation on the north facing surface due to the lower solar altitude which was double the magnitude recorded in February. The diffused solar radiation on the southern wall remained at a similar magnitude in May as it was in summer.

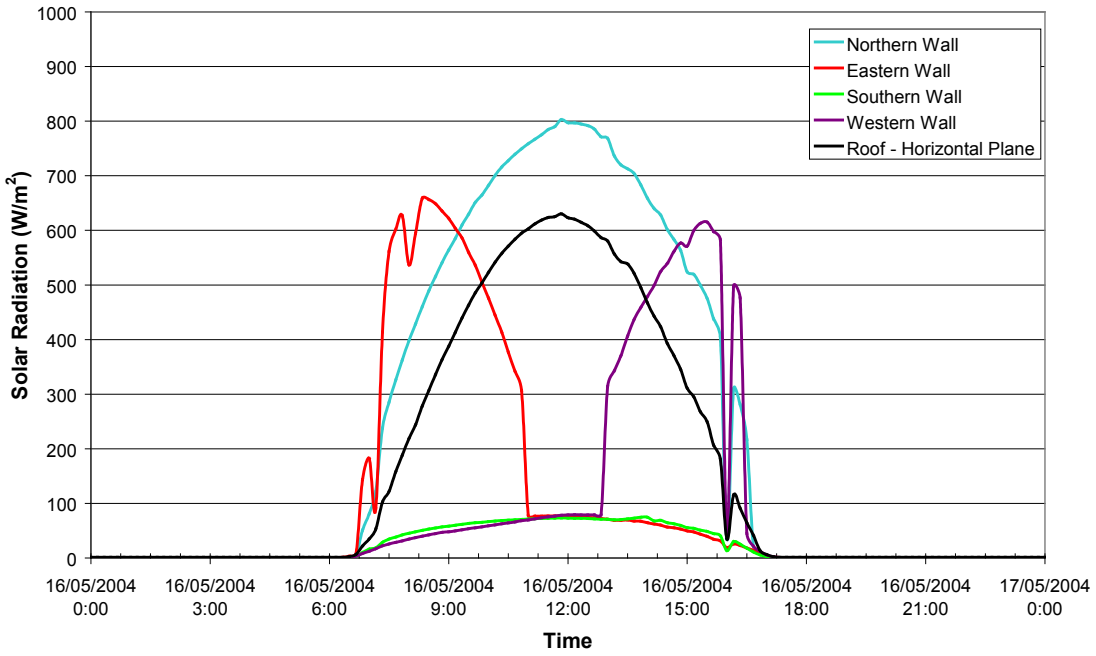

Figure 4.10 Incident Solar Radiation on Modules External Surfaces for 16th May 2004

The large solar influence throughout the entire day on the northern facing wall caused it to act as the primary heat source for the modules. This also created a prolonged period of heat release by the northern wall into the internal space of the CB module. Generally the northern wall consistently provided the most heat to the room while all the other walls were predominately removing this heat.

The total energy envelopes for the heat entering and leaving through the internal surface of the modules are shown in Figure 4.11 for the entire month of May 2004. The total energy exchange was actually larger for the cooler conditions than in the hot February period, with the walling systems being much more “active” during May.

The temperatures of the BV module occurred earlier and were higher than the CB module despite less total energy typically flowing in. The heat into the CB module did not flow into the room until later into the day as a result of the thermal lag, evidenced by both the heat flux readings and the observed time of the maximum module temperature. This delayed flow was responsible for the reduced temperature drop at night. The BV module had greater heat loss through the northern wall and did not transmit as much heat into the room. While the peak heat flows of both modules were similar, the CB module peak flow occurred later and was maintained at a higher rate for longer.

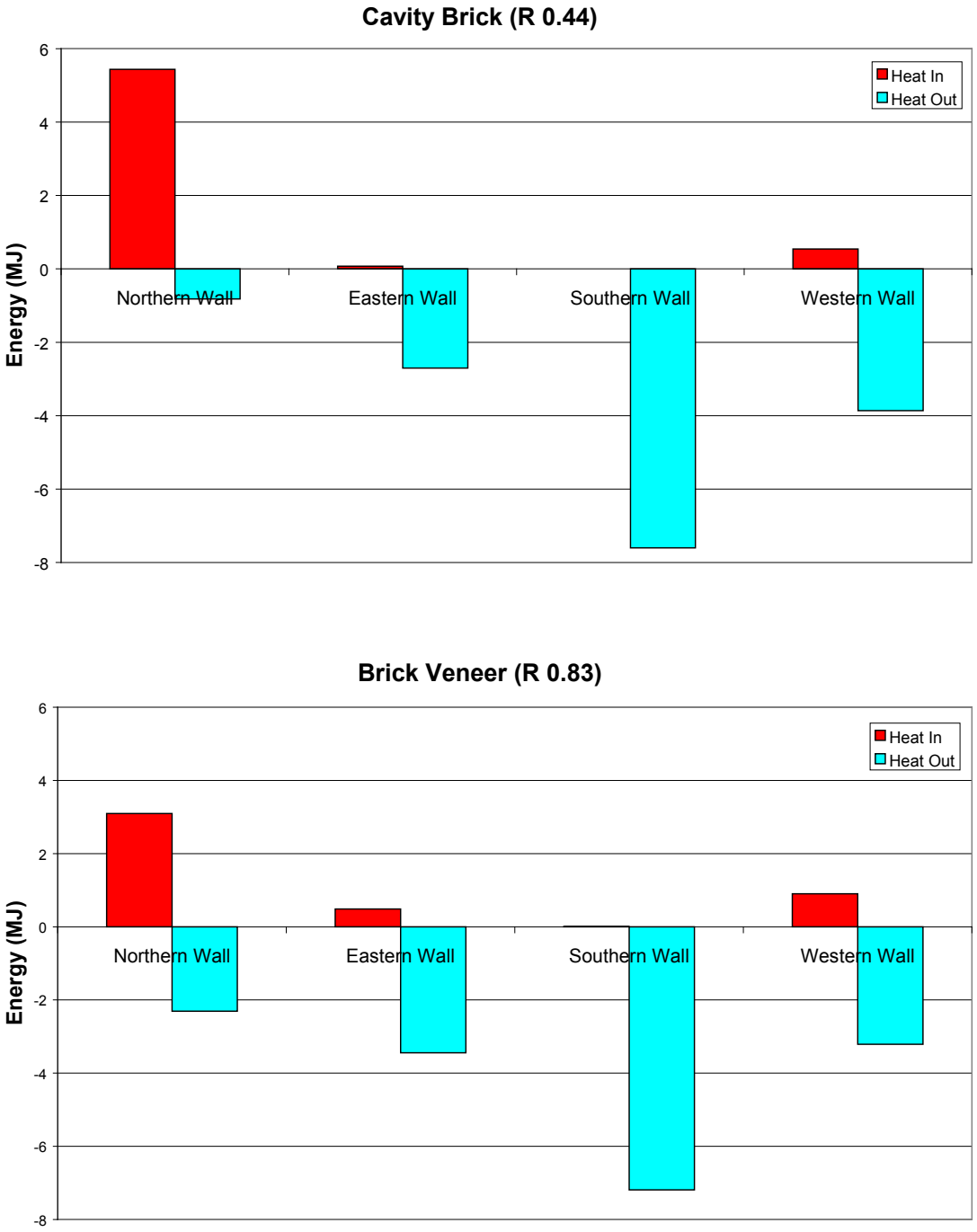

Figure 4.11 Total Energy Envelope of Internal Surfaces (May 2004)

The southern wall for both modules removed heat from the room throughout the entire day and was the main driver in regards to reducing the internal temperatures of both modules as observed in the calculated total energy envelopes. The southern wall did not receive any direct sunlight on the external surface and was therefore only driven by the external temperature and diffused radiation as well as responding to the internal temperature of the module. For the CB module heat absorption was strongest during the day due to the higher internal temperature driving heat into the cooler southern wall (which remained cooler for longer due to the thermal lag). This loss reduced into the evening as the internal temperature reduced and the southern wall temperature increased to a peak at approximately 8 p.m. However, the opposite occurred for the BV module as the lower thermal mass does not produce as much thermal lag. Heat loss was actually

minimised during the day and increased through the night until morning. This also added to the increased diurnal swing of the module and the rapid temperature drop into the night.

Slightly more heat entered through the BV eastern wall than for the CB module due to the shorter thermal lag. Heat flowed into the room while the sun was still incident for BV. In the case of the CB module it is likely that the sun would have passed over before the time lag of the wall had been overcome, this would then result in a heat flow reversal were heat is flowing in both through and back out of the wall.

4.3. Comparison of Insulated Light Weight and Insulated Cavity Brick Modules

4.3.1. Overview

The original module tests described in Chapter 4.2 involved the direct comparison of the conventional cavity brick and brick veneer walling systems. These comparisons were comprehensive and involved four seasons. As the testing program expanded, more modules were added and a large range of variables investigated. This made it more difficult for the direct comparison of all walling systems under the same conditions as progressive changes were made.

The original cavity brick module was converted to insulated cavity brick in July 2005 (see Table 3.2). To install the insulation, the exterior brickwork skin was removed and an R1.0 polystyrene sheet was attached to the cavity face of the interior brickwork skin. The exterior skin was then rebuilt with the cavity width maintained at 50mm (excluding insulation). The R-value of the insulated cavity brick wall was determined using the guarded hot box and found to be 1.30 m^2K/W.

The insulated lightweight module was completed in December 2005 (Module IV, Table 3.2). The module construction has been described in detail in Chapter 3, with the walls consisting of an external 2-3mm cream acrylic render on 2mm cfc (fibro-cement) sheets mounted on a timber stud frame with R1.5 glasswool batts between the studs. The interior was lined with 10mm plasterboard painted white. The R-value determined in the guarded hot box test was 1.51 m^2K/W.

As can be seen from Table 3.2, there was a limited period in late 2005 and early to mid 2006 when the performance of the Insulated Cavity Brick (InsCB) module and the Insulated Lightweight module (InsLW) could be directly compared. The comparisons for typical hot and cool weather conditions follow.

4.3.2. Hot Weather Conditions

4.3.2.1. Temperature Variations and Thermal Lag

The data for the insulated lightweight module presented for this time period was limited to room air, roof air and the full western wall temperature and heat flux profiles as other instrumentation had yet to be installed. The free-floating performance of the InsLW and InsCB modules over a 4 week period, across December 2005 to January 2006, is compared. This also included the heat wave in January 2006 where on New Years Day the external temperature peaked at approximately 45°C as shown in Figures 4.12 and 4.13.

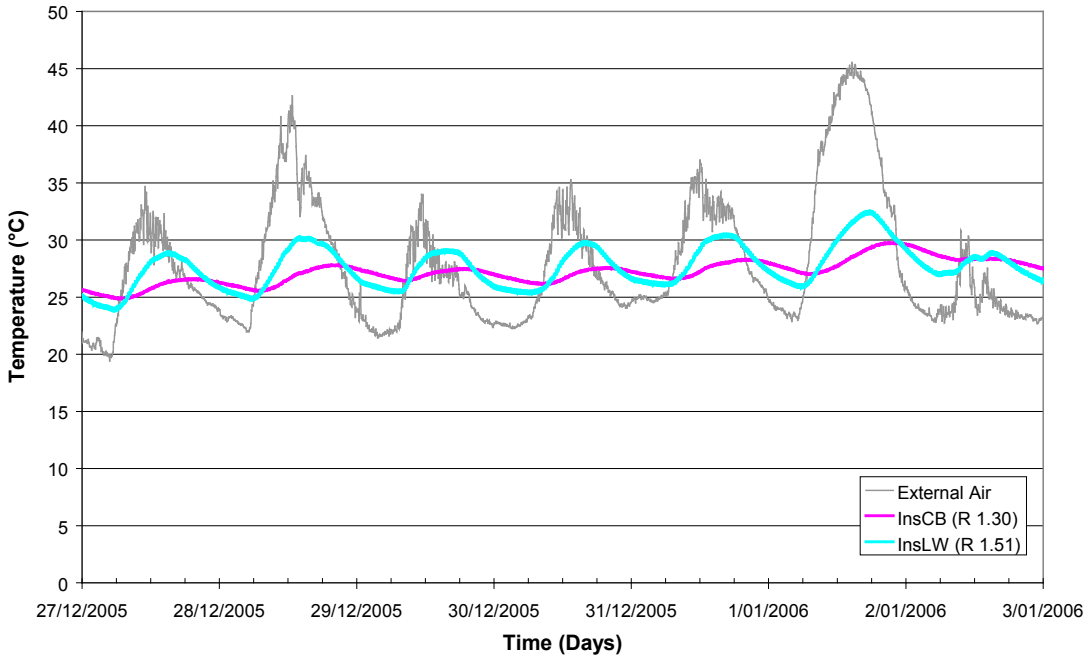

Figure 4.12 Internal and external temperature for Insulated Light Weight and Insulated Cavity Brick modules – New Years Period January 2006

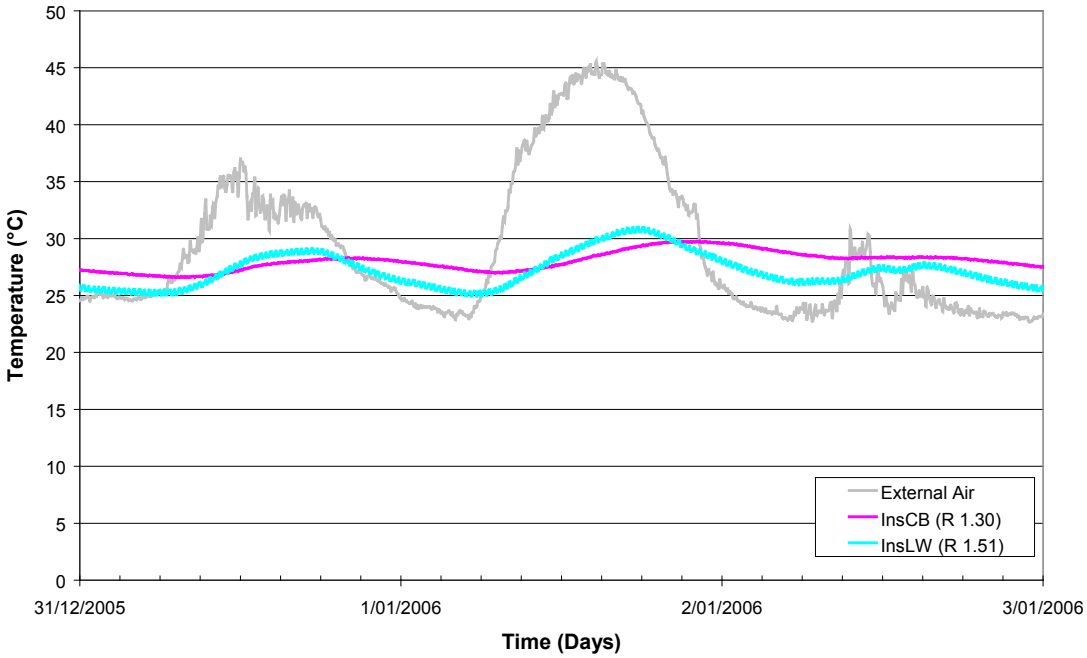

Figure 4.13 Internal and external temperature for Insulated Light Weight and Insulated Cavity Brick modules. – New Years Day January 2006

As can be seen from Figure 4.13, the peak temperatures for the InsCB module occurred at approximately 10-11pm depending on the input conditions. This lag was similar to the CB module. Typically the InsLW module peaked at approximately 5-6pm. Previous results showed that InsBV peaked at 8-9pm under similar conditions.

The average daily temperature swing for the InsLW module was 3.9°C, compared to 1.5°C for the InsCB module. On average the swing of the InsCB module was 40% of the total InsLW module swing. The InsLW module also exhibited higher peak temperatures (28.2°C average peak for this period which was 1.5°C higher than for the InsCB module). Despite the nightly temperatures being lower for the InsLW module due to the more rapid internal temperature changes with the external driving factors, the average internal temperature for the 4 week period for the InsLW module was 26.2°C, which was higher than the 25.9°C for the InsCB module.

It is significant to note that despite the fact that the R-values for two walling systems differing by only 0.2 m^2K/W (1.30 m^2K/W for the InsCB module and 1.51 m^2K/W for the InsLW module), their performance was vastly different, both in terms of maximum and minimum temperatures, and the thermal lag. This can be directly attributed to the presence of thermal mass in the InsCB system, and in particular the presence of thermal mass on the inside of the cavity wall insulation. In comparison, the InsLW system, although having high thermal resistance, had virtually no thermal mass and therefore lacked the ability to absorb and release heat. This can be clearly seen in Figure 4.12 in relation to the diurnal swing, internal temperature range and thermal lag (for example, on the hot New Year's Day, the InsLW system had an internal temperature swing of 6.5°C which was more than twice the swing of the 2.8°C for the InsCB system).

4.3.2.2. Through-Wall Heat Flux

Due to instrumentation limitations heat flux and temperature data could only be collected for the western wall of the InsLW module, therefore no energy envelope calculations could be performed. The primary analysis showed heat readily passed through the InsLW walling system into the module. Not only did this occur under direct solar incidence on the external surfaces but even the diffused radiation during the morning was sufficient to transmit heat into the internal space. The diffused solar radiation promoted an inward flow of heat by providing a sufficiently large temperature differential. Since no thermal mass was present in the walls of the module the effect on the walling system was immediate. This behaviour was not observed in the modules with thermal mass which exhibited a delayed response.

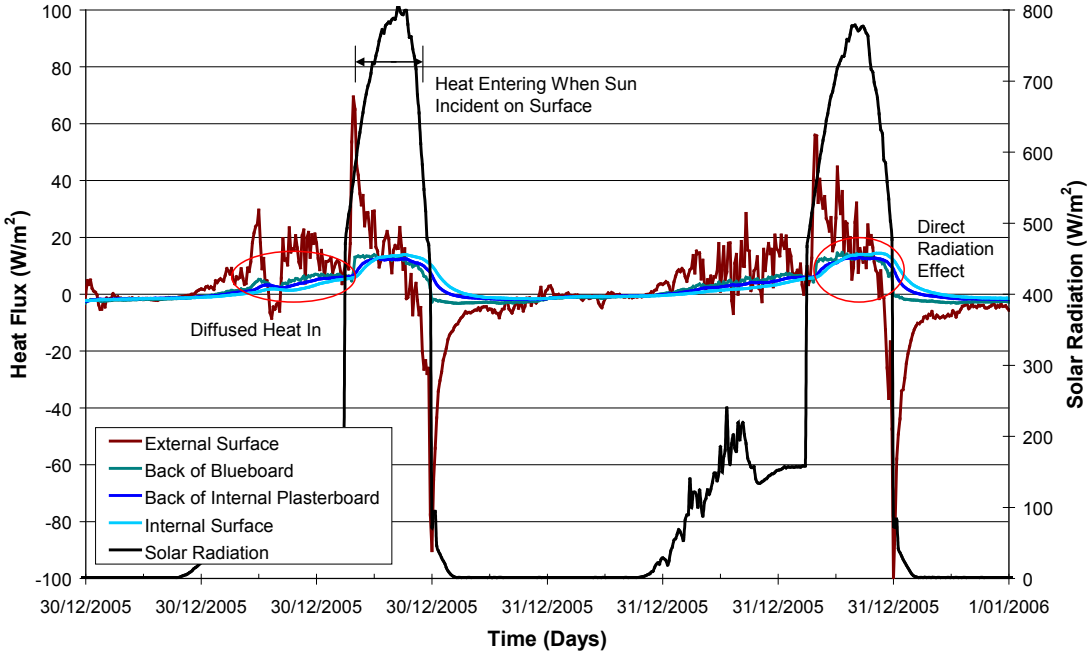

Figure 4.14 Western Wall Incident Solar Radiation and Heat Flux Profile

The behaviour of the heat flux profile across the InsLW western wall also indicated that the quantity of heat being absorbed peaked and decreased before the maximum surface temperature was developed at around 3pm (see Figure 4.14). This was most likely due to the relatively low heat capacity of the wall which results in the surface temperature rising quickly and thus allowing the re-radiation of the incoming solar radiation. There was no further attenuation of flux through the InsLW wall (unlike the cavity brick walls) with the maximum internal peak flux on New Years day being around 13W/m^2 (as Figure 4.13).

From the InsCB modules heat flux sensor reading it can be observed that the cavity insulation appeared to uncouple the interior skin from the exterior, with the observed incoming heat flux values being lower than 5W/m^2. The variations in the interior wall heat flux were most likely due to the wall responding to minor fluctuations in indoor air temperature.

4.3.3. Cold Weather Conditions

4.3.3.1. Temperature Variations and Thermal Lag

The performance of the InsLW and InsCB modules through May and June 2006 can be compared in Figure 4.15. The solar influence on the thermal mass surfaces in the InsCB played a big part as it absorbed heat which was later transmitted through the walling envelope to maintain higher internal temperatures than the InsLW. The dampening of the thermal mass reduced the influence of the weather creating much more stable internal conditions.

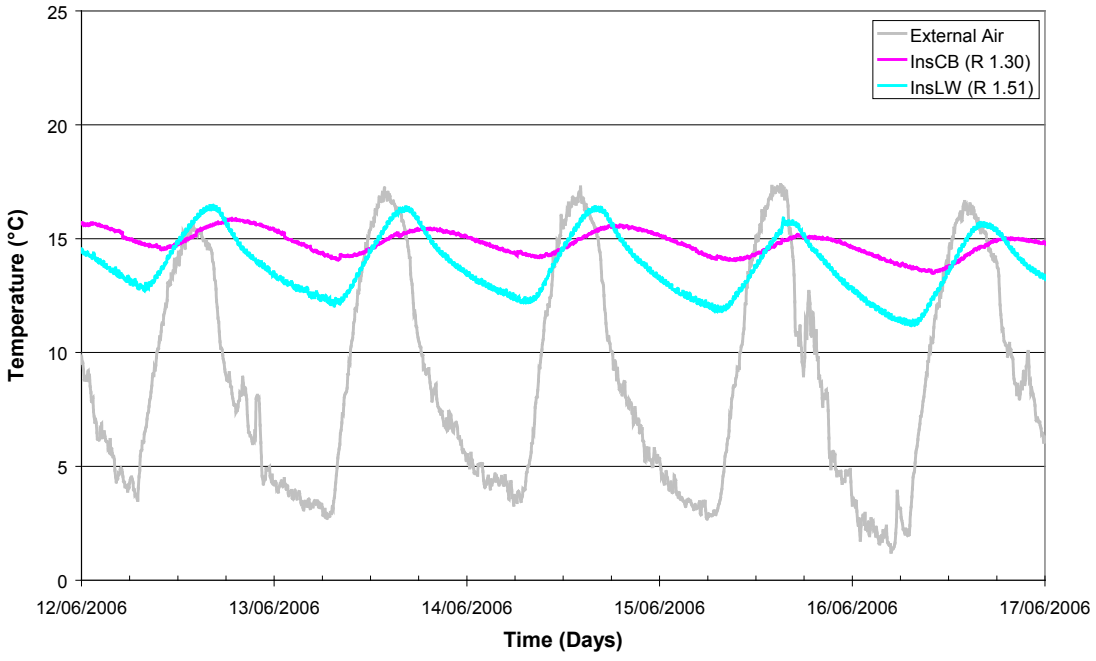

Figure 4.15 Internal and external temperature for InsLW and InsCB modules

The InsLW module provided little offset in regards to the peaks and troughs with the general trend of the InsLW following the external temperature. The InsCB not only had an greater reduction in temperature swing compared to the InsLW but also offset the peak temperatures which added even further dampening to the internal temperature. The internal space of the InsCB did not experience the maximum effect of the external weather until a delay of about 8 hours. By that time the external conditions had again changed. As a result, the peak weather influence of the day had less impact on the system with the greater thermal mass.

Overall the InsCB module maintained a higher internal temperature under cold conditions for most of the day compared to the InsLW module. The InsLW did peak at a higher temperature during the day but this period was limited due to the rapid influence of the external environment which readily reduced the internal temperature as a result of the lack of thermal mass in the walling system.

4.3.3.2. Through-Wall Heat Flux

The total energy envelopes for the InsLW and InsCB modules over 4 weeks through May and June 2006 are shown in Figure 4.16. Heat readily flowed into the InsLW when the sun was incident on the external wall surfaces with little time lag between the incidence on the external surface and the heat passing through into the internal space. Also once the solar incidence passed, heat immediately flowed back out through the wall. For the InsLW module, a large proportion of the heat gain came from the slab, as the internal temperature dropped much lower in comparison to the InsCB module. However, the heat from the slab flowing into the room was not sufficient to match the performance of the InsCB module. In this latter case, the internal temperature of the InsCB module was not low enough for the slab influence to be significant.

Heat loss was minimised into the night in the InsCB due to the delayed heat flow through the walling system. There were higher heat gains through all the internal wall surfaces for the InsLW module, yet on average the internal temperature was lower despite the walls having a higher R-value than for the InsCB module. The heat entering the InsLW module as shown in Figure 4.16 only occurred during the day due to the direct response of the walling system and the lack of thermal lag accounting for the higher peak temperature. As no heat was reradiated by the InsLW walling system at night, for winter conditions interior temperatures undesirably dropped below the InsCB module.

A slight gain of heat occurred through the southern wall of the InsLW module despite only receiving diffused solar radiation. While this gain was relatively negligible, it demonstrates the lack of thermal lag in the system. The temperature difference across the InsLW walls produced a very quick response across the whole wall system. The heavier walls have a delayed and reduced effect as could be inferred from the energy envelope of the InsCB southern wall. The maximum external air temperature during the day could not solely provide the driving force to transmit heat through the InsCB southern wall as the thermal lag prevented the instantaneous heat transmission which occurred for the InsLW walls.

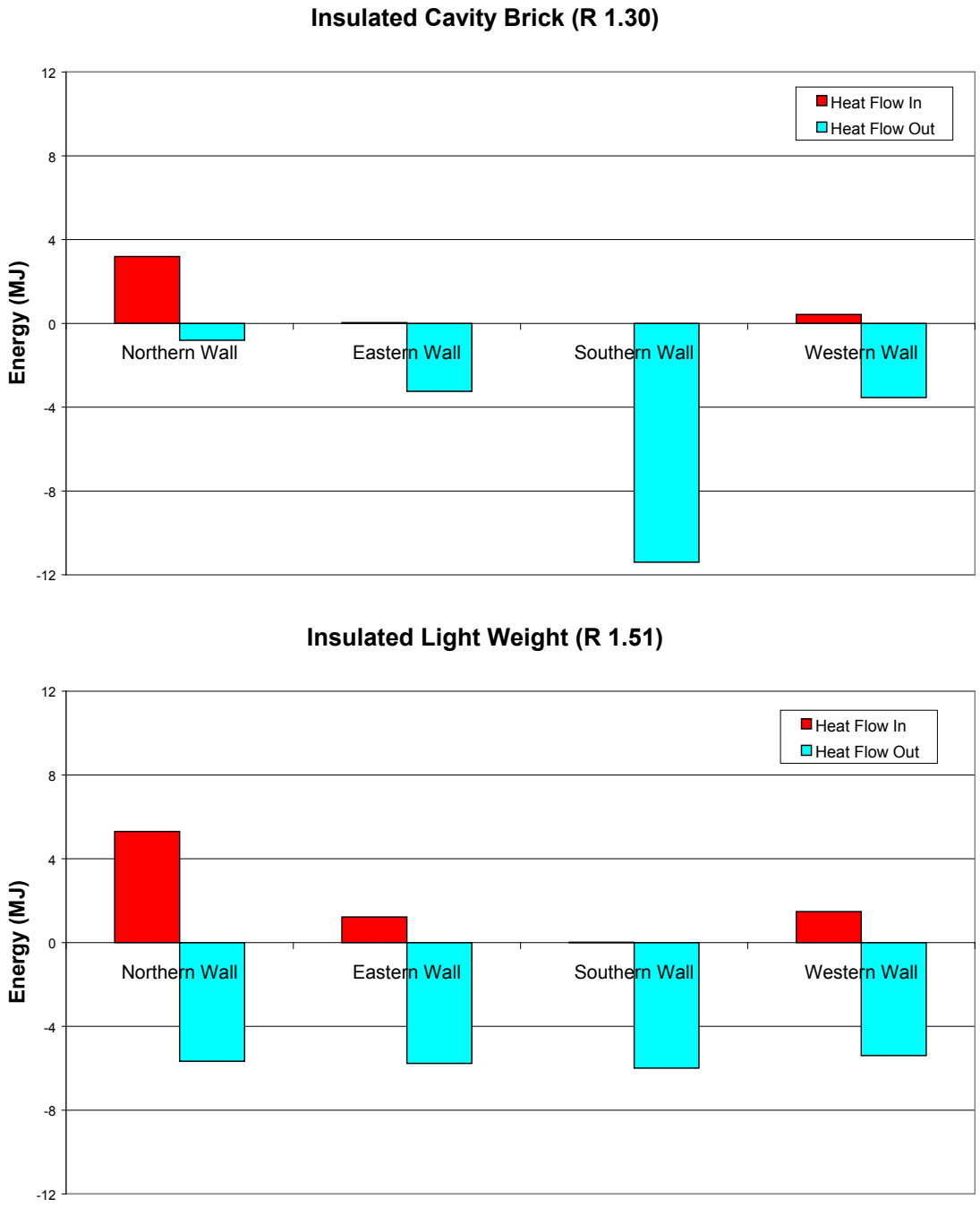

Figure 4.16 Total energy envelopes for the internal surfaces of the InsLW and InsCB modules – 4 Weeks through May-June 2006

The insulation in the cavity of the insulated cavity brick certainly aided in the reduction of the heat lost through the wall. It provided an added barrier between the internal room and the external conditions, with the internal mass further moderated the internal temperature.

4.4. Key findings

This chapter has described tests on housing modules which contained no major openings, thus allowing the thermal properties and behaviour of wall systems themselves to be studied. The bulk of direct comparison related to conventional cavity brick and brick veneer constructions, with some of the later studies related to insulated cavity brick and lightweight constructions. Further analysis will include a more in depth statistical analysis to provide a comparison across different time frames and provide a better insight into the variations in the mechanisms between the constructions. This will form part of the Phase II report.
The following summarises the key findings:

- Wall thermal mass and accompanying thermal lag played a key role in controlling the magnitude and timing of the maximum and minimum internal temperatures. The effects of high (and low) external temperatures were ameliorated and the magnitude of the diurnal swings reduced. Cavity brickwork, brick veneer and insulated cavity brickwork attenuated the effect of solar radiation to varying degrees by releasing the stored heat back to the outside environment, thereby reducing the net heat flux entering through the wall. This was not case for the insulated lightweight walls which had higher thermal resistance but no thermal mass. As a result, there was a greater variation in internal temperatures and no thermal lag exhibited by the InsLW module.

- The internal temperature was governed by the heat entering and leaving via the walls. The resultant diurnal temperature swings were small (2-3°C for the cavity brick module and 3-5°C for the brick veneer during Feb 2004). The internal temperature was maintained at a given level due to the continual flow of heat into and out of the room from the heavy masonry walling. This effect was therefore more pronounced for the cavity brick modules than the brick veneer module and insulated lightweight. The InsLW system had a diurnal swing more than twice the InsCB during hot conditions.

- The southern wall tended to be always cooler than the internal air as it did not receive any direct solar radiation on its external surface and consequently heat generally flowed out through this surface. However for the InsLW construction, due to the lack of thermal mass, the effect was greatly reduced and more dependent on the temperature difference across the wall which dictated the direction and magnitude of heat flow.

- In winter, heat predominantly entered the buildings via the northern wall and in summer via the western and eastern walls. The performance and the effectiveness of wall orientation can vary seasonally as a result of the varying solar angle – in particular the introduction of the northern wall as a heat source from the low solar angle in winter.

- There was a strong influence on the building envelope from the impingement of solar radiation. The InsLW module responded directly in reaction to the external environment with a rapid increase and reduction in temperature rates for this system due to its low internal thermal mass. Walls also immediately transmitted heat through into the module when solar radiation was incident on the external surface.

- It is clear that the thermal response of a building is influenced by both the thermal resistance of the walls and their thermal mass. Different behaviour characteristics were observed for the InsCB, InsBV and InsLW modules, even though their R-values were similar.

- The InsLW module was on average warmer than the CB module during the warmer conditions and on average cooler than InsCB module during cooler conditions. The daily internal temperature swing for the InsLW was also much higher than for both the CB and InsCB modules.

5. THERMAL TEST MODULES - WITH A NORTH FACING WINDOW

5.1. Introduction

The initial module studies described in Chapter 4 were focused on the fundamental behaviour and heat transfer mechanisms for the individual wall systems. This was achieved by minimising roof effects with a heavily insulated ceiling, and the complete absence of openings (thus avoiding direct solar ingress).
As detailed in Chapter 3, a major opening was later installed in the northern wall of each module to permit solar access. This allowed the subsequent study of solar-passive mechanisms and the interaction with the various components of the modules. The interiors of the modules were allowed to either "free float" or be "controlled" to enable both scenarios to be studied.

This chapter presents the results of the studies and in particular considers the effect of the opening on internal temperature conditions and energy demands for a range of seasonal effects for the various module types. All results presented here correspond to cases with no carpet, ventilation or curtain operation included.

5.2. Impact of a North Facing Window on Internal Temperature

The presence of a major opening in the northern facing wall had a major influence on the thermal performance of the test modules. This is illustrated in Figure 5.1, (Sugo et al., 2004) which shows a comparison of internal temperature for cavity brick modules with and without a window for the conditions experienced in early June, 2004 (as can be seen from Table 3.2, this was a brief period when the two modules could be directly compared).

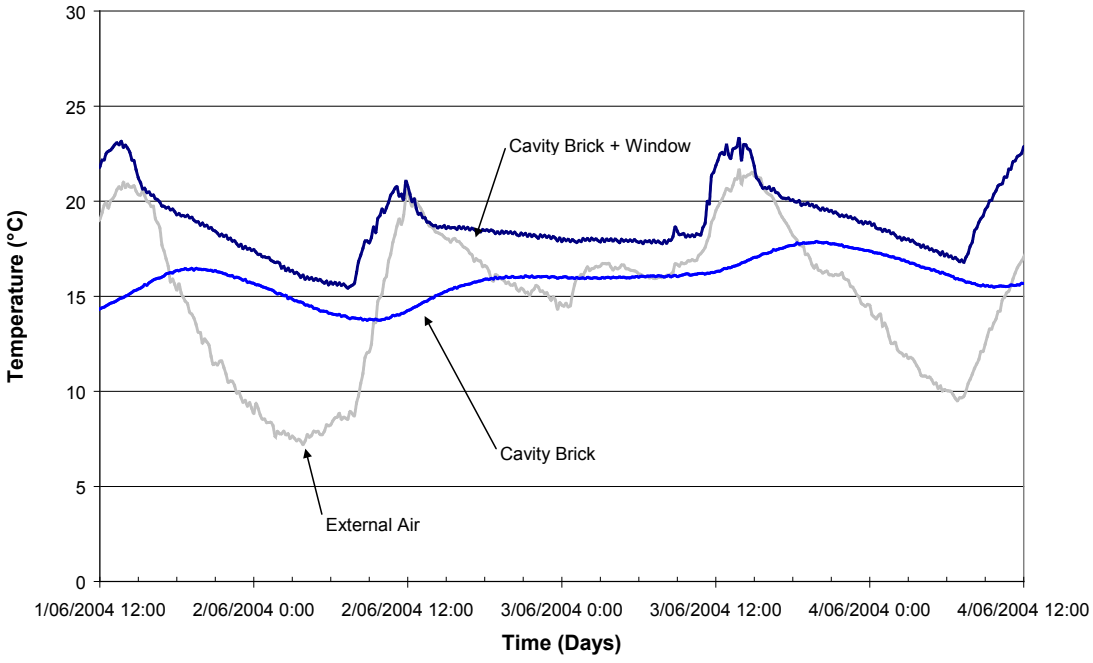

Figure 5.1 External and internal air temperatures for the cavity brick module, with and without a window, June 2004.

The windowless module had a typical diurnal swing of 2-3°C with a mean internal temperature of 15.6°C. The peak daily temperatures were also delayed with respect to the peak external temperature.

The cavity brick module with the addition of a north facing window consistently exhibited higher temperatures, warmer than both the external air and the windowless module. This was due to the direct solar gain entering the building. Internal temperatures ranged between 15-24°C for the module with the window and night temperatures were 7-8°C higher than the external air. The time lag between the maximum external and internal temperatures for the windowless cavity brick module was approximately 7-8 hours. The peak internal temperatures of the module with a window occurred nearly simultaneously with the external air.

5.2.1. Seasonal Variations of Solar Gain

The response of all of the modules with a window was strongly influenced by the weather conditions, with the incoming solar radiation via the window being the dominant driver of the internal temperature (Sugo et al., 2007). The variation in the solar angle with season for the windowless modules had some effect on the internal temperatures and the thermal performance of the modules. With a north facing window this effect was greatly amplified, with distinct differences in the internal temperature behaviour from season to season. Solar gain in winter was much greater than in summer as shown in Figure 5.2 for the CB module. The hottest internal temperatures experienced by the modules did not necessarily occur in the middle of summer as some later results show, but rather either side of the season when external temperatures were still moderate and the lower solar angle resulted in larger solar ingress through the window. This effect is particularly highlighted in the 12 month observation schedule described in Section 5.5 where internal thermal mass is particularly needed to aid in offsetting the temperatures rise.

As can be seen from Figure 5.2 the peak incident solar radiation falling on the north-facing window (measured in the north facing vertical plane) for the 17th and 18th of July 2005 was in the order of 800 W/m^2 with 500-600 W/m^2 entering the building.

The contrasting behaviour during summer can be seen from Figure 5.2 which shows the typical solar gain through the CB module window during January 2005. Due to the high solar altitude at this time of the year no direct radiation was recorded at mid-height through the window. The observed values were due to the reflected and diffuse radiation components. This energy entered the building from 6:30 am until 7pm, peaking in the order of 120 W/m^2 at 12:30 pm. After 7 pm, heat was lost via the window with the peak value being 23 W/m^2 at 5 am.

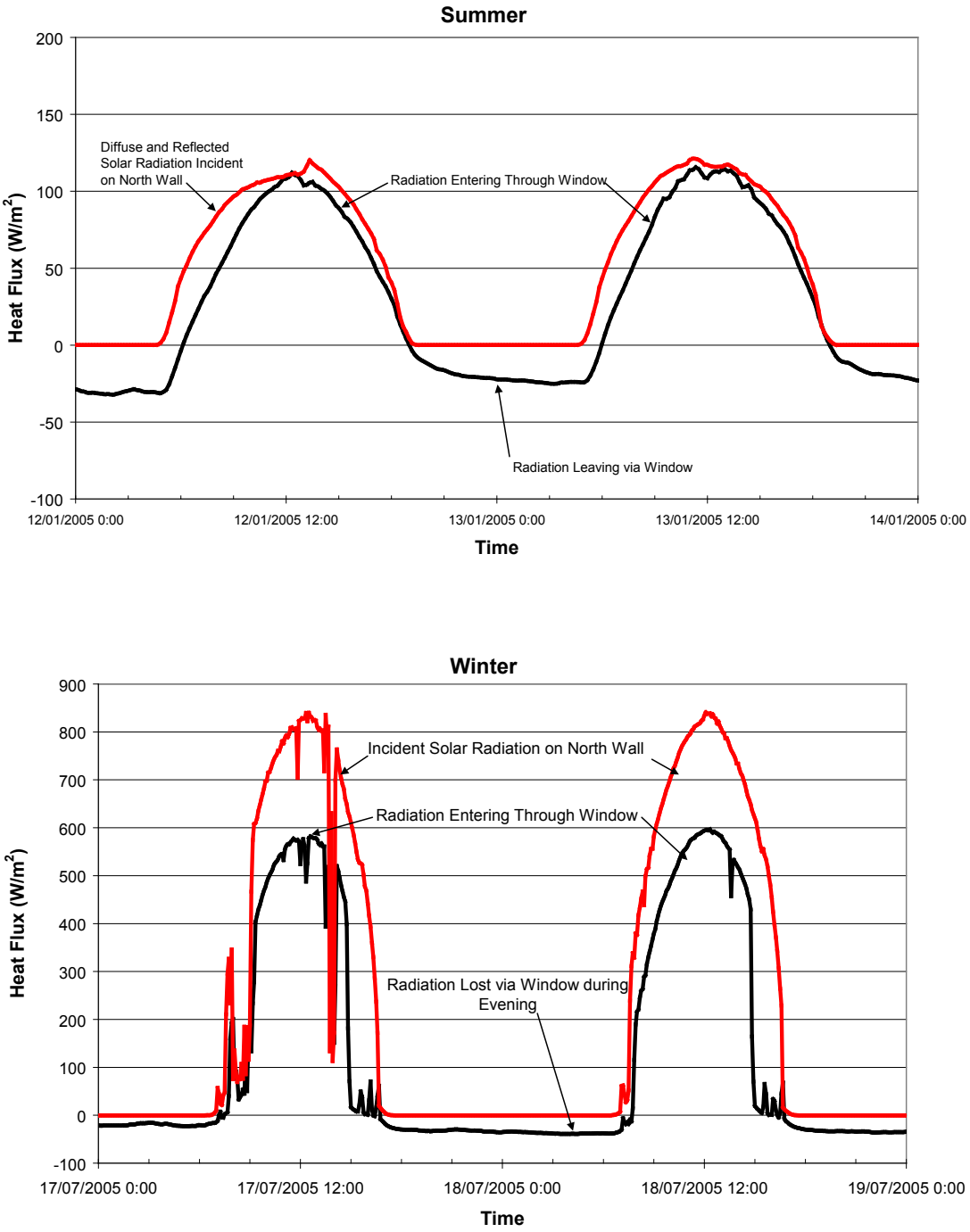

Figure 5.2 Solar radiation gains in summer and winter for the CB module

5.2.2. Energy Envelopes

The energy movements for each building module depended upon the nature of the module (construction type, the presence of windows etc.), the seasons and the weather conditions. It is useful to study the magnitude and direction of energy flows for each component surface of a module, as it gives a good indication of the heat transfer mechanisms which are taking place. This can be illustrated by comparing the internal envelope energy summary shown in Figure 5.3 for one week in August 2004 for the CB module with a window opening in the northern wall to the InsCB without a window. The dominant role of the window opening is very clearly illustrated with the bulk of inward flowing energy coming from that source. Over the

observation period there was significant radiant heat flow in through the window; 27.7 MJ entered through the CB brick window whereas only 5.8 MJ was transmitted through the InsCB modules northern wall. Inward energy flow from other internal wall surfaces was small.

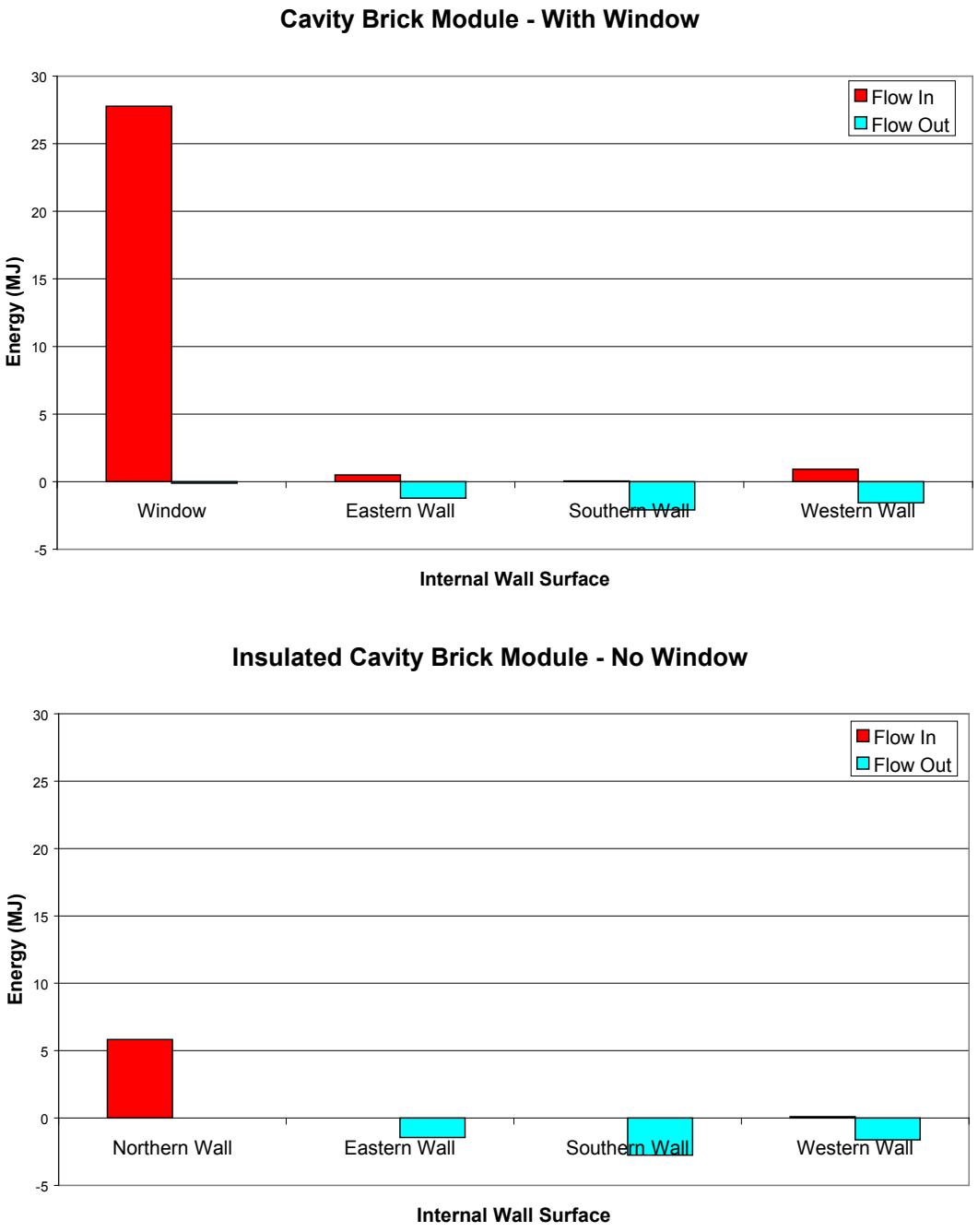

Figure 5.3 An example of the total energy exchange for the CB module with window and InsCB without the window.

5.2.3. Slab Response

As described in Chapter 3, heat flux sensors were located on the slab adjacent to the window and in the far south-east corner of each module (Sugo et al., 2007). This allowed the extent of solar radiation influence on the slab through the window to be quantified. Typical results for the CB module are shown in Figure 5.4 for summer and winter conditions. For winter, the area of the slab which received direct solar radiation was heated during the day to approximately 30˚C, absorbing at a maximum approximately 210 W/m^2 of the incoming flux as shown in Figure 5.4 (a). The balance of the incoming energy was redistributed in the module via convection and/or radiation. The energy stored in the area of the slab near the window was released back into the internal air space at a steady 30 W/m^2 from 3 pm to 7 am as the room air temperature dropped and incoming solar radiation decreased. In contrast, the remaining portion of the slab which did not receive direct sunlight continued to absorb small amounts of heat but at a decreasing rate until about 10 pm when it then started to release heat into internal air space peaking at 10 W/m^2 at 7am.

Under summer conditions, (Figure 5.4 (b)), due to higher solar elevation the energy absorbed by the slab adjacent to the window was much less (peaking at approximately 25 W/m^2). Consequently, less energy was available to be released back into the room during the evening.

The slab influence was also investigated in the project with the installation of carpet and underlay. While the results are not presented here, removing the thermal mass of the slab had a negative impact on the InsLW and InsBV modules by increasing the peak room temperatures by up to 2-3°C. No discernable impact was found on the InsCB and CB modules which have internal thermal mass present in the walling system.

From the above it is clear that the addition of a window to the north facing wall of the modules significantly alters the entire behaviour of the system with the solar gain entering through the window becoming the primary driving force of the building. These results illustrate well one of the key underlying principles of solar passive-design and the mechanisms at play within an actual dwelling.

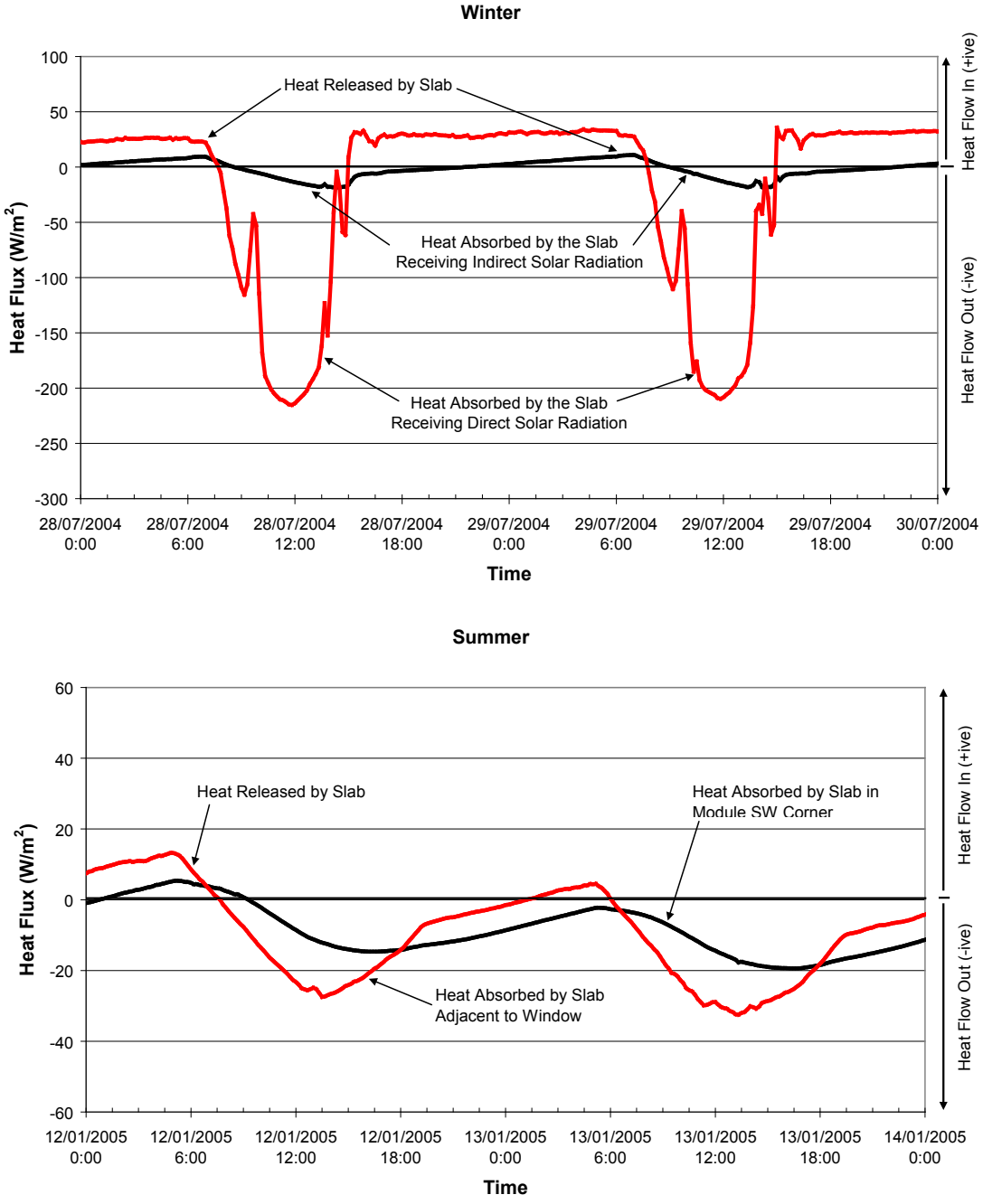

Figure 5.4 Heat released and absorbed by a slab for typical summer and winter conditions.

5.3. Free Floating Conditions

This section describes the behaviour of the modules under free-floating conditions for various seasons.

5.3.1. Spring weather conditions (October 2006)

5.3.1.1. Temperature variations

The behaviour of the four modules during October 2006 provides a good basis for comparison (see Figure 5.5). The weather for this period was typical for October with warm north-westerlies followed by cool changes. On average the external temperature swing was large, up to 13°C. External temperatures regularly peaked over 25°C with several days above 30°C. This combined with the lower solar angle also produced large temperature swings within the modules, up to 11°C for the InsLW in one case. The internal air temperatures of the modules could be grouped into two distinct trends: one for the systems with significant internal thermal mass (CB and InsCB), with InsCB being warmer overall; and the other for systems without internal thermal mass (uninsulated BV and InsLW). Note that this data contains results from the uninsulated brick veneer module.

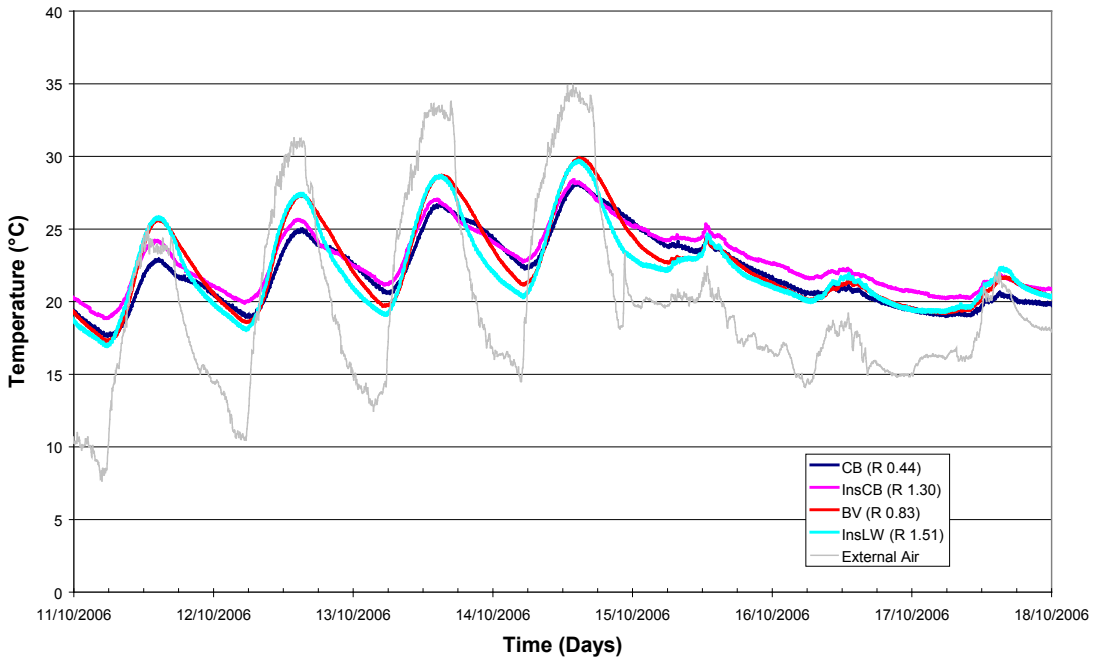

Figure 5.5 Temperature profiles for four modules, October 2006

For the period shown in Figure 5.5, the uninsulated BV and InsLW modules peaked approximately 2ºC warmer than the CB and InsCB modules during the day and 1-2ºC cooler during the night, reflecting the influence of the thermal mass on dampening the diurnal swing within the CB and InsCB systems. The InsCB held marginally warmer temperatures for two days after the cool change, reflecting the role of the cavity insulation by reducing outwards heat flow from the internal skin and the thermal mass. A summary of the observed temperature variations for the modules is given in Table 5.1

The InsLW module exhibited on average the highest diurnal temperature swing (7°C) which was 0.7°C greater than the uninsulated BV (6.3°C). The InsLW module consistently had slightly higher peak daily

temperatures over the month, with an average peak temperature of 25.6°C, compared to 25.2°C for the uninsulated BV (a result of the insulation in the InsLW system retaining heat within the module during the day).

The uninsulated BV module showed a limited degree of heat removal during the day, but the effect of this thermal lag was lower as thermal mass only existed in the external brick skin. Consequently, heat passed through the envelope later during the day resulting in the temperature of the uninsulated BV module not decreasing as rapidly as for the InsLW module. The uninsulated BV module also had a slightly higher mean temperature than the InsLW module as a result of it not reaching as low a minimum at night and smaller diurnal swing. While the mean temperatures of the uninsulated BV and InsLW were similar, the InsLW module had the least desirable characteristics of all modules (including the uninsulated BV) during this time period of October 2006, with the highest daily peak temperature on average and the greatest diurnal swing. The InsLW module had the least capacity for self-regulation particularly at times during the year when solar-passive principles can be utilised to a maximum.

Table 5.1 Temperature variations for 4 weeks in October 2006

Temperature (°C)	Uninsulated BV	InsCB	CB	InsLW	External Air
Mean Daily	21.9	22.3	21.3	21.7	18.4
Mean Daily Min	18.9	20.4	19.2	18.6	11.7
Mean Daily Max	25.2	24.6	23.5	25.6	25.3
Mean Range	6.3	4.2	4.2	7.0	13.6

Note: *Mean Daily* indicates the average daily temperature for the 4 week period, *Mean Daily Min/Max* is minimum/maximum daily temperature average for the 4 week period, *Mean Range* is an average of daily span between minimum and maximum temperatures for the 4 week period.

Both the InsCB and the CB modules followed similar temperature trends but typically the temperatures in the InsCB were offset approximately 1°C higher than the CB module which reflected the role of the cavity insulation. This was generally consistent over October 2006. Diurnal swings of both modules were identical at an average of 4.2°C. This was approximately 2°C and 2.8°C lower than the uninsulated BV and InsLW modules respectively, and directly due to the dampening effect of the thermal mass. This resulted in cooler day time peak temperatures and warmer night temperatures than the modules without internal thermal mass.

5.3.1.2. Through-Wall Heat Flux and Energy Envelopes

The corresponding wall heat flux profiles for 3 typical days within October 2006 are shown for each of the modules in Figures 5.6, 5.7 and 5.8 and are characteristic of heat movements for this season.

It is apparent in Figures 5.6 and 5.7 that for the eastern and western walls of the InsLW module, heat was only transmitted through the walling system when the sun was incident on the respective external surface, or in the case of the southern wall, when the external temperature and/or diffused solar radiation was at the sufficient level. However, it was the inability of the InsLW module to counter the incoming solar gain through the window which produced the high temperature during the day. Also, no heat was reradiated back into the room once the sun set due to the lack of thermal mass in this walling system. Throughout the night heat was lost to the outside from the internal space through all walls as well as the window. This produced the sudden drop in internal temperature and the lowest minimum temperature of all four modules. The InsLW module shows little response in producing heat flows to counteract the natural weather conditions.

The maximum heat transmitted through the western wall of the uninsulated BV module also exhibited a pronounced peak, with a similar peak to the InsLW but at a later time. The peak heat flow through the western wall of the uninsulated BV module occurred approximately 2 hours after that for the InsLW and continued to add heat to the room albeit at a decaying rate until approximately 5:30am. This reflected the role of the thermal mass of the external veneer which created a delay in the time for the heat to flow through the wall as a result of the solar incidence. The average peak internal temperature of the uninsulated BV module was therefore not as high as the InsLW module with the walls of the uninsulated BV module also providing a marginal amount of heat absorption. In the case of the eastern wall internal surface very little heat even travelled through the wall as a result of the morning sun. However heat release into the room peaked suddenly during the late afternoon and decayed rapidly through the night (Figure 5.6). Even with this limited capacity to add heat to the room, nightly temperatures were marginally warmer compared to the InsLW module despite the BV module being uninsulated.

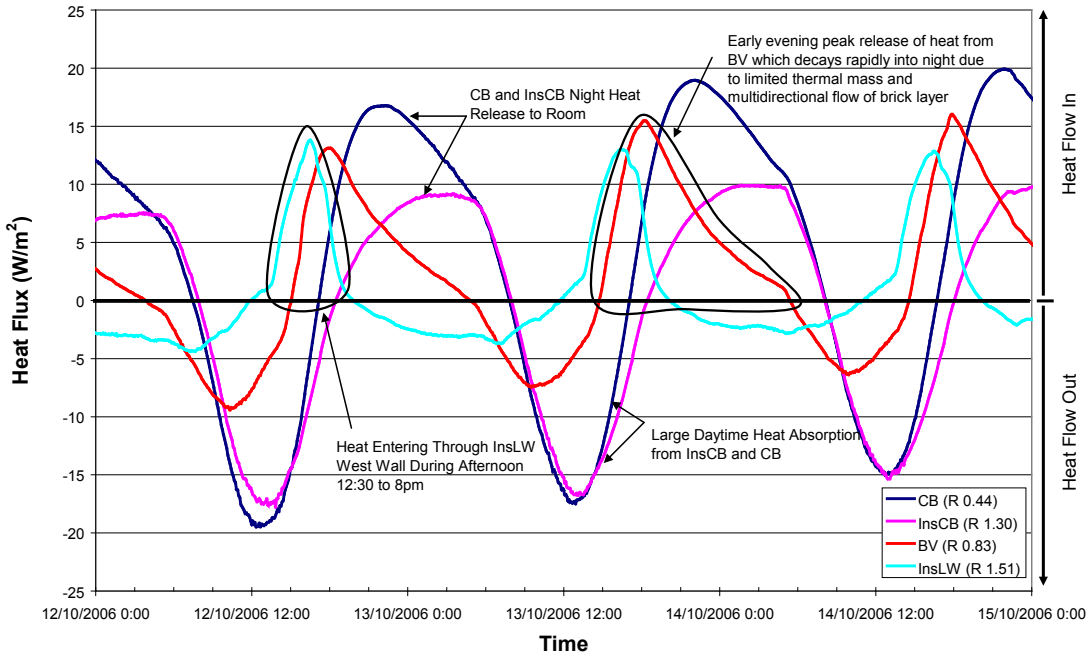

Figure 5.6 Western wall internal surface heat fluxes, October 2006

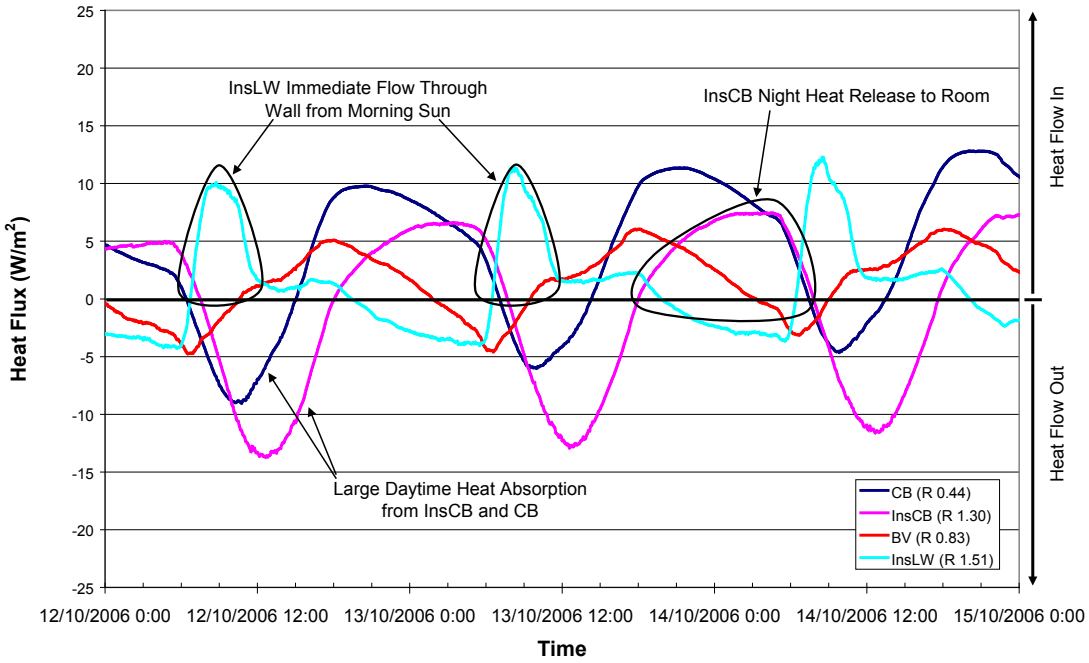

Figure 5.7 Eastern wall internal surface heat fluxes, October 2006

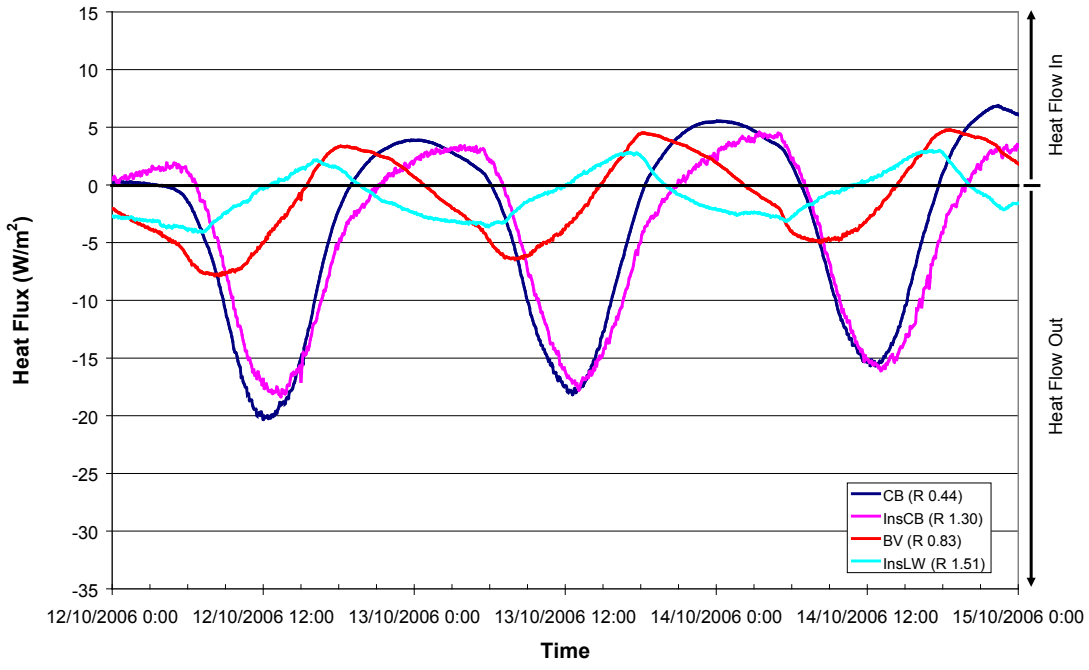

Figure 5.8 Southern wall internal surface heat fluxes, October 2006

While the InsCB and CB modules had similar trends in regards to the internal temperature, differences existed in the heat flows for each wall. While both modules strongly absorbed heat during the day to counter the solar gain which helped to reduce the peak temperature, the CB module was prone to releasing heat into the room initially at a more accelerated rate than the InsCB, with the heat then tapering off into the evening. The InsCB module had a gradually increasing rate of heat flow back into the room that appeared to plateau into the morning as the internal temperatures dropped further. This trend of heat release for both InsCB and CB walls was also seen to occur at other times during the year, but with the magnitudes being dependent on season.

The heat stored within the internal layer of the CB module flowed readily both into the room and into the cavity. This accounts for the heat release being rapid at first and then decaying through the evening (Figures 5.6 and 5.7). In the case of the InsCB walls, the insulation attached to the cavity surface of the internal brick layer restricted the heat loss to the cavity by isolating the internal skin from the external environment, thus maintaining more heat in the internal brick layer which in turn promoted a more continual flow into the room. The heat flow into the room actually increased into the night as reduced internal temperatures increased the driving force to remove heat from the brick.

5.3.2. Hot weather conditions

5.3.2.1. Temperature variations

The summer results for January 2007 presented here consist of three weeks of data for CB, InsBV and InsLW. Due to data acquisition problems no results were obtained for InsCB. However, the comparative difference between the InsCB module to the InsBV and the CB modules can be observed from the 12 month testing schedule as reported in Section 5.5. The weather conditions experienced did not include any heat wave conditions, with the daytime temperatures not overly high on average and only occasionally peaking above 30°C. However night temperatures were typical of summer conditions. Figure 5.9/10 shows the temperature profiles for the CB, InsBV and InsLW modules for a 6 day period in mid-January 2006. Note that for these results and all following, the brick veneer module included R1.5 insulation as described in Section 3.

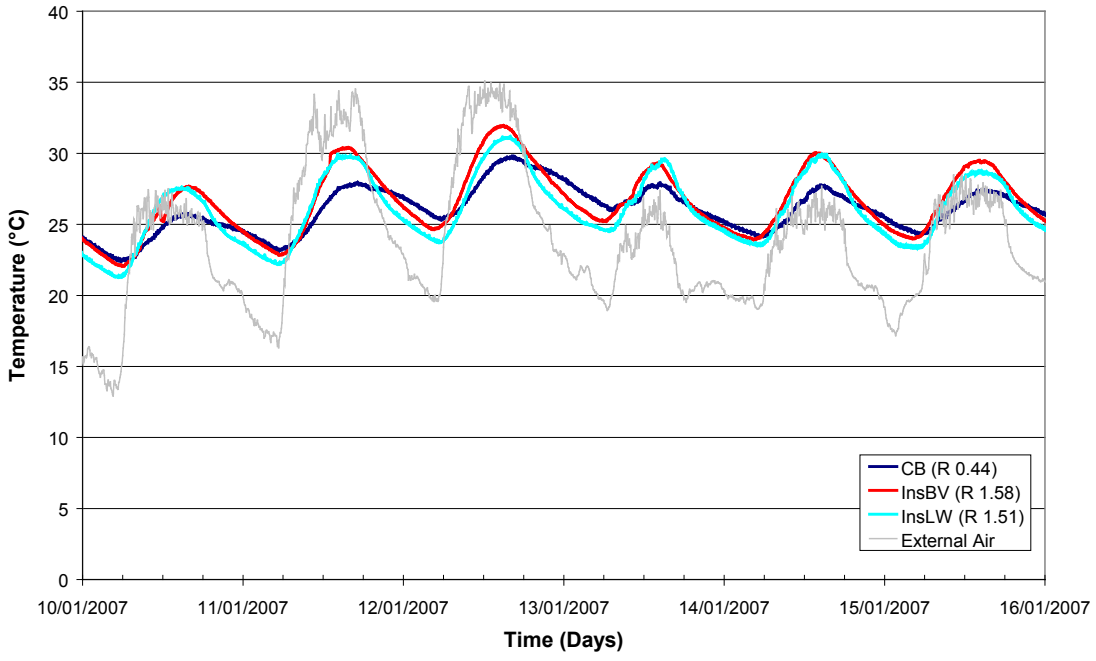

Figure 5.9 Temperature profiles for CB, InsBV and InsLW modules, January 2007.

The temperature profiles shown in Figure 5.9 demonstrate behaviour which was similar to that observed for the other time periods. The InsLW and the InsBV modules had the highest internal daily temperature and rapidly lost heat through the night. Even after warm periods, the InsLW and InsBV modules peaked to higher temperatures faster than the CB module. Under these conditions the InsBV module had on average the highest peak daily temperature, slightly exceeding the InsLW module by 0.2°C, though the InsLW module dropped to the lowest minima on average at night due to lack of thermal mass in the walling system.

Both the InsLW and InsBV modules temperatures reduced to values below the CB module, but this did not occur until the evening between the hours of 7pm to 11pm depending on external conditions. The average temperatures for each of the modules over the 3 week period from the 1st to the 21st of January 2007 are given in Table 5.2.

Table 5.2 Temperature variations for 3 weeks in January, 2007

Temperature (°C)	InsBV	CB	InsLW	External Air
Mean Daily	25.74	25.17	25.27	23.36
Min Daily Mean	23.29	23.52	22.71	18.30
Max Daily Mean	28.55	26.79	28.36	29.90
Mean Range	5.26	3.27	5.66	11.59

Note: *Mean Daily* indicates the average daily temperature for the 4 week period, *Mean Daily Min/Max* is minimum/maximum daily temperature average for the 4 week period, *Mean Range* is an average of daily span between minimum and maximum temperatures for the 4 week period.

It can be seen from Table 5.2 that the CB module had the lowest mean temperature under these summer conditions; it had also on average the lowest daily peak temperatures. The mean temperature range of the CB module was also the lowest, with a daily average of 3.27°C. This was a direct effect of the thermal mass dampening the temperature fluctuations. Both the InsLW and InsBV modules had significantly higher average temperature ranges than the CB, with 5.66°C and 5.26°C respectively. Again, InsLW had the highest diurnal temperature swing which created the most unstable internal conditions. This indicates that the external brickwork skin of brick veneer did have a small influence in reducing internal temperature swings. However, this effect is certainly not of the same magnitude as the influence of an internal brickwork skin. The higher temperatures exhibited by the InsBV and InsLW modules resulted from the inability of the internal wall surfaces to absorb heat to counter the incoming solar gain. For other seasonal conditions, the InsBV module was able to do this to a limited degree, but under summer conditions there appeared to be little benefit. The InsLW module however showed little to no evidence of countering solar gains to reduce the high internal day temperatures. There was a slight thermal lag observed for the InsBV system, but the thermal mass of the external skin had insufficient thermal lag to allow a heat flow reversal to occur once the external temperature had decreased. However, the small amount of thermal lag present did result in a lower rate of temperature drop and higher minimum night temperatures compared to the InsLW module.

5.3.2.2. Through-Wall Heat Flux

As shown in Figures 5.10 – 5.12 and the total energy envelope in 5.13, a much larger quantity of heat was absorbed by the CB module during the day than the InsBV and InsLW modules. The southern and western walls restricted the CB module temperature rise during the day. The CB module did maintain slightly higher temperatures at night compared to the InsBV and InsLW modules and whilst this release of heat to the interior is beneficial during cooler periods it may not be so during hot periods if the ambient temperatures are already high. However it should be noted that the temperature difference at night between the CB and the InsBV and InsLW modules is not as significant as the difference during the day due to the overheating that occurs in the modules without internal thermal mass.

While the eastern wall of the CB module actually absorbed less heat in total through the internal surface than the InsLW module it can be seen from Figure 5.10 that the heat absorbance by the CB module occurred during the day which acts to counter the solar gain while the InsLW lost heat at night through the wall. A large quantity of heat did pass from the eastern wall of the CB module at night (Figure 5.10 and 5.12) into the internal space, which was predominately from the transmission of heat due to the solar incidence during the morning, therefore the eastern wall of the CB module appears to do little to reduce temperatures during

summer. Despite this, the CB eastern wall delayed the heat flow into the room whereas the InsLW walling system transmitted heat through the wall during the day when it is least wanted and essentially acted as a secondary heat source.

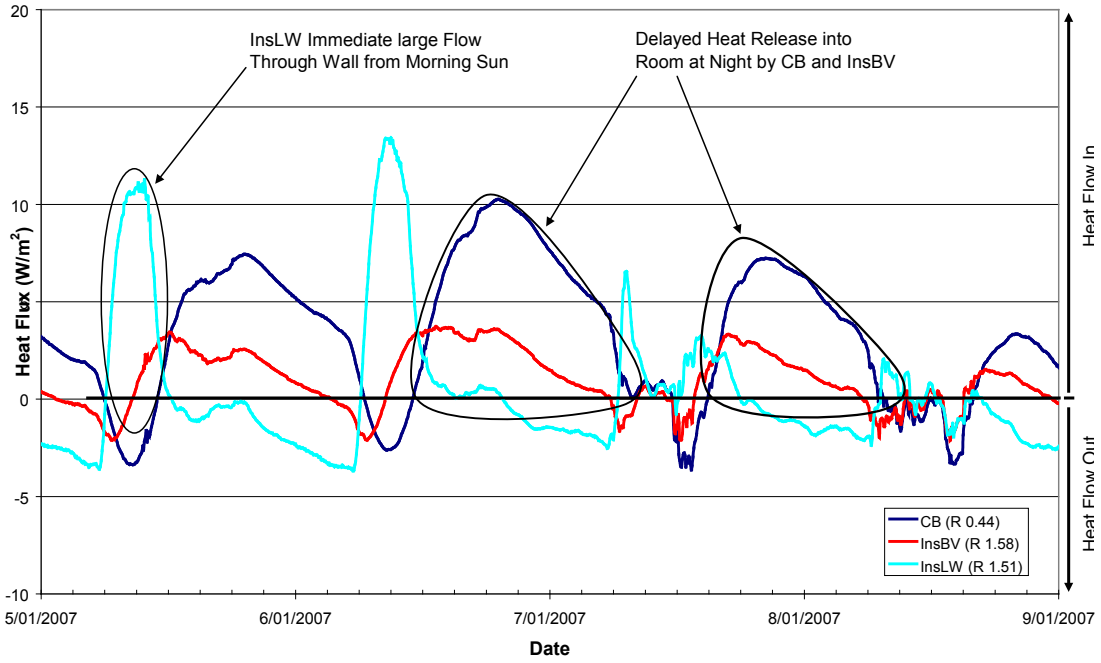

Figure 5.10 Eastern walls internal surface heat fluxes, January 2007

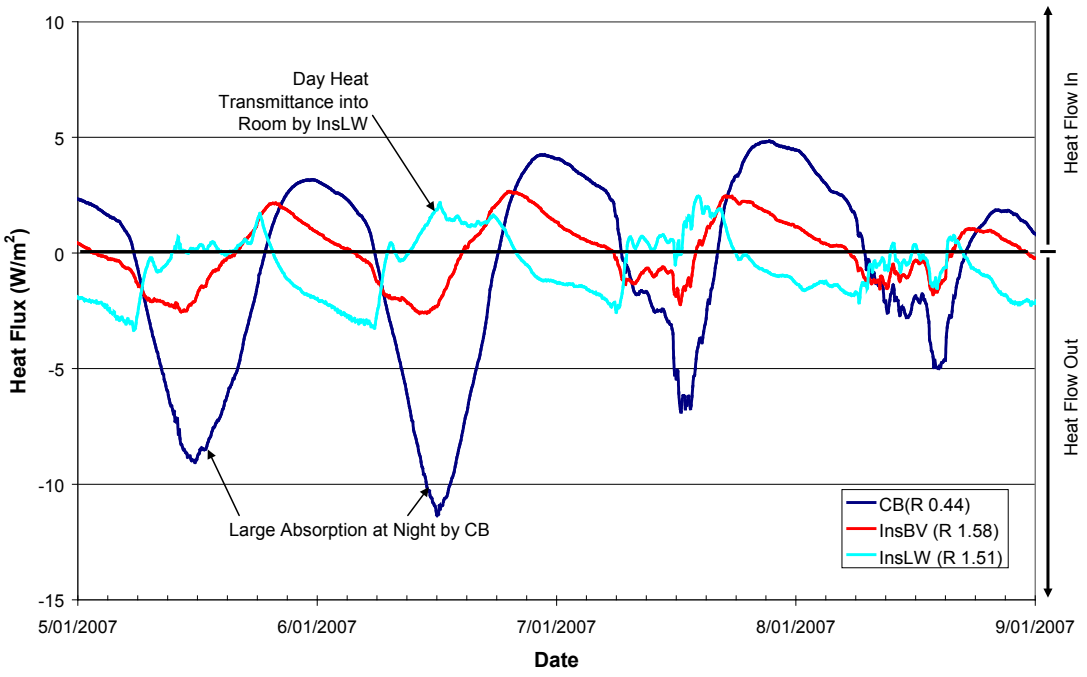

Figure 5.11 Southern walls internal surface heat fluxes, January 2007

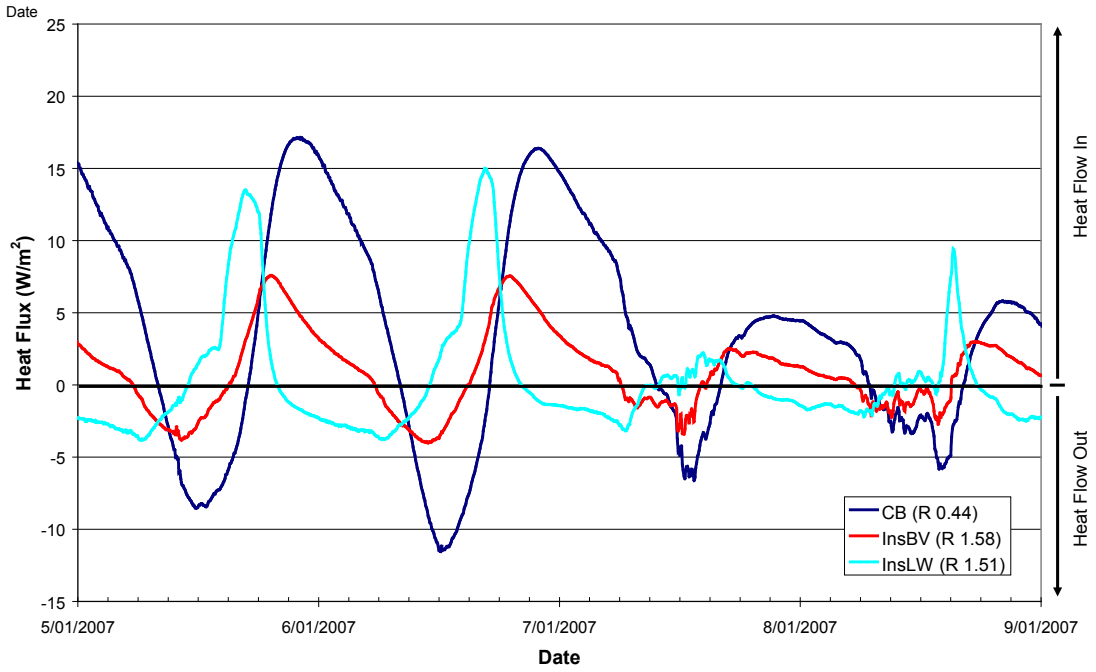

Figure 5.12 Western walls internal surface heat fluxes, January 2007

The InsLW module lost heat consistently at night resulting in the large temperature drop. While the InsLW would readily decrease temperature at night, it was at the expense of high temperatures during the day, as the walling envelope did not have the capacity to absorb heat from the room. As can be seen from Figures 5.10 to 5.12, the walls actually added heat during the day during the least desirable time periods of 7am to 12 noon for the eastern wall and 11am to 8pm for the western wall. The large temperature swing also reduces thermal comfort levels.

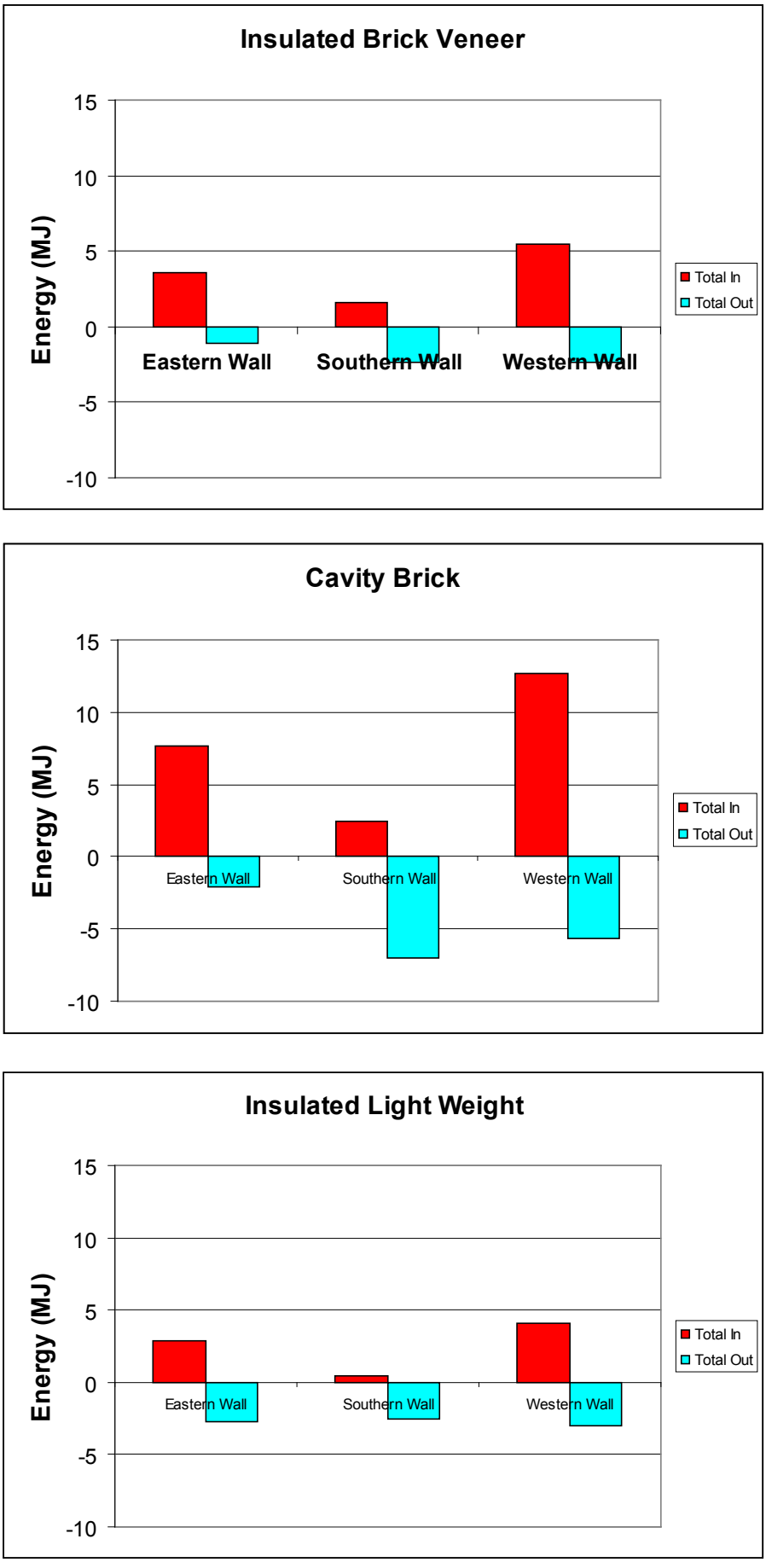

Figure 5.13 Total energy envelopes of internal surfaces, three weeks January 2007

5.3.3. Cold weather conditions

5.3.3.1. Temperature variations

Typical cold weather behaviour for the CB, InsBV, InsCB and Ins LW modules can be observed by studying their response during May 2007. Under these conditions there was a large solar passive influence which resulted in internal temperatures significantly higher than the external air (up to 13°C for the InsLW module). This was directly the result of the solar gain through the window in the northern wall. As can be seen from Figure 5.14 there was a marked difference in the response across the modules, with the two systems without internal thermal mass (InsLW and InsBV) exhibiting significantly higher peak temperatures during the day due to the inability to absorb the incoming solar gain. The InsCB module had the least temperature variation and the CB module remained coolest throughout.

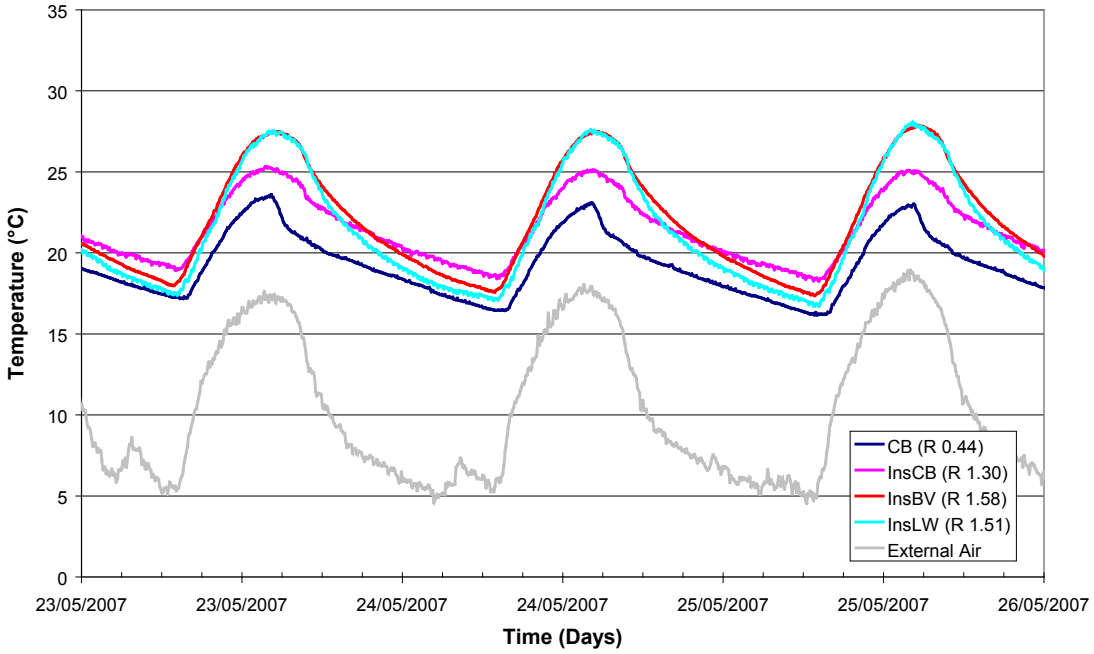

Figure 5.14 Temperature profiles for four modules, May 2007

Figure 5.14 illustrates that the InsBV and InsLW modules were by far the warmest modules during the day, with both having similar trends and similar temperatures. After 5pm the InsLW module began to decrease in temperature at a faster rate and reached a slightly lower minimum than that of the InsBV module. The InsBV was slightly warmer at night than the InsLW as the heat stored in exterior brickwork skin of the brick veneer western wall during the day was progressively released back into the room at night which is beneficial in winter (Figure 5.18).

The InsCB and CB modules followed a similar trend but with the internal temperature of the CB module being consistently approximately 2°C less than the InsCB module. An analysis of the cold weather temperatures for a 2 week winter period (17th May to 31st May 2006) is summarised in Table 5.3. This confirms that the addition of cavity brick insulation produced a shift in temperature, and internal thermal mass reduced the effect of the solar gain.

The cavity insulation of the InsCB module limited the release the heat stored in the internal skin to the cavity. The InsLW and InsBV modules typically peaked 2.2°C higher than the InsCB module. The InsCB

module maintained the warmest internal temperature from 10pm to 8am due to the release of heat back into the room at night. Both the InsCB and CB modules appeared to cool at a linear rate but with differing offsets whereas the InsBV and InsLW modules showed an almost exponential decrease.

Table 5.3 Temperature variations for 2 weeks in May, 2007

Temperature (°C)	InsBV	InsCB	CB	InsLW	External Air
Mean Daily	22.8	22.2	20.3	22.4	14.38
Min Daily Mean	19.0	19.6	17.9	18.5	8.70
Max Daily Mean	27. 8	25.6	23.8	27.9	21.28
Mean Range	8.7	5.9	5.9	9.4	12.58

Note: *Mean Daily* indicates the average daily temperature for the 4 week period, *Mean Daily Min/Max* is minimum/maximum daily temperature average for the 4 week period, *Mean Range* is an average of daily span between minimum and maximum temperatures for the 4 week period.

With regards to the temperature swings (mean range) in the modules as shown in Table 5.3, the InsBV and InsLW modules had the highest internal temperature swing on average with 8.7°C and 9.4°C respectively, reflecting the lack of internal thermal mass which can improve the stability of the internal temperature. Internal thermal mass has a greater interaction with the internal room space and as a result the average temperature swing was lower for the InsCB and CB modules with both being 5.9°C.

The CB module was consistently the coolest of all four modules. Under these conditions the heat added to the room due to the solar gain was absorbed by the internal brick skin. As no insulation existed in the cavity, this absorbed heat more readily passed into the cooler cavity and further outwards into the external brick skin. The InsCB module maintained a consistently higher temperature than the CB as the insulation isolated the internal skin and limited the heat loss at night resulting in a total net gain of heat into the room from all walls at night, providing greatly improved performance over InsBV and InsLW throughout the entire day.

5.3.3.2. Through-Wall Heat Flux and Energy Envelopes

The sum of the energy movements for the eastern, southern and western walls for the two week period in May 2007 is shown in Figure 5.15. The solar gain through all north facing windows was similar and over the entire 2 week period, a total of approximately 165 MJ/m^2 entered each individual module. Loss through the window at night varied between modules as this was dependant on the internal room temperature of the respective module.

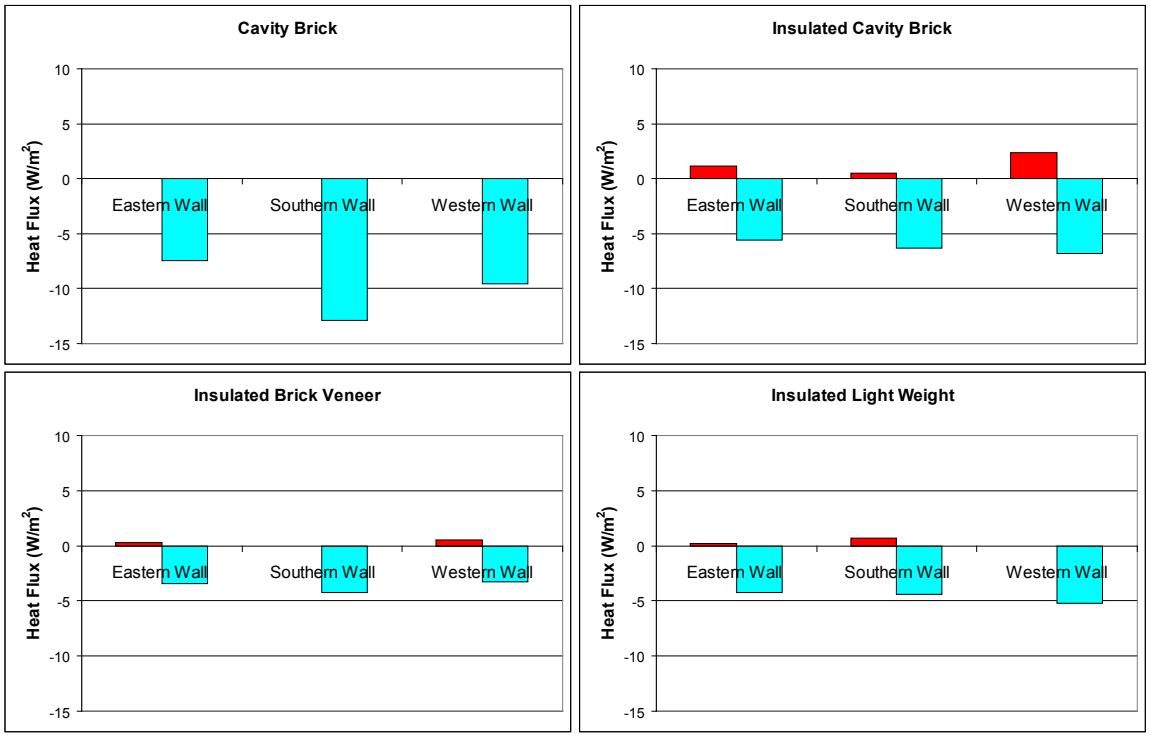

Figure 5.15 Total energy envelopes for internal surfaces, 2 week period in May, 2007

From the total energy envelopes it is evident that for all modules heat predominately flowed out from the internal space. This was a result of the high solar gain and cool external temperatures. However it was the time of day in which the heat flow direction occurred which had the greatest impact on the internal temperatures. The internal wall heat movements for a three day period in May 2007 are shown in Figures 5.16, 5.17, and 5.18.

The CB module provided the most cooling effect of all modules as seen by the heat flux envelope where a large amount of heat flowed out of the module but little or no heat was released back into the room from the walls. There was strong absorption during the day which effectively countered the high solar gain through the window. Heat tended to flow into the cavity due to the low cavity temperature, though the magnitude of this loss was reduced at night due to the decrease in internal temperature and solar ingress. The CB module's minimum nightly temperatures were similar to the InsLW module.

In comparison to the InsCB, the InsLW module had slightly less heat loss out of the walling envelope. However it was the time during the day in which the heat was lost that was critical to the performance of the modules. The InsCB module released heat into the room at night whereas at the same time the InsLW module consistently lost heat from all walls. Also due to the lack of thermal mass there was also little absorption of heat during the day by the InsLW internal wall surfaces to counter the solar gain. As a result the InsLW module exhibited high temperatures during the day and low temperatures at night, giving it the highest diurnal swing of all the modules.

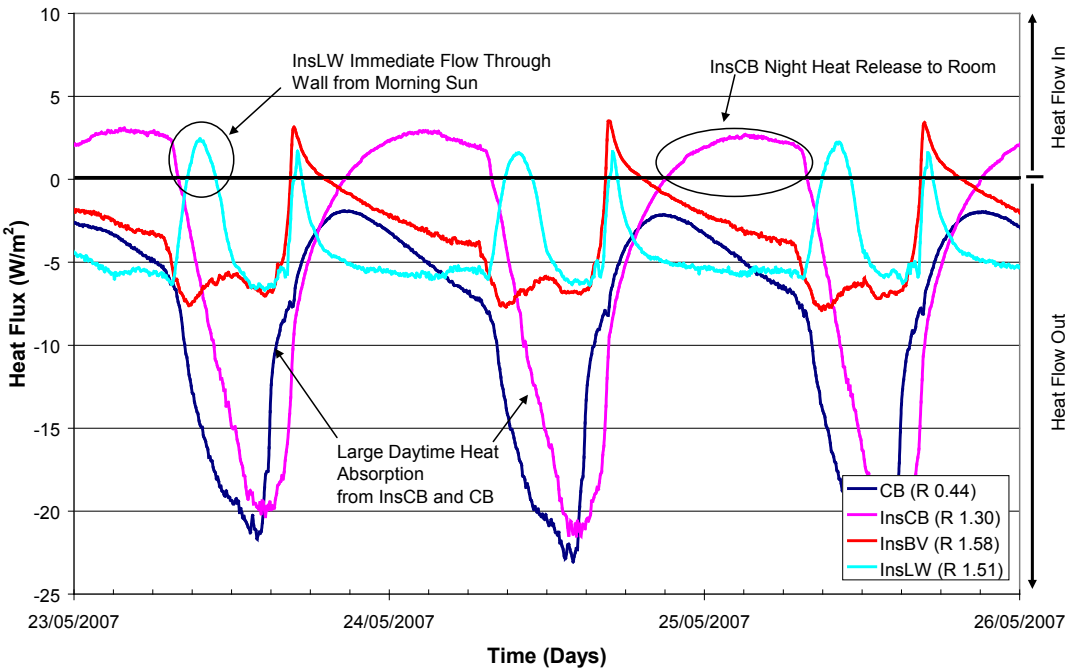

Figure 5.16 Eastern walls internal surface heat fluxes for three days in May, 2007

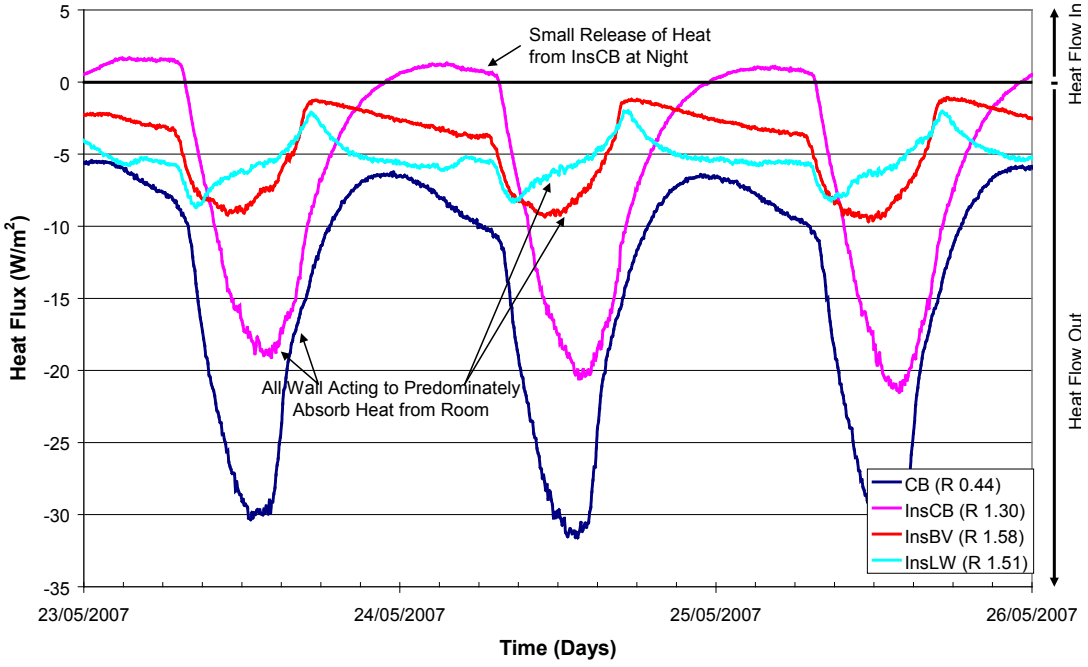

Figure 5.17 Southern walls internal surface heat fluxes for three days in May, 2007

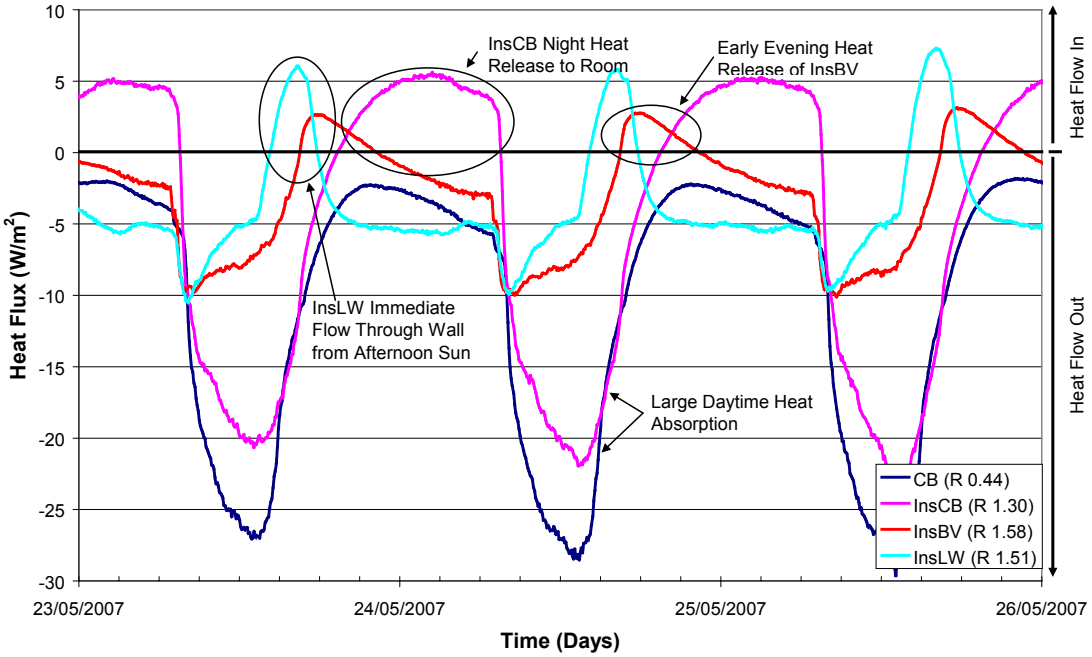

Figure 5.18 Western walls internal surface heat fluxes for three days in May, 2007

Due to cavity insulation, the InsCB module did not suffer the heat loss through the walling system into the cavity as was observed for the CB module. Due to the internal thermal mass, heat was mostly removed from the room during the day, thus countering the solar gain. The southern and western walls of the InsCB module had much less outgoing heat than its CB counterparts whereas the eastern wall had slightly less loss for InsCB. As a result of this, the InsCB module had higher daytime temperatures than its uninsulated counterpart. The other significant factor was the night time release of heat back into the room by the InsCB module, which was far greater than for all other modules. The combination of internal thermal mass and cavity insulation thus created the most stable internal temperature of all modules and provided ideal solar passive performance.

The InsBV behaved similarly to the InsLW, however there was a reduced outward flow of heat through the walls during the night which resulted in marginally warmer temperatures at night. This was directly due to the external veneer of brickwork.

5.4. Artificially Controlled Internal Conditions

5.4.1. Introduction

This series of tests were performed to assess the performance of the various walling systems under internally controlled conditions. By maintaining the interior of each module within a given temperature range the energy demands as a result of each walling system could be assessed. The air-conditioning system to control the temperature within each module was a commercial fan unit consisting of a chilled water heat exchanger and a resistive heat element connected to ductwork (a more detailed description is given in Section 3.3). The cooling energy was measured by monitoring the flow rate and the temperature rise of the chilled water after it passed through a heat exchanger. Heating energy was measured directly using the controller output to the current valve which switched the heater element on and off. The fans were 400W units and the heat generated by this unit was added to the energy calculation. Calibration of the cooling and heating system was performed for each module. The energy was calculated as a 'net' value representing the energy required to maintain the module within the set comfort levels.

The comfort levels were assessed on the basis of lower and upper internal temperatures set at 18°C and 24°C respectively. The systems were programmed to maintain this defined internal temperature range by a 'hysteresis' type cycle. Heating was activated when the internal air temperature fell below 18ºC and continued until 20ºC was reached at which point the heater was turned 'off'. The building would always "free-float" between 20-22°C with cooling being activated at 24ºC and continuing until 22ºC was attained.

The system operated by determining the average temperature of two thermostats located on the southern and western walls, situated so as to not receive any direct solar radiation.

5.4.2. Energy Demands of the Four Modules in October 2007

The following results for the CB, InsCB, InsBV, and InsLW modules were obtained from the month of October 2007 which represented late spring conditions consisting of cool nights and relatively warm days. Prior to this observation period, the modules were run under "controlled conditions" for a period of three weeks to minimise any influence from the slab-on-ground and module thermal history. For this period the curtains were also closed at night (Sugo et al., 2008).

Figure 5.19 shows the external/internal air temperatures for 3 days in late September/early October. It can be observed that there were times when only the InsLW and InsBV modules required additional heating at night or cooling during the day whilst at other times, under more extreme conditions at above 30ºC, all modules required cooling.

Each observed week showed a consistent pattern, with the InsLW module having a more frequent and higher cooling demand than all other modules. The InsLW and InsBV modules also required heating at times, reflecting the lack of internal thermal mass in reducing diurnal swings. At this time of year the high external diurnal temperature swings with a 'comfortable' mean external temperature combined with moderate solar ingress were ideal conditions for the passive contribution of internal thermal mass.

The total energy demand for the month of October for each of the modules is presented in Figure 5.20 and confirms the greater need for heating and cooling energy for the InsLW and InsBV modules.

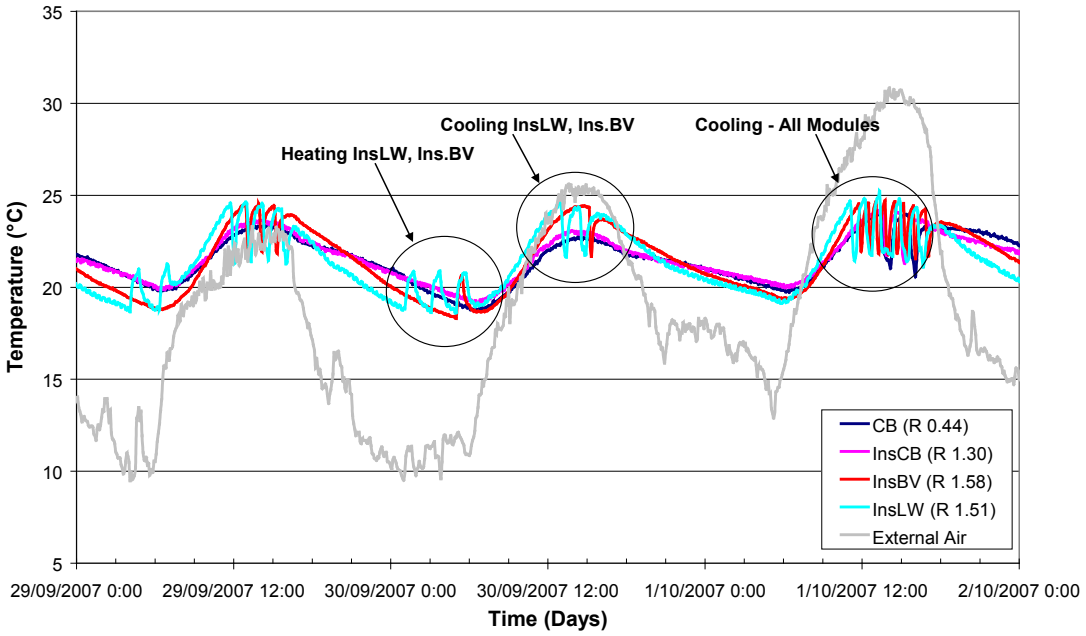

Figure 5.19 Modules under controlled conditions, August/ October 2007

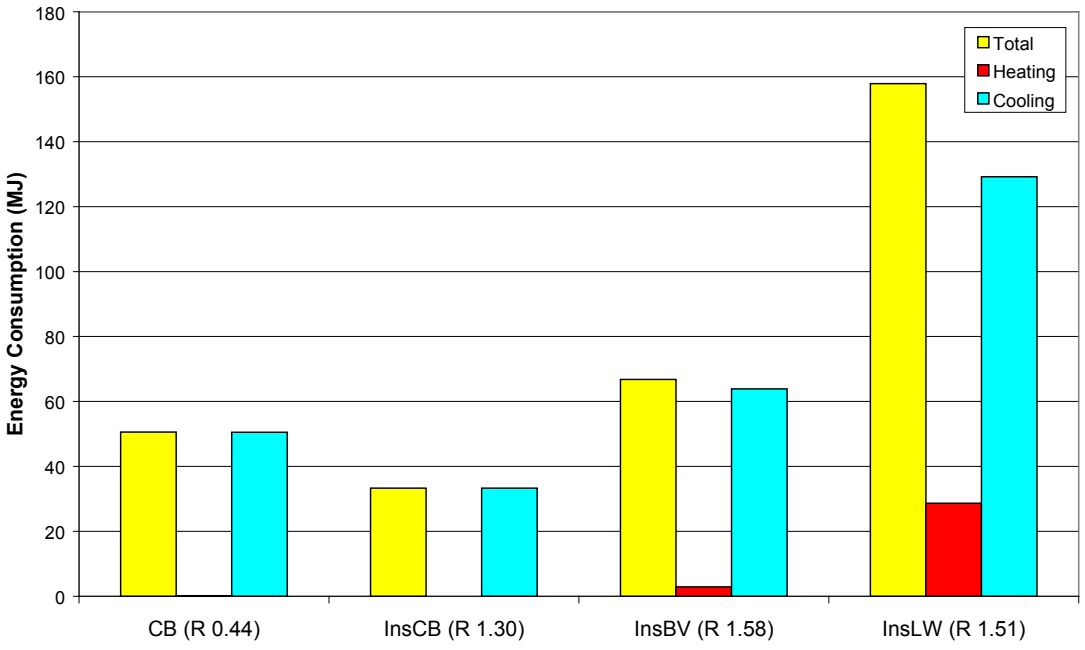

Figure 5.20 Total energy consumption, October 2007

For the InsLW module, there was generally a direct correlation between heating or cooling energy demand and external temperature, with the response of this module (with no thermal mass) directly related to the weather conditions. This was not the case for the other modules. For these weather conditions the CB and InsCB modules required limited cooling and no heating.

The favourable energy values for the CB and InsCB modules provide strong evidence for the benefits of thermal mass under “controlled” conditions since the InsLW module required a greater amount of heating/ cooling energy despite its higher R-value. The difference in energy demand for these two walling systems

would therefore be due to the presence of internal thermal mass and to a lesser extent, the external mass. Note that under these weather conditions, the CB (R 0.44) module with the lowest R-Value performed similarly to the InsCB (R 1.30) module and required far less energy than the InsLW (R 1.51) construction.

A summary of energy demand and external air conditions over the 4 week period is presented in Table 5.4. Each successive week in the observation period showed a consistent pattern with the InsLW module having a more frequent and higher cooling demand than the InsBV module, with the CB and InsCB modules being the lowest. The LW and InsBV modules also required heating at times.

Table 5.4 Summary of the cooling/heating demands for October 2007

Week Ending	Energy Usage (MJ)											
	InsLW			InsBV			InsCB			CB		
	Heat	Cool	Total	Heat	Cool	Total	Heat	Cool	Total	Heat	Cool	Total
4/10/2007	28.7	129.2	157.9	2.9	63.9	66.8	0.0	33.3	33.3	0.0	50.5	50.6
11/10/2007	23.4	71.8	95.2	0.0	28.9	28.9	0.0	7.1	7.1	0.0	6.0	6.0
18/10/2007	32.0	63.4	95.4	8.7	33.2	41.8	0.0	16.6	16.6	0.0	39.5	39.5
25/10/2007	15.3	86.5	101.8	2.4	49.7	52.1	0.0	22.3	22.3	0.0	40.8	40.8
Total Consuption	99.4	351.0	450.4	14.0	175.6	189.6	0.0	79.4	79.4	0.1	136.8	136.9
Weekly Average	**24.9**	**87.8**	**112.6**	**3.5**	**43.9**	**47.4**	**0.0**	**19.9**	**19.9**	**0.0**	**34.2**	**34.2**
Total Energy Ratio*	**5.7**			**2.4**			**1.0**			**1.7**		

*Relative to the InsCB module

5.4.3. Energy Demands of the Four Modules in July and August

The following results are for cold weather conditions and relate to a typical 6 week winter period from early July to mid-August 2008. All modules were fitted with carpet, and the curtains closed at night. The typical behaviour of the modules for a 3 day period under controlled conditions is shown in Figure 5.21, together with the corresponding variations in external temperature. There were less heating/cooling interventions for the CB and InsCB modules as a result of the internal thermal mass dampening the internal temperature fluctuations. Overall the weekly average energy use was of a significantly higher magnitude than for the previous October results (Page et al., 2009).

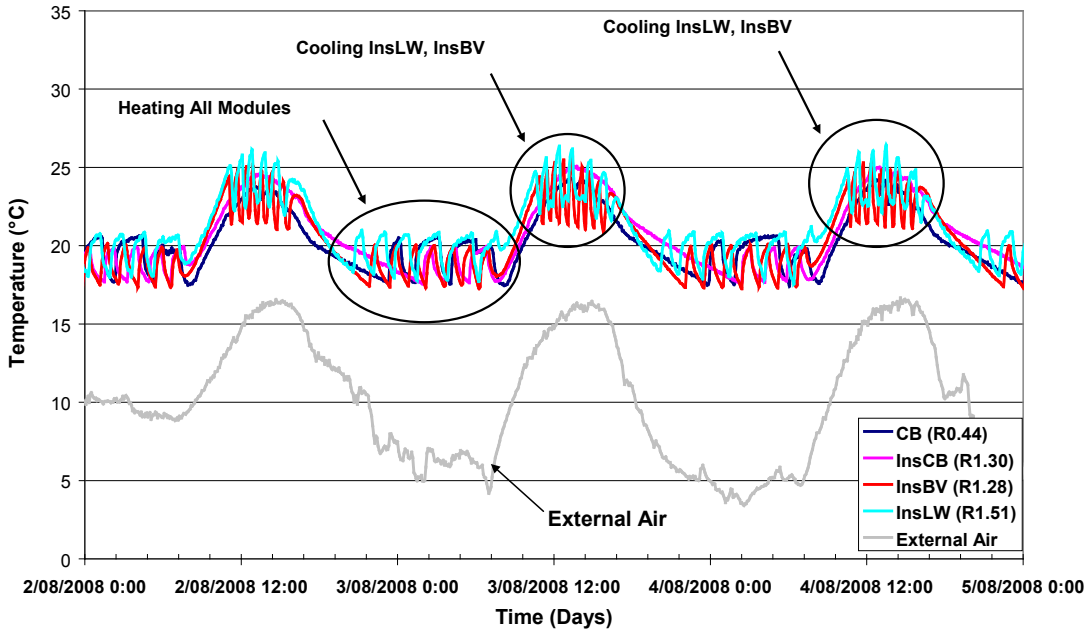

Figure 5.21 Modules under controlled conditions, August 2008

The total energy usage for the full 6 week period of the four modules is shown in Figure 5.22 and Table 5.5. The bulk of the energy consumption was for heating, however during the day, cooling was often required by both the InsLW and InsBV modules. This was due to the tendency of these modules to overheat from solar ingress through the opening in the northern wall. As the internal skin of the InsLW and InsBV providing no cooling ability it was necessary for the air conditioning system to compensate. The internal thermal mass of the InsCB and CB provided enough inherent absorption of the solar gain to not require additional cooling to make up the difference to keep temperatures from rising above the preset 24°C. This was also evident under the previously described free floating conditions. The winter sun was low and was therefore the primary driving factor for the behaviour of the modules.

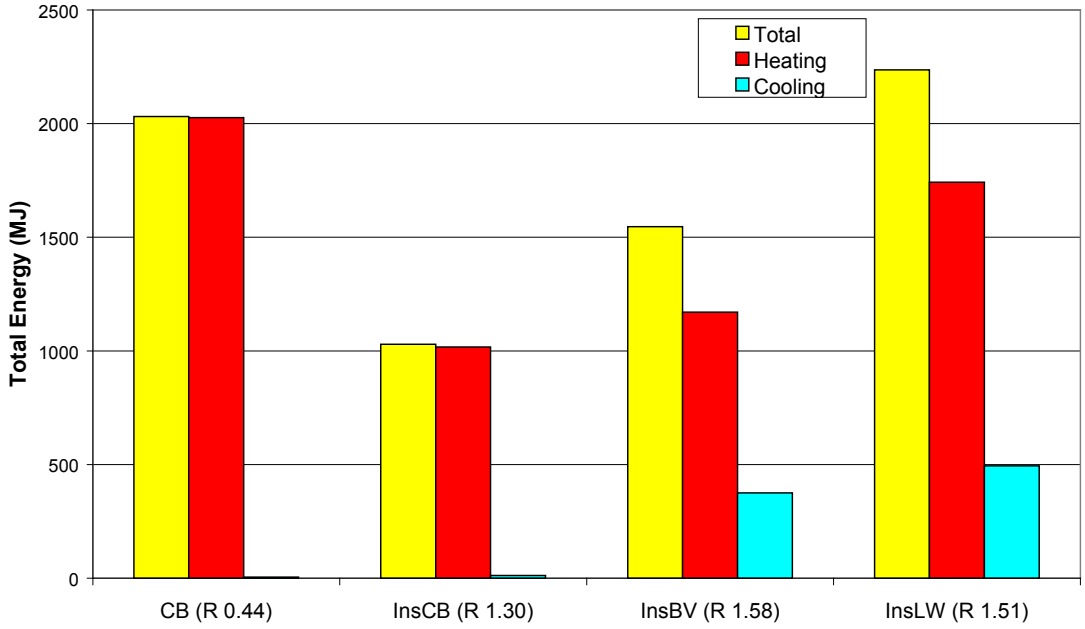

Figure 5.22 Total energy consumption, July/August 2008

Table 5.5 Summary of the cooling/heating demands for July/August, 2008

Week Ending	Energy Usage (MJ)											
	InsLW			InsBV			InsCB			CB		
	Heat	Cool	Total	Heat	Cool	Total	Heat	Cool	Total	Heat	Cool	Total
10/07/2008	244.0	62.5	306.5	156.5	42.6	199.1	117.4	0.0	117.4	273.4	0.0	273.4
17/07/2008	283.3	120.2	403.5	184.8	90.6	275.4	150.5	10.5	161.0	323.2	4.9	328.1
24/07/2008	255.5	84.2	339.7	174.8	69.9	244.8	128.6	1.7	130.3	288.0	0.0	288.0
31/07/2008	316.4	76.1	392.5	226.6	59.5	286.1	224.8	0.0	224.8	408.5	0.0	408.5
7/08/2008	294.7	87.7	382.4	194.2	63.9	258.1	163.1	0.0	163.1	319.0	0.0	319.0
14/08/2008	348.0	63.4	411.4	233.8	49.1	282.9	232.9	0.0	232.9	414.4	0.0	414.4
Total Consuption	1741.9	494.1	2236.0	1170.7	375.6	1546.4	1017.3	12.2	1029.5	2026.5	4.9	2031.4
Weekly Average	**290.3**	**82.4**	**372.7**	**195.1**	**62.6**	**257.7**	**169.6**	**2.0**	**171.6**	**337.8**	**0.8**	**338.6**
Heating Energy Ratio*	**1.7**			**1.2**			**1.0**			**2.0**		
Cooling Energy Ratio*	**40.6**			**30.8**			**1.0**			**0.4**		
Total Energy Ratio*	**2.2**			**1.5**			**1.0**			**2**		

*Relative to the InsCB module

It can be seen from Figure 5.22 and Table 5.5 that under cold weather conditions the InsCB module had the lowest energy requirements for both heating and cooling. In contrast to the heavy walling modules, the InsLW and to a lesser extent the InsBV module (without internal thermal mass) had limited capacity for self-regulation, with the heat flows being driven purely by the external conditions. The lack of internal thermal mass resulted in higher daytime temperatures and artificial cooling was required to offset the solar heat gain. Towards the end of the day internal temperatures dropped with the external conditions at a faster rate compared to the CB and InsCB as little heat was released back into the room from the walling system.

The primary basis for the superior performance of the InsCB module was the contribution of the internal brick skin. During the day, heating of the interior from the low winter sun was offset by the ability of the internal thermal mass of the CB and InsCB walls to absorb heat. This prevented the day-time overheating which was observed in the InsLW and InsBV modules.

From the surface heat flux movements shown in Figure 5.23, it can be seen that for the western wall, the heat stored in the internal skins of the CB and InsCB walls was released back into the room once the internal temperature dropped. All internal wall surfaces of the InsCB module released heat back into the room. The polystyrene insulation attached to the cavity side of the internal leaf promoted the flow of heat into the room rather than heat flowing through into the cooler cavity. The internal surfaces of all other modules continued to remove heat from the room (see for example, the heat flux movements for the eastern walls shown in Figure 5.24). The CB module suffered as it had no heat release back into the module from the eastern and southern walls. In this case, due to the lack of cavity insulation, the thermal mass had no resistive barrier between the cavity and the external environment and as a result, the artificially added heat was more easily transmitted through the wall.

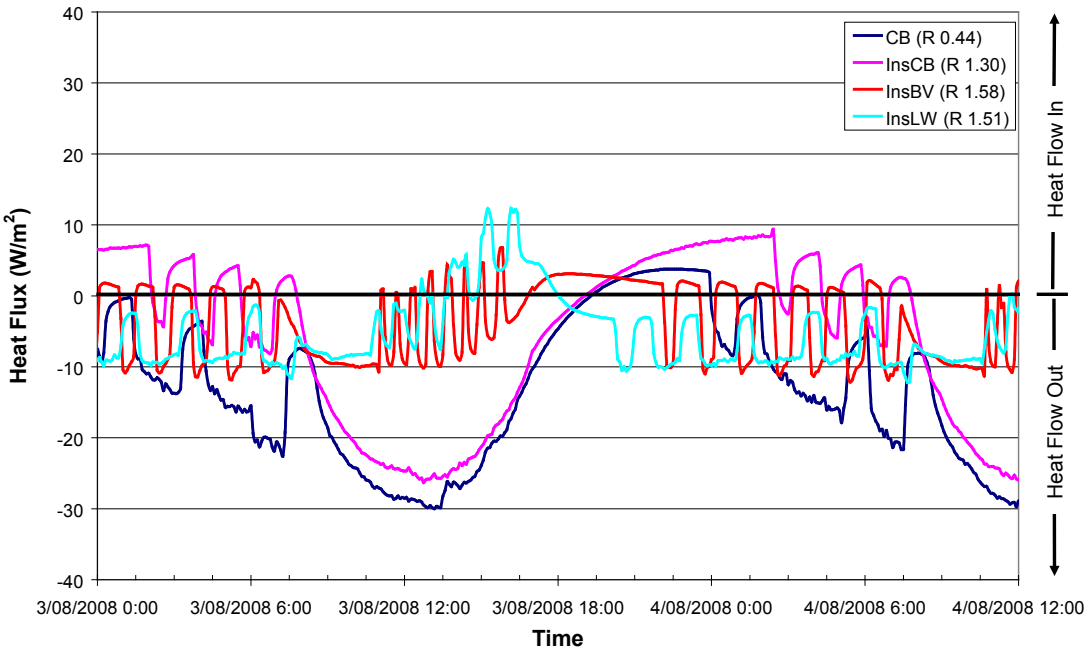

Figure 5.23 Western walls internal surface heat fluxes, August 2008

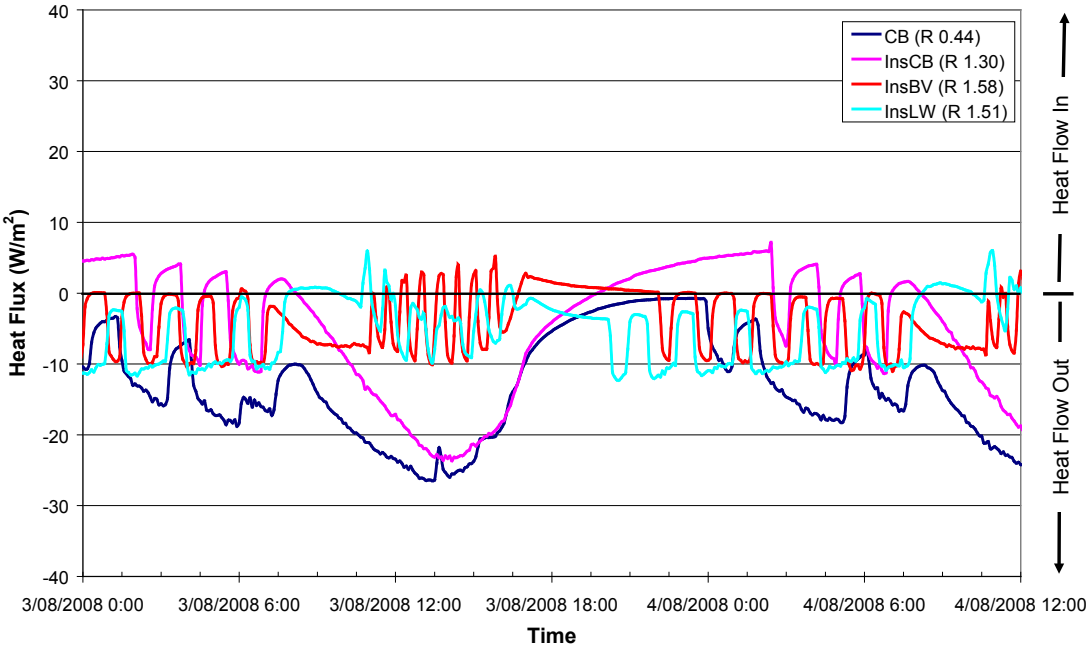

Figure 5.24 Eastern walls internal surface heat fluxes, August 2008

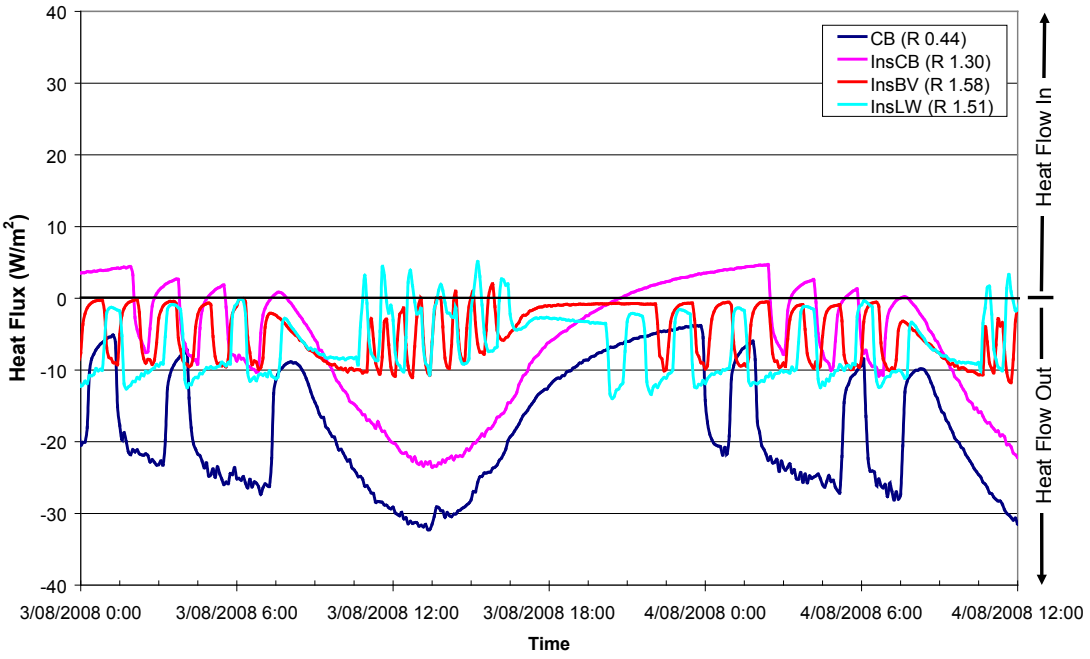

Figure 5.25 Southern walls internal surface heat fluxes, August 2008

The two alternative extreme cases of high thermal mass with no insulation (*CB*), and insulation with no thermal mass (*InsLW*), both required much higher energy consumption. Despite the InsLW module having an R-value 14% higher than the InsCB, the InsLW module required 117% more energy. Even the InsBV module, with an R-value 16% greater than the InsCB module used 50% more energy (reflecting the contribution of the thermal mass of the interior skin). It is clear that there is no direct correlation between building performance and wall R-value alone; the best solution lies with an appropriate combination of wall insulation and thermal mass.

5.5. 12 Month Parallel Observation Period for the CB, InsCB, InsBV and InsRBV modules, October 2008 to 2009

5.5.1. Overview

In the latter stages of the investigation the InsLW module was converted to reverse brick veneer (InsRBV) as seen in Table 3.2. This allowed a direct comparison of the performance of this relatively novel system with the other walling systems (CB, InsCB and InsBV). The decision was based on the results showing that of all the existing modules at the time insulated lightweight was the worst performing with the most undesirable thermal characteristics and the least effective in adhering to solar-passive design principles. The insulated lightweight module had the least desirable characteristics during free floating conditions with the highest temperatures during the day and the largest diurnal swing. Air conditioning results also showed high energy consumption.

A 12 month observation schedule was introduced to provide consistent experimental results under all seasonal conditions for both free floating and air conditioned states with no alteration of any other variable related to the modules.

Prior to the observation schedule commencing, all carpet and underlay was removed, as well as the screen doors on the north facing window assembly. The internal partition walls still remained. As described in Section 3.4 the InsBV and InsRBV modules contained partition walls which were timber stud frame, while the InsCB and CB module contained brick masonry partition walls. No ventilation took place over the 12 months of testing.

Ideally, data from 6 weeks of each season was to be obtained for both free floating and controlled conditions. However testing changeover required a period of stabilisation to remove or add thermal history due to the air conditioning. This produced a slight variation between the numbers of weeks tested for each season and moved the testing period to surround either side of the ideal mid season interval.

5.5.2. Free Floating Conditions

5.5.2.1. Summer

5.5.2.1.1. Temperature Trends

An insight into the comparative behaviour of the various walling systems can be obtained by studying the internal temperature trends over the full data collection period. The summer period for data collection consisted of a 5 week period of 34 days, with a 1 week prior settling after the spring air conditioning cycle. With regards to the weather, a total 23 of the 34 days peaked at over 30°C, with the average night temperature being 16.5°C. Conditions varied from an average daily maximum temperature of 30°C to several cooler periods when temperatures peaked at between 20-25°C. The temperature profiles for 1 week are shown in Figure 5.26.

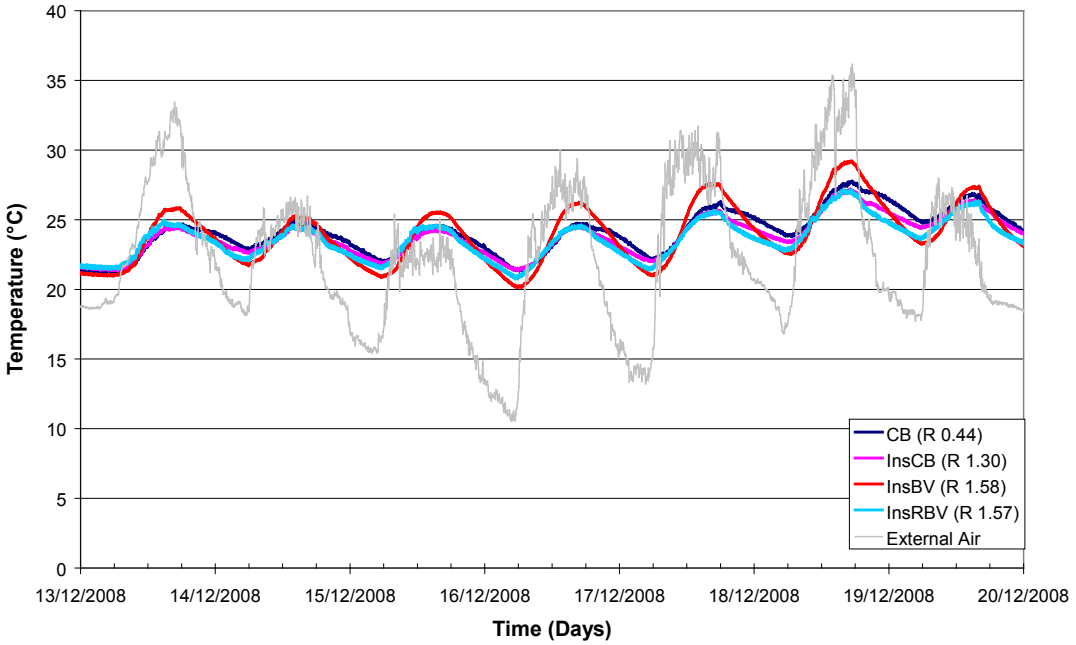

Figure 5.26 Temperature profiles for four modules, December 2008

The mean internal temperatures together with standard deviations calculated from the entire data collection period of 5 weeks are shown in Figure 5.27. The total mean internal temperatures do not recognise the daily temperature oscillation as a response to the external weather conditions, therefore the standard deviation was also considered. The calculated standard deviations are the average standard deviation of all 34 days and represent the internal diurnal swing experienced as a result of the external driving factors.

The InsBV and InsCB modules both had identical mean temperatures yet their behaviour to the external conditions was significantly different with regards to the diurnal swing which demonstrates why mean temperature cannot be solely considered. The InsBV module exhibited a much larger temperature oscillation about the mean than the modules with internal thermal mass, having almost double the standard deviation of InsCB and easily peaking to the highest daily temperature of all modules. The high diurnal swing within the InsBV module would result in a greatly reduced level of thermal comfort. The modules with internal mass had more stable internal temperatures. All standard deviations for the InsCB, CB and InsRBV modules were similar. The InsCB module had the lowest standard deviation as a result of the combination of the internal and external thermal mass as well as the cavity insulation. The CB module also had a lower standard deviation than the InsRBV module due to the presence of the external thermal mass. Thermal mass provided a definite dampening effect on the internal temperature swing.

The CB module had the highest mean temperature. This was primarily due to a combination of a prolonged higher temperature at night and the higher peak temperatures during the day compared to the InsCB and InsRBV modules. The InsRBV module was consistently cooler than all modules except for the overnight minima when the InsBV module temperature rapidly reduced. The internal temperature of the InsRBV module dropped more rapidly than both the InsCB and CB modules as it lacked the external skin of thermal mass, accounting for the higher standard deviation.

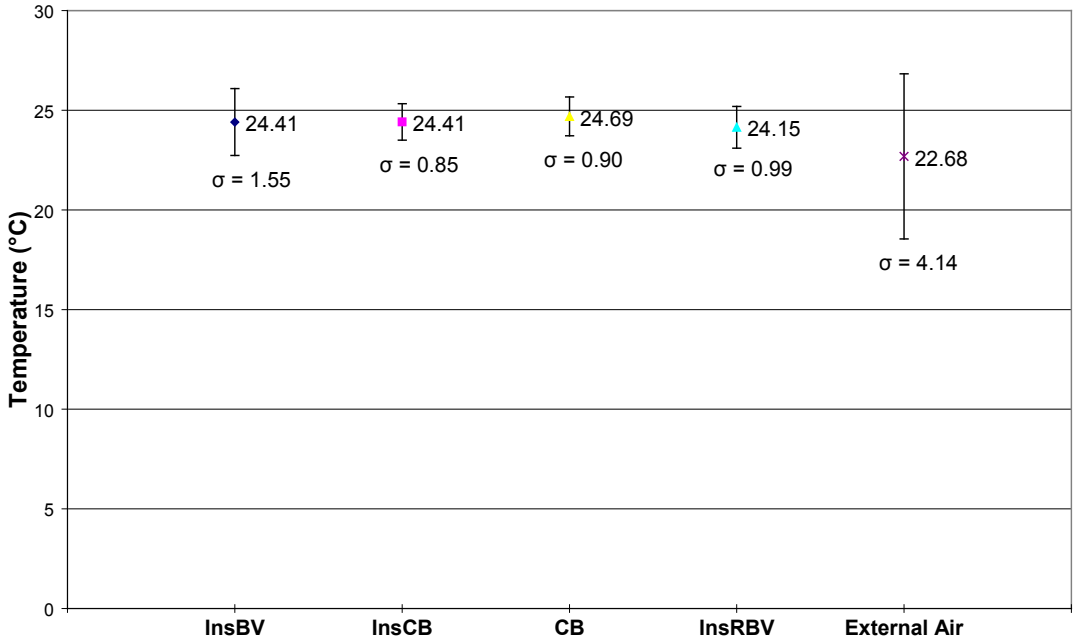

Figure 5.27 Mean module temperatures and standard deviations – summer 2008-2009

The lack of internal thermal mass in the InsBV module leads to the internal temperature being less stable than the other modules. The InsBV module overheated during the day and rapidly lost temperature at night. The rapid evening loss of heat may be a positive for systems with low internal mass in hot conditions but it is highly questionable as to whether this benefit is sufficient given the high internal daytime air temperature.

5.5.2.1.2. Heat Flow Analysis

The measured heat fluxes for the perimeter walls give a good indication of module behaviour. As with all thermal systems the modules responded in such a manner to reach equilibrium with the driving force. The time of this process depends on the wall construction type, with high mass materials such as the brick masonry walls responding at a slower rate compared to the lightweight construction and bulk insulation. Energy envelopes were split into day and night in order to assess the inherent heating and cooling mechanisms of the constructions individually. In the heat flux study "day" was defined as the period when the horizontal plane solar radiation (measured on the roof) was greater than 10W/m^2. Heat fluxes defined as "Night" cover the remainder of the 24 hour period.

Average Daily Heat Flux

The average heat flux during the day, both into and out of the modules for the western, southern and eastern walls is shown in Figure 5.28. For summer conditions it was desirable for the module to remove as much heat as possible from the internal space with minimum gain into the room, however this effect was not as strongly observed during summer due to the high solar angle.

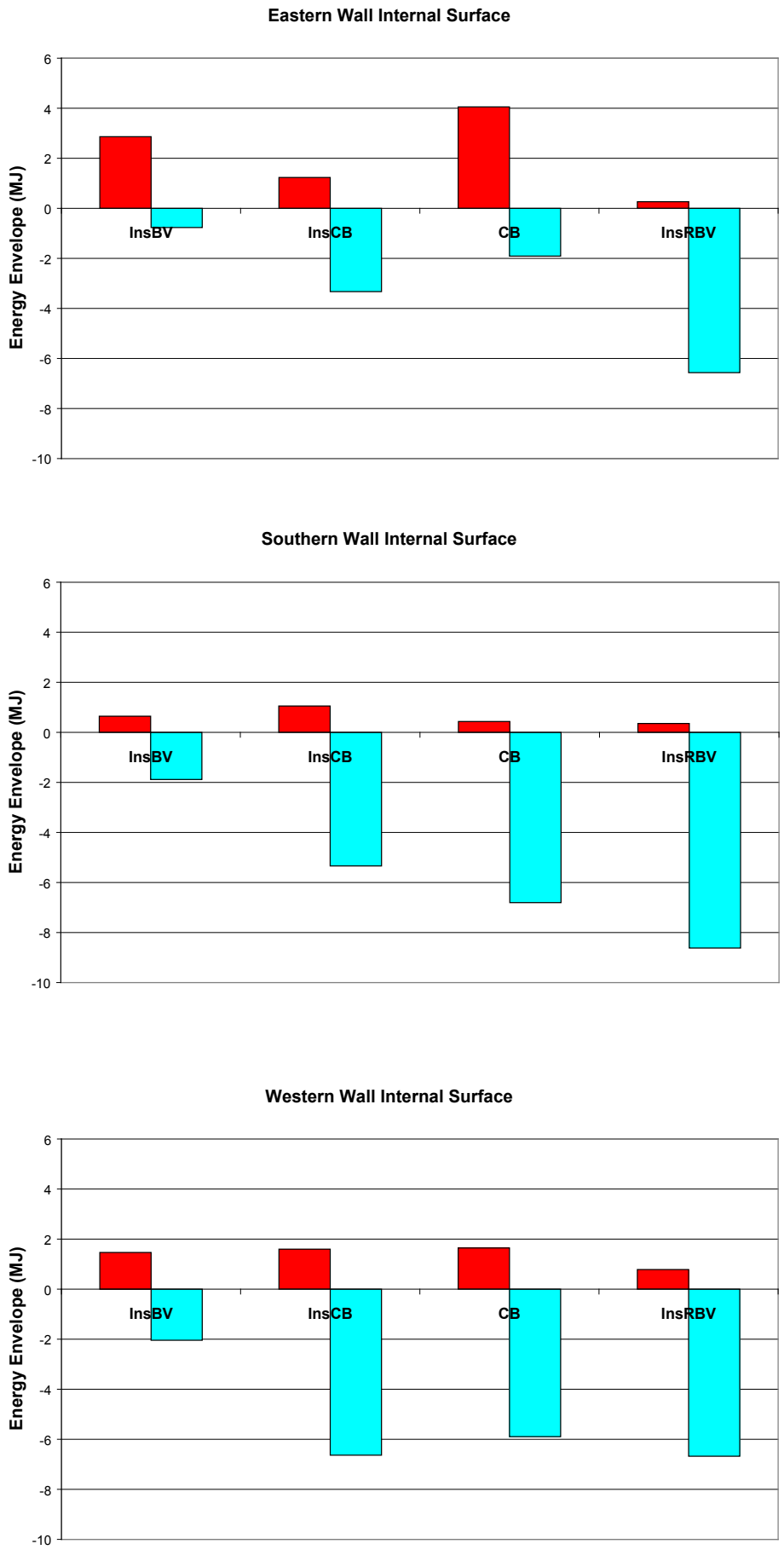

Figure 5.28 Heat absorbed and released over the "day" period – summer 2008-2009

The first key observation was the lack of heat absorbed by all perimeter walls in the InsBV module compared to the remaining modules which had internal skins incorporating thermal mass. This lack of internal thermal mass was responsible for the internal temperatures during the day being significantly higher in the InsBV module than the other modules as there was less absorption by the walls to compensate for the high external temperatures and the solar gain through the window.

Apart from the heat entering through the northern window a large portion of heat also entered the InsBV and CB modules through the eastern wall during the day. The lack of insulation in the CB walling system also resulted in a higher flow of heat into the room from the early morning sun which was incident on the eastern wall; this initial flow occurred at a later time than that for the InsBV module due to the thermal lag of the wall but continued for a longer period of time, from 9am to midnight. However it was not the addition of heat from the wall that caused the overheating in the InsBV, rather it was the lack of the ability of the module to remove the incoming heat from the solar gain. The eastern wall inward flow was small in contrast to the solar gain through the north facing window.

The eastern wall of the InsRBV module provided a great deal of cooling to the module compared to the other constructions, with over double the absorption seen for the InsCB module. This could account in part for the lower daily internal temperature of the InsRBV module. The southern wall of the InsRBV module also provided increased cooling ability compared to the other modules.

For the western walls, all the modules with interior brickwork skins behaved in a similar fashion during the day, removing heat from the room. The InsCB and CB modules however released more into the room than the InsRBV, as a result of the contribution of the external brickwork skin of those modules.

Average Nightly Heat Flux

The monitored average nightly heat fluxes relate to the response of the modules to the decreasing internal temperature driven by the external conditions. "*Night*" was defined as the period when the horizontal plane solar radiation was less than 10W/m^2. The heat flux for the eastern, southern and western internal wall surfaces is shown in Figure 5.29. It can be seen that during this period all walls predominately released heat back into the room due to the reduction in internal temperature.

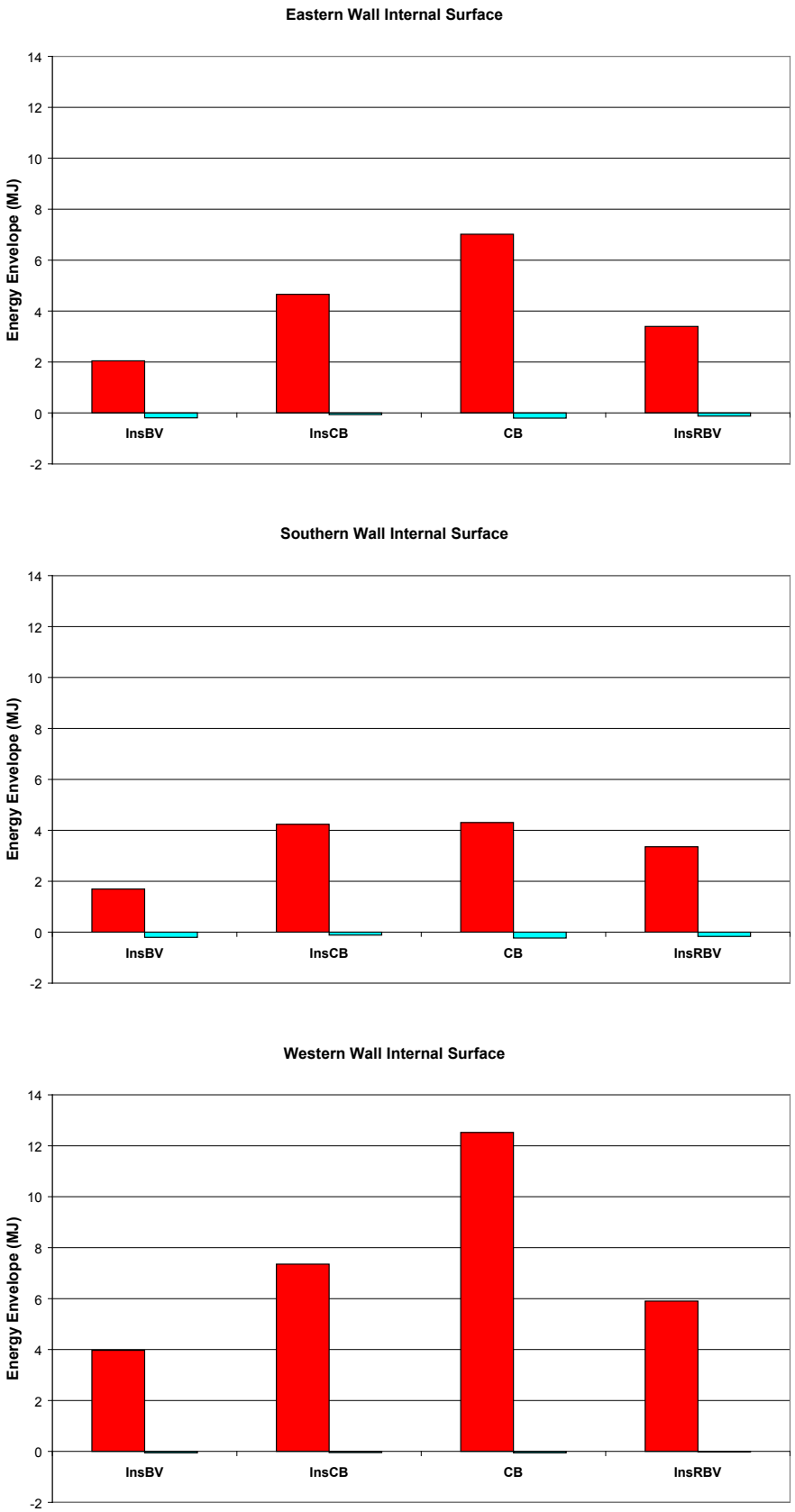

Figure 5.29 Heat absorbed and released over the "night" period – summer 2008-2009

As conditions cooled, heat from the wall of the CB module was released at a faster rate than that for the InsCB and InsRBV modules. This rate of heat released then decreased through the evening as the heat storage became exhausted. The large amount of heat released from the walls by the CB module resulted from the contribution of the external as well as the internal brick skin due to absence of cavity insulation.

As a result of the large flow of heat into the CB module it maintained a higher night mean temperature. The InsBV module released the least amount of heat into the room as the internal skin of the perimeter walls contained little thermal mass. As a result, this module had the most rapid internal temperature drop as it responded readily to the external conditions.

Both the InsBV and CB modules had characteristics which make them less desirable constructions under these conditions. The InsCB module was slightly warmer than the InsRBV module as it had slightly more heat release into the module. However this resulted in a smaller standard deviation and therefore more stable internal conditions. For these summer conditions, insulation in the eastern and western walls plus internal thermal mass is beneficial.

5.5.2.2. Winter

5.5.2.2.1. Temperature Trends

The external temperature profile for the 5 week winter period is shown in Figure 5.30. Early in the observation period external temperatures were moderate but became cooler in the later weeks, with overnight minima approaching 5°C.

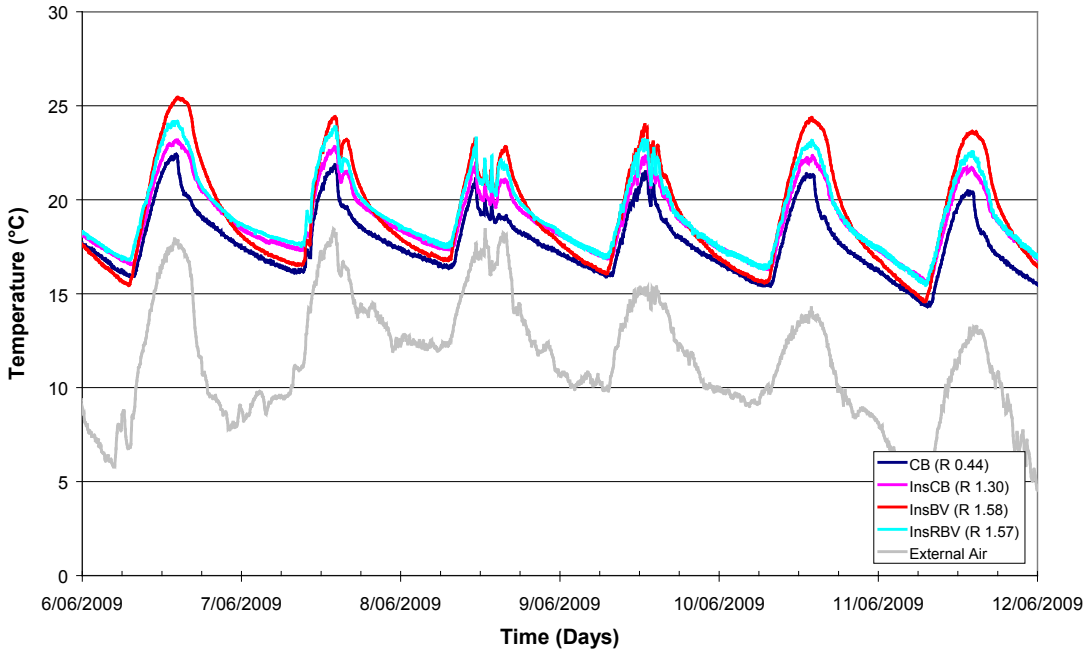

Figure 5.30 Temperature profiles for four modules – winter 2009

The mean internal temperatures and standard deviations for the entire data collection period of 5 weeks for each of the modules and external air temperature are shown in Figure 5.31.

As can be seen from Figure 5.31, all module internal temperatures were significantly higher than the external temperature due to the solar gain through the northern window. The CB module exhibited the lowest average mean temperature of all modules. The uninsulated cavity of the CB module remained cool promoting a continual outward flow of heat. The CB also had the smallest standard deviation and therefore diurnal swing.

The InsRBV module had the highest mean temperatures of all the modules. The mean temperature of the InsBV was higher than both the InsCB and CB modules, but again the InsBV module had the largest standard deviation as a result of the lack of internal thermal mass.

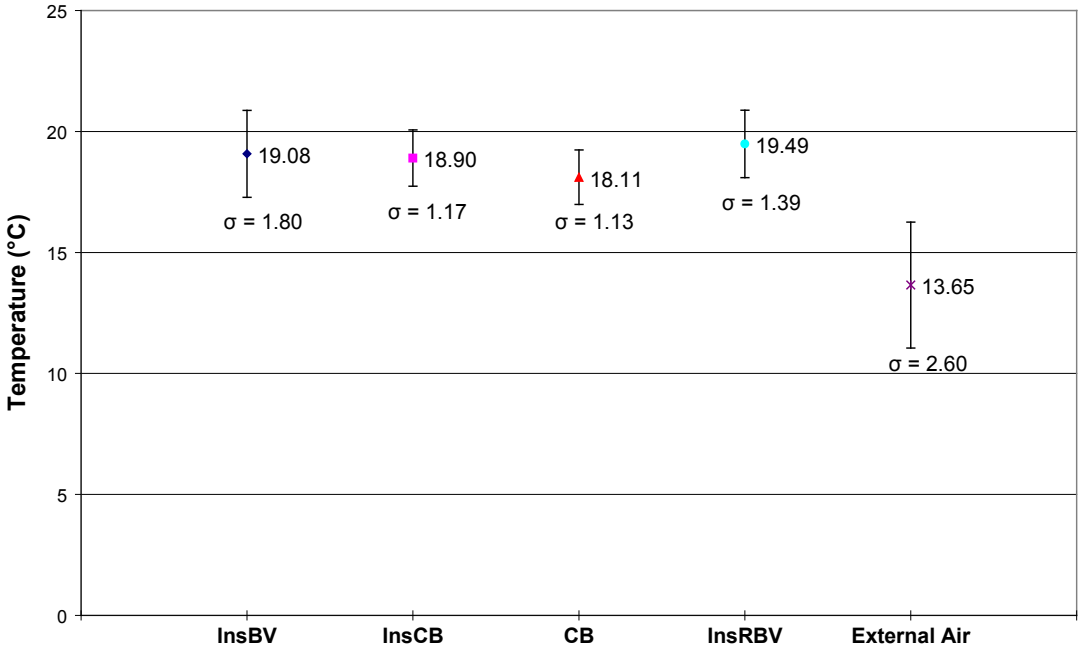

Figure 5.31 Mean module temperatures and standard deviations – winter 2009

The InsCB and CB modules had similar standard deviations and identical temperature trends with only a temperature offset differentiating the two. The InsRBV module had a larger standard deviation than both CB and InsCB due to the absence of a heavy external skin (and lack of thermal mass).

5.5.2.2.2. Heat Flow Analysis

The heat flow for the eastern, southern and western walls for each of the four modules are shown in Figure 5.32 and 5.33 respectively for the “day” and “night” periods. It is evident that there was a continual heat flow outward during the day from all four modules, with the magnitude varying with construction type. The rapid heating of the InsBV module, as seen previously, may be beneficial during the day in winter, but the temperature increase was the largest which also results in the least thermal stability. A corresponding rapid loss of temperature took place into the evening as no heat was released into the room from the insulated timber stud frame.

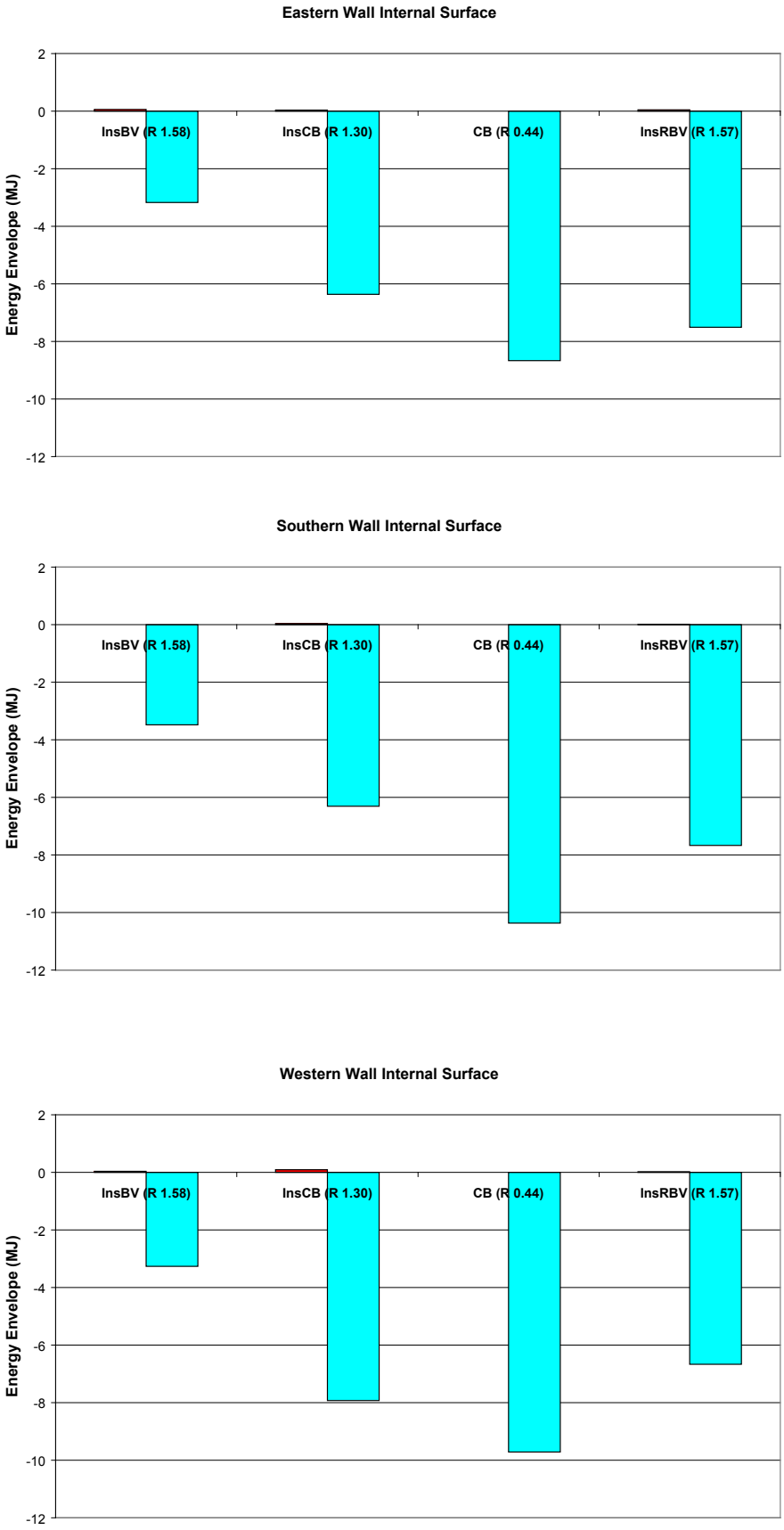

Figure 5.32 Heat absorbed and released over "*day*" period – winter 2009

As can be seen from Figure 5.33 the CB module continued to lose heat from the internal space throughout

the night. There was a slight addition of heat back into the room from the western wall, but this was insignificant compared to the loss. This was due to the lack of insulation in the cavity. Cavity temperatures and cavity surfaces of the brick remained cool promoting an outward flow from the internal space.

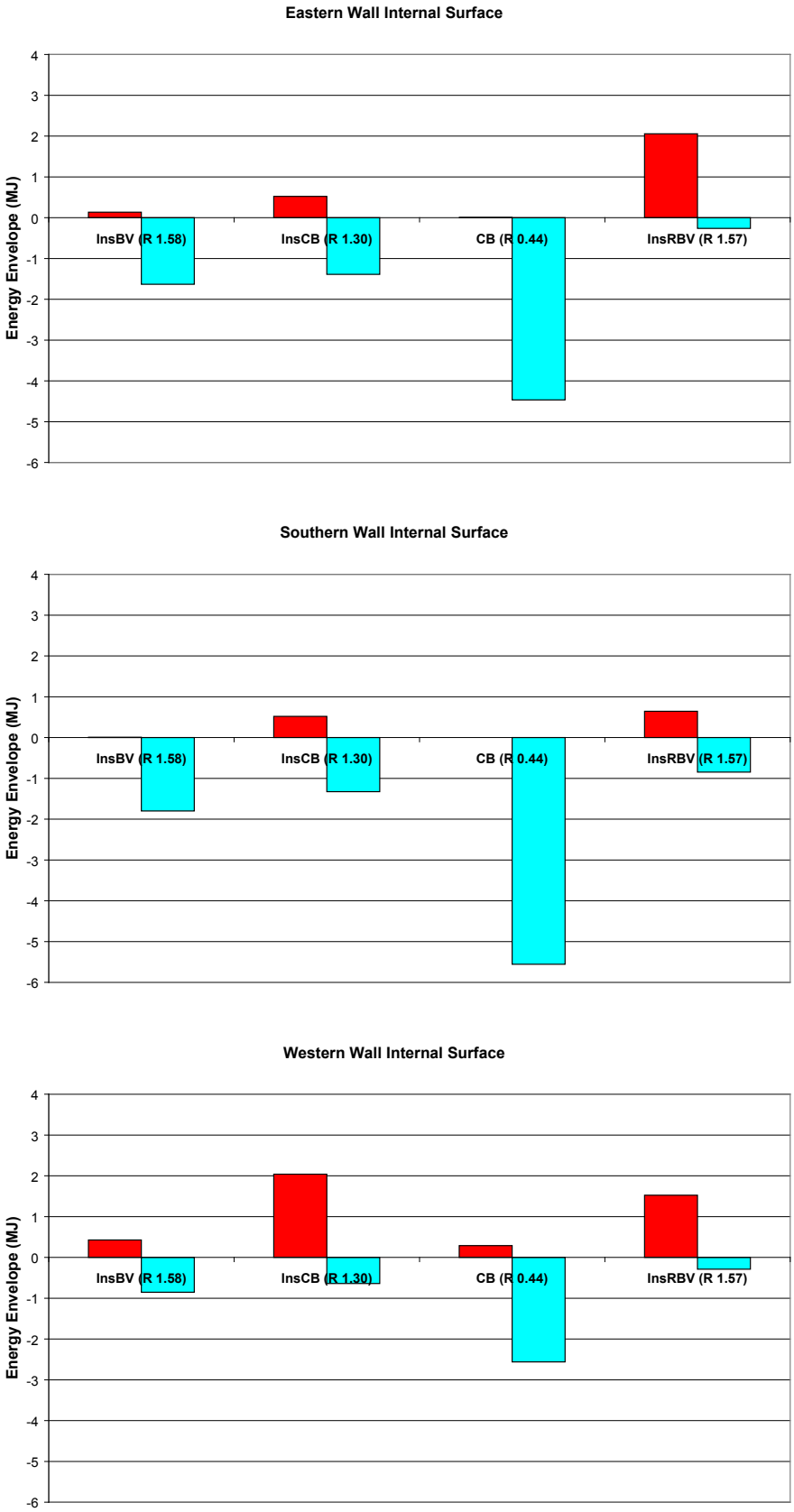

Figure 5.33 Heat absorbed and released over "night" period – winter 2009

There was almost no heat released back into the room at night from the InsBV module due to the lack of internal thermal mass in the walling system. The CB module absorbed heat from the room during both the day and night resulting in the coolest temperatures. The InsRBV and InsCB modules performed quite well under these conditions, with the greatest amount of heat released back into the internal space at night and with a lesser magnitude of heat loss during the day compared to the CB module.

Differences did arise between the InsRBV and InsCB modules in terms of the heat flow back into the internal space from the eastern wall. The InsRBV module released a much larger quantity of heat into the room, whereas the InsCB module lost more heat through the eastern wall at night than was transmitted into the room.

The lightweight external skin of the InsRBV module during the day allowed more heat to flow from the incident solar radiation on the external surface of the wall through the insulation to the cavity side of the internal brick skin. The lower time lag in this case was a benefit. For the InsCB module the external brick skin slowed the heat flow until after the sun had moved from the surface, the insulation then lowered this small heat flow even further, thus maintaining a cooler temperature on the cavity surface of the internal brickwork skin. This limited the capacity of the InsCB eastern wall to transmit heat back into the room as the temperatures dropped. Despite this there was little discernible difference between the InsCB and InsRBV internal temperatures at night.

5.5.2.3. Autumn

5.5.2.3.1. Temperature Trends

The autumn period consisted of a total of 4 weeks of data collection, with 1 week prior settling period after the summer air conditioning cycle. The weather was mostly cloudy with few clear days. Maximum temperatures were warm, ranging predominately between 25°C and 30°C (see Figure 5.34). Night time minima had greater variation ranging from cool nights close to 10°C to warmer temperatures of 20°C. External temperatures were lower than summer by 1.68°C on average, however the northern wall radiation was nearly three times greater than in summer due to the lower angle of the sun. This resulted in larger solar ingress into the modules and higher internal temperatures than summer, despite the external temperatures being lower.

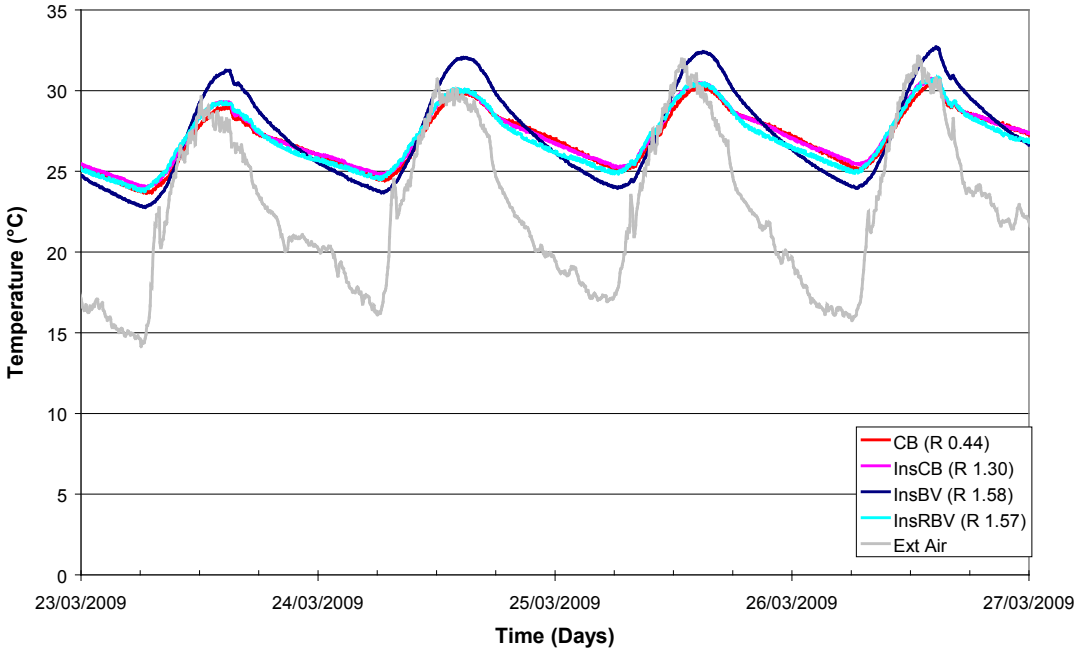

Figure 5.34 Module temperature profiles for the four week autumn period

The mean internal temperature calculated for the entire data collection period of 4 weeks is given in Figure 5.35. The InsBV module, as seen during other time periods had the highest peak temperatures and a larger rate of temperature fluctuation with the lowest minimum temperatures during the night.

The InsCB and CB modules' trends were almost identical, with the CB module having slightly lower temperatures overall. The InsRBV module followed the same trend as InsCB and CB which is consistent with the presence of internal thermal mass. During the morning and up to the peak temperature during the day, the InsRBV behaviour tended to be similar to the InsCB module. However during the afternoon and with the night temperature decrease, the drop in temperature occurred at a slightly faster rate resulting in a marginally cooler internal temperature than both InsCB and CB for most of the night.

Compared to summer, all autumn standard deviations were higher due to a combination of the higher solar gain and lower external temperatures. The InsBV module was the most adversely affected with an increase of 0.49 as it lacked internal thermal mass. This increase was 29% greater than that for the standard deviation increase of the InsCB module. The high resistance of the internal skin of the walls without thermal mass resulted in the solar heat gain staying within the InsBV module. Night time loss through the window was then not countered by a release of absorbed heat and a large diurnal swing resulted.

The CB module was the least affected by the increased solar gain from summer to autumn. The standard deviation of the InsCB and CB modules were similar, however the temperatures varied due to the tendency of the heat in the CB wall encountering less resistance in the uninsulated cavity, allowing greater outward heat flow.

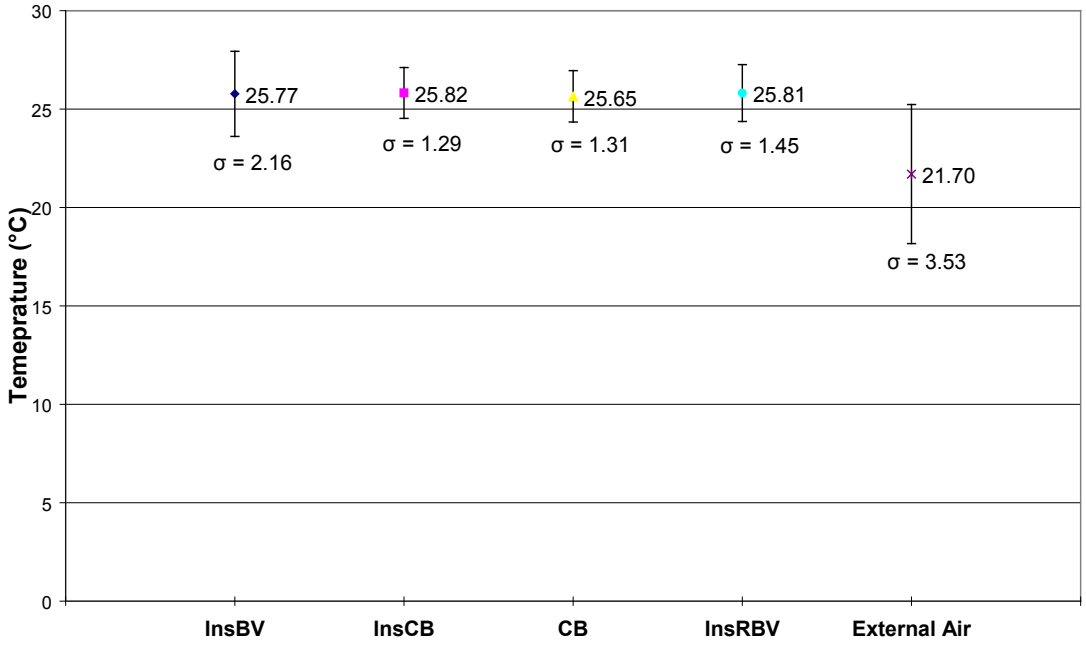

Figure 5.35 Mean module temperatures and standard deviations – autumn 2009

5.5.2.3.2. Heat Flow Analysis

The average heat flux for the "day" period is shown in Figure 5.36. Compared to summer, the heat fluxes for autumn during the day are much greater as a result of the higher solar gain. It can be seen that the CB module responded most strongly with large increases in heat absorbed by the walls. The southern wall provided the most cooling benefit and the CB western wall provided marginally higher absorption than the other modules. The CB eastern wall had similar behaviour as for the InsCB module.

The InsRBV module's heat loss through the eastern wall was greater than for the InsCB module, indicating that it provides an increased cooling effect; this is also consistent with other results through the year. The western walls of the InsCB and CB modules were the predominant source of heat loss for those modules during the day.

The lack of absorption by all walls on the InsBV module was again responsible for the overheating which is observed in the general temperature trend. The internal stud frame wall with insulation acts to hold heat in the room rather than remove it. A larger portion of heat compared to the other modules also entered the room through the eastern wall.

For all systems, the predominant source of heat absorption through the day was the southern wall. The CB had by far the largest absorption through the southern wall due to the lack of insulation in the cavity which promoted a continual high rate of outward flow, and this was certainly beneficial in regards to maintaining the cooler internal temperatures. The highest outward flow for the western wall was also observed for the CB module. Overall the CB walling systems was the most effective in maintaining lower internal temperatures by countering the solar gain.

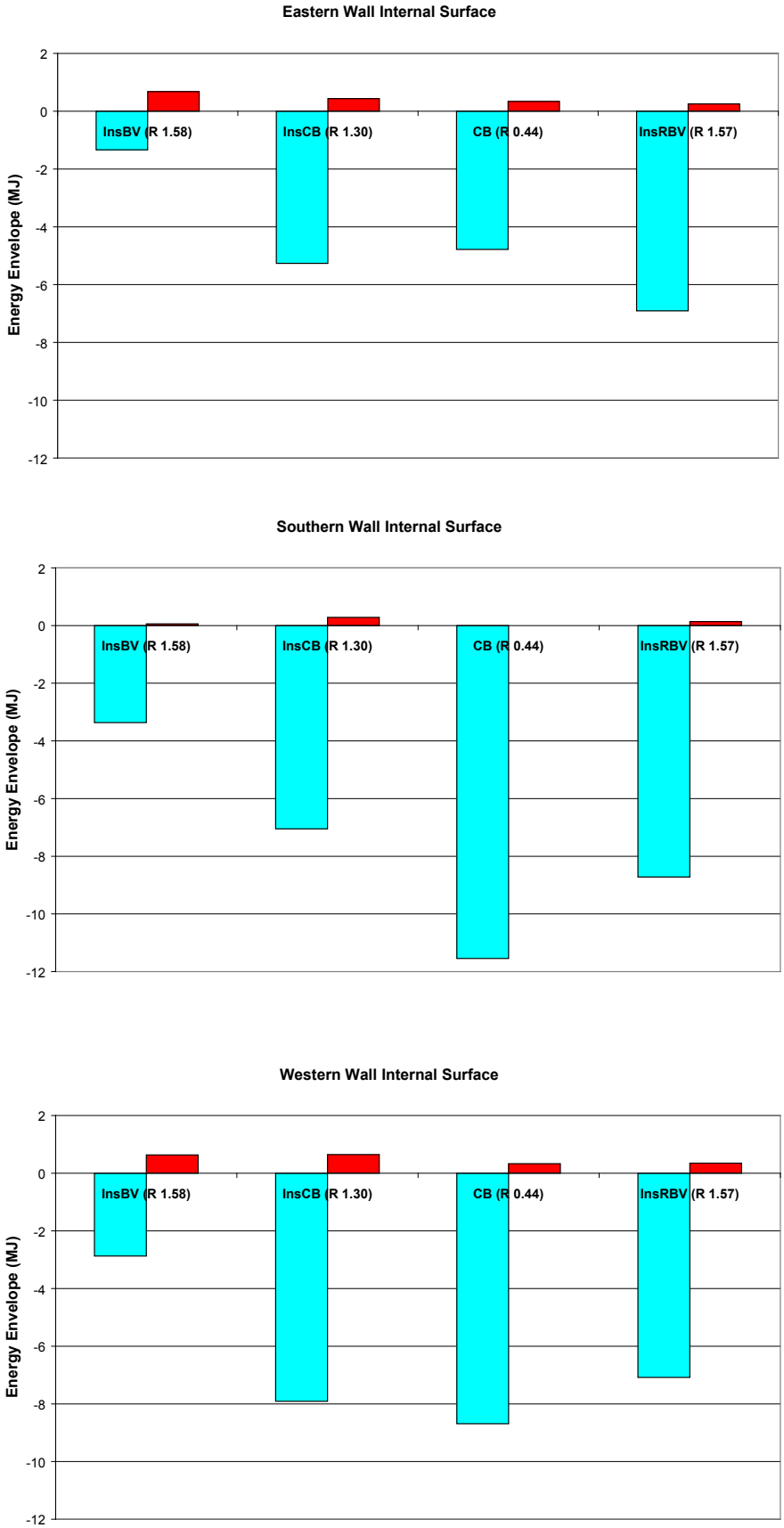

Figure 5.36 Heat absorbed and released over "day" period – autumn 2009

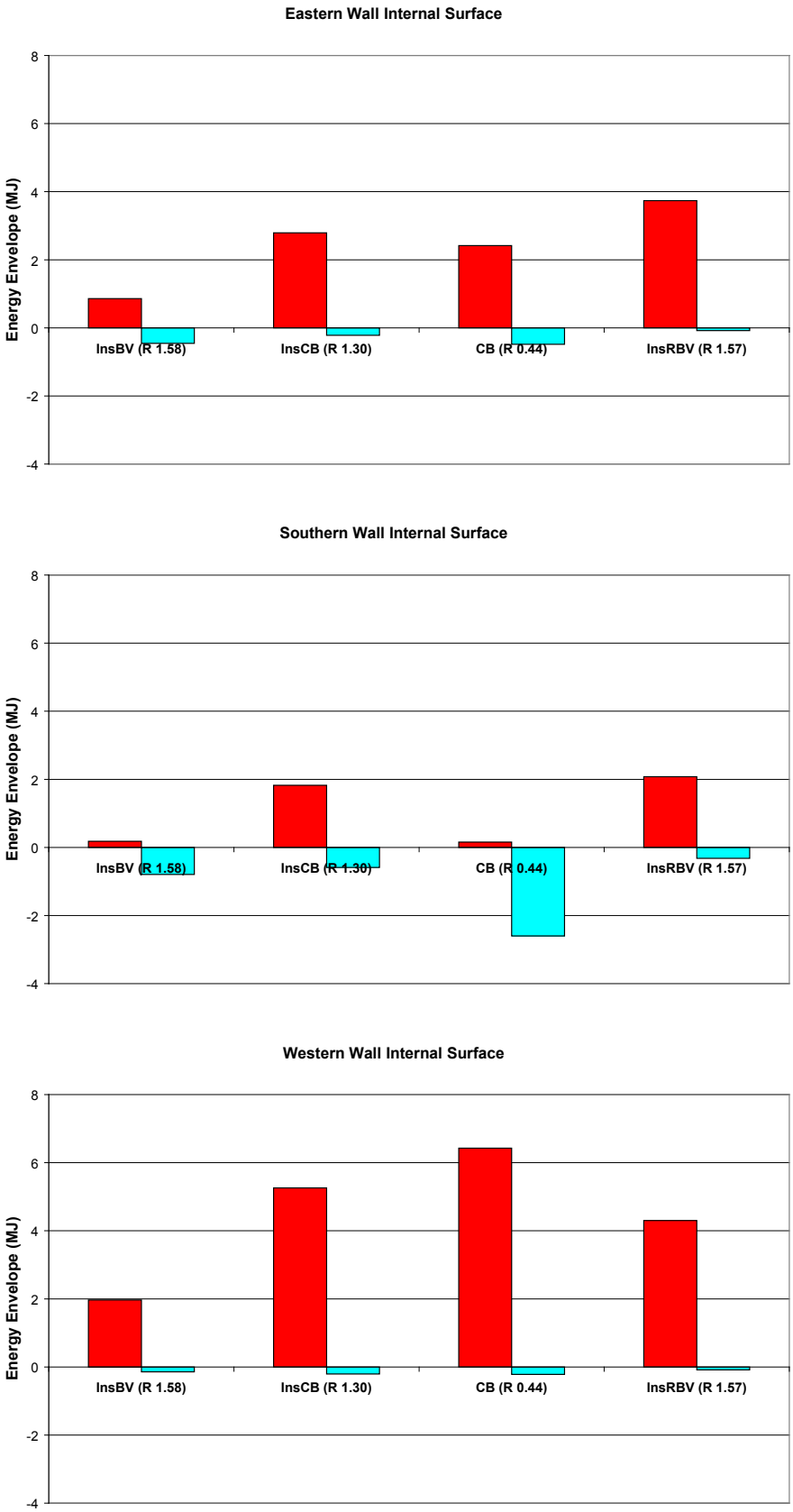

Figure 5.37 Heat absorbed and released over night period – autumn 2009

The average heat fluxes both in and out of the modules for the “night” period are shown in Figure 5.37.

In all modules the western wall was dominant at night in releasing most of the heat into the room. This heat was predominately sourced from the solar gain through the window during the day and the heat passing through the walling system from the afternoon.

Due to presence of cavity insulation, the InsCB and InsRBV module had a similar heat release trend back into the room at night. However the western wall of the InsRBV module did not provide the same heating effect as either the InsCB or CB module. This was one reason why the module tended to be slightly cooler at night as the western wall heat release typically occurred from evening to sunrise. It should be noted that while the CB module had a higher release of heat from the western wall into the room, a significant quantity of heat loss occurred through the southern wall at night (Figure 5.37).

5.5.2.4. Spring

5.5.2.4.1. Temperature Trends

The spring period had a 5 week collection consisting of a complete 34 days, with a 2 weeks prior settling after the winter air conditioning cycle. Generally over spring the conditions were sunny with over half the days being clear. An average temperature of 16.5°C was recorded. Daily temperatures nearly always exceeded 20°C, occasionally peaking over 25°C. Minimum night temperatures typically ranged between 5-10°C (see Figure 5.39).

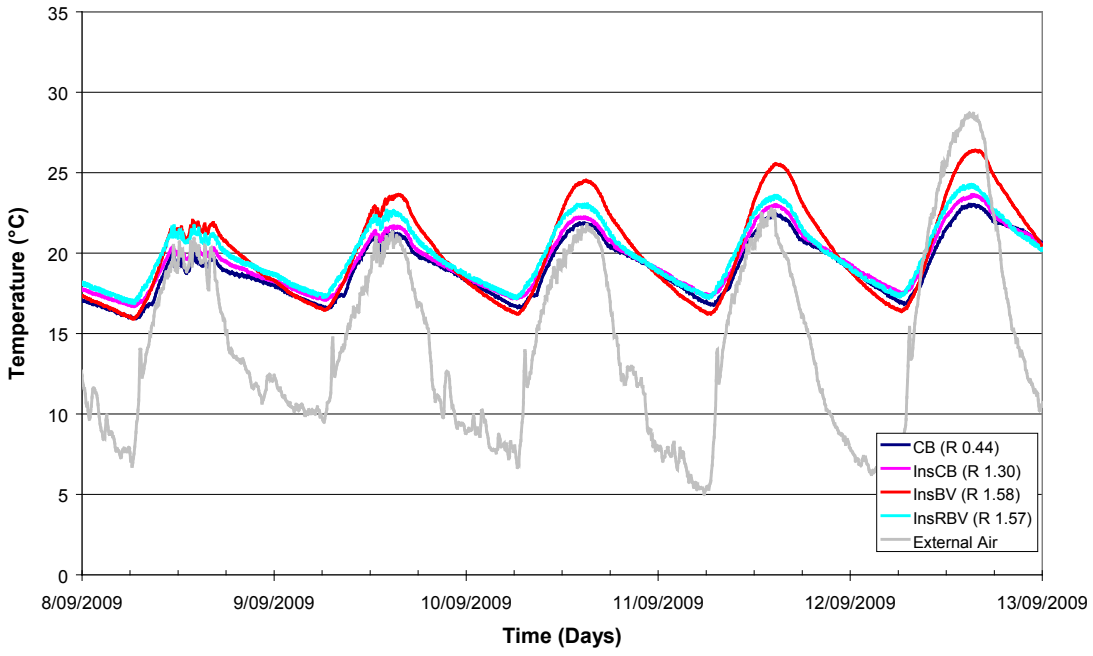

Figure 5.39 Internal module temperatures for selected spring week

The mean internal temperatures and standard deviations for the entire data collection period of 5 weeks for each of the modules and external air are shown in Figure 5.40.

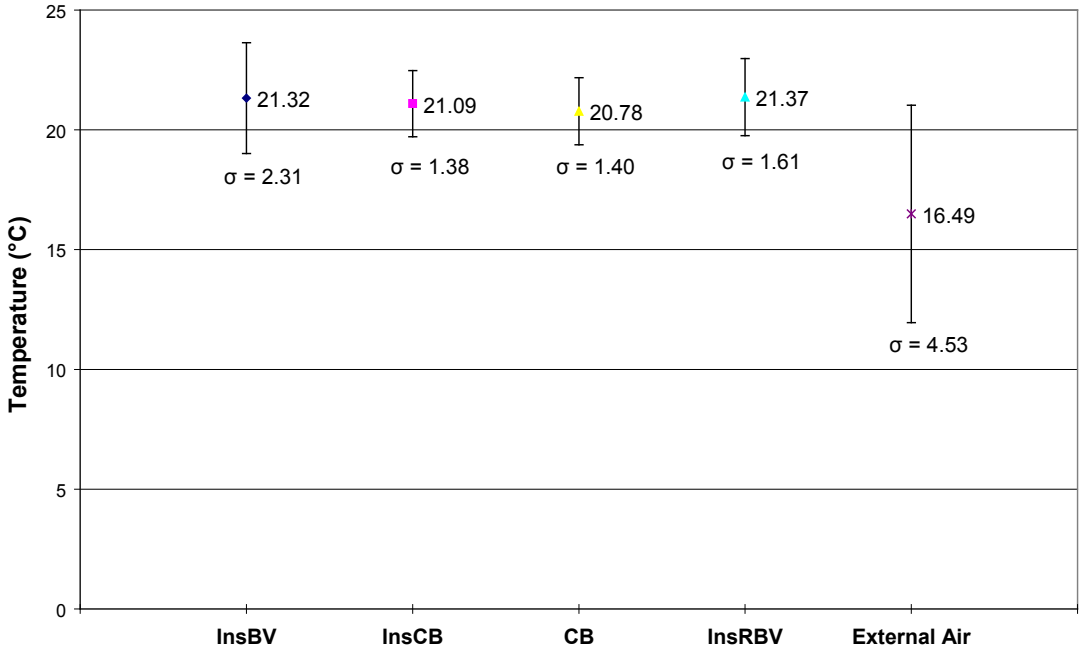

Figure 5.40 Mean module temperatures and standard deviations – spring 2009

The spring collection period had the most stable internal temperatures of all the seasons. The modules with internal thermal mass, InsCB, CB and InsRBV, all performed relatively similarly with slight differences pertaining to the distribution of mass and insulation throughout the construction. The InsRBV module was slightly warmer than the InsCB module during the day due to the solar gain effect which was also observed during autumn. The InsRBV module also had the highest mean temperature of all modules at 21.37°C which was only 0.05°C above the InsBV module. The InsBV was only slightly lower on average due to the evening temperature reduction. Again, the InsBV module had the largest standard deviation due to the lack of internal thermal mass which again demonstrated overheating during the day compared to the other modules. The InsRBV module produced the highest temperature swings of the modules with internal thermal mass.

5.5.2.4.2. Heat Flow Analysis

The average heat flux for the "day" period is shown in Figure 5.41. The walling systems of all four modules predominately removed heat from the room during the day. The InsBV module had the lowest absorption due to the lacking thermal mass on the interior wall surface. The southern and western walls were more active for the modules with internal thermal mass. Absorption through the southern CB module wall was the largest.

It is also worth noting that the InsRBV had the largest heat loss from the room into the eastern wall. This is a result of the lack of exterior thermal mass. The delayed heat flow through the wall from the incident morning sun on the external surface is also of a lesser magnitude as the insulated timber stud frame stores little of this heat.

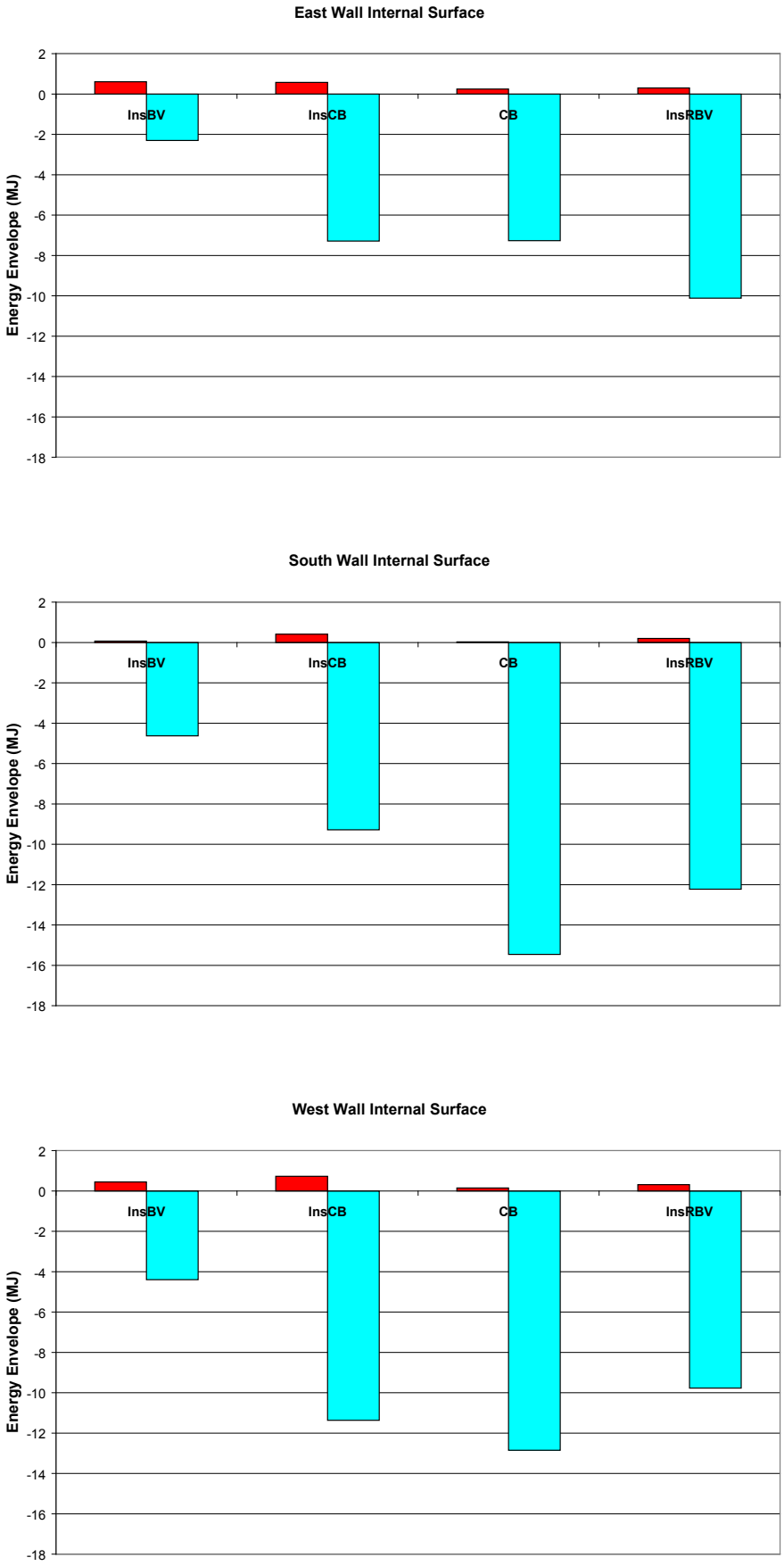

Figure 5.41 Heat absorbed and released over "day" period – spring 2009

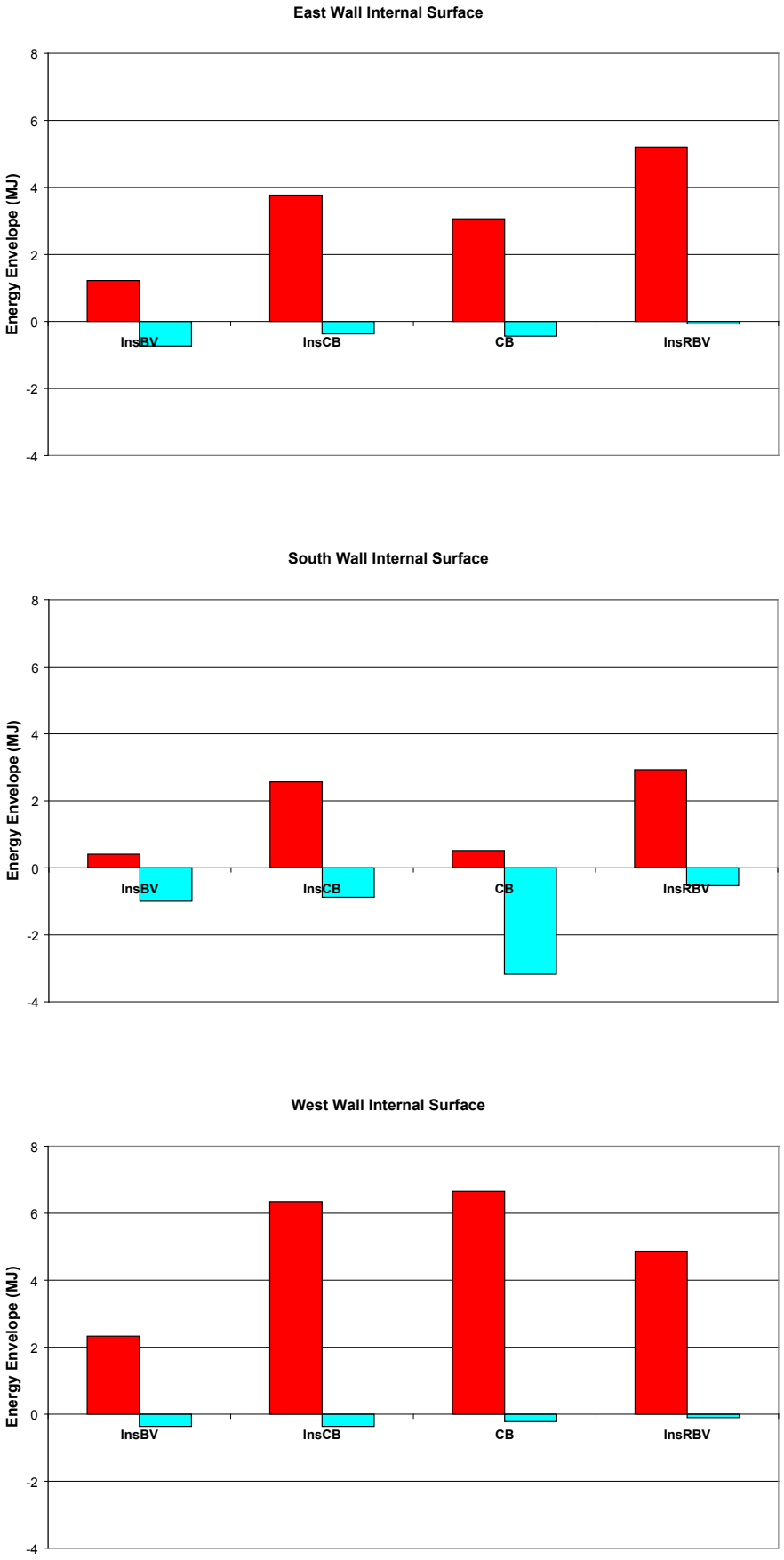

Figure 5.42 Heat absorbed and released over night period – spring 2009

The average heat fluxes both in and out of the modules for the "night" period are shown in Figure 5.42.

The CB module southern wall continued to lose heat throughout the evening. Whereas InsCB and InsRBV generally released heat back to the room from the southern wall due to the additional of insulation behind the internal thermal mass skin.

Both the InsCB and CB modules release a similar amount of heat into the room from the western wall from the combined effect of the heat absorbed from the room during the day and also the transmission of heat through the wall from the exterior due to the afternoon solar incidence. The InsRBV has a slightly lower release of heat as it lacks the exterior skin of thermal mass

5.5.3. Artificially controlled internal conditions

5.5.3.1. Energy Demands in Spring 2008

Air conditioning was operated in spring for a 5 week period in October 2008. The weather conditions were moderate with a few warm 30°C plus days and only several nights reaching as low as 10°C.

The typical response of four modules for part of the last week of October is shown in Figure 5.43 and 5.44. The InsBV was typically the first module during the day to require cooling. Heating was only required at the beginning of the testing period which was towards the end of October. External temperatures increased into November and no further heating was required. Only one heating cycle for the InsBV and CB modules was required over the whole 5 weeks.

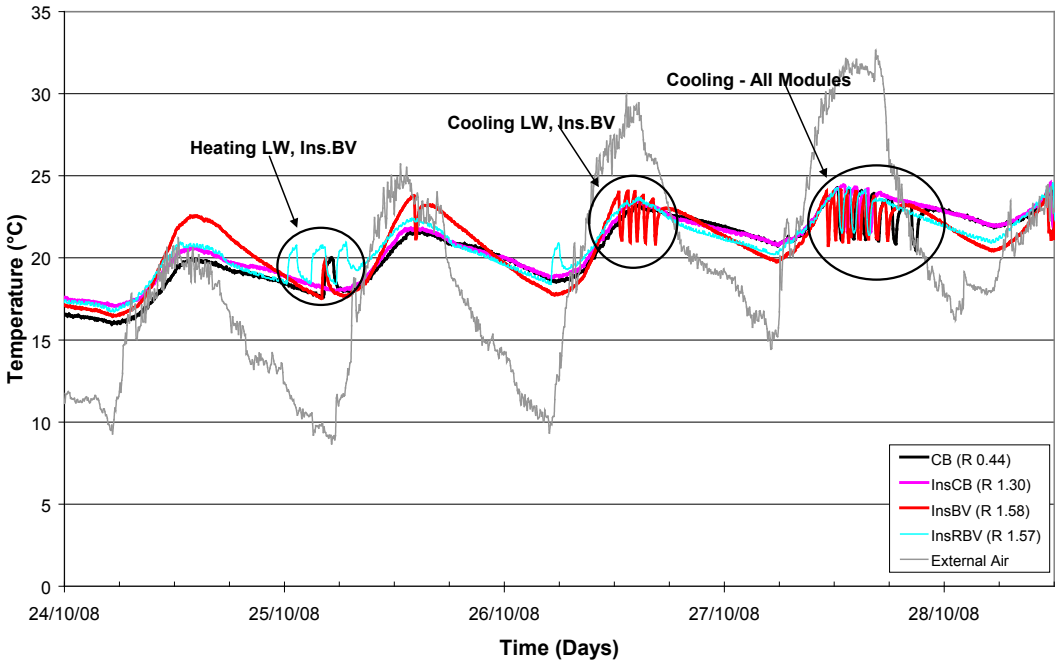

Figure 5.43 Heating/cooling behaviour for modules under controlled conditions – spring 2008

When cooling was required, the CB module would tend to continue with the cycles into the evening as shown in Figure 5.44 and during the warmer days the cycles would also be activated for longer. This resulted in a similar energy consumption figure to the InsBV module over spring. The InsCB module's

cooling cycles were typically activated only 30 minutes after the CB module in the morning and did not extend into the night, in fact more cooling cycles were required for the InsBV module despite it having no internal thermal mass in the walling system.

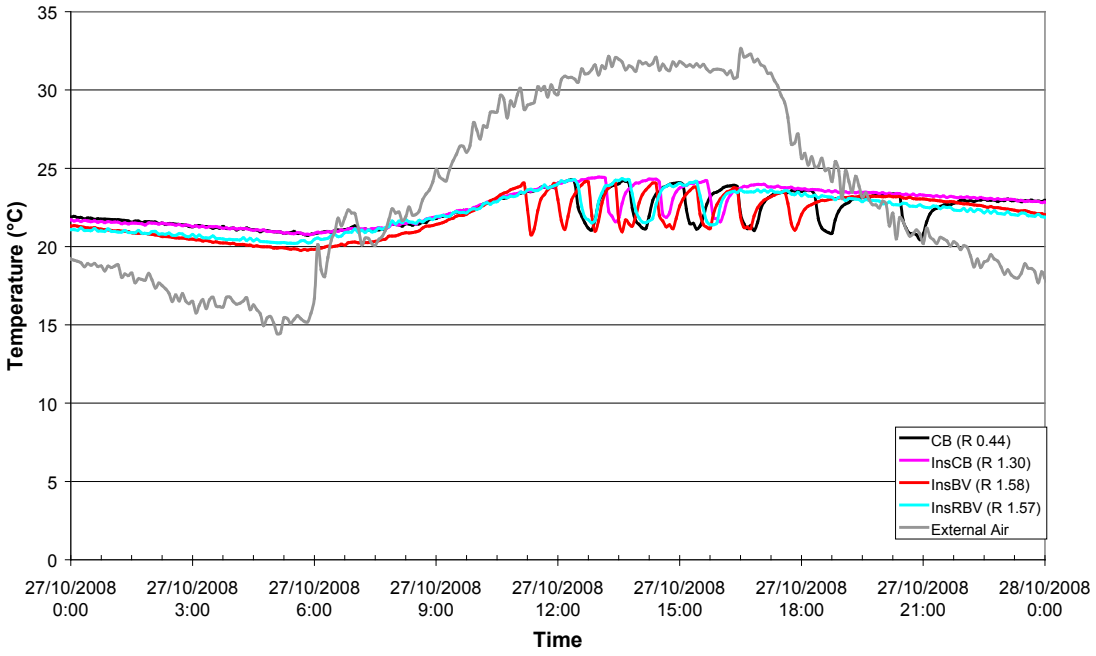

Figure 5.44 Typical module cooling behaviour - 27th October 2008

The total energy consumption for all four modules over the spring collection period can be observed in Figure 5.45. The week to week numerical results are given in Table 5.11 together with the relative performance normalised against that of the most efficient InsCB module.

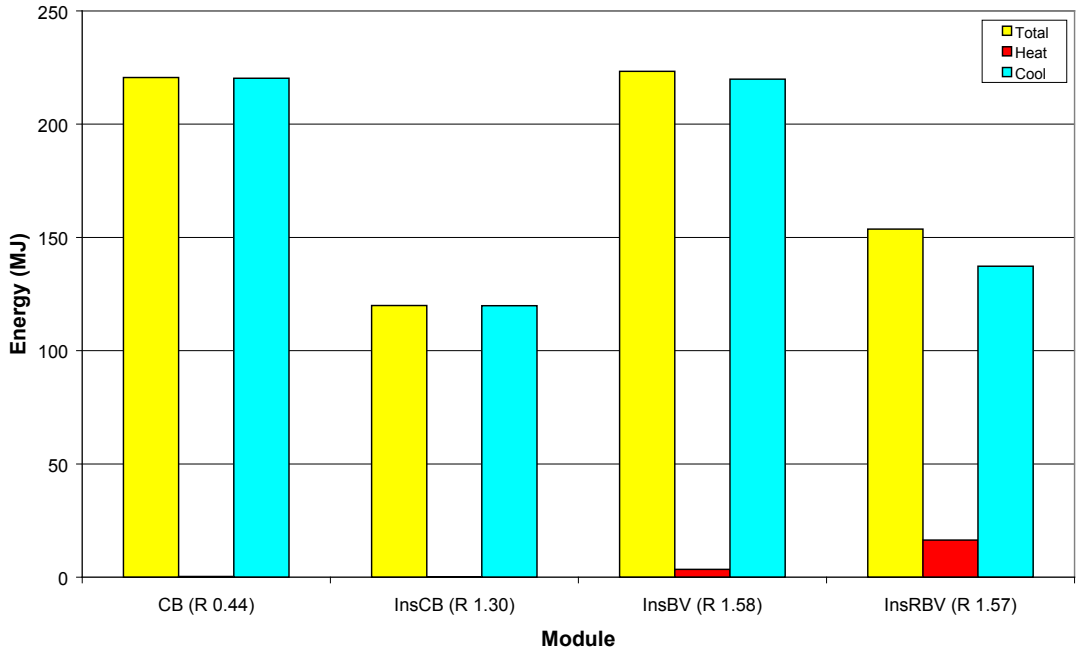

Figure 5.45 Total energy consumption over 5 week period – spring 2008

The differences in energy use between the InsCB and InsRBV modules were primarily due to heating load required by the InsRBV module as the cooling loads were similar. This was consistent with the free floating data which indicated that the InsRBV module had lower night time temperatures that were directly associated with the lack of an external skin with thermal mass. The external skin of thermal mass in the InsCB module aids in regulating the cavity surface of the internal skin promoting added heat flow into the room rather than to the outside environment. Generally little heating was required for any of the modules as few nights dropped to temperatures low enough to activate the system.

The InsBV module more readily required cooling due to its propensity to overheat compared to the other modules. However the CB module required cooling later in the day (Figure 5.44) which accounts for the relatively similar energy requirements to the InsBV module over the 5 week period.

Table 5.11 Energy demand per week – spring 2008

Week Ending	Energy Usage (MJ)											
	Insulated Reverse Brick Veneer			Insulated Brick Veneer			Insulated Cavity Brick			Cavity Brick		
	Heat	Cool	Total	Heat	Cool	Total	Heat	Cool	Total	Heat	Cool	Total
30/10/2008	25.7	13.4	39.0	2.7	45.5	48.2	0.0	11.8	11.8	7.1	27.9	35.0
6/11/2008	0.1	46.1	46.2	0.1	63.5	63.6	0.1	36.3	36.4	0.1	69.6	69.7
13/11/2008	0.0	20.8	20.8	0.2	55.9	56.0	0.0	22.2	22.2	0.1	41.3	41.4
20/11/2008	0.1	60.3	60.4	0.2	71.1	71.4	0.0	57.5	57.6	0.1	99.2	99.3
27/11/2008	16.2	10.2	26.4	3.0	29.3	32.3	0.0	3.8	3.8	0.0	10.2	10.3
Total Consumption	**42.1**	**150.7**	**192.7**	**6.2**	**265.3**	**271.5**	**0.1**	**131.6**	**131.7**	**7.4**	**248.1**	**255.6**
Weekly Average	**8.4**	**30.1**	**38.5**	**1.2**	**53.1**	**54.3**	**0.0**	**26.3**	**26.3**	**1.5**	**49.6**	**51.1**
Heating Energy Ratio*	**311.1**			**45.7**			**1.0**			**54.9**		
Cooling Energy Ratio*	**1.1**			**2.0**			**1.0**			**1.9**		
Total Energy Ratio*	**1.5**			**2.1**			**1.0**			**1.9**		

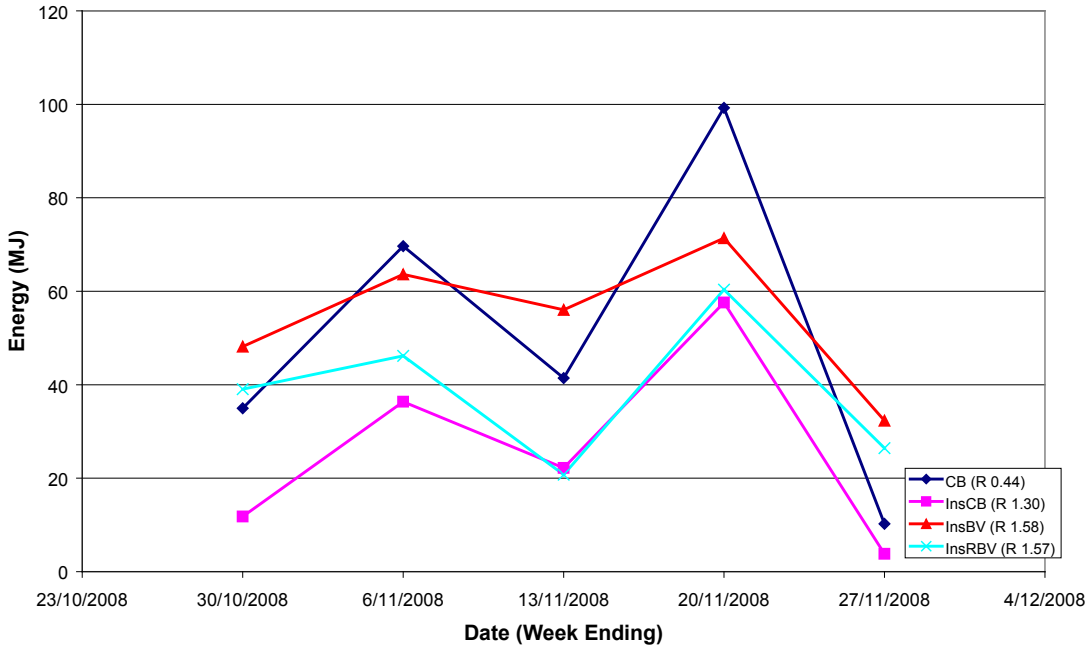

Figure 5.46 Energy use trend per week – spring 2008

While no trend was visible in energy use from week to week due to varying weather conditions there did appear to be a relationship in energy use between each module (apart from the overlapping of the CB and InsBV module in the third week), see Figure 5.46 and Table 5.11. This difference was due to increased cooling load. Warmer conditions appeared to affect the CB module more strongly than the InsBV module. The energy use of the CB module increased at a higher rate than the InsBV following a slight rise in external conditions. This extra supply was due to the prolonged cooling through the night.

5.5.3.2. Energy Demands in Summer 2009

Air conditioning was operating for the summer period through the months of January and February 2009. The data only corresponds to four weeks as the final week of data was unfortunately corrupted. The first three weeks of data collection were very hot with consistent temperatures above 30°C, regularly occurring from as early as 9am and continuing into the early evening. Solar radiation was also high during the day due to limited cloud cover. A cool change occurred in the final week and little cooling was required in that period. The response of the modules for a 3 day period in early February is shown in Figure 5.47.

The hot weather pushed the capacity of the external heat exchanger to its limits as it was originally intended for use on only two modules. It was therefore difficult to provide adequate cooling to all four sheds in the extreme heat, particularly when attempting to cool water to the 7°C set point with the high external temperatures. Consequently the internal temperatures were not reduced to the 22°C cut-off, but rather maintained between 22 and 23°C.

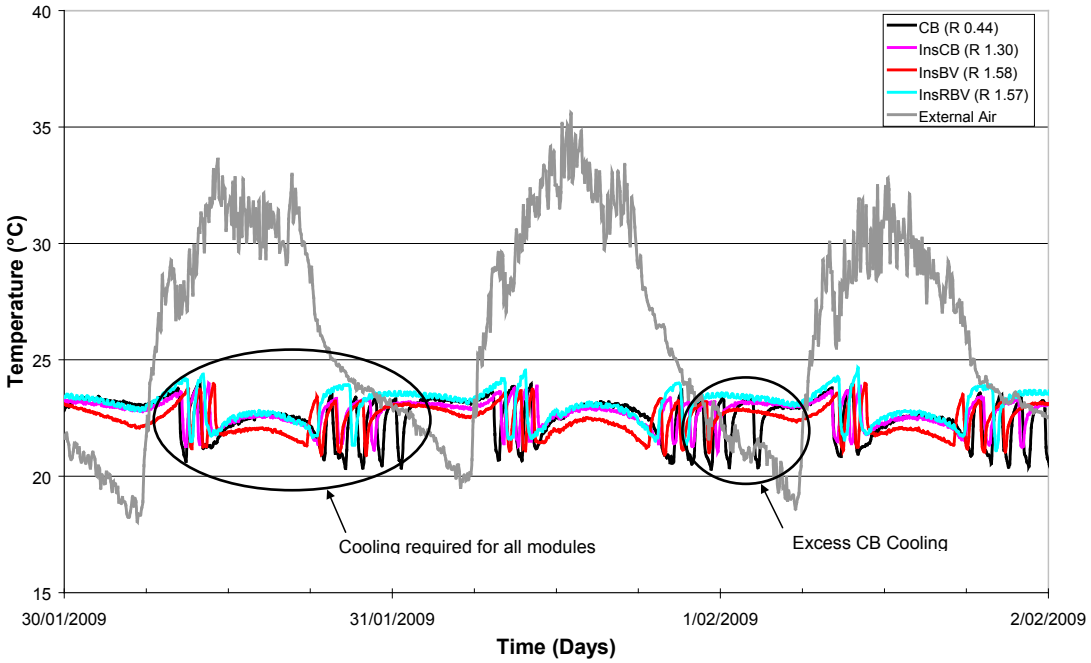

Figure 5.47 Cooling Behaviour for modules under control conditions– summer 2009

Due to the extreme heat, the energy use of the four modules was almost identical across the hot period (see Figure 5.48), with the exception of the CB module which required extra cooling into the evening and early morning. This effect was similar to that observed under spring conditions.

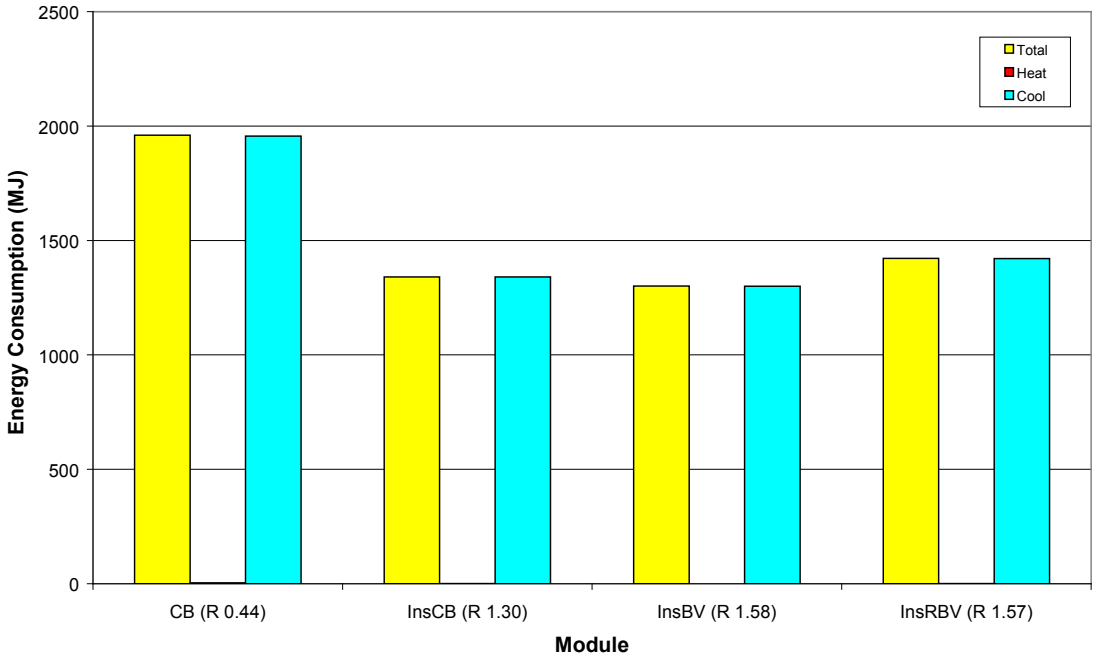

Figure 5.48 Total energy consumption over 4 week period – summer 2009

The overall energy use was high as a result of the internal temperature failing to reach the 22°C cut-off point. This resulted in the system operating nearly continually during the day. The InsRBV module used 121MJ more energy than the InsBV module and while in other seasonal periods this variation may be considered significant, in the context of these results it only corresponded to a difference of 9%, though this summer behaviour may not be truly representative of what would have occurred if the system operated with full functionality. The weekly energy demands for each module are summarised in Table 5.12

Table 5.12 Energy demand per week – summer 2009

Week Ending	Energy Usage (MJ)											
	Insulated Reverse Brick Veneer			Insulated Brick		Veneer	Insulated Cavity		Brick	Cavity Brick		
	Heat	Cool	Total	Heat	Cool	Total	Heat	Cool	Total	Heat	Cool	Total
22/01/2009	0.1	258.1	258.2	0.0	252.5	252.5	0.1	254.6	254.7	0.2	374.5	374.7
29/01/2009	0.2	340.2	340.4	0.0	302.8	302.8	0.1	319.3	319.4	0.3	460.3	460.6
5/02/2009	0.2	432.2	432.4	0.1	388.0	388.1	0.1	405.3	405.3	3.1	599.2	602.3
12/02/2009	0.4	345.9	346.3	0.0	310.9	311.0	0.1	335.2	335.3	0.2	489.3	489.4
19/02/2009	0.1	44.4	44.4	0.1	46.0	46.1	0.0	26.2	26.2	0.0	33.2	33.2
Total Consumption	**0.9**	**1420.8**	**1421.7**	**0.2**	**1300.3**	**1300.5**	**0.4**	**1340.6**	**1341.0**	**3.8**	**1956.5**	**1960.2**
Weekly Average	**0.2**	**284.2**	**284.3**	**0.0**	**260.1**	**260.1**	**0.1**	**268.2**	**268.2**	**0.8**	**391.3**	**392.0**
Heating Energy Ratio*	**2.2**			**0.5**			**1.0**			**8.9**		
Cooling Energy Ratio*	**1.1**			**1.0**			**1.0**			**1.5**		
Total Energy Ratio*	**1.1**			**1.0**			**1.0**			**1.5**		

5.5.3.3. Energy Demands in Autumn 2009

The autumn air conditioning observation period consisted of four weeks of data collected over April and May 2009 with a 2 week prior settling period. External temperatures regularly peaked at around 22-23°C, however the low solar angle created the need for artificial cooling to maintain the internal temperature below 24°C. The typical response for a 4 day period in April is shown in Figure 5.49. Note the high cooling requirements over this period as a result of the solar gain despite external air temperatures being relatively mild.

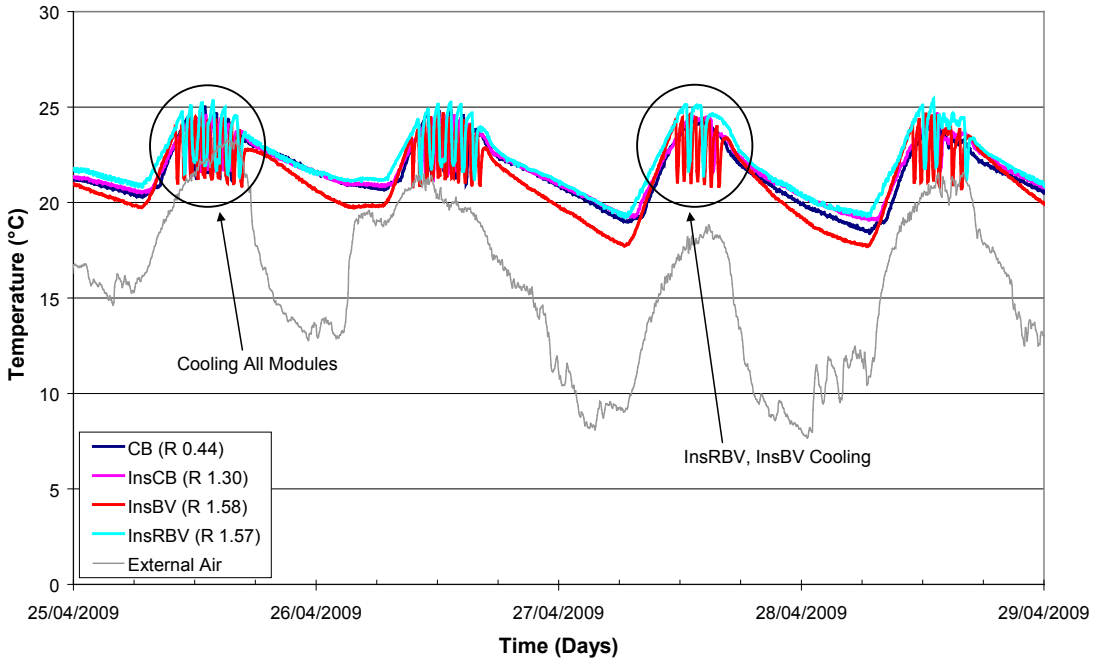

Figure 5.49 Internal temperatures of modules under controlled conditions – winter 2009

As with past results the InsCB module again was the most energy efficient. The InsBV module was the most energy intensive requiring 214% more energy than the InsCB module; this was due to the air conditioning system reacting to the high diurnal swing of the module. This was also observed in the October 2007 air conditioning data for the InsLW where the high diurnal swing resulted in high energy consumption. The InsBV and InsRBV modules both required similar amounts of heating energy, but had differing cooling requirements.

As conditions became cooler into May heating was necessary towards the end of the final week of data collection. Comparing the performance of the InsCB and CB modules it appeared that in terms of cooling, insulation in the cavity had little impact until the onset of cooler weather. The total energy consumption for the 4 week autumn period for each of the modules is shown in Figure 5.50.

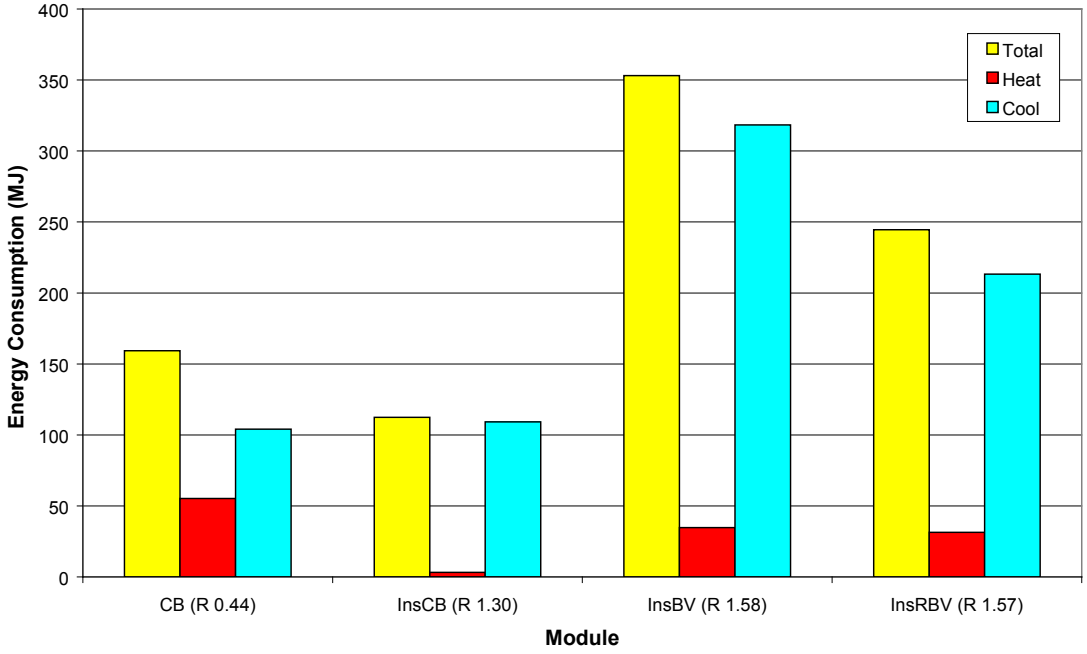

Figure 5.50 Total energy consumption – autumn 2008

The InsBV and InsRBV modules reflect the behaviour seen in the free floating results in that the high solar gain with cool to moderate external air temperatures (averaging 15.7°C) lead to high internal temperatures, which in turn produced a much greater need for artificial cooling. Under these conditions the performance of the InsCB module was superior to the InsRBV module (InsCB required approximately a third of the energy). This demonstrates the importance of the external brickwork skin during periods of high solar gain.

The performance of the InsBV and InsRBV modules show that under these weather conditions, a single skin of brickwork (whether on the external or internal side of the walling envelope) did not provide the benefits of double brickwork. However the single skin of internal brickwork in the InsRBV module provided some benefit over the single external skin of the InsBV module (see Figure 5.50). The capacity of the InsRBV module to offset high solar gain appeared to be less than both the InsCB and CB.

Values of weekly energy consumption are presented in Table 5.13, including a comparison of the total energy used against that for the InsCB module. The largest variation for the InsCB module occurred in the final week where heating was required. All modules required greater heating needs than the InsCB module.

Table 5.13 Energy demand per week - autumn

Week Ending	Energy Usage (MJ)											
	Insulated Reverse Brick Veneer			Insulated Brick Veneer			Insulated Cavity Brick			Cavity Brick		
	Heat	Cool	Total	Heat	Cool	Total	Heat	Cool	Total	Heat	Cool	Total
16/04/2009	0.1	161.7	161.8	0.1	161.4	161.5	0.0	118.4	118.4	0.2	142.4	142.6
23/04/2009	0.0	86.3	86.3	0.1	89.5	89.6	0.0	50.6	50.6	0.1	61.5	61.5
30/04/2009	0.0	53.1	53.1	0.1	85.9	86.1	0.0	28.4	28.4	0.1	30.1	30.2
7/05/2009	0.0	60.7	60.7	0.1	91.8	91.9	0.0	28.4	28.4	0.1	12.5	12.5
14/05/2009	31.3	13.2	44.5	34.5	51.1	85.5	3.1	1.8	4.9	55.1	0.0	55.1
Total Consumption	**31.5**	**374.9**	**406.4**	**34.9**	**479.7**	**514.5**	**3.2**	**227.6**	**230.8**	**55.5**	**246.4**	**301.9**
Weekly Average	**6.3**	**75.0**	**81.3**	**7.0**	**95.9**	**102.9**	**0.6**	**45.5**	**46.2**	**11.1**	**49.3**	**60.4**
Heating Energy Ratio*	**9.7**			**10.8**			**1.0**			**17.2**		
Cooling Energy Ratio*	**1.6**			**2.1**			**1.0**			**1.1**		
Total Energy Ratio*	**1.8**			**2.2**			**1.0**			**1.3**		

5.5.3.4. Energy Demands in Winter 2009

The winter results were obtained for a 5 week period in July and August 2009 proceded by a 3 week settling in period. Peak daytime external temperatures rarely reached 19°C with a few days exceeding 20°C. Night temperatures consistently dropped below 5°C. The general trend of the mean external temperature was flat, reflecting the winter conditions.

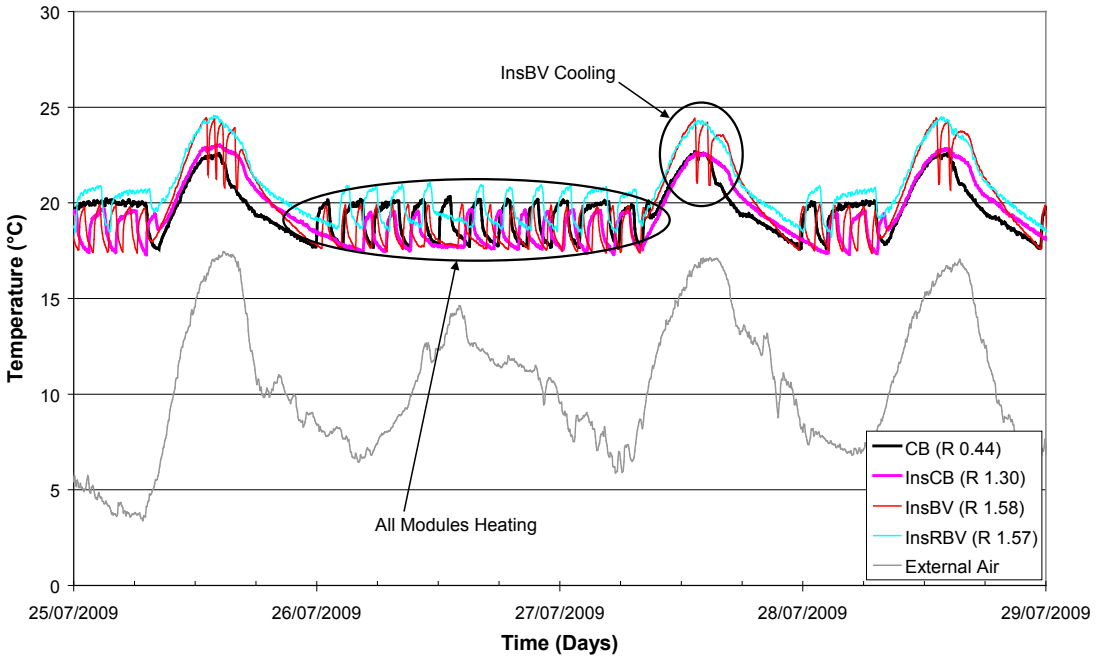

Figure 5.51 Internal temperatures of modules under controlled conditions – winter 2009

During this winter period the air conditioning system was consistently required. Heating was regularly activated at night and also during the colder days when little solar radiation was present. The typical response for a 6 day period in July is shown in Figure 5.51. Both the InsBV and InsRBV modules peaked consistently at the upper range of the air conditioning systems setting of 24°C. The InsBV module often activated the

cooling; the InsRBV module approached but did not exceed this limit. The InsCB and CB modules peaked at similar temperatures which were typically 1.5-2.0°C cooler than the InsRBV and InsBV modules.

Heating was the predominant source of energy consumption during winter, however some cooling was required for the InsBV module to maintain the internal space within the comfort zone and offset the solar gain (the internal insulated timber frame has limited capacity to do this). As seen in Figure 5.51, this cooling was a consistent requirement during the final 4 weeks of data collection (even though this cooling need was minimal compared to heating).

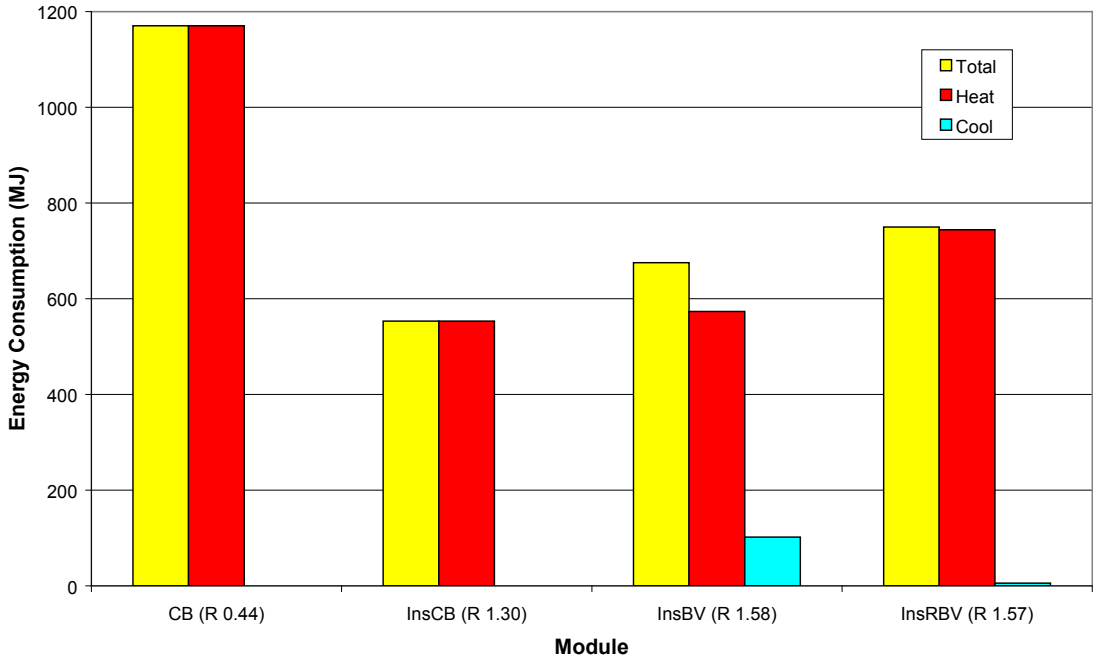

Figure 5.52 Total energy consumption over 5 week period – winter 2009

The heating requirements of the InsCB and InsBV modules were very similar with a total difference of only 20MJ. The InsBV module often required more heating cycles, occurring earlier in the evening than for the InsCB module. The similar consumption figures were a result of the extended heating periods for the InsCB module. The InsRBV module appeared to suffer in both cases with earlier activation than the InsCB module and extended heating periods. The CB module was even further to the extreme as a result of it being the coolest module under these conditions together with the lack of cavity insulation to prevent internal heat flowing to the exterior. The total energy consumption of the 5 week period for each of the modules is shown in Figure 5.52.

Table 5.14 Energy demand per week – winter 2009

Week Ending	Energy Usage (MJ)											
	Insulated Reverse Brick Veneer			Insulated Brick Veneer			Insulated Cavity Brick			Cavity Brick		
	Heat	Cool	Total	Heat	Cool	Total	Heat	Cool	Total	Heat	Cool	Total
16/07/2009	271.0	0.0	271.0	191.7	0.0	191.7	224.4	0.0	224.4	415.4	0.0	415.4
23/07/2009	186.2	3.9	190.2	142.7	34.5	177.2	143.2	0.0	143.2	283.9	0.0	283.9
30/07/2009	214.4	0.0	214.4	162.5	19.0	181.6	155.5	0.0	155.5	334.0	0.0	334.0
6/08/2009	193.9	0.0	193.9	145.0	24.8	169.8	136.3	0.0	136.3	304.0	0.0	304.0
13/08/2009	149.4	1.9	151.3	123.2	23.6	146.7	118.3	0.0	118.3	248.4	0.0	248.4
Total Consumption	**1014.9**	**5.8**	**1020.7**	**765.1**	**101.9**	**867.0**	**777.6**	**0.0**	**777.6**	**1585.7**	**0.0**	**1585.7**
Weekly Average	**203.0**	**1.2**	**204.1**	**153.0**	**20.4**	**173.4**	**155.5**	**0.0**	**155.5**	**317.1**	**0.0**	**317.1**
Heating Energy Ratio*	**1.3**			**1.0**			**1.0**			**2.0**		
Total Energy Ratio*	**1.3**			**1.1**			**1.0**			**2.0**		

5.5.4. Key findings

The study presented in this chapter has described the free floating and controlled conditions for various walling systems in the thermal test modules with a north facing window. The following key findings have been drawn:

Free Floating

The free floating study of the various walling systems indicates that thermal mass (particularly internal thermal mass), and wall insulation can be used to advantage in improving the thermal performance. Thermal mass is an effective form of heat storage to regulate internal temperatures and temperature fluctuations. In terms of thermal comfort this was particularly the case for walls with internal thermal mass, whose performance was also markedly enhanced by the inclusion of cavity insulation.

The following is a summary of the main findings:

- The presence of the window became the dominant driving factor in the thermal performance of the building.
- The combination of solar radiation on the external wall surface and heat entering the building via the window in some cases resulted in a bi-directional heat flow in the walls.
- The diurnal swing was much higher in conditions with high solar gain.
- InsLW module had a much less capacity for dampening the internal temperature variations and consistently had the highest diurnal swing. The BV constructions had a slightly lower diurnal swing, however it was InsCB and CB modules which had the best dampening ability.
- The InsLW and InsBV constructions would consistently peak to higher temperatures than InsCB and CB. The insulated internal skin essentially ‘traps’ heat in the module space, whereas InsCB and CB modules absorb heat from the room which counters the effect of the solar gain.
- Solar incidence on the external surfaces of the InsLW module provided an immediate flow of heat into the room through the walling system as no thermal mass was present to produce a thermal lag. These walls then acted as ‘secondary’ heat sources during the day while the sun was incident. BV constructions also showed this but with a slightly reduced and delayed effect due to the thermal lag of the exterior skin.
- During winter, internal thermal mass with a backing of insulation was a superior construction as it promoted heat release into the room during the evening to maintain warmer temperatures.
- The InsCB module provided the most consistent and predictable behaviour across all time periods with heat absorption during day and heat release and night.
- The InsRBV module performed marginally better than the InsCB module in summer and winter but seemed to suffer during periods with high solar gain when compared to InsCB and CB modules. The CB module performed best when the solar gain was high.

Controlled Internal Conditions

The following is a summary of the main findings for controlled internal conditions:

- InsCB always consumed less energy than other constructions to maintain the internal temperature with the specified range. The internal thermal mass combined with the cavity insulation aided the system in reducing energy consumption due to solar passive effects.
- No correlation between R-Value and energy consumption was found.
- InsLW and InsBV often required more heating and cooling cycles due to their inherent properties which produced large diurnal swings.
- The InsLW module was typically the first to activate either heating or cooling due to the rapid response to the driving conditions. InsLW consistently had the highest energy consumption.
- There appears to be no correlation between R-Value and energy consumption. The InsLW module performed marginally worse than CB in July/August 2008 and considerably worse in October 2007 despite having an R-Value three times greater.
- Energy consumption is strongly dependant on the external driving conditions and the energy demand of the modules varies depending on this.
- The use of lightweight high insulating interior skins did not reduce air conditioning loads. In fact the InsCB module consistently performed the best and used the least energy. The internal thermal mass with the insulation in the cavity to isolate it from the exterior environment, and the external skin which increased thermal lag appeared to assist in reducing the use of the air conditioner by absorbed daily solar gain and releasing heat at night.

General conclusions concerning the InsRBV module

The conversion of the InsLW to InsRBV modules certainly improved the thermal performance compared to that of the original construction. However under certain conditions the benefit of both internal and external thermal mass combined with insulation was lacking. This was not a case with the InsCB module.

Investigations into the heat flow through the walls indicated that the additional external thermal mass provided increased dampening of the external conditions and also helped to decrease the environmental impact on the cavity surface of the internal thermal mass. Externally clad insulation alone did not provide this form of cavity dampening and due to this; the internal thermal mass was acted upon on both the internal and external surfaces, reducing the capacity to lessen the temperature rise from the solar gain. This could also be one factor why under driven conditions the InsRBV used more energy than InsCB. This did not mean that InsRBV cannot provide a comfortable passive living space, it was a definite improvement over other constructions however the assembly itself was in no way perfect and appears to possibly lack a degree of thermoregulation in comparison to the InsCB under higher solar gain. Nevertheless, the InsRBV performed strongly during the summer and winter collection periods.

5.6. The effects of insulation and thermal mass - statistical analysis

5.6.1. Introduction

This section has been prepared by Dr Trevor Moffiet and will be published as a separate paper shortly (Moffiet et al.).

As indicated previously and summarised in Table 3.2, data on the thermal performance of the modules was collected over an eight year period with a large range of variables considered. The breadth of the study, together with the limited numbers of modules, meant that in many cases it was not feasible to replicate identical conditions in all four modules to allow direct comparison under the same weather conditions. To more effectively interrogate the large body of data collected, statistical techniques have been used (See section 3.2). These studies are ongoing, and detailed results and findings will form part of the Phase 2 report. A preliminary analysis to investigate the influence of thermal mass and thermal insulation on the performance of walling systems is presented here to illustrate the approach along with some preliminary findings. Statistical models provide a way to objectively summarise and compare the average affects of the main variables taking into account the influence of the weather conditions over several years as well as "noise" caused by unspecified and/or uncontrolled sources of variation in the real world. In the following study, statistical modelling has to been used to enable comparisons between modules that existed in mutually exclusive time periods.

5.6.2. Statistical Model

Data selected from the housing energy efficiency database for the statistical analysis covered the period 2002-2008 and consisted of the following conditions and variables:

- Free-floating cases
- No venting of the modules
- Curtains were not present or were opened both day and night
- Window/door screens were not present

The six module configurations over the course of the research of BV, InsBV, CB, InsCB, InsLW, InsRBV did not comprise a balanced experimental design with respect to the presence of insulation and the placement of high thermal mass in the wall system and therefore their effects could not be modelled directly. Such analysis was only possible by statistical models especially designed to compare the performance of the six modules that exhibited particular insulation/thermal mass combinations rather than to directly model the effects of insulation and thermal mass. In addition, many combinations of the main construction variables and their modifications were not present in the data across all seasons.

To enable effective representation of the basic building configurations across the four seasons no distinction was made between module states that contained internal partition walls and those that did not. However, the data could still be categorised by the presence or absence of high interior thermal mass located in the walling envelope of the partition walls.

For purposes of analysis, all temperature data were simplified and divided as an average into four periods of

day. The model was developed to predict the average temperature of each quarter day (Q-Day) and provide the resulting profile.

A total day was divided as follows:

- N1: 12:00am to sunrise
- D1: sunrise to 12:00pm
- D2: 12:00pm to sunset
- N2: sunset to 12:00 am

Note: D1 and D2 – day periods, N1 and N2 – night periods.

Each single day was defined according to a *through-day mean temperature profile* (TDMT profile) as shown in Figure 5.53, by a set of three straight lines that connect the four points given by the mean air temperatures corresponding to each quarter of the day. A similar TDMT profile was defined for the mean external temperatures. Differences in profile slope, or amplitude, between corresponding line segments of internal and external profiles were indicators of a room's sensitivity to short term changes in external temperatures. Lower amplitudes of change indicated lower sensitivity. A room that was very sensitive to external conditions exhibited profiles more similar to those of the external profile with a displacement in average temperature. The sensitivity was most evident in the line segments from D1 to D2 and D2 to N2 as those periods are aligned with high increases and decreases of external temperatures related to the rise and fall of the sun through the day.

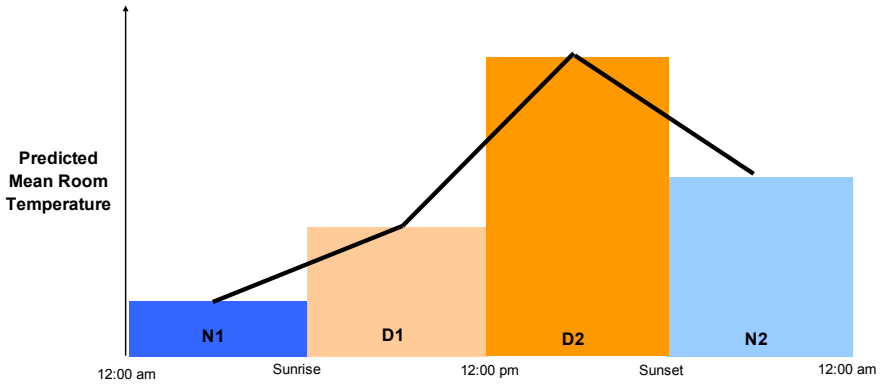

Figure 5.53 A schematic to illustrate a TDMT profile over four periods of the day. In defining this profile plot, the mean temperature for each period is assigned to the middle of each period.

The method used for statistical modelling/analysis was generalised linear modelling (GLM). The interest was in the prediction of average internal module air temperatures across four periods of the day by season using a parsimonious set of meaningful predictor variables.

The explanatory variables used for modelling were:

- Mean External Air Temperature (Continuous variable: average temperature in period of day)
- Basic Configuration (Categorical variable: The six module wall systems)

- Season (Categorical variable: Autumn, Winter, Spring Summer)
- Q Day (Categorical variable: four periods of the day)
- Basic Building Configuration * Q Day (A 2-way Interaction term)
- Basic Building Configuration * Season (A 2-way Interaction term)
- Season * Q Day (A 2-way Interaction term)
- Basic Building Configuration * Season* Q Day (A 3-way Interaction term)

Other variables that were considered but were not included in modelling were solar radiation (measured on each side of the building and the roof), solar altitude, wind direction and wind speed. The potential for these physical variables to contribute to improved model predictions were assessed relative to the model residuals and found to add little in regards to the predicted results. Note that the contributions to room temperature by 'solar radiation' and 'solar altitude' were effectively correlated to the variables 'external temperature' and 'season'.

While it was recognised that the internal air temperatures of the modules were dynamically influenced through lagged heat flows, time lags were not modelled directly. The statistical model was effectively a static model that made some allowances for the differences in module dynamics by the inclusion of interaction terms which allowed for building responses to be different to each other within different periods of the day and within different seasons.

The statistical model returned an R^2 value of 87% (see Table A.1, Appendix A) indicating a reasonably strong predictive model given the low number of explanatory variables (three) and their interactions. Each of the model variables was indicated to be highly statistically significant with p-values <0.0001 (see Table A.2, Appendix A).

Details on the significance of predictor variables, model summaries and confidence intervals can be found in Appendix A.

5.6.3. Results and discussion

The overall significance of the model suggested that the mean internal air temperature is influenced by several parameters such as the mean external air temperature, the wall configuration, the period of the day and the season. It meant that some or all of the seasonal and daily mean internal air temperatures were moderated differently by the different wall constructions.

Figure 5.54 is a graphical summary of the averaged modelled effects for the CB and BV modules. The purpose of this plot is to visually highlight average thermal mass and insulation effects for a given external air temperature profile. The thermal mass effect was characterised by a low slope of the line segment that represents the change in average air temperature between the second (D1) and third periods of the day (D2). The slope was less for buildings that had high interior thermal mass compared to buildings that had low interior thermal mass.

The insulated and uninsulated CB modules exhibited approximately parallel temperature profiles to each other. The insulated and uninsulated BV modules also had roughly parallel temperature profiles. The thermal

resistance effect was characterised by the displacement between the approximately parallel TDMT profiles for an insulated building and its uninsulated counterpart.

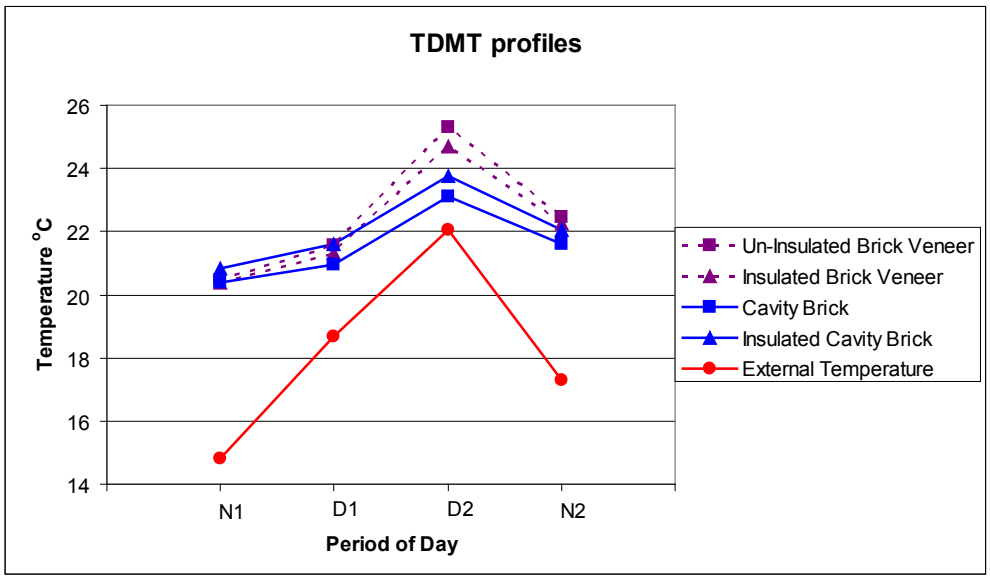

Figure 5.54 Summary of the modelled TDMT profiles for the cavity brick and brick veneer modules averaged across the four seasons.

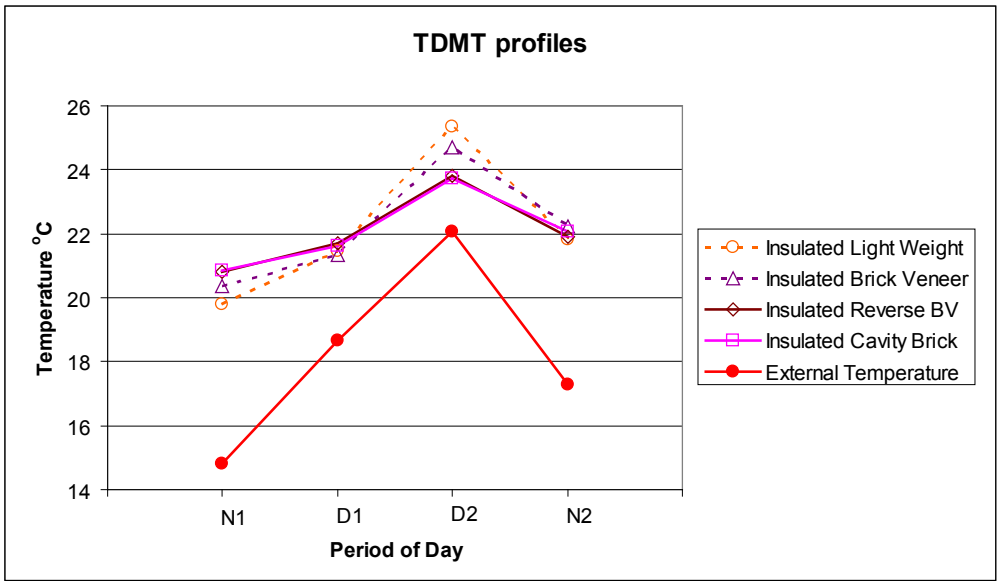

Figure 5.55 Summary of the modelled TDMT profiles for the insulated modules averaged across the four seasons.

The averaged TDMT profiles for all of the insulated modules are shown in Figure 5.55. The purpose of this plot is to visually highlight average thermal mass effects for a given external temperature profile. The InsLW module, which had the lowest internal and external thermal masses of all of the modules, exhibited a TDMT profile that was closest to that of the external temperature. Its interior temperature was the most sensitive to external temperature changes.

The next most sensitive was the InsBV module and equally least sensitive were the InsCB and InsRBV modules. The intermediate positioning of the TDMT profile for the InsBV module was indicative that its

external thermal mass was having some moderating influence on internal air temperature swings compared to the InsLW module.

The InsRBV module exhibited a TDMT profile that was parallel to and approximately coincident with the InsCB profile on average. However, when examined by season these two profiles were seen to separate. The thermal mass effects by season are summarised numerically in Figure 5.56 as well as Tables 5.15 and 5.16 which show the estimated mean temperature differences (swings) between the 3rd (D2) and 2nd (D1) periods of the day by season for each building, given the mean external air temperature swings between the same periods in the day.

Table 5.15 Thermal mass effects on internal temperature swings

	Estimated 95% Confidence intervals for ($Temp_{InternalD2}$-$Temp_{InternalD1}$) given ($Temp_{ExternalD2}$-$Temp_{ExternalD1}$).			
	Autumn (°C)	Winter (°C)	Spring (°C)	Summer (°C)
External Air	3.9	4.1	3	2.5
BV	4.3 ±0.83	3.9 ±0.47	3.5 ±0.37	3.3 ±0.7
InsBV	3.9 ±0.42	3.7 ±0.47	3 ±0.74	2.9 ±0.57
InsLW	4.1 ±0.68	4.3 ±0.48	3.4 ±0.38	3.7 ±0.52
CB	2.3 ±0.32	2.3 ±0.26	2 ±0.25	2 ±0.28
InsCB	2.5 ±0.42	2.4 ±0.44	1.8 ±0.39	1.8 ±0.55
InsRBV	2.5 ±0.59	2.6 ±0.86	1.8 ±0.86	1.5 ±0.59

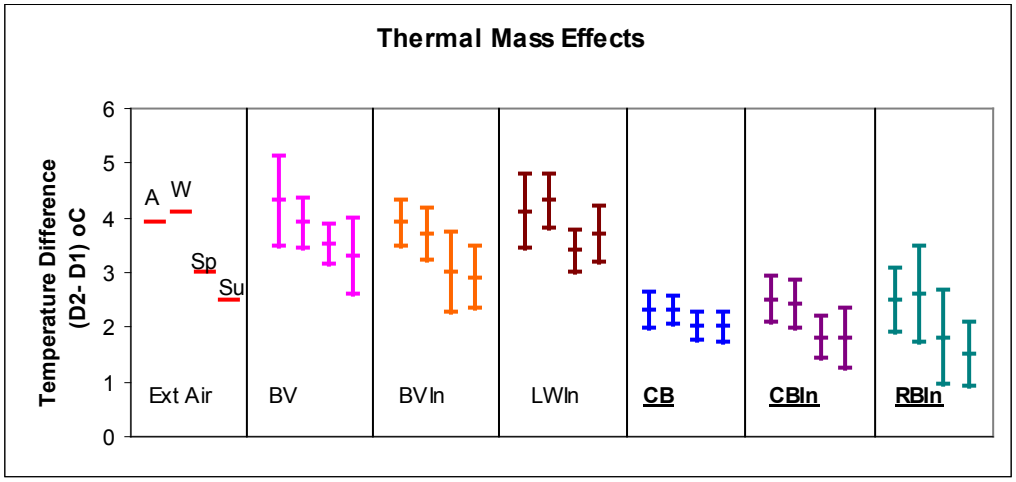

Figure 5.56 Graphical summary of Table 5.15. Buildings with high internal thermal mass are indicated in bold and underlined.

Table 5.16 Thermal resistance (insulation) effect

	Estimated 95% Confidence intervals for (mean Temp $_{insulated}$ – mean temperature $_{uninsulated}$) given the means of the external air temperatures shown in Appendix A, Table A.3	
	InsBV – BV (°C)	InsCB – CB (°C)
Autumn	0.07 ±0.48	0.65 ±0.27
Winter	-0.15 ±0.33	1.03 ±0.26
Spring	0.15 ±0.42	0.95 ±0.24
Summer	-1.2 ±0.46	-0.47 ±0.31

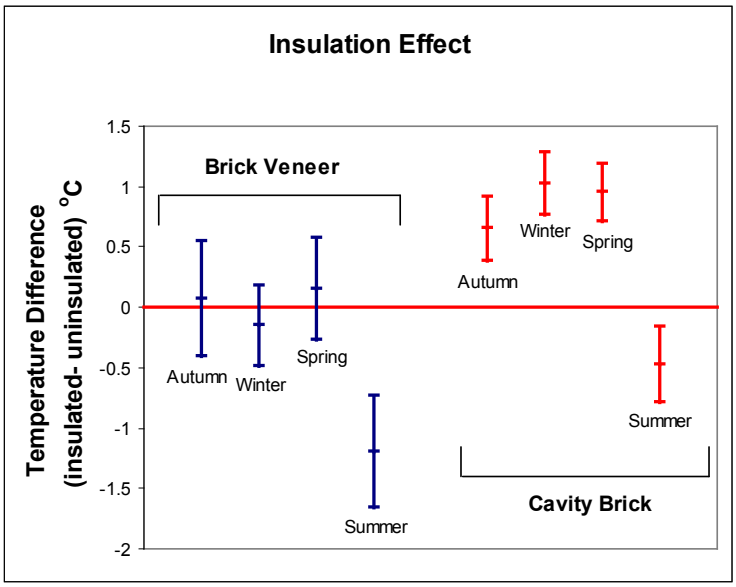

Figure 5.57 Graphical summary of Table 5.16.

The magnitude and direction of displacement of an insulated module profile relative to an uninsulated module profile was affected by the season and position of the insulation relative to the distribution of the thermal mass. For example, adding insulation to the CB module caused a shift towards higher internal air temperatures in winter (Ave difference= 1.03 ± 0.26 °C, 95% C.I) but had a small shift down in temperature for summer (Ave difference =-0.47 ± 0.31 °C, 95% C.I) (see Table 5.16 and Figure 5.57).

Adding insulation to the BV module caused a shift to lower temperatures in summer (Ave difference =-1.2 ± 0.46 °C, 95% C.I) but had no significant effect in winter, autumn or spring (see Table 5.16 and Figure 5.57). It was not unexpected that the CB and BV modules would behave differently to each other with the introduction of an insulation layer between the outer and inner leaves of the building envelope as different thermal mass layers were effectively being isolated from the room interior and exterior.

5.6.4. Summary of statistical results

The resulting statistical model of the TDMT profile for each system was used to draw inferences on the effects of the different wall systems on room thermal behaviour.

Similar to the reported findings of existing literature, it was found that the cross-sectional arrangements of thermal mass and insulation layers in the wall system are order and seasonally dependent in terms of the effect on the thermal behaviour of the room. The general effect of adding an internal high thermal mass layer, to an otherwise lightweight wall construction, was to reduce the amplitude of the TDMT profile. The general effect of adding an insulation layer between the interior and exterior leaves of an otherwise uninsulated wall system, was to displace the mean of its TDMT profile relative to the mean of the external temperature profile. The magnitudes and directions of the displacements depended on the season and the cross-sectional distributions of the thermal mass layers relative to the insulation and the interior. It should be noted however, that the general effects of the insulation and thermal mass described in this study were dependent on the thermal test modules configurations and conditions experienced as located at the University of Newcastle. The results indicate that if internal air temperature swings are allowed to occur because of building design and/or building operation then the inclusion of interior thermal mass in the design becomes critical for modulating those swings. This suggests that building codes which prescribe energy efficient construction methods and materials should allow for natural variation in building purposes by recognising the importance of thermal mass / thermal resistance combinations to suit design for purpose.

5.7. Overall Summary

It is evident from observations that the InsBV had lowest outward flow of all four modules, it also had the highest daytime temperature. There was a definite benefit to be gained by having internal thermal mass. The InsRBV had highest flow out in summer, accounting for lowest temperature. Significant difference came from the east wall flow compared to other modules. The CB was coolest module in autumn primarily due to the South wall, possibly due to lower outside temp and high solar ingress producing this higher flow, combined with lack of insulation within the wall.

6. THERMAL MODELLING – SIMULATION STUDY

6.1. Introduction

This research project presented a unique opportunity to develop and verify thermal modelling software because of availability of a large body of data on the thermal performance of real structures. Two software packages have been developed: a comprehensive modelling package based on first principles, NUMBERS (Newcastle University Modelling and Building Energy Rating Software) (Luo et al., 2006, 2007, 2008, 2010); and a predictive software tool based on a fuzzy neural network approach. These packages are described in detail in the following sections.

6.2. Development of NUMBERS Software*

6.2.1. Overview of the software

The NUMBERS software (Newcastle University Modelling and Building Energy Rating Software) was developed in-house as part of the overall thermal project. NUMBERS is a building simulation tool built from first principles that is capable of predicting the thermal performance of a building envelope for any given set of climatic data, building floor plan, walling construction and building orientation.

The software allows the user to construct a numerical representation of an actual building by positioning together walls, floors and ceilings to form zones to construct the desired building. NUMBERS can handle multi-zone and multi-story buildings by calculating the exchange of thermal energy between zones, determined from solutions of the conservation of mass and energy laws. The governing equations for each walling system and consequently each zone can be obtained by using the "Finite Volume Method (FVM)", the "Conduction Transfer Function (CTF)", or a hybrid approach combining both the FVM and the CTF. These methods are dependent on the floor plan, building configuration, climatic data and boundary conditions.

NUMBERS can predict the zone air temperatures of a building or the energy consumption necessary to maintain comfortable internal conditions. For free-floating zone temperature predictions the indoor air temperatures, time lags and decrement factors can be determined from NUMBERS, while for air conditioned scenarios the energy consumption can be predicted. Thermal radiation heat fluxes of the inner zone surfaces are determined by exchange areas with their view factors established accurately by a polygon-polygon view factor method.

NUMBERS operates by a zonal method where the floor plan of a building is divided into distinct zones; typically this will be the selection of individual rooms as zones with dividing walls of the desired materials between. Each room or area is therefore considered individually. Attic spaces are also included as an individual zone.

An overview of the structure of the program is shown in Figure 6.1.

* Dr Caimao Luo is the developer of the NUMBERS software package and the present chapter has been contributed by him

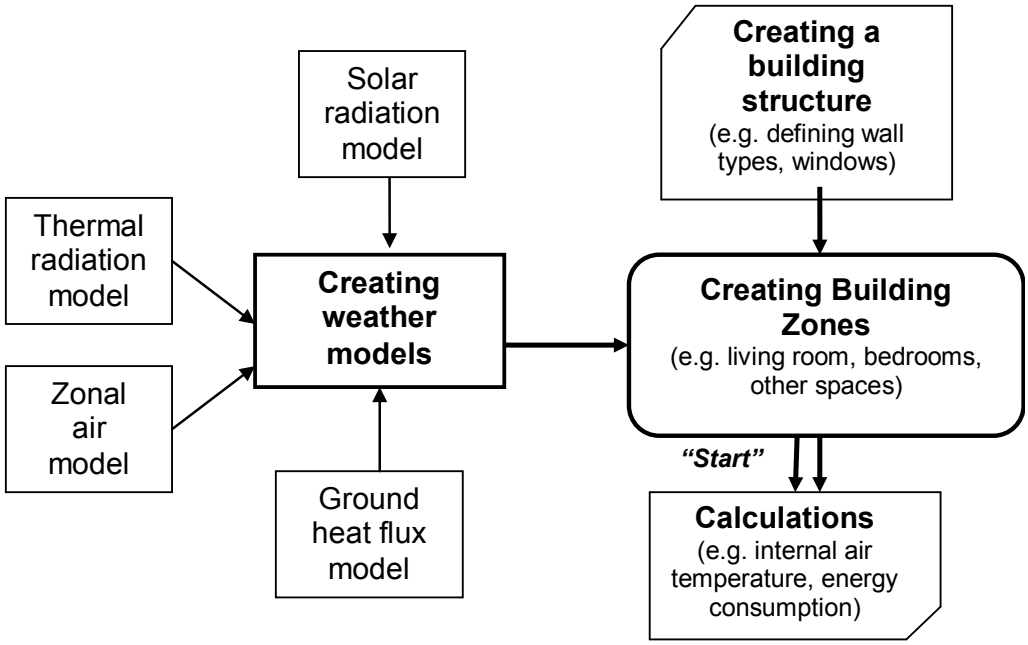

Figure 6.1 Flow chart of NUMBERS structure

6.2.2. Fundamental sub-models in the Building Energy Simulation Program

NUMBERS incorporates a series of fundamental sub-models to reproduce the essential features of the environmental conditions and building properties. A brief description of each of these sub-models is included here. Further details, including the appropriate mathematical derivations are contained in Appendix B.

6.2.2.1. Weather model

This model determines the heat flux of the exterior surfaces due to short/long wavelength radiation. The model was therefore used to predict the net beam and diffuse radiation on the outer surfaces based on the direct radiation on a plane normal to the solar beam, the global solar radiation and diffuse radiation on a horizontal surface; and the convective heat transfer coefficient based on the geometry of the building and the wind speed and direction. Details of the relationships used are given in Appendix B.1.1.

6.2.2.2. Wall Thermal Conduction Models

The purpose of the wall module is to determine the heat fluxes and temperatures on both surfaces of a wall or wall element. Two different approaches were incorporated into the software, with the selection of the appropriate method being left to the user:

a) Finite volume method (FVM)

The basic concept of the finite volume method is to divide any material layer into three sections with two inner nodes and two surface nodes, and to use some algebra to remove the variables at the inner nodes as shown in (Luo et al., 2008). The advantage of this method is that for most building materials the resulting discretised equations do not involve any inner nodes. An air gap is treated as a special construction layer and included in the calculation. The final solution for the wall provides the heat flux and temperature at any layer surface in the wall. Full details of this approach are given in Section B.1.2.1.

b) Conduction transfer function method (CTF)

The basic idea of the CTF method is to define the inner and outer wall surface heat flux at the current time nΔt as a function of the inner or outer surface temperature at times nΔt, (n-1)Δt, (n-2)Δt, (n-3)Δt …and the surface heat flux at the previous times (n-1)Δt, (n-2)Δt, (n-3)Δt …. Details of this method with appropriate descriptions are given in Section B.1.2.2.

It should be noted that the CTF method uses the heat flux and temperature at both ends of a wall, not the construction layer surface for the FVM as computational state variables, leading to less governing equations than the FVM. However, for "heavy" wall systems such as a cavity brick system, the ground floor (if treated as a "wall"), the cutoff terms nz and nq could be very large and the resulting CTF coefficients are not reliable (see Section B.1.2.2). NUMBERS therefore also provides a hybrid method which combines the advantages of the CTF and FVM methods, with the CTF method employed for the "*light*" wall system and FVM for the "*heavy*" wall system.

6.2.2.3. Ground/Floor Model

As shown in Figure 6.2, the ground floor is assumed to be a "wall" comprising several layers of construction, with an air gap and 10 layers of soil each with a thickness of 0.1 m. The heat flux at the lower surface of the deepest layer is assumed zero.

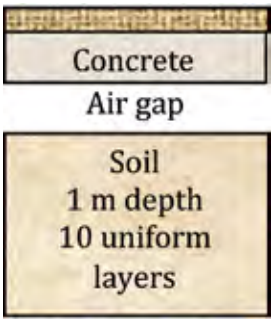

Figure 6.2 Boundary conditions at a typical floor

6.2.2.4. Window Model

This model predicts the area of sunshine on the floor, the opposite wall and neighbouring walls, taking into account the window location, geometry of the room, solar elevation and the solar azimuth (See Section B.1.4).

6.2.2.5. Zone Model

This model establishes the energy balance equations applied to the zone model (See Section B.1.5).

6.2.3. Software Input and Output Parameters

Weather data are used to calculate the heat flux and the convective heat transfer coefficients on the outer wall/roof surfaces. At the same time, relative humidity (*RH*) in the atmosphere can be used to determine the indoor RH based on the air exchange between the building zones and outside atmosphere. Apart from the weather data, input parameters are required for the construction materials, widow details, wall details, zonal definition details and shading factor for external walls (See Section B.1.6). Input is menu driven via

a user friendly interface as outlined in Section B.3. A post processing data file is provided as output with details of all the relevant parameters to define the thermal behaviour.

6.2.4. Validation of NUMBERS against housing module measurements

Since a large body of data on the thermal performance of the housing modules exists, the performance predicted by NUMBERS could be compared to the real data for a range of walling types and weather conditions. The weather data used in the validation of the software was collected from on-site measurements. The thermal properties used for cavity brick, brick veneer and light walls are given in Tables 6.1 to 6.3. The thermal properties for the roof and ground are listed in Tables 6.4 and 6.5.

The room air temperatures obtained by NUMBERS and measurements for the thermal modules without any windows for hot and cold weather conditions are given in Figures 6.3-6.4 for the cavity brick and brick veneer wall systems. Similar comparisons for modules with the northern wall are given in Figures 6.5 to 6.7. It can be observed that the numerical predictions and experimental measurements agree within reasonable error. This error could be caused by inaccuracy in the assumption related to the thermal properties of the building materials, the convective heat transfer coefficient (*CHTC*) of the inner/outer wall surfaces, solar radiation models and the infiltration air exchange between the inside and outside of the building. Note that the overall temperature trends as well as the peak values are reproduced well for all seasons.

Table 6.1 Thermal properties for a cavity brick wall

Layers	Thermal capacitance [ρC_p (J/m^{3}K)]	Thermal conductivity [k (Wm/K)]	Thickness [m]	Thermal resistance [m^{2}K/W]
Brick	1.197e6	0.6515	0.11	
Air Gap	-	-	-	0.1311
Brick	9.24e5	0.1695	0.01	
Plaster board	9.24e5	0.1695	0.01	

Table 6.2 Thermal properties for a brick veneer wall

Layers	Thermal capacitance [ρC_p (J/m^{3}K)]	Thermal conductivity [k (Wm/K)]	Thickness [m]	Thermal resistance [m^{2}K/W]
Brick	1.197e6	0.6515	0.11	
Air Gap	-	-	-	0.4736
Aluminium sheet	2.358e6	221.0	0.001	
Air gap	-	-	-	0.4736
Plaster board	9.24e5	0.1695	0.01	

Table 6.3 Thermal properties for a light weight wall

Layers	Thermal capacitance [ρC_p (J/m^{3}K)]	Thermal conductivity [k (Wm/K)]	Thickness [m]	Thermal resistance [m^{2}K/W]
Fibre-cement	1.680e6	0.5	0.009	
Air Gap	-	-	-	0.1576
Rockwool Batt R 1.5	2.944e4	0.1299	0.09	
Plaster board	9.24e5	0.1695	0.01	

Table 6.4 Thermal properties for a clay tiles roof

Layers	Thermal capacitance [ρC_p (J/m^{3}K)]	Thermal conductivity [k (Wm/K)]	Thickness [m]	Thermal resistance [m^{2}K/W]
Clay tiles	1.770e6	0.8403	0.005	
Air Gap	-	-	-	0.299
Aluminium	2.358e6	200.0	0.001	

Table 6.5 Thermal properties for the ground

Layers	Thermal capacitance [ρC_p (J/m^{3}K)]	Thermal conductivity [k (Wm/K)]	Thickness [m]	Thermal resistance [m^{2}K/W]
soil	1.613e6	1.205	4.2	
concrete	2.112e6	1.449	0.2	

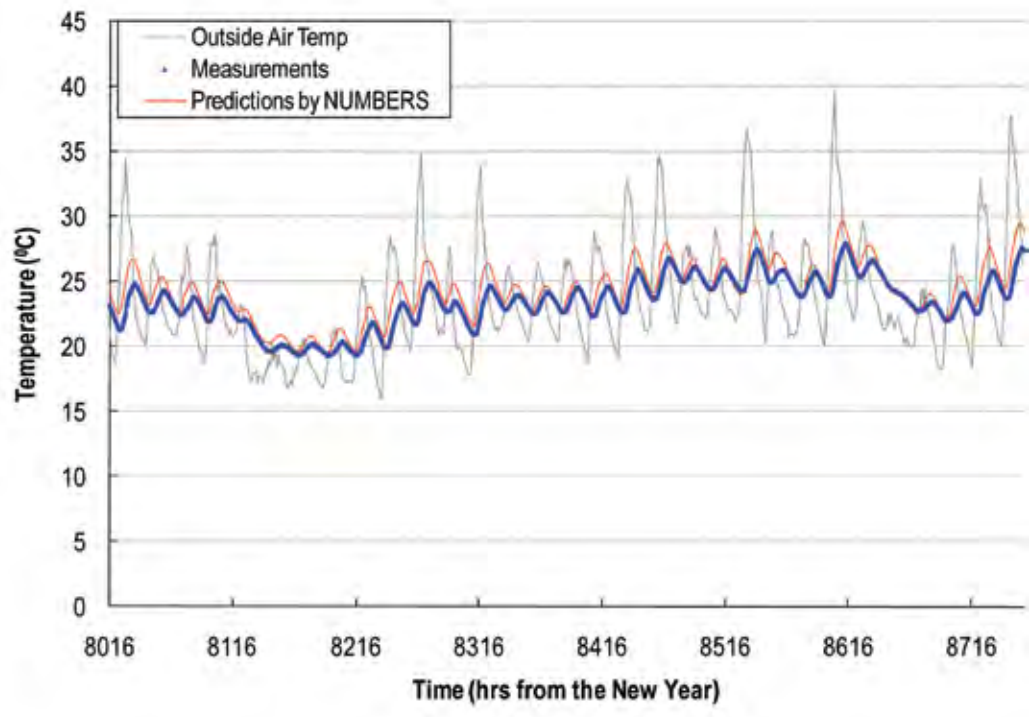

Figure 6.3 Comparison of the room air temperature between the measurements and predictions from NUMBERS for the CB module without the window for the hot weather conditions (December, 2003)

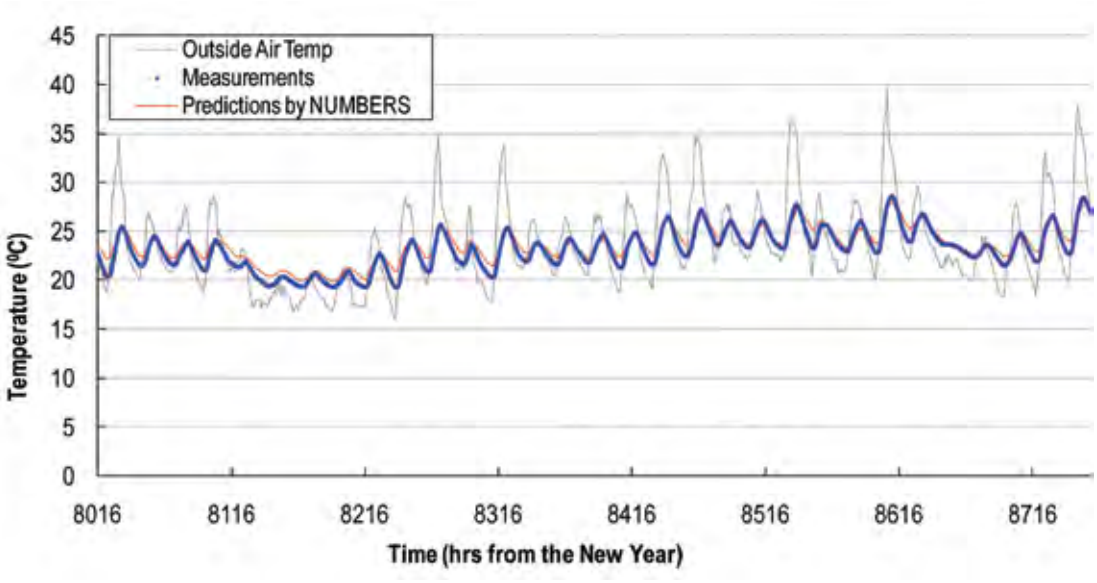

Figure 6.4 Comparison of the room air temperature between the measurements and predictions from NUMBERS for the BV module without a window in December, 2003

Similar comparison for the modules with the northern facing window for the CB, InsLW and BV modules and seasons are given in Figures 6.5-6.7.

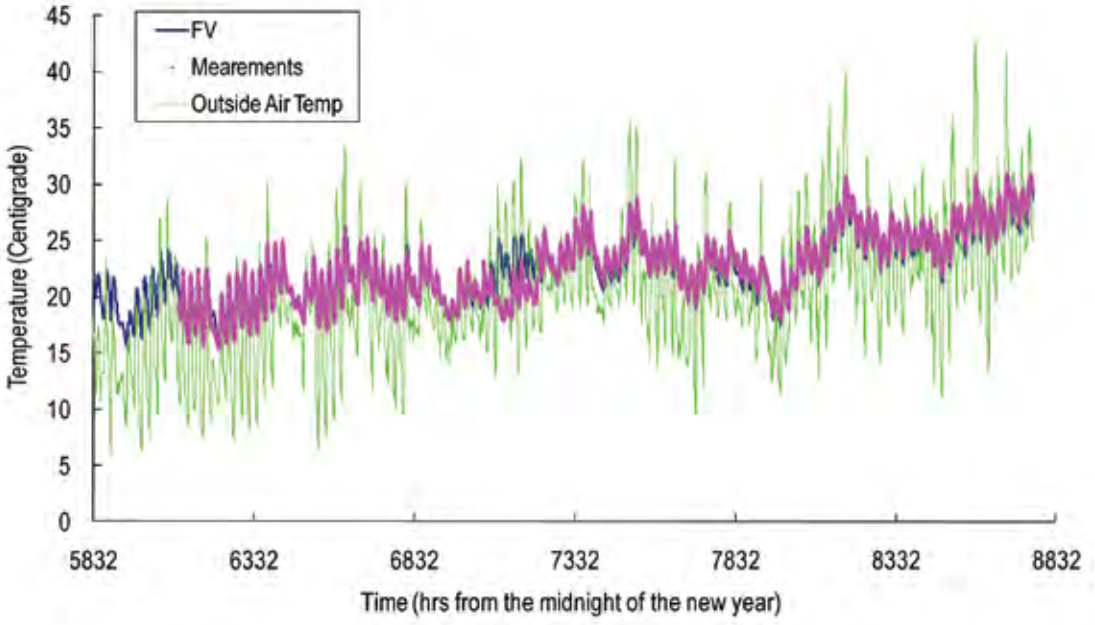

Figure 6.5 Comparison of the room air temperature between the measurements and predictions from NUMBERS for the CB module with a window (from September to December, 2005)

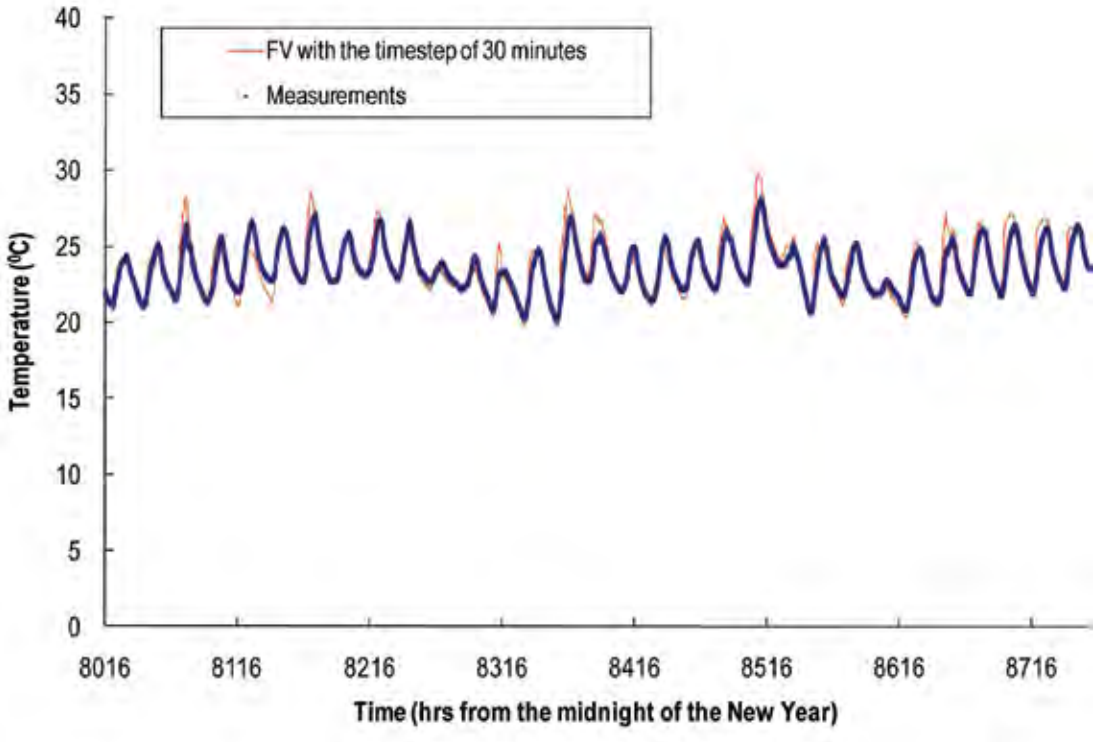

Figure 6.6 Comparison of the room air temperature between the measurements and predictions from NUMBERS for the InsLW module with a window for the hot weather conditions (December, 2007)

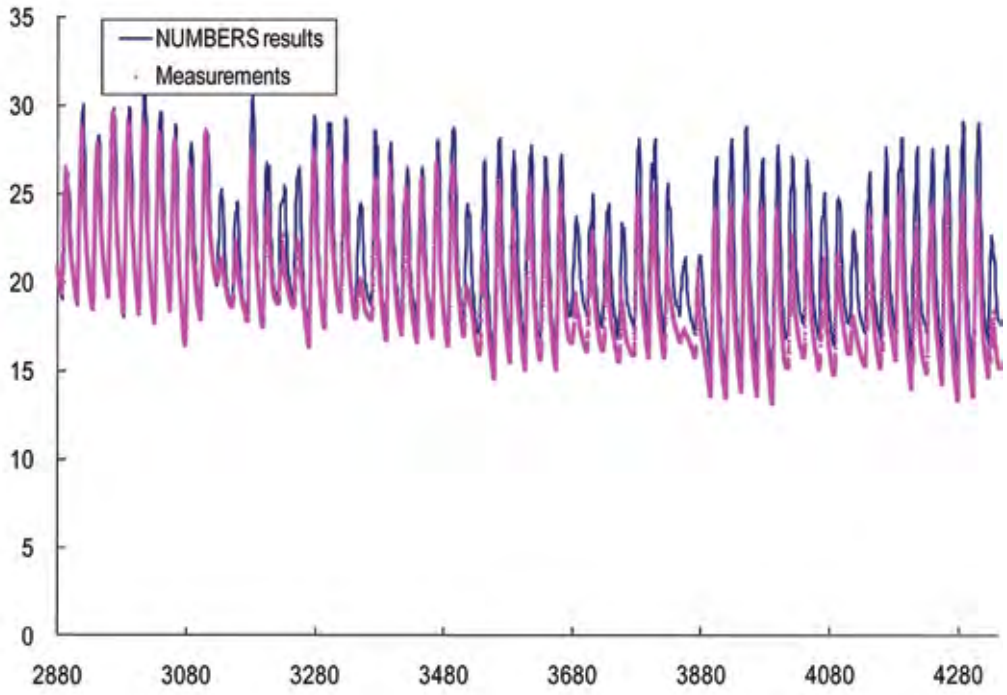

Figure 6.7 Comparison of the room air temperature between the measurements and predictions from NUMBERS for the BV module with a window for the cold weather conditions (May and June, 2006)

6.2.5. Validation of NUMBERS using Ashrae-Standard

6.2.5.1. Introduction

An accepted means of verifying a thermal modelling software package is to use the provisions of the ASHRAE Standard (*ASHRAE Standard, 2007*). This "BESTEST" procedure involves using the software to model the thermal behaviour of a standard building, and compare results with a range of other software packages.

6.2.5.2. Building Geometry and Wall properties

The basic geometry of cases 600, 610, 620 and 630 from the ASHRAE Standard is a 48 m^2 floor area, single storey, low mass building with rectangular prism geometry as illustrated in Figure 6.8. The required properties of the wall materials are given in Table B.1.

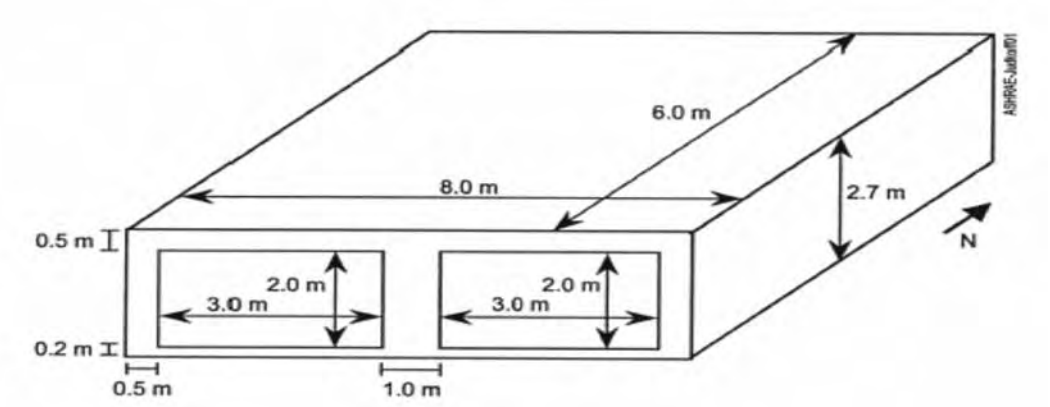

Figure 6.8 Isometric south windows - unshaded (case 600) (*ASHRAE*)

For CASE 600, the geometry is shown in Figure 6.8. This includes a 12 m^2 southern facing window.

For Case 610, the geometry is the same as for Case 600 except for addition of an overhang for the southern facing window. The horizontal overhang is assumed to extend the entire length of the southern wall.

For Case 620, the geometry is same as for Case 600 except for the changed window orientation as shown in Figure 6.9. The original 12 m^2 south-facing window is changed to 6 m^2 of window area facing east and 6 m^2 of window area facing west.

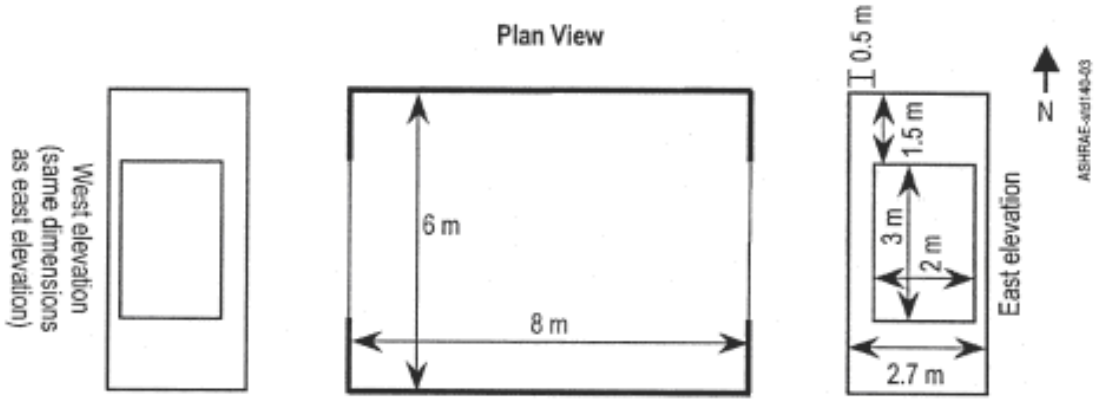

Figure 6.9 East and west window (case 620) (*ASHRAE*)

For Case 630, the geometry is the same as for Case 620 except that shading devices are added to the east and west windows as shown in Figure 6.10.

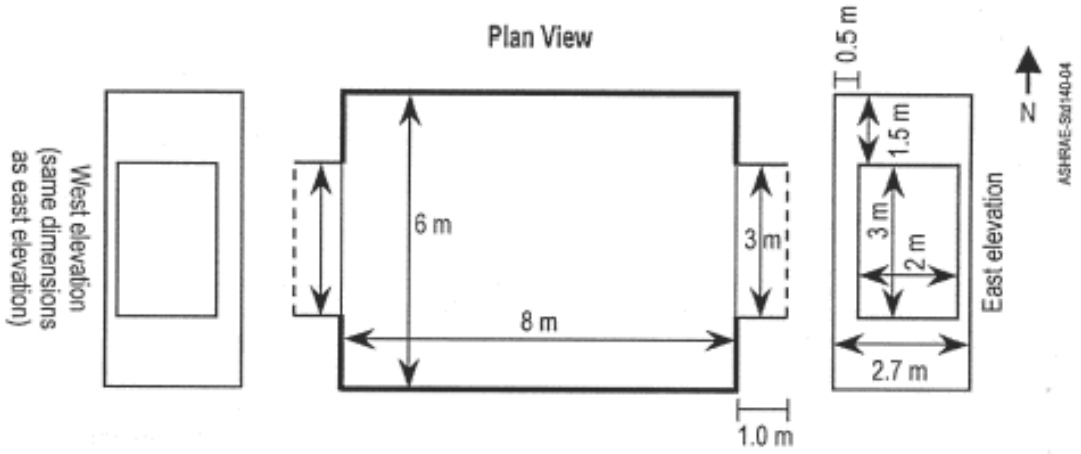

Figure 6.10 East and west window shading (case 630) (*ASHRAE*)

6.2.5.3. Heat transfer, window, infiltration and solar radiation properties

All of the properties needed for modelling the thermal performance of the test module are given in the ASHRAE Standard, and then are tabulated in Tables B.2–B.8. It should be noted that the outside surface convective heat transfer coefficients were determined automatically in NUMBERS, as well as the angular dependence of optical properties with the input at normal incidence. The interior solar distribution due to the solar radiation from open windows is also calculated by NUMBERS itself.

The weather data used in the application of the NUMBERS software was that provided by the ASHRAE Standard.

6.2.5.4. Comparison of NUMBERS result with other software results from the ASHRAE BESTTEST Standard

The final results from NUMBERS are tabulated in Tables 6.6 and 6.7. It can be seen that the Results from NUMBERS are within the range of the other reported results for all the cases investigated. From the detailed study, the cooling loads are sensitive to the overhang due to its effect on the solar radiation entering into the room zone through windows. From the comparisons, it is clear that NUMBERS satisfies the BESTEST procedures and can be assumed to be as representative of real behaviour as other modelling software.

Table 6.6 BESTTEST annual heating loads for selective available software

CASE	ESP	DOE2	SERIRES	S3PAS	TRNSYS	TASE	NUMBERS
	UK-DMU	USA	UK-BRE	SPAIN	BEL/UK	FIN.	Australia
	[MWh]	[MWh]	[MWh]	[MWh]	[MWh]	[MWh]	[MWh]
600	4.296	5.709	5.596	4.882	4.872	5.362	4.908
610	4.355	5.786	5.620	4.971	4.970	5.383	4.912
620	4.613	5.944	5.734	5.564	5.073	5.728	4.912
630	5.050	6.469	6.001	6.095	5.624		4.975

Table 6.7 BESTTEST annual cooling loads for selective available software

CASE	ESP	DOE2	SERIRES	S3PAS	TRNSYS	TASE	NUMBERS
	UK-DMU	USA	UK-BRE	SPAIN	BEL/UK	FINLAND	Australia
	[MWh]	[MWh]	[MWh]	[MWh]	[MWh]	[MWh]	[MWh]
600	6.137	7.079	7.964	6.492	6.492	6.778	6.309
610	3.915	4.852	5.778	4.764	4.601	5.506	5.159
620	3.417	4.334	5.004	4.011	3.901	4.351	4.580
630	2.129	2.489	3.701	2.489	2.416		3.324

6.2.6. Conclusions

This section has given an overview of the development and verification of NUMBERS software. The general concept was determined from the energy balance equation and is related to the "Finite Volume Method", the "Conduction Transfer Function", and/or the combination of both methods into a hybrid approach. These methods, linked with the structure and configuration of a building, together with the climatic data and boundary conditions, were implemented into NUMBERS to predict the internal temperature under free floating conditions as well as energy consumption. The accuracy of the software has been shown to be reasonable, and depends on the reliability of several parameters such as beam solar radiation heat flux, wind speed and its direction, atmospheric air temperature and indoor air temperature. The details of the applications together with mathematical solutions and derivations can be found in Appendix B and relevant publication (Luo et al., 2006, 2007, 2008, 2010).

6.3. Thermal modelling by Fuzzy Neural Network approach

6.3.1. Introduction

The objective of this project was to use the large data base available as a resource to develop predictive software based on a fuzzy neural network approach. This software would be capable of making a speedy assessment of the thermal performance of a building, and thus serve as a useful tool for preliminary assessment before a more complex simulation was made. The model can examine the internal thermal comfort in terms of the thermo-physical properties of the building envelope for typical Australian residential buildings under varying climatic conditions. This type of model has a relatively simple architecture, is computationally inexpensive and can be trained using experimental and theoretical data. The models developed for predicting the indoor temperature were trained principally from data from the four test housing modules under free-floating conditions (as described in Chapters 3-5). This aspect of the overall project was carried out as a PhD program by Haitham A. M. Alasha'ary and the full details can be found in this thesis dissertation (Alasha'ary H. A. M., 2010) and publications (Alasha'ary et al., 2008, 2009).

The neuro-fuzzy modelling approach employed was the so-called adaptive neuro-fuzzy inference system (ANFIS). An innovative hybrid modelling and prediction system referred to as adaptive neuro-fuzzy inference system (ANFIS) of Sugeno-type has been used for this study. Four different versions of an ANFIS based model were developed from experimental data using a large set of real time-series weather and surface temperature data collected from the four test modules.

The results obtained from this study demonstrate that the neuro-fuzzy model is capable of accurately predicting the room temperature and thus, the thermal performance of such buildings. It also has the potential of providing a computationally efficient and inexpensive predictive tool for the more effective thermal design of housing.

6.3.2. Overview of the Fuzzy Neural model

The experimental investigation has involved the study of the behaviour of cavity brick (CB), brick veneer (BV) and lightweight (LW) constructions, as well as the effect of insulation and major wall openings (windows).

In the neuro-fuzzy approach the model has been trained using the experimental data collected from the test modules. An innovative hybrid modelling and prediction system referred to as adaptive neuro-fuzzy interference system (ANFIS) of Sugeno-type has been used.

The development of the model had five stages which are outlined in the flowchart shown in Figure 6.11. The preliminary stage (Stage I) involved the collection of adequate information and background material as the underlying modelling approach in order to establish a solid ground for understanding of the relevant concepts. The next step was collecting and extracting the necessary input/output data from the databases that held all measurements related to the test modules. The acquired data was then grouped into "training" and "validation" data sets according to the test modules to which they belonged.

Stage II was concerned with the development and training of three preliminary versions of the neuro-fuzzy model as well as performing a sensitivity analysis on the developed models. The versions differed in terms of the type and number of input variables used for the prediction of the indoor temperature. This stage also involved the evaluation of the "trained" models using the validation data sets.

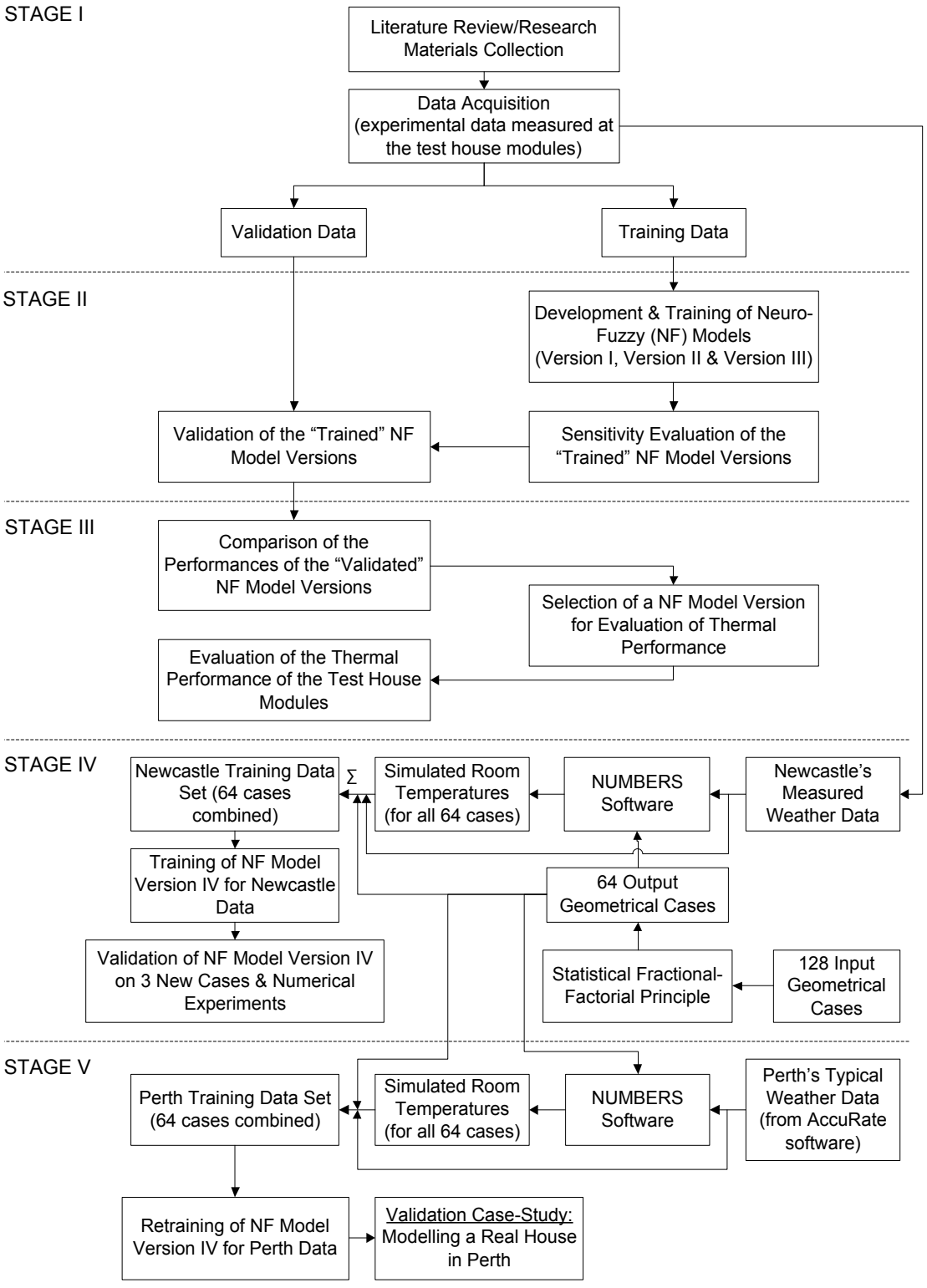

Figure 6.11: Flowchart outlining the entire system.

In Stage III the three neuro-fuzzy versions were compared to one another in terms of their performance and accuracy. A final decision was made as to which particular model was the most effective in performing the next procedure which involved evaluating the thermal performance of the four test modules in terms of internal thermal comfort.

Stage IV was aimed at making the study more comprehensive and involved the development of the final

version of the neuro-fuzzy model (Version IV). In this stage hypothetical modules made up of the same walling types as the experimental phase were each created with a full matrix of different wall and window area combinations as well as shading factors. To avoid complexity, a statistical fractional-factorial principle was then employed to reduce the size of the initial combinational matrix to a smaller partial matrix containing fewer combinations, yet still giving a clear picture of the behaviour and properties of the entire original matrix.

Finally, to validate the usefulness and practicability of the neuro-fuzzy model, Stage V consisted of a case study modelling a typical real house located in Western Australia. A more detailed description of the ANFIS approach is given in Appendix C.

6.3.3. Objectives of the neuro-fuzzy application

The application was intended to analyse the thermal performance of a building under free-floating conditions in terms of internal thermal comfort only. Energy consumption and economical factors were not taken into account in the study.

The study was performed using a synergetic neuro-fuzzy modelling technique that utilised the concepts of both fuzzy logic systems (FLSs) and artificial neural networks (ANNs) benefiting from the combination of their individual advantages to provide a powerful hybrid modelling tool. The particular neuro-fuzzy model utilised is called ANFIS (adaptive neuro-fuzzy inference system) of the Sugeno type, which is a modelling and predictive paradigm capable of predicting certain behaviours and patterns based on a set of training data.

The objectives of the neuro-fuzzy application were:

- To develop a neuro-fuzzy model and assess its capability to predict the room temperature in residential structures based on experimental climatic data collected from the four purpose-built thermal test housing modules.

- To evaluate the thermal performance of the Newcastle test modules based on the predictions obtained from the neuro-fuzzy model for a diverse range of climate conditions.

- To build a fast and effective predictive tool that could potentially be used by architects and developers for the prediction of the thermal performance of residential buildings during the planning stage. This would serve as a tool to assess the adequacy of alternative preliminary designs in terms of energy efficiency.

6.3.4. Performance of ANFIS Models

6.3.4.1. ANFIS Version III

The selected ANFIS Version III was trained against independent training data sets obtained from the test modules (BV, InsLW and CB). As each model was progressively refined, its generalisation capability was examined for all modules by predicting their internal air temperatures based on the experimental observations of the four climatic parameters (see Table 6.8).

The block diagram of ANFIS Version III shown in Figure 6.12 illustrates the input and output variables involved.

Table 6.8: Description of the input variables used for the four versions of the ANFIS model

Model Version	Number of Inputs	Input variables	Predicted Output
Version I	6	Interior surface temperatures: Properties of the northern, southern, eastern and western walls; ceiling and slab	Room air temperature
Version II	6	Exterior surface temperatures: Properties of the northern, southern, eastern and western walls; roof and underground	
Version III	4	External climatic data: *Outside air temperature, wind speed, wind direction and horizontal-plane solar radiation*.	
Version IV	13	External climatic data + time + building geometry: Time of day, outside air temperature, wind speed, wind direction and horizontal-plane solar radiation, north wall area ratio, north, south, east and west window area ratio; wall shading factor, window shading factor and walling type	

Note that ANFIS Version III was "trained" with experimental data obtained from the module tests. The data used for testing Version IV was generated using the NUMBERS software package.

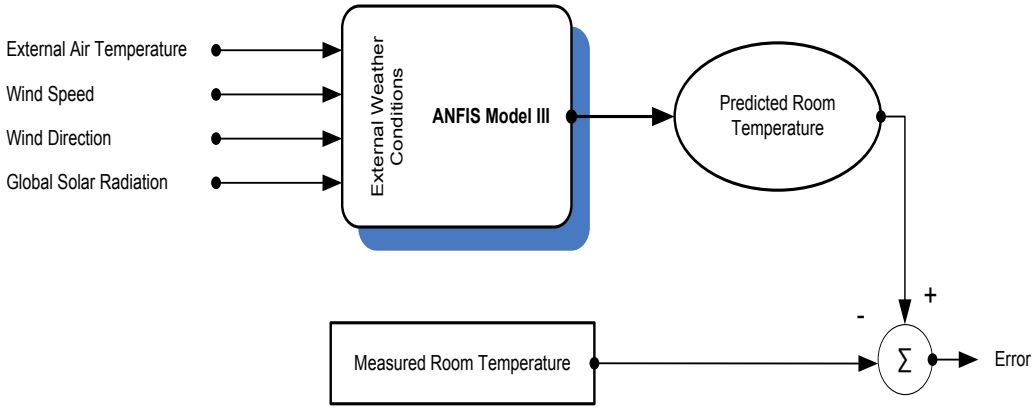

Figure 6.12: Block diagram of ANFIS Version III indicating the input/output variables.

To evaluate and validate the performance and accuracy of the ANFIS model, the "trained" ANFIS Version III was validated against "unused" validation data sets (i.e. data from module observation periods not used in the training phase). Numerical predictions for the room temperatures were generated by ANFIS Version III and then compared with the actual measurements. Figure 6.18 shows examples of the predicted room temperature obtained by ANFIS Version III compared to the corresponding measured room temperature for the BV test house module. The percentage error is also shown.

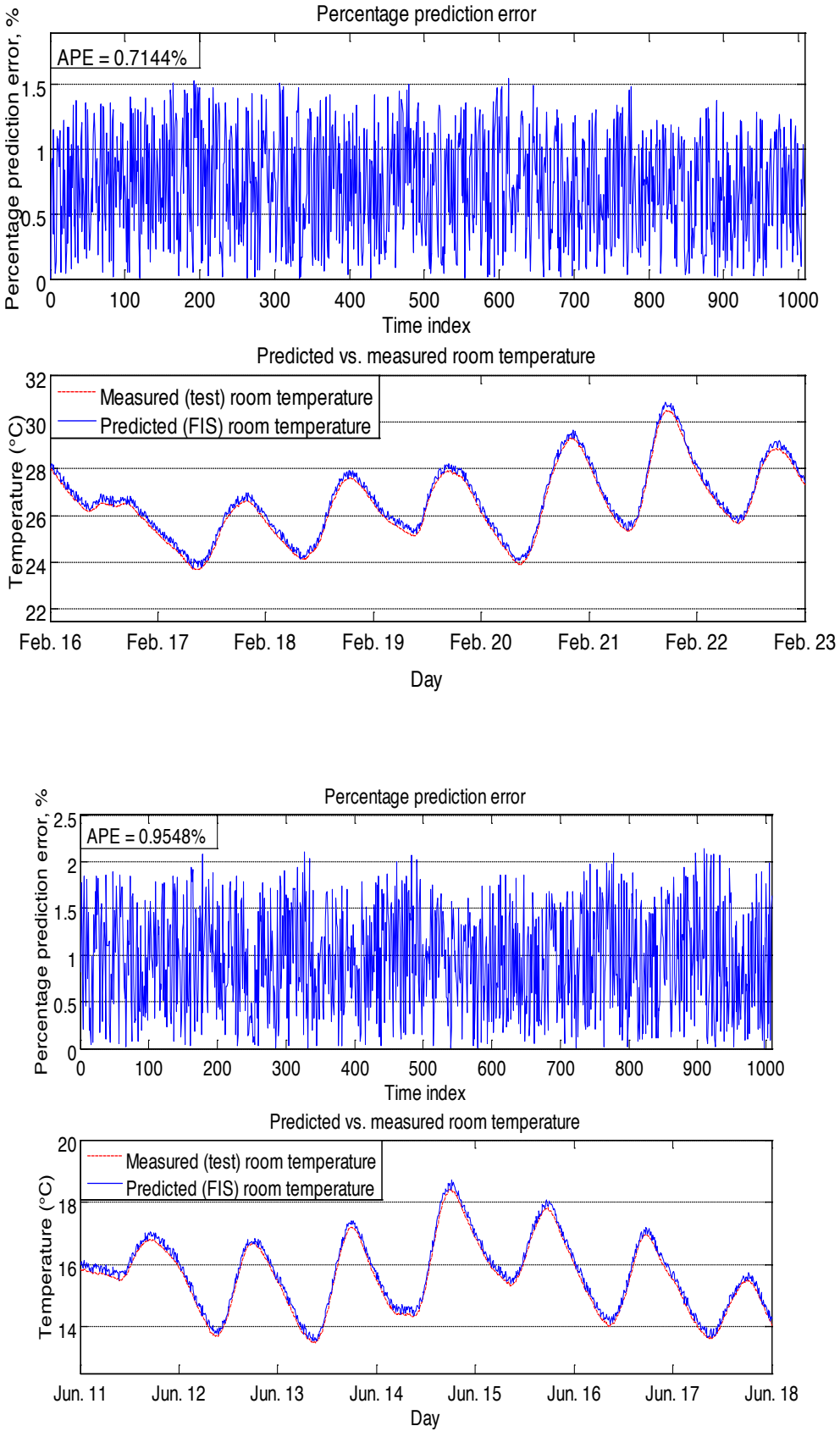

Figure 6.13 ANFIS Version III - measured vs. predicted room temperature for the BV module: (Top) summer: 16th – 22nd, February 2004, (Bottom) winter: 11th – 17th June 2004.

The predictions for other modules for one week periods representing the hottest and coldest climatic cycles of the calendar year can be found in the dissertation, with the agreement being good in all cases [Alasha'ary H. A. M, 2010]. Note the internal room temperature was predicted with a small error for all modules. The largest discrepancy was observed for the InsLW module in which the error curve diverged by a maximum value of approximately 2.7% and an average of about 1.2%.

It can therefore be concluded that ANFIS Version III exhibits very good performance in terms of room temperature predictions compared to the corresponding room temperature measurements.

6.3.4.2. ANFIS Version IV

ANFIS Version IV deals with hypothetical houses constructed of defined geometries from walling types BV, CB and LW and the performance evaluated from data derived using the NUMBERS software. To cover a broad range of configurations the building envelope for each hypothetical housing module was expressed in terms of a number of key variables, namely: the wall area; the window area; the wall shading factor; and the window shading factor (see Table 6.8). A block diagram of the Model Version IV is shown in Figure 6.14.

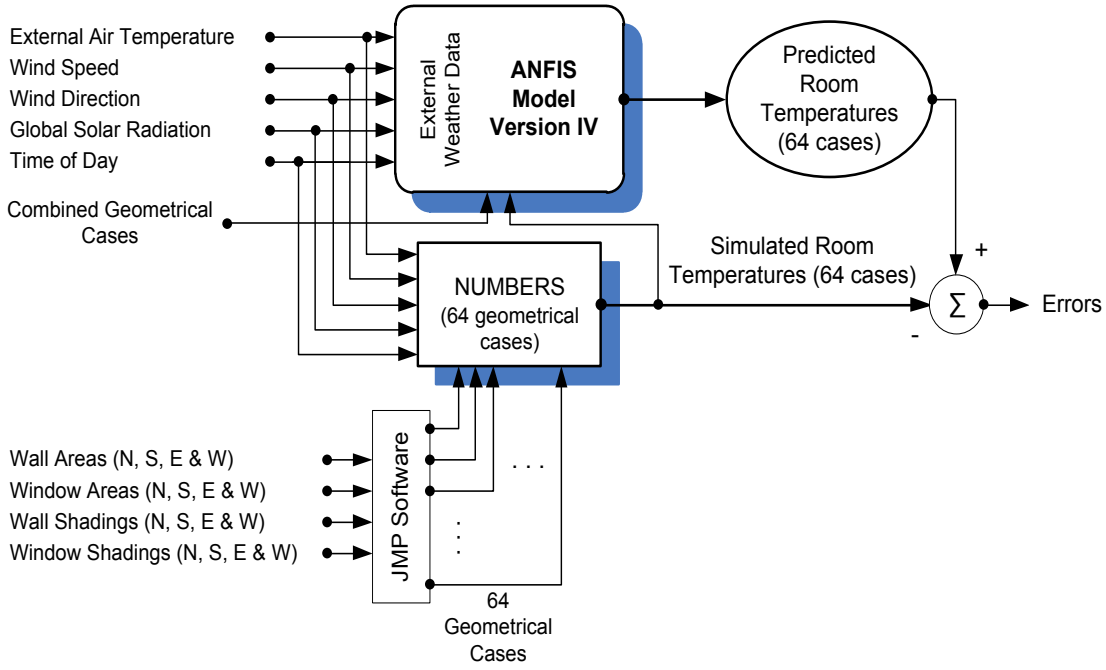

Figure 6.14: Block diagram of ANFIS model Version IV indicating the input/output variables.

Once the 192 geometries were simulated by NUMBERS, they were then combined into a single massive training data set in preparation for model Version IV training which was achieved using the input/output data sets available from the real test house modules and those obtained from NUMBERS simulations. This super training data set was represented by an enormous 1,681,920 x 14 matrix (14 refers to the 13 weather/geometrical input variables as well as the single simulated room temperature).

This ANFIS-based model Version IV was developed and trained to comprehend all geometrical configurations of the three hypothetical modules represented by the JMP-generated corresponding patterns. It had a five-rule, 13-input structure and was similar in architecture to those used in the first three versions. An epoch value of 500 was employed to train this model version which was sufficient to allow the model to attain a steady-state condition (when the training error is minimal).

Some or all of the four variables was varied to generate distinct geometrical configurations. Each variable was expressed in terms of the percentage of total surface area using a three-level assignment (lower, middle and upper). In addition, the effect of a rectangular floor plan was taken into account by considering wall areas of different sizes facing in the north, south, east and west directions. This increased the number of key variables to 16 implying that 3^{16} or 43,046,721 permutations would have to be considered per module if a three-level full-factorial approach was to be implemented. Given that there are three hypothetical modules, the number of required runs with NUMBERS software would be 129,140,163 which - with an average run time of 5 minutes - would take about 1229 years to complete!

Given that the full-factorial approach was impractical, a more appropriate method had to be adopted based on the partial-factorial approach using a set of simplifying assumptions:

Each hypothetical module had a rectangular floor plan comprising identical opposite sides (e.g. a pair of north/south walls had identical dimensions).

- The ceiling height was identical to that of the test house modules, i.e. 2.45 m.
- The total wall surface area of all hypothetical modules was kept constant and equal to that of the test house modules, i.e. 58.8 m^2 (i.e. 6 m x 2.45 m x 4).
- Each wall incorporated a centrally-located single-glazed window.
- The window/wall aspect ratio was kept unchanged, i.e. window height/wall height = window length/ wall length.
- Wall shading was the same on all walls at all times. Window shading was treated similarly.

Assumption 1 implies that once the area of a specific wall is known, the area of the other walls can be automatically determined resulting in a single key factor rather than four to express the wall orientation. For example, if the area of the northern wall is 35% of the total wall surface area, then the surface areas of the southern, eastern and western walls will be 35%, 15% and 15% of the total wall surface area, respectively.

Assumption 6 indicates that all walls must have the same amount of shading. Also, all windows should have similar shading levels. This again eliminates the effect of orientation and, thereby, reduces the number of shading-related variations to two rather than eight (i.e. one for wall and another for window).

The above assumptions effectively reduced the number of key variables from 16 to 7 (i.e. one key variable of wall area, four key variables of window area and two key variables of wall/window shading each at three levels of lower, middle and upper) requiring 3^7 = 2,187 permutations for each module (see Table 6.9).

Table 6.9 Proposed three-level proportional assignment of each variable factor

Key Variable	3-level ratio assignment			Comment
	Lower	Middle	Upper	
Oriented wall area	15%	25%	35%	Indicates the proportion of the oriented wall area to the total wall surface area
Window area	25%	50%	75%	Indicates the proportion of the window area with respect to the respective wall area
Wall shading	25%	50%	75%	Indicates the shaded proportion of the respective wall
Window shading	25%	50%	75%	Indicates the shaded proportion of the respective window

The percentage values assigned to lower, middle and upper levels for each key variable were adopted from the data reported in the literature for typical residential buildings in Australia.

The JMP statistical analysis of variables revealed that the effect of the middle level assignment on the overall characteristic of a given building module was indeed minimal and as such a two-level assignment (i.e. lower and upper) was quite sufficient. This finding allowed a further simplification of the problem implying that only $2^7 = 128$ permutations were needed to fully describe a given building module.

Using these 128 combinations as inputs to the JMP software, JMP was able to reduce this number by 50% resulting in 64 combinations representing the initial system without much loss of information or characteristics of the system. As such, the total number of numerical runs with NUMBERS for the three modules altogether was reduced to a manageable value of 192 (= 3 x 64).

The ANFIS Version IV results are presented for the three hypothetical modules only for the first case. Each module was validated against two 1-week periods representing cold and hot climatic conditions. Figure 6.15 shows an example of the validation results for the hypothetical BV module.

The performance of ANFIS Version IV was not quite as good as for the ANFIS Versions I-III in terms of validation of the results. However, it was still reasonable for this more generalised case and is within the 10% error tolerance set for this study.

The predicted temperature curve (solid blue line) tracks the simulated temperature curve (dashed red line) quite well maintaining the trend in all cases. The error curve on top of each plot tracks the relative deviation between the two temperature plots and confirms the satisfactory performance of ANFIS Version IV.

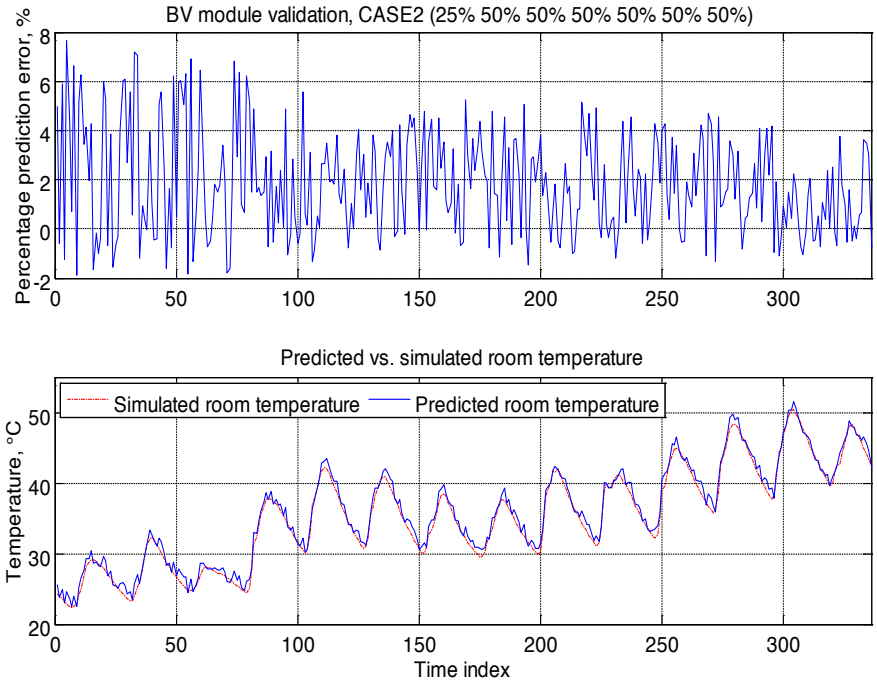

Figure 6.15: Simulated vs. predicted room temperature of the BV hypothetical module.
Note: all percentages describe the 7-dimensional space generated by the seven geometrical variables, i.e. the northern, eastern and western walls and the window areas.

6.3.5. Conclusions

This section has given an overview of the development of a Fuzzy Neural model for predicting the internal temperatures of housing constructed from different walling systems. The general concepts and techniques used to develop and "train" the model from the observed experimental results from the housing tests modules have been presented. It has also been demonstrated that it is applicable to a wider range of housing than the simple test modules. More complex details of the development and applications of the module can be found in Appendix C and in the doctoral dissertation of Haitham A. M. Alasha'ary and other subsequent publications (Alasha'ary H. A. M, 2010).

6.4. Summary

Two thermal modelling software packages have been developed as part of this investigation, and then have been described in this chapter. One of the packages (NUMBERS) is based on first principles, incorporating within it theoretical, first principles models for weather, thermal conduction of walls, ground/slab and windows. Using a zonal approach, this program is capable of predicting the resulting internal conditions from a given set of weather conditions.

The second package is a fast, predictive tool based on a fuzzy neural network approach; with the model "educated" using data collected from the housing test modules.

Both models are capable of predicting building behaviour, the Fuzzy Neural model being most useful for fast, preliminary analysis and NUMBERS being used for more complex analysis of building behaviour.

7. SMART UTILISATION OF THERMAL MASS – HYBRID APPROACH

7.1. Overview

The normal convention in designing a house is to use the same walling system for the full building envelope. Typically this is selected on the basis of aesthetics and economics. However, applying the principles of solar-passive design and using the various wall characteristics to their full advantage, it may be more effective to use a range of walling types strategically located to obtain the most efficient thermal performance. This chapter presents the results of an investigation into the use of hybrid walling systems in this manner.

The results of a combined numerical, statistical and experimental study concerned with the use of dissimilar walling systems on the external parts of a given building envelope are summarised. The rational behind the "hybrid wall" concept is to achieve a more effective distribution of thermal mass across the envelope and, hence, improve the overall thermal performance of the building. The effectiveness of the "hybrid wall" concept was investigated using a series of hypothetical building modules of common Australian residential constructions, namely Light Weight (*LW*), Brick Veneer (*BV*), Reverse Brick Veneer (*RBV*) and Cavity Brick (*CB*). These designs were examined numerically using the commercial energy rating tool "*AccuRate*", statistically using JMP software and experimentally using a novel bench-scale setup. The performance of each design was evaluated on the basis of its energy consumption. The numerical predictions and experimental data highlighted that the eastern and western walls have the most impact on the energy consumption under Australian climatic conditions. It was found that considerable reductions in the energy consumption could therefore be achieved through the use of high thermal mass insulated walls on the eastern and western sides of the building envelope. The key features of this investigation are presented here. More details can be found in Ms. K. Gregory PhD dissertation (Gregory K. E., 2010) and related publications (Gregory et al., 2008, 2009)

7.2. Numerical Studies

7.2.1. AccuRate Software

AccuRate is an energy rating tool developed by the Australian Commonwealth Scientific and Industrial Research Organisation (*CSIRO*). The main purpose of the software is to predict the energy consumption for air-conditioned buildings and the zone air temperatures for free-floating buildings. It allows for the comparison of the thermal performance of different styles and designs of buildings. It is an indicator of the energy needed to be added or removed to keep the conditioned floor area of the building comfortable. AccuRate assigns a star rating to a residential building based on its calculated annual heating and cooling energy requirements.

The software requires detailed information about the building such as orientation, construction type, insulation levels, window size, shading, overshadowing, ventilation to name a few. The mathematical basis of the AccuRate software is the "Frequency Response" method in which the systems inputs and outputs are viewed as being sinusoidal in time. The building is assumed to consist of a number of zones each comprised of elements, such as the floor, roof, ceiling, walls and windows. Each building element is considered to be composed of a series of homogeneous layers, referred to as "slabs". By combining the response of

the individual slabs, the response of the building to a given input file can be determined. The input file is usually in the form of a weather data file, which is a year of data representing typical climatic conditions for a given geographical location (outdoor dry bulb air temperature, relative humidity, wind speed, wind direction, global solar radiation on the horizontal plane, diffuse solar radiation on the horizontal plan, cloud index, pressure). In the case of Newcastle, the year 1974 has been selected as a typical weather pattern for the Newcastle area. This input data for AccuRate cannot be changed by the user.

The model calculates heating and cooling energy data on an hourly basis over a period of one year. The output from the model is a simple report detailing the quantity of heating and cooling energy that would be required to maintain conditions within the building to the assigned comfort zone. A one-to-ten star rating is given to the building corresponding to the energy performance with ten stars given to the most efficient building design. Star ratings correspond to different energy consumption rates depending upon the climate zone.

AccuRate is a second generation energy rating tool. The upgrade of the previous NatHERS software (NatHERS) has seen improvements in natural ventilation modelling, user-defined constructions, improved modelling of roof spaces, sub-floor spaces, skylights and horizontal reflective air gaps, and the availability of many more zones.

The heating and cooling temperatures are set by AccuRate and cannot be changed by the user. The thermo stat settings for the Newcastle climate zone can be seen in Table 7.1 below:

Table 7.1 AccuRate's Thermostat Setting

Area	Actual Location	BCA Climate Zone	AccuRate Climate Zone	Heating Living, Kitchen, other zones	Heating Bedroom Zones 00:00 – 07:00	Heating Bedroom Zones 08:00 – 16:00	Cooling All Zones
Newcastle	Williamtown	5	15	20	15	18	25

7.2.2. JMP Statistical Software

JMP is a division of SAS Institute Inc. (SAS) and was developed by John Sall and others to perform simple and complex statistical analyses. It provides a comprehensive set of statistical tools as well as design of experiment and statistical quality control. It dynamically links statistics with graphics to interactively explore, understand, and visualise data.

In this application of JMP, multiple linear regressions using the stepwise method for selection of a variable into the model was used. The influence of a variable or interactions of variables, errors and other factors are all calculated and presented within the model. To ensure the model logically represented the data, manual override by the investigator was used so as the main effects were selected first, followed by sensible interactions. This model allows for the effect of each wall on energy consumption to be quantified. The model developed can also be used as an energy consumption predicting tool rather than using a complex thermodynamic model such as AccuRate.

7.3. Hybrid Wall Study

For this comparative study relatively simple idealised hypothetical building envelopes were considered rather than a complete house. This allowed the direct comparison of various forms of building envelopes without the complexities which would be present if a complete house design was considered. Three envelope types were considered (Figure 7.1):

- Module A: Module A is a 6 m square module, consisting of only the exterior walling systems under investigation and with no doors, internal walls or windows.

- Module B: The physical configuration of this module was based on Module A with an additional 2.05 m x 2.84 m single glazed 6.38 mm thick window on the northern wall to examine the effects of solar radiation entering the modules.

- Module C: Module C was a modified version of Module B in which internal walls of bare brickwork panels 2 m by 1 m have been added to examine the effect of additional thermal mass. In previous studies, it was found that Module C with a north facing window and internal bare brick wall was the most energy efficient module.

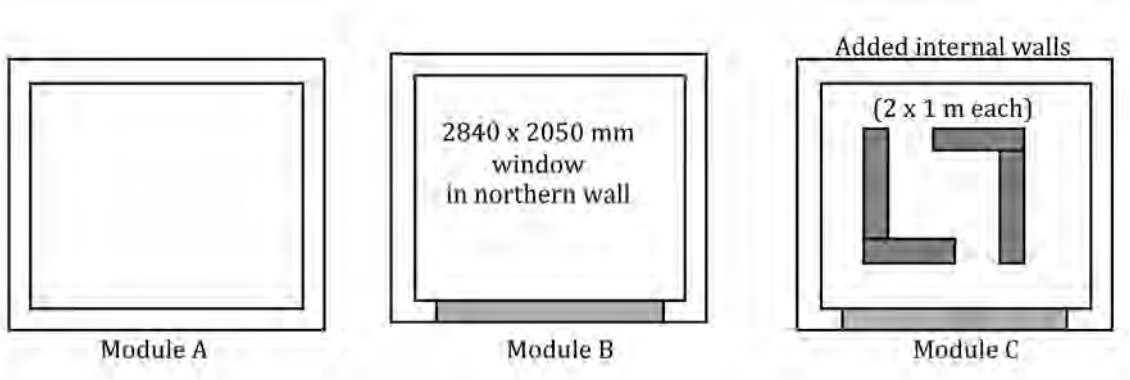

Figure 7.1 Plan views of building modules considered in this study

Each module was assumed to be constructed on a 100 mm reinforced concrete slab-on-ground. No floor coverings were present to ensure the thermal mass of the slab was exposed. The roof construction was assumed to be from light coloured tiles with reflective foil underlay, at a pitch of 22 degrees with a plasterboard ceiling and R 3.5 m^2K/W glass insulation batts.

Each module was initially modelled with a uniform walling system in which the Northern (N), Southern (S), Eastern (E), and Western (W) walls had identical construction. The resulting energy consumption for each module is shown in Table 7.2.

Table 7.2 Energy consumption (MJ/m² per annum) for uniform walling systems for each building module

	Module A	Module B	Module C
Insulated Cavity Brick (***ICB***)	72.4	45.5	42.4
Insulated Reverse Brick Veneer (***IRBV***)	68	46.3	42.5
Insulated Brick Veneer (***IBV***)	65.5	72.5	50.7
Insulated Light Weight (***ILW***)	75.6	75.8	60.1
Brick Veneer (***BV***)	82	62.9	60.7
Cavity Brick (***CB***)	131.8	83.9	82.5
Reverse Brick Veneer (***RBV***)	170.9	121.1	120.5
Light Weight (**LW**)	202.9	206.3	184.2

Note: Acronyms describing walling system differs here form previous chapters as data/analysis originates from K. Gregory thesis (Gregory, 2010)

In the case of Module A the use of a uniform IBV walling system results in the lowest energy consumption of 65.5 MJ/m² per annum. For Modules B and C, however, the ICB walling system had the lowest energy consumption of 45.5 MJ/m² per annum and 42.4 MJ/m² per annum, respectively.

Table 7.3: Combinations for hybrid walling studies

Case	Northern Wall (*N*)	Eastern Wall (*E*)	Southern Wall (*S*)	Western Wall (*W*)	Star Rating	Energy [MJ/m²]
1	BV	BV	ICB	BV	5.4	78.8
2	BV	ICB	ICB	ICB	5.6	73.9
3	ICB	BV	BV	BV	5.3	79.1
4	BV	BV	BV	ICB	5.4	78.2
5	ICB	BV	ICB	ICB	5.6	74.3
6	ICB	ICB	BV	ICB	5.6	74.4
7	ICB	ICB	ICB	BV	5.6	74.3
8	BV	ICB	BV	BV	5.5	78.8
9	BV	ICB	BV	ICB	5.5	75.7
10	BV	BV	ICB	ICB	5.5	75.4
11	ICB	ICB	BV	BV	5.5	77
12	BV	ICB	ICB	BV	5.5	76.3
13	ICB	BV	BV	ICB	5.5	75.9
14	ICB	BV	ICB	BV	5.5	75.4
15	ICB	ICB	ICB	ICB	5.7	72.4
16	BV	BV	BV	BV	5.2	82

It would be desirable to model the interaction of each of the different walling systems, (LW, BV, RBV, CB, ILW, IBV, IRBV, and ICB) on each different orientation (N, S, E and W). This, however, leads to a total of 4096 combinations of case studies. As it was not practical to model this many permutations, the case studies needed to be reduced. Hence, each walling system was studied in combination with the ICB construction, which was the best performing construction for the uniform, walling system case. Using BV as an example, the possible wall combination together with the resulting energy consumption and star rating obtained from AccuRate, are given in Table 7.3.

As can be seen from Table 7.3 there are 16 different combinations. This was repeated for each walling system resulting in 112 combinations per module or 336 combinations in total. All combinations were modelled in rating mode, where the amount of energy needed to be added or removed to the module to keep the module within a specific temperature range (18 – 25°C) was calculated.

Results for Module A are plotted in Figure 7.2. It can be seen that the energy consumption of a uniform module can be decreased by installing ICB walls. In the case of the LW construction the energy consumption was largely decreased by installing ICB walls, and their most efficient position was on the southern or western wall. This modification on the western wall offered an energy saving of 43.3 MJ/m^2 per annum. Furthermore by combining ICB walls on the southern and western, or eastern and western, or southern and eastern, energy consumption was further decreased by 36.3 MJ/m^2 per annum. This trend was also evident in the RBV and CB modules. Installing ICB walls in the BV, IBV, ILW and IRBV constructions did not offer a significant improvement in energy efficiency.

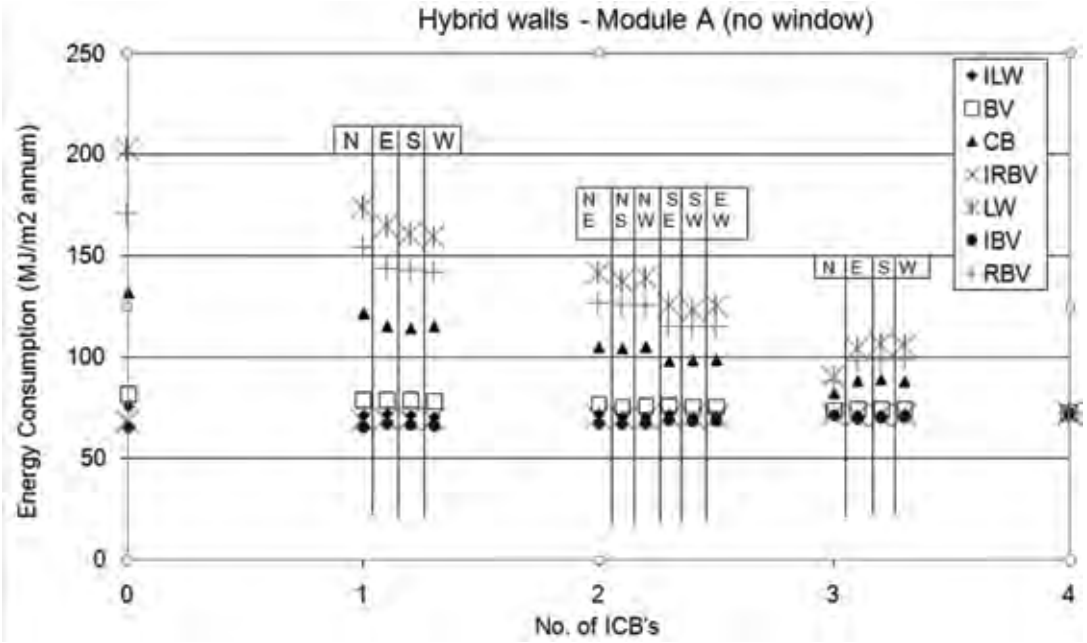

Figure 7.2: Energy consumption for Module A predicted by AccuRate energy rating software.

The results for a similar study for Module B are presented in Figure 7.3. It is evident from Figure 7.3 that LW and RBV walling systems once again had a similar profile to the LW system in Module A. Although now, installing one ICB wall on the western or eastern side of the envelope had the most influence on reducing energy consumption by 61.7 MJ/m^2 per annum.

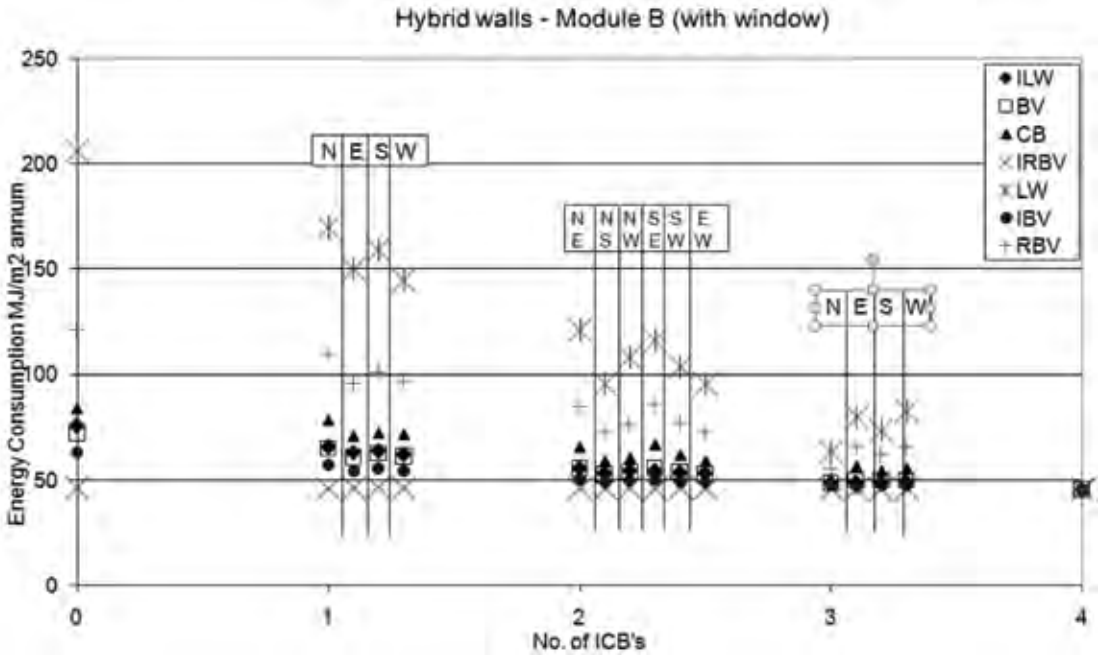

Figure 7.3 Energy consumption for Module B predicted by AccuRate energy rating software

Once again, installing ICB walls in CB, BV, IBV, ILW and IRBV constructions did not offer a significant improvement in energy efficiency.

For Module C, Figure 7.4, it was again evident that the eastern and western walls had the most influence in reducing energy efficiency with an ICB wall on the western wall saving 51.6 MJ/m^2 per annum. Although in combination, the northern and eastern wall can decrease energy consumption by 94.9 MJ/m^2 per annum compared to a uniform LW module.

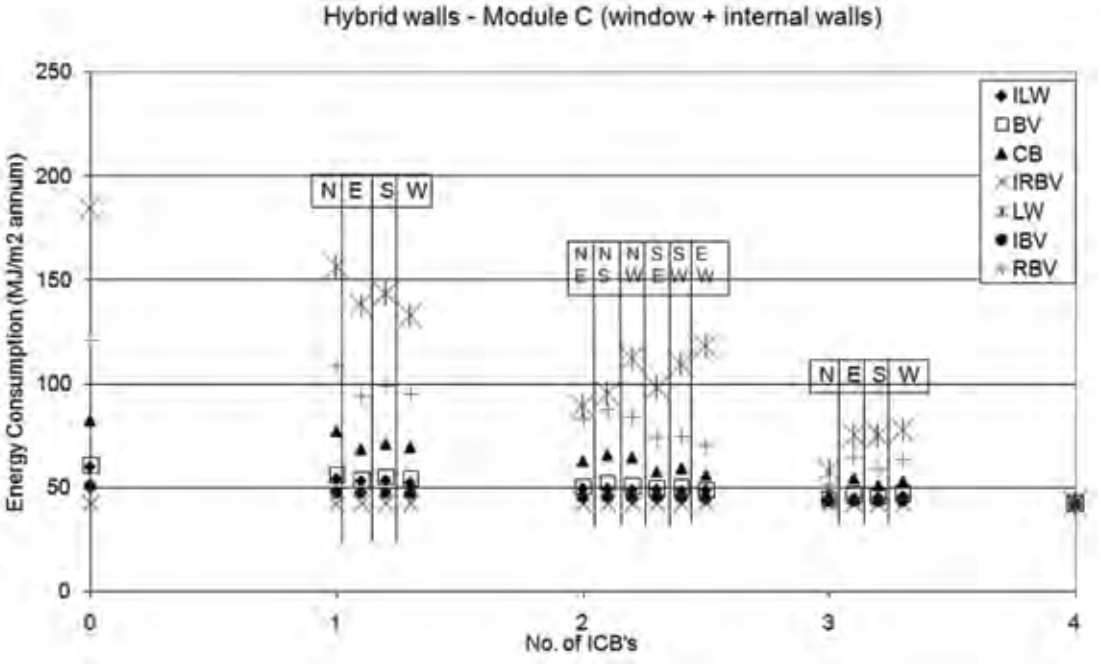

Figure 7.4 Energy consumption for Module C predicted by AccuRate energy rating software

In Modules B and C, the CB performance was closer to the BV although it was intuitively expected that CB would have better performance than BV.

7.3.1. JMP Analysis

The AccuRate predictions for each module were also analysed with the JMP statistical software and a multiple linear model was developed. It was based on the structure of each walling system: external thermal mass (*O_TM*), internal layer of thermal mass of the external wall (*I_TM*) and the variable (*I*) showing if insulation was present (1 = yes, 0 = no), see Table 7.4.

Table 7.4: Properties for each walling system *O_TM*, *I_TM* and *I* presence

Material	O_TM [kJ/K]	I [-]	I_TM [kJ/K]
BV	2352.1	0	133.1
CB	2352.1	0	2352.1
RBV	145.2	0	2352.1
LW	145.2	0	133.1
IBV	2352.1	1	133.1
ICB	2352.1	1	2352.1
IRBV	145.2	1	2352.1
ILW	145.2	1	133.1

There were several aspects of the analysis that may affect the results obtained from JMP. The factor space was analysed using a 3D scatter plot (Figure 7.5) and it was found that all extremes of the ranges of each variable were used leading to a good fit for the model.

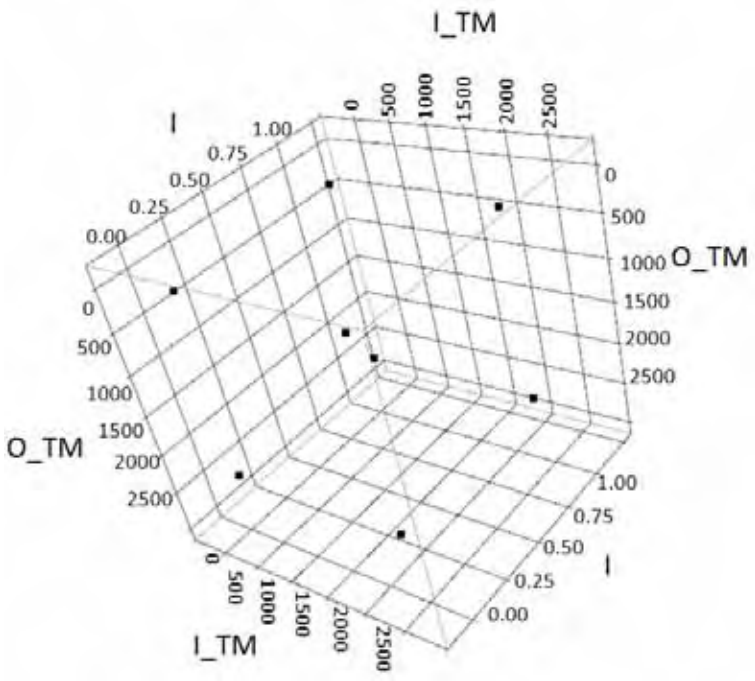

Figure 7.5 3D scatter plot from JMP for uniform modules (the data points are predictions by AccuRate energy rating software)

Relevant JMP models were developed for each building module and from this the influence of the properties of each walling system was quantified by comparing their engineering significance (see Figure 7.6). Engineering significance is a statistical term used to describe the influence the change of a variable has on another variable. The JMP model calculates an estimate for the influence of the variable within the model. In this case to determine the engineering significance, the whole range of a variable, for example, O_TM, from the lowest value (145.2 kJ/K) to the highest value (2352.1 kJ/K) is the estimate (-0.0007993) multiplied by the range (2207 MJ/m^2 per annum). This was when O_TM changes from the lowest to the highest value on the northern wall of module A, having an effect of reducing the energy consumption by 2 MJ/m^2 per annum.

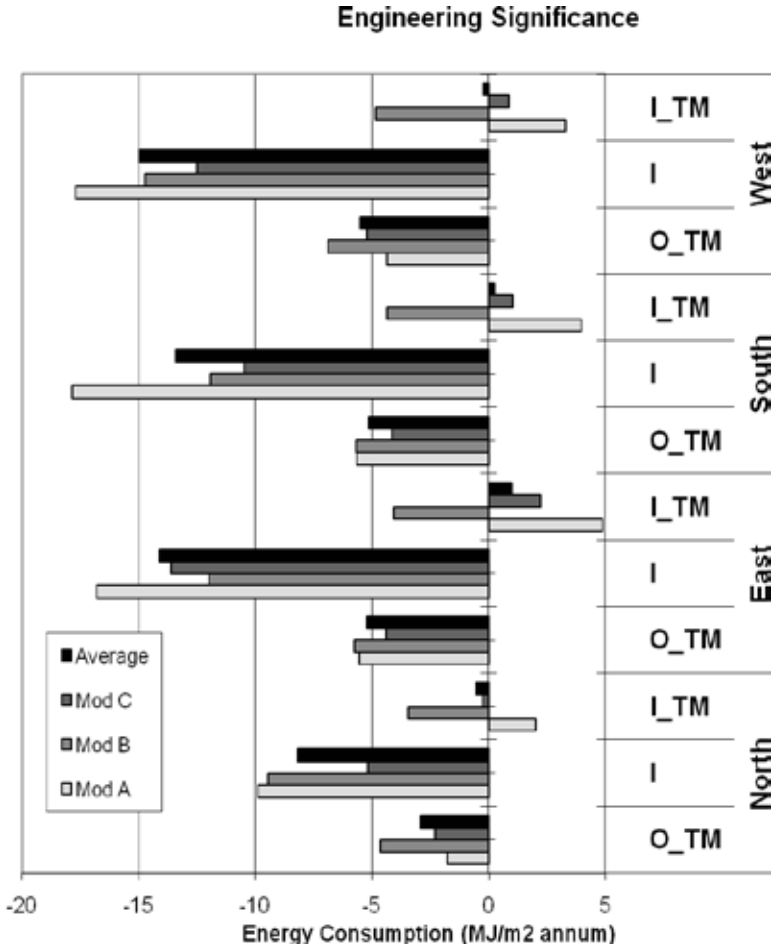

Figure 7.6 Engineering significance of O_TM, I_TM (kJ/K) and I on each wall orientation for each module on energy consumption (MJ/m2 per annum)

As Figure 7.6 indicated for Module A the most influential walls were the western then southern followed by the eastern wall. Insulation on all walls decreased energy consumption dramatically, and had a higher impact on energy consumption than thermal mass. The I_TM on all orientations will increase energy consumption. This was due to the module not having a window and the thermal mass having limited interaction with the internal environment.

The effects of installing a window in Module B can be seen with the reduction of the influence of insulation, with the western wall clearly having the most influence here. Also with a window present I_TM was able to be utilised, decreasing energy consumption.

Overall the northern and western walls performed similarly requiring high insulation, O_TM and I_TM,

whereas, the southern and eastern walls performed similarly requiring high insulation and O_TM, but low I_TM. From this the most efficient module would consist of ICB on the northern and western walls and IBV on the east and south. The energy consumptions for this design are given in Table 7.5.

Table 7.5: Energy Consumption (MJ/m2 per annum) for ICB on the north and west walls and IBV on the east and south for all building modules

Module A	Module B	Module C
67	49.8	45.6

JMP can also identify interactions between different aspects of the wall. Relevant plots generated are given in Figures 7.7-7.9 and the interactions between O_TM and insulation, and O_TM and I_TM determined (solid lines). The interaction between I_TM and insulation was also predicted (dotted line).

If a wall was insulated, and O_TM was increased, energy consumption was also increased, as shown in Figure 7.7, for Module A. This was due to the module consisting of only external walls, and radiation from the sun cannot enter the module. On the other hand, if a wall was insulated and the I_TM was increased, energy consumption was slightly decreased. This demonstrated the interaction of the thermal mass with the internal environment.

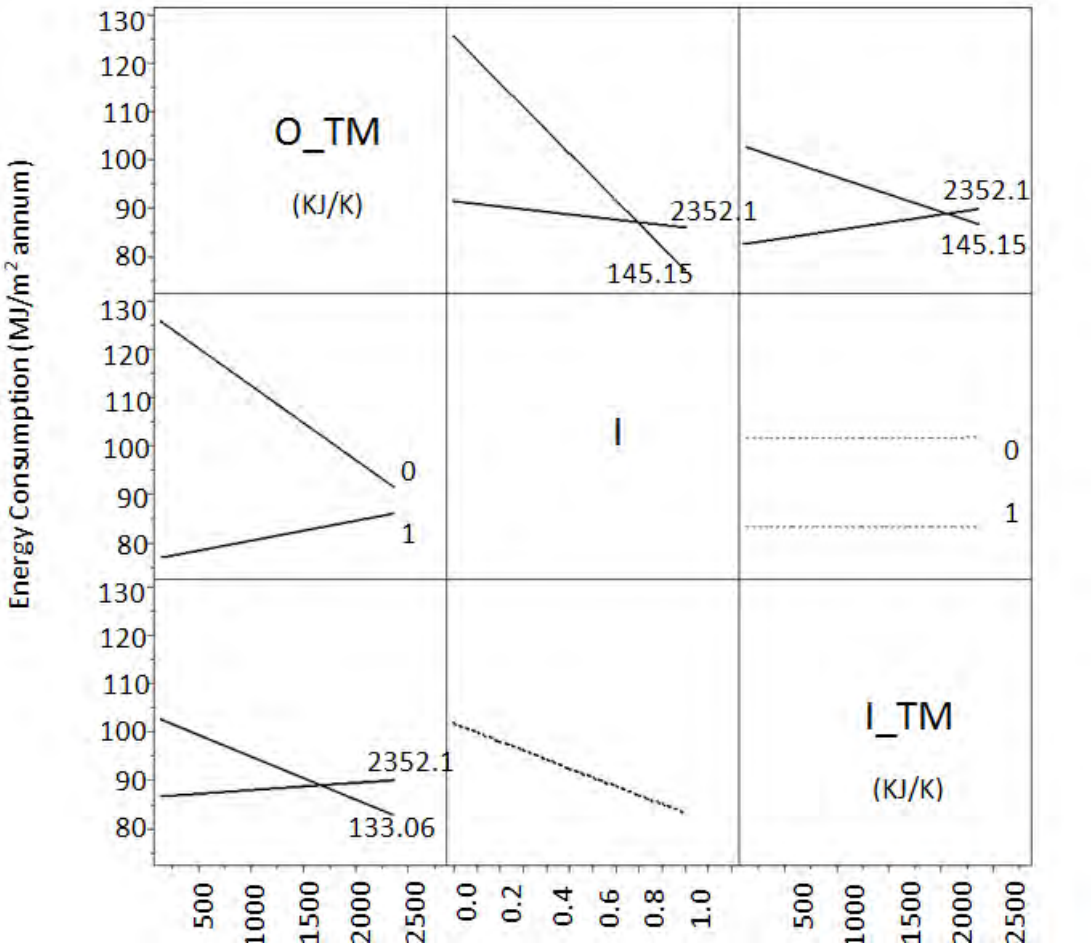

Figure 7.7 Walling structure interactions for Module A

When a wall is not insulated, increasing the O_TM dramatically reduces the energy consumption, while increasing the I_TM slightly increases energy consumption.

The interactions for Module B shown in Figure 7.8 were slightly different to those of Module A. For Module B, a wall that was not insulated and had high I_TM, energy consumption would be reduced at the same rate as if insulation was present. This showed that by installing a window, radiation was able to enter the module enabling the I_TM to function to its potential and counter the solar gain.

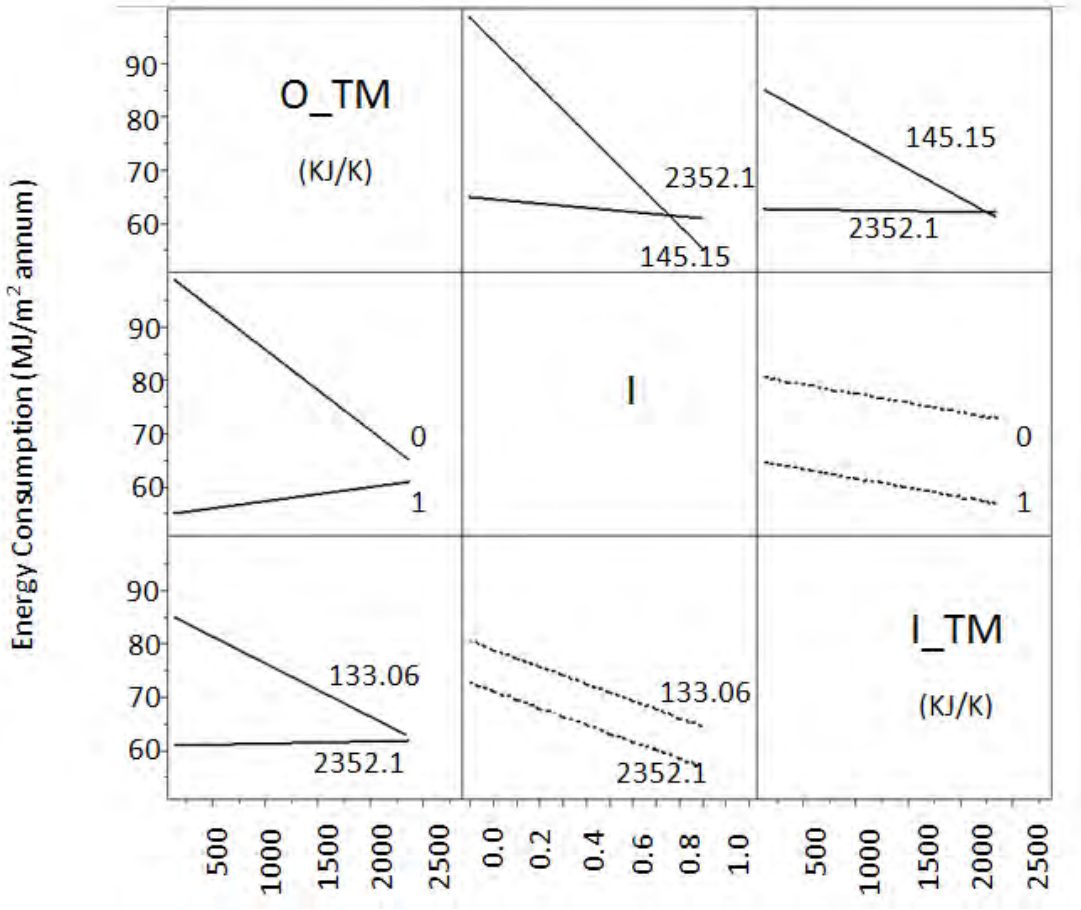

Figure 7.8 Walling structure interactions for Module B

In the case of Module C (see Figure 7.9) interactions were different once again. The increase of O_TM with I_TM did not have a large effect on energy consumption. But once again, the effect of thermal mass with insulation was the same for Modules A and B.

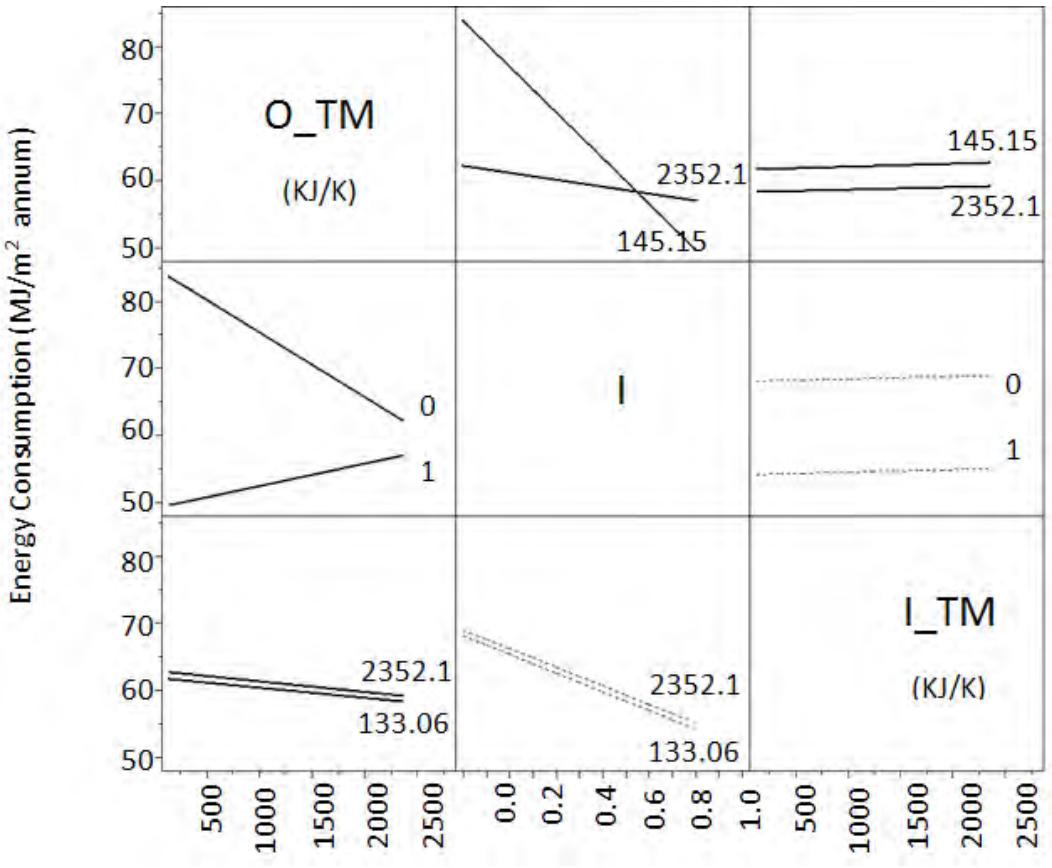

Figure 7.9 Walling structure interactions for Module C

To allow the findings to be used in a practical sense, a selection of six different hybrid designs were used for further analysis, see Figure 7.10. Comparisons in performance were based on an analysis with AccuRate, engineering significance, and the interaction plots from JMP. The modules were selected on their performance in Module B as Module B was thought to perform in manner similar to a real house, since solar radiation was able to enter the module. To obtain a good comparison of hybrid walling systems, very good, good, and poor performing modules were used in the study.

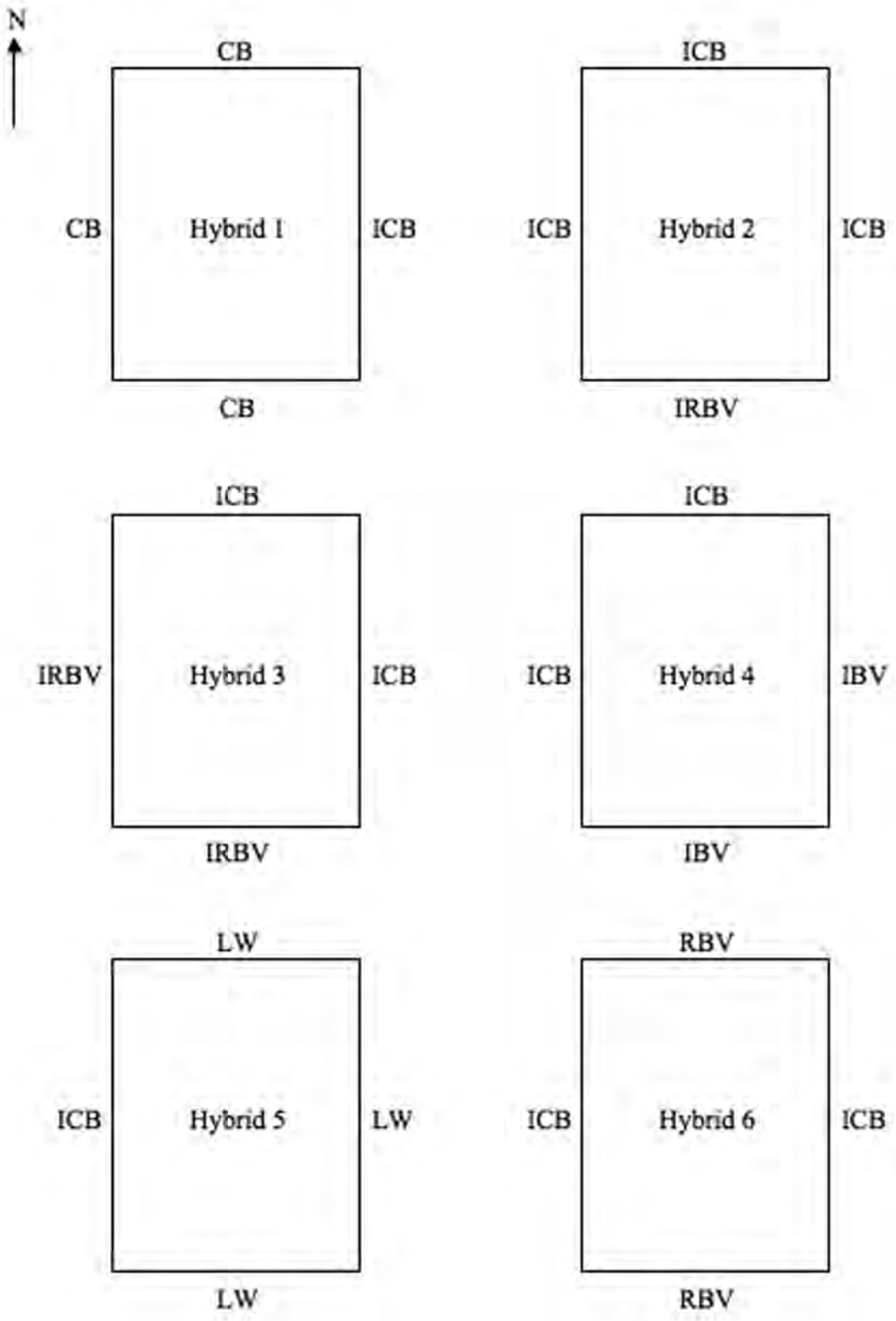

Figure 7.10 Six selected Hybrid Module for further analysis

The energy consumption for the uniform and hybrid modules for Module B construction, calculated using AccuRate, are shown in Figure 7.11.

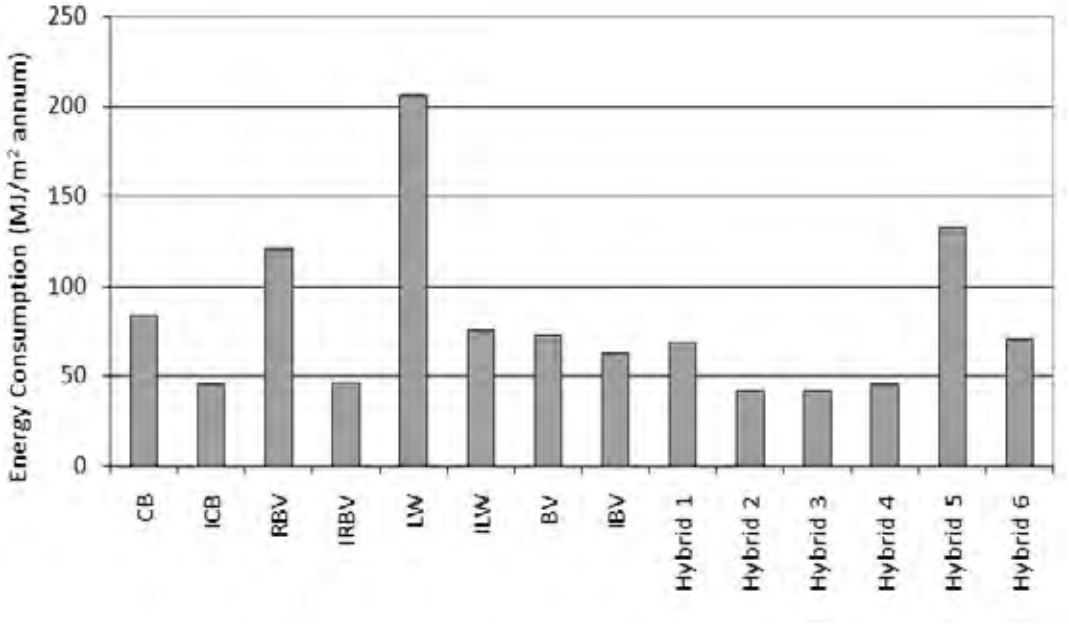

Figure 7.11 Energy consumption of uniform and hybrid modules for Module B

Hybrid 5 was clearly the worst performer of the hybrid designs, as it consisted of mainly LW walls and only one ICB wall, although, the addition of an ICB western wall for the LW did result in a dramatic decrease in energy consumption of 73.7 MJ/m^2 per annum. As mentioned earlier, the eastern and western walls were major players in the transfer of heat, and this was again demonstrated by the reduction in energy consumption in hybrid 6 with a decrease of 50.9 MJ/m^2 per annum from a uniform system of RBV.

Hybrid 2 and hybrid 3 performed very similarly to the uniform systems of ICB and IRBV, and hence the change between these walling systems was not significant.

7.3.2. Decrement Factor Study

To further analyse the performance of the hybrid modules, the wall decrement factors were also studied. This involved the results from the AccuRate analysis as well as comparison with the results obtained from the bench scale experimental study described in Section 2.2. The decrement factor is shown in Equation 1 and is the difference of the inside temperature with the desired room temperature over the temperature difference of the outside temperature with the same desired temperature.

$$Decrement\ Factor = \frac{T_i - T_D}{T_o - T_D} \qquad (1)$$

Where: T_D is the desired room temperature
T_i is the inside average daily temperature
T_o is the outside average daily temperature

The decrement factor can only be applied to a single wall and requires the surface temperature of the outside and inside of the wall. AccuRate did not supply this information in the output, hence a Temperature Difference Ratio (TDR) was used here (equation 2), derived from the decrement factor to compare AccuRate and the bench scale results.

$$TDR = \frac{T_{inside}^{\max} - T_{inside}^{\min}}{T_{outside}^{\max} - T_{outside}^{\min}} \quad (2)$$

Where T is the air temperature

A low decrement factor is desired as this will offer the least temperature fluctuation. Hence, in the derived TDR, a lower value was also desired.

The TDR results from AccuRate and the bench-scale setup for Module A presented in Figure 7.12, display an average TDR difference of 0.132, although the trend was the same in both methods. The difference in results may be due to the TDR for AccuRate being calculated over one year, whereas the TDR for the bench-scale setup was calculated over three days of experimental runs. To verify this, several days were selected from the AccuRate cycle for hybrid design 6, and the TDR was calculated. It was found that the TDR values ranged from 0.295 to 0.604, depending on the particular weather for that day, and time of year. An average of these was taken and found to be 0.438, which is relatively close to the yearly value of 0.403.

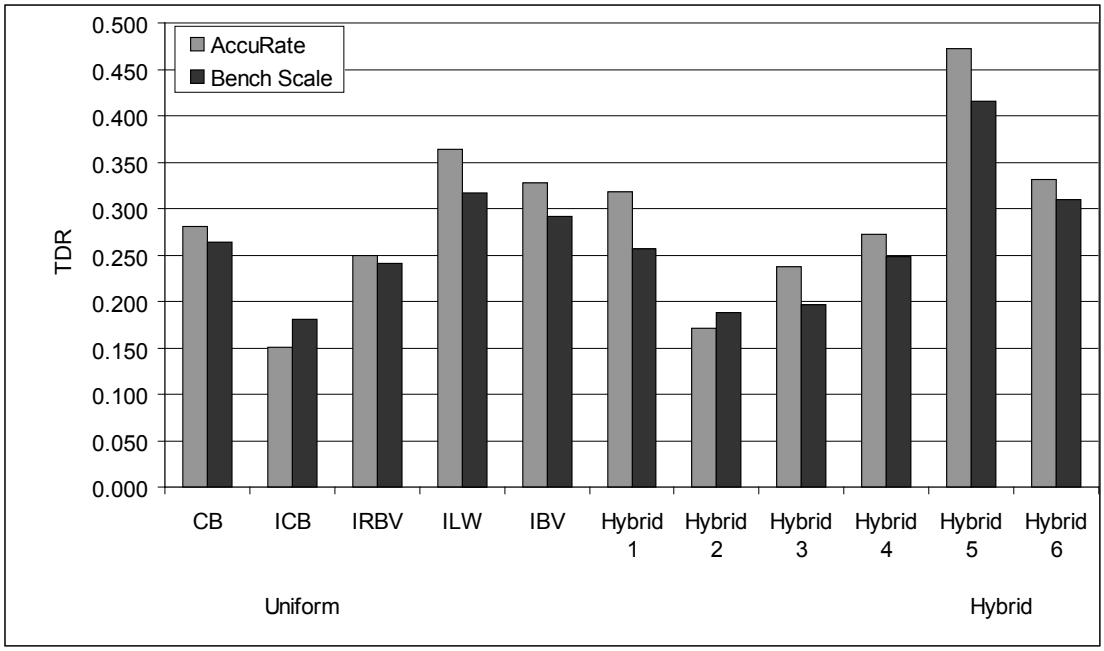

Figure 7.12 TDR results for AccuRate and the Bench Scale Model for uniform and hybrid modules in Module A

The AccuRate TDR results were very similar for hybrid 2 and hybrid 3, and the uniform modules of ICB and IRBV, although results from the bench-scale setup showed IRBV to be slightly higher that the other designs and more comparable to hybrid 4.

The uniform and hybrid systems have been ranked in Figure 7.13 from best performing to worst performing based on their energy consumption and TDR.

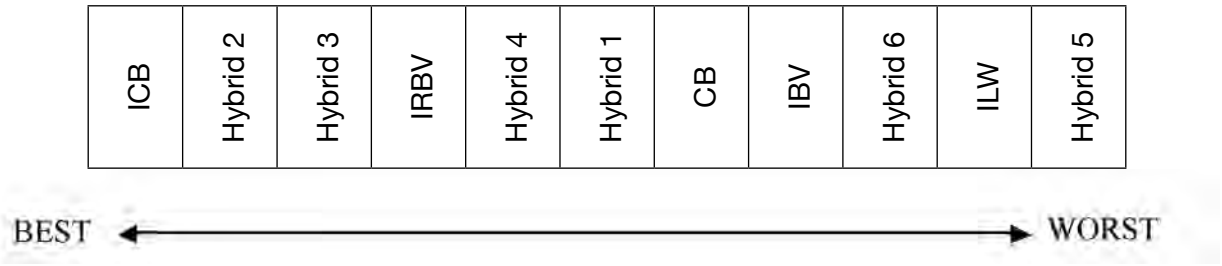

Figure 7.13: Best to worst performing designs

The best performing hybrid designs involved the use of ICB and IRBV. This was expected as these walling systems were also the best two performing uniform designs. Better applications of the hybrid walling idea can be seen in hybrid 5 and hybrid 6 (see Figure 7.11) when the energy consumption of these designs is reduced by the addition of ICB walls.

7.3.3. Thermal Lag Study

Another method used for assessing the thermal efficiency of a building material is thermal lag. This is the amount of time taken for heat to be conducted through a material. A small thermal lag resulting in a quick change in internal temperature causes thermal comfort within the module to diminish. The desired temperature profile is a slow change, hence a large thermal lag. This allows the thermal energy to be slowly released into the module maintaining thermal comfort.

Figure 7.14 compares the thermal lag for the bench-scale setup and AccuRate predictions for all module types. As expected, the modules with the higher level of thermal mass (CB, ICB, IRBV, Hybrid2 and Hybrid3) exhibited the greatest thermal lag. For constructions with a large amount of thermal mass, CB and ICB, the bench-scale setup tended to over predict the thermal lag by approximately 2 hours. In the hybrid systems, hybrid 2, 3 and 4 all predicted higher than Accurate. These hybrid designs all contained insulation, and hence, the insulation was performing better than expected within the bench scale setup. Lighter mass constructions such as ILW, IBV and hybrid 5 compared very closely to the AccuRate predictions.

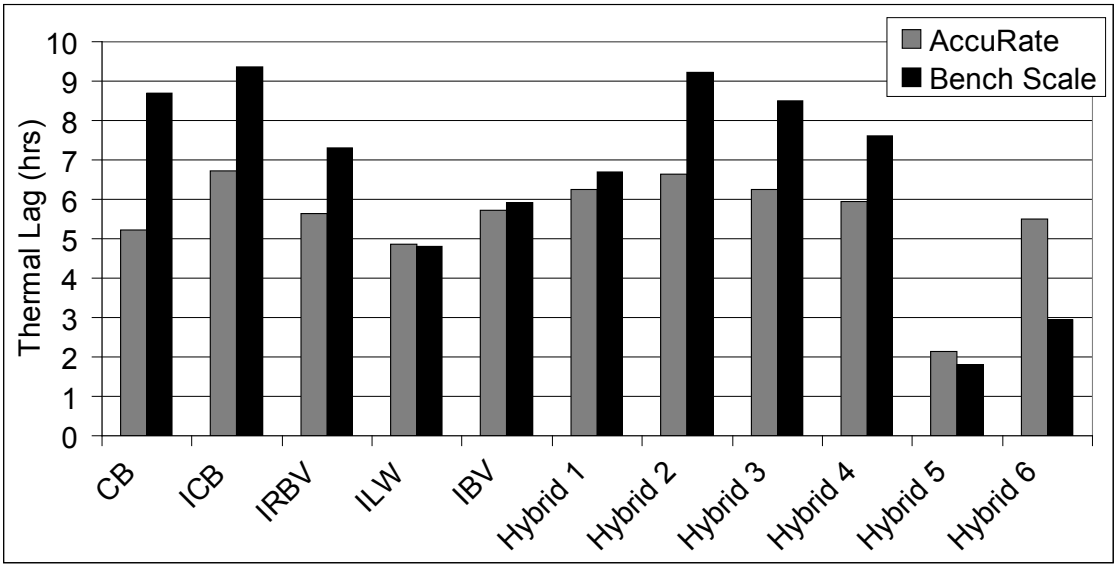

Figure 7.14 Comparison of Thermal Lag for AccuRate Predictions and Bench-Scale Setup

Heat was only able to enter the bench-scale setup through the northern wall, where the heating element was attached. In contrast, AccuRate models real world situations where heat is transferred through several walls, and this affects the thermal lag value. Despite this deference, the bench scale results had similar trends to the AccuRate predictions, allowing a thermal performance comparison between designs.

7.4. Case Studies (Hybrid wall application to real house)

7.4.1. Introduction

The module results give a good indication of the thermal performance of various walling systems and demonstrate the advantages that can be obtained by the use of a hybrid walling system. To investigate the influence of this concept on a real house, preliminary analyses were performed on a typical house incorporating the hybrid concept using AccuRate for Newcastle and Perth weather conditions.

A series of case studies were conducted to examine the performance of six of the previous hybrid designs within the context of a real floor plan rather than hypothetical modules. For this purpose an 8 star house designed and built by HIA GreenSmart Professionals, Jade Projects in partnership with Think Brick Australia was selected. The construction of this house which is referred to as the base-house (Figure 7.15) took only 18 weeks at a cost of $200,000. The base-house was built to demonstrate the findings from the University of Newcastle study of the thermal performance of Australian housing. The house is located in the Revolution Road display development in Perth's south eastern suburb of Seville Grove. To be included in the development each home had to have a minimum 5 star rating and show considerable energy and water savings through its design and construction. This particular house achieves an 8-star rating in the Building Energy Rating Services (BERS) system. The BERS system is similar to the AccuRate Software, using the same calculating engine with a slightly different user interface.

A series of experimental measurements of the indoor air temperature was also performed to assess the thermal performance of the base-house. The case studies presented in this chapter initially focused on the comparison between measurements and predictions using AccuRate and NUMBERS. The focus was then shifted to the implementation of the six hybrid wall designs to the floor plan of the base-house. The thermal performance of the resulting building envelopes were examined using AccuRate. The calculations associated with the six hybrid case studies were carried out for both Perth and Newcastle climatic conditions. More details can be found in the PhD K. Gregory dissertation (Gregory, 2010).

Figure 7.15 Entrance of the base-house.

7.4.2. The Base-House Design

The floor plan of the base-house can be seen in Figure 7.16.

The side of the house with the main living areas (family/dining) is orientated north. This allows the thermal mass in the tiled concrete flooring and double clay brick walls to absorb and release warmth in the winter and 'coolth' in summer. Sufficient shading is provided in the summer months and can be removed in the winter months.

The glazing to floor area is 22.4 % which is less than the 25% as recommended in the literature. Windows and doors have been weather sealed to prevent infiltration and have also been strategically placed to maximise cross ventilation, especially in this area which experiences Perth's famous 'Fremantle Doctor' afternoon breezes.

The house has been fitted with numerous sensors, temperature, heat flux, humidity etc. allowing the data to be compared with the numerical results.

Variation of this base-house were simulated for this study, with changes only made to the exterior walling systems, either uniform or hybrid designs, for both Perth and Newcastle weather conditions.

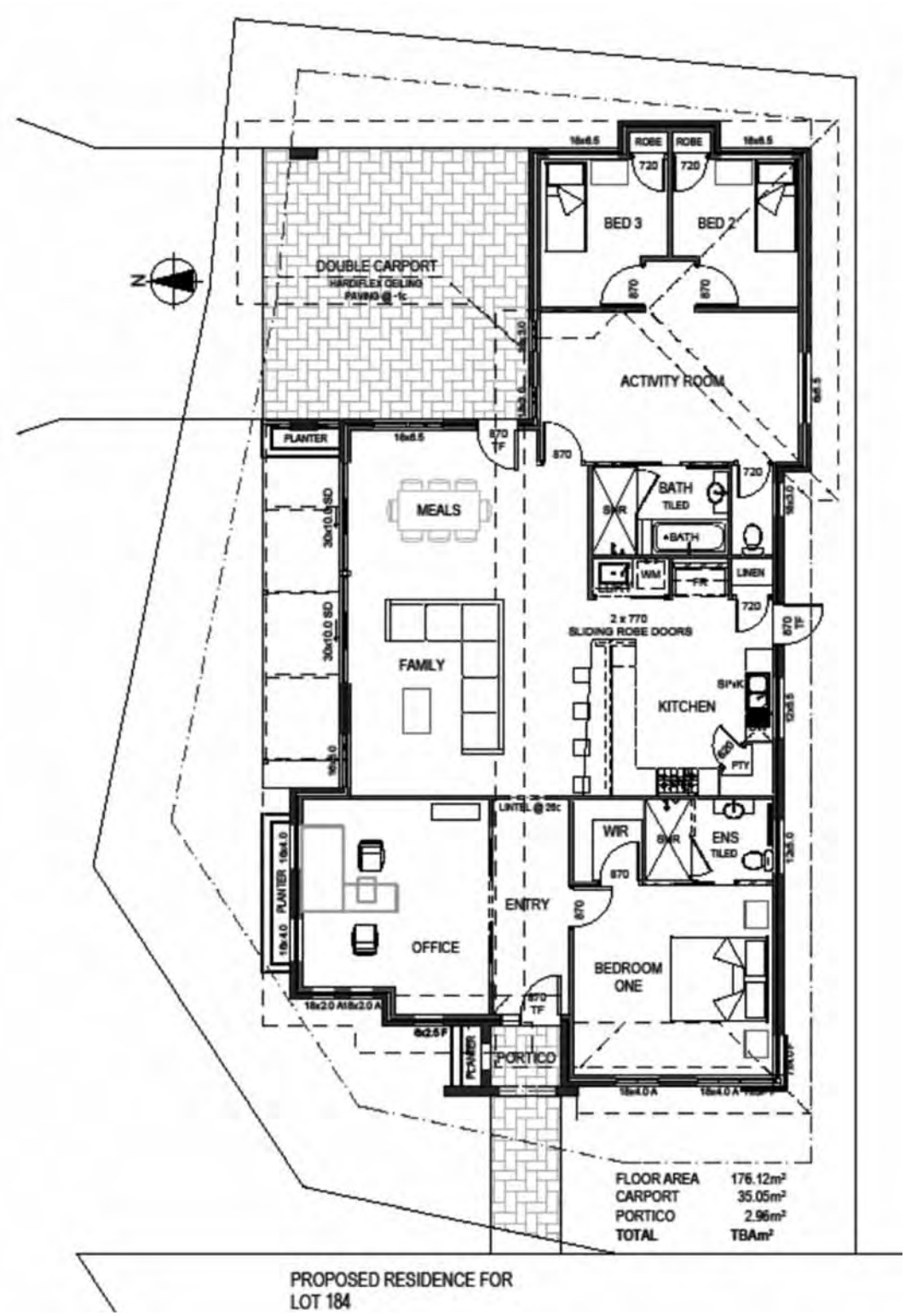

Figure 7.16 Floor plan of the base-house.

7.4.3. Energy Efficiency Analysis of Uniform and Hybrid Designs in the Base-House in Newcastle and Perth

Using the numerical model AccuRate, the six hybrid designs previously selected in the module study were modelled in both Newcastle and Perth weather conditions using the base-house floor plan. Within the base-house all walls facing a particular direction (i.e. north, south, east or west) had the same construction as denoted by the hybrid design.

Hybrid 2 and hybrid 3 perform similarly to the uniform constructions of IRBV and ICB. As the energy consumption of the uniform designs of IRBV and ICB are almost identical it is not surprising that hybrids of the two constructions also perform similarly. This particular implementation of the hybrid wall concept is not advantageous as a reduction in energy consumption is not achieved.

It is clear that by adding ICB walls to the poor performing uniform constructions, such as LW or RBV, energy consumption is significantly decreased as in hybrid 5 and hybrid 6 respectively, with an average decrease of 17.45 MJ/m^2 annum.

By adding ICB walls to the eastern and western walls of the base-house, an RBV/ICB, hybrid 6, structure can perform more like a CB structure. So in this application instead of having a uniform CB design with 8 walls of brickwork, the hybrid design, hybrid 6, has only 6 walls of brickwork. This demonstrates that the thermal mass and insulation is located in more appropriate places to achieve a better thermal performance.

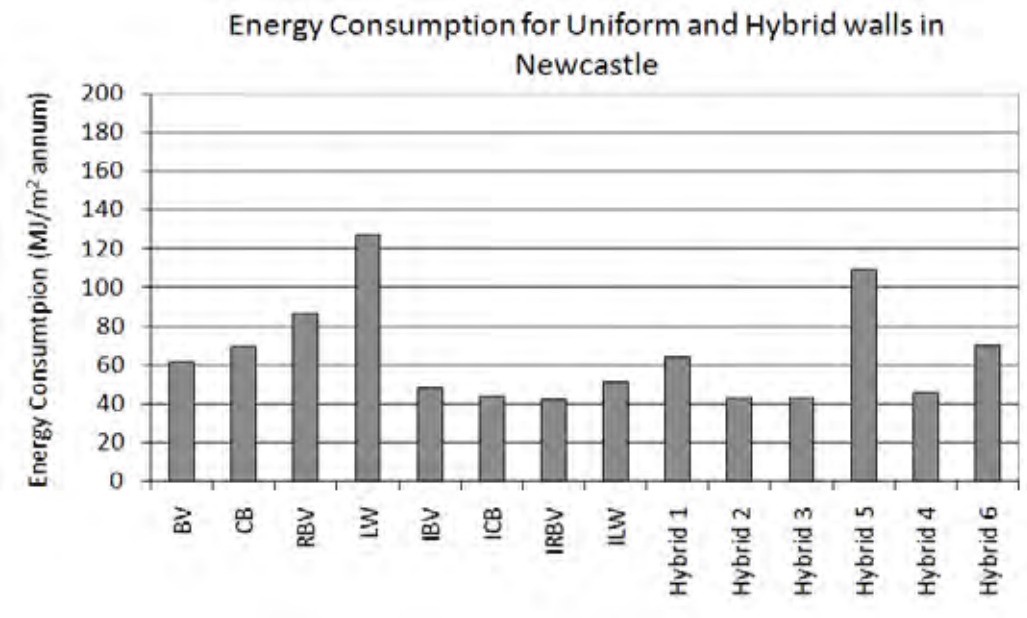

Figure 7.17 Energy Consumption for Uniform and Hybrid walls in Newcastle.

Once again, IRBV and ICB constructions perform very similarly to hybrid 2 and hybrid 3, although in Perth it is evident that IRBV has slightly lower energy consumption than ICB. With the combination of the two constructions in the hybrid designs the difference is negligible.

In both Newcastle and Perth, IBV performs slightly worse than IRBV and ICB although the hybrid design, hybrid 4, achieves an energy consumption value very close to that of hybrid 2 and 3.

Once again, it is evident in Perth that there is a large decrease in energy consumption comparing LW construction to hybrid 5 and RBV to hybrid 6, with an average decrease of 24.7 MJ/m^2 annum. This is a good example of the hybrid wall concept and the benefits in energy consumption reduction.

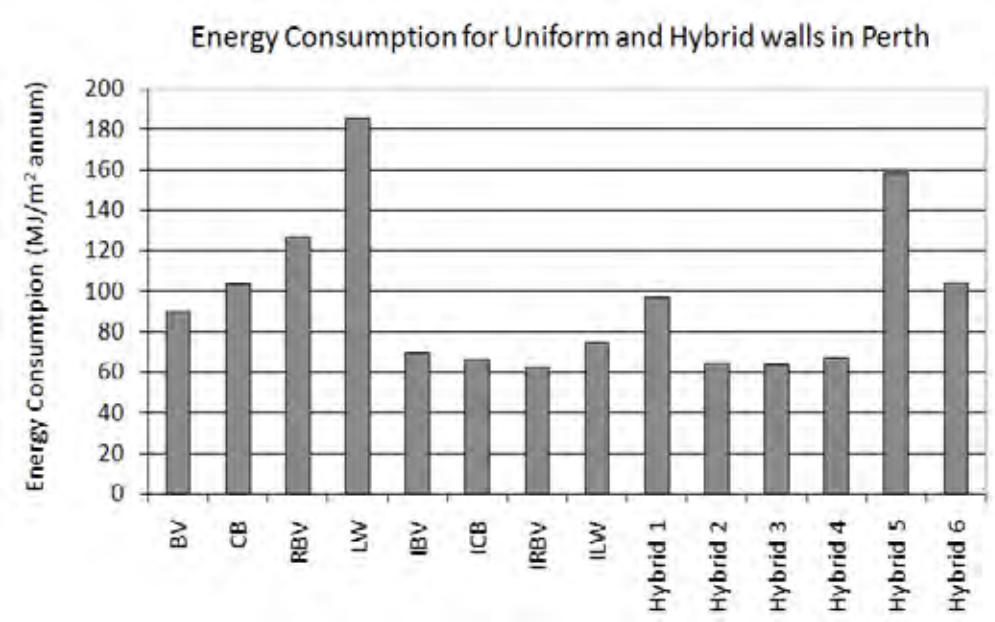

Figure 7.18 Energy consumption for uniform and hybrid walls in Perth.

Analysis of the base-house in Perth shows a similar trend to that of Newcastle. In Perth it is clear that energy consumption is somewhat higher than in Newcastle.

7.5. CONCLUSIONS

The study described in this chapter has shown that the use of the hybrid walling concept has the potential to significantly improve thermal performance in particular cases. This was shown initially in relation to the performance of a series of hypothetical modules, and then illustrated by the application of the concept to a typical house. When part of a solar-passive design, the use of hybrid walling certainly offers an additional technique to enhance thermal performance.

8. REFERENCES

1. AccuRate Manual, CSIRO, ACS -AIR Organisation, Editor, 2004.

2. Alash'ary H.A., Moghataderi B., Page A.W. & Sugo H.O., *Application of a Neuro-Fuzzy Model to Evaluate the Thermal Performance of Typical Australian Residential Masonry Buildings-II*. Proc. 2nd Canadian Conference on Effective Design of Structures, McMaster University, Hamilton, Ontario, Canada (May 2008): 651-661

3. Alasha'ary H., Moghtaderi B., Page A., Sugo H., *A Neuro-Fuzzy Model for Prediction of the Indoor Temperature in Typical Australian Residential Buildings,* International Journal of Energy and Buildings 41(7): 703-710, 2009

4. Alasha'ary H. A. M., *Neuro-fuzzy modelling of the thermal performance of typical Australian residential buildings*, PhD thesis, Faculty of Engineering & Built Environment, The University of Newcastle, Newcastle 2010, p. 239

5. Alashaary H. Moghtaderi B., Sugo H. and Page A.W., *Application of a Neuro-Fuzzy Model to Evaluate the Thermal Performance of Typical Australian Residential Masonry Buildings*. Proc. 14th International Brick and Block Masonry Conference, Sydney, The University of Newcastle, NSW, Australia; 567-578, February 2008

6. American Society for Testing Materials: ASTM C 1363-97, *Standard Test Method for the Thermal Performance of Building Assemblies by Means of a Hot Box Apparatus*, Philadelphia, USA. 1997

7. American Society for Testing Materials: ASTM C 236-89, *Standard Test Method for Steady-State Thermal Performance of Building Assemblies by Means of a Guarded Hot Box*, Philadelphia, USA, 1989

8. *ASHRAE Standard, Standard Method of Test For The Evaluation of Building Energy Analysis Computer Programs*, American Society of Heating, Refrigerating and Air-Conditioning Engineers, Inc.: Atlanta, 2007

9. Australian Residential Building Sector Greenhouse Gas Emissions, Australian Greenhouse Office, 2004. D.o.E.a.H, pp. 1990-2010

10. Australian Standard, AS 2627.1—1993, *Thermal insulation of dwellings, Thermal insulation of roof/ceilings and walls in dwellings*, Standards Australia, Homebush, NSW 2140, 1993

11. Australian Standard, AS/NZS 4859.1, *Materials for the Thermal Insulation of Buildings – Part 1: General Criteria and Technical Provisions*, 2002

12. BASIX and Building Code of Australia, About the House, 2005, www.aboutthe.house.com.au.

13. Burch, D. M., Remmert, W. E., Krintz, D. F. and Barnes C. S., *A Field Study of the Effect of Wall Mass on the Heating and Cooling Loads of Residential Buildings*, Proceedings of the Building Thermal Mass Seminar, Knoxville, Tennessee, NBS, pp.265-312, USA, 1982.

14. Clark, M.G., Sugo, H.O., Page, A.W., *Thermal Performance of Australian Masonry Housing – A Preliminary Study*, Proc. 9th NAMC, Clemson, South Carolina, June, 2003, pp 597 – 60

15. Clarke R. E., *Measurement Report MHF-1440 Thermal Transmission Properties of a sheet of Polystyrene Foam*, CSIRO, May 2002.

16. Dale J. D., Kostiuk L. W. and Hatzinikolas M. *Thermal Performance of an Insulated Masonry Structure in a Northern Climate*. In: The proceedings of the 3rd North American Masonry Conference (NAMC), TMS, USA, June 1985; pp. 2-12.

17. Delsante, A., *Is the New Generation of Building Energy Rating Software up to the Task?*, A Review of AccuRate, ABCB Conference "Building Australia's Future 2005", Surfers Paradise: CSIRO Manufacturing and Infrastructure Technology, 2005.

18. FirstRate, available from: http://www.sustainability.vic.gov.au/www/html/1491-energy-rating-with-firstrate.asp

19. Gregory K. E., *Smart Utilisation of Thermal Mass in Masonry Buildings*, PhD thesis, Faculty of Engineering & Built Environment, The University of Newcastle, Newcastle 2010, p. 222

20. Gregory, K.E, Moghtaderi., B., Page, A., *Use of Dissimilar Walling Systems on Residential Building Envelops for Improving Their Thermal Performance*, Journal of Green Building, 4 (2), pp. 109-125, 2009

21. Gregory, K.E, Moghtaderi., B., Sugo, H., Page, A., *A Thermal Performance Study of Common Australian Residential Construction Systems in Hypothetical Modules*, Proceedings of the 14th IBMAC, Sydney, NSW (2008)

22. Gregory, K.E, Moghtaderi., B., Sugo, H., Page, A., Assessment of thermal performance of two masonry walling designs for housing using a combined theoretical and experimental approach, CCEDS-II: 2nd Canadian Conference on Effective Design of Structures: Sustainability of Civil Engineering Structures, McMasters University, Toronto, Canada (2008)

23. Gregory, K.E, Moghtaderi., B., Sugo, H., Page, A., *Effect of Thermal Mass on the Thermal Performance of Various Australian Residential Constructions Systems,* Energy and Buildings, 40(4) 459-465 (2008)

24. Hay, J.E. and J.A. Davies, *Calculations of the solar radiation on a inclined surface,* in Proc. of First Canadian Solar Radiation Data Workshop, Ministry Of Supply and Services, Canada, 1980.

25. Jayamaha, S.E.G., N.E. Wijeysundera, and S.K. Chou, *Measurement of the heat transfer coefficient for walls,* Building and Environment, 31(5), 1996, pp. 399-407.

26. JMP Software, JMP Statistical Discovery Software, http://www.jmp.com/

27. Luo C, Moghtaderi B, Sugo S, Page A.W., *Time Lags and Decrement Factors for Multi-layer Materials*, Building Simulation 2007, Proc. 10th Int. Building Performance Simulation Association, Beijing, China, Sept, 2007, pp. 95-100

28. Luo C., Moghtaderi B., and Page A. W., *Determining the Thermal Capacitance, Conductivity and*

the Convective Heat Transfer Coefficient of a Brick Wall by Annually Monitored Temperatures and Total Heat Fluxes, Energy & Buildings, (2010), doi: 10.1016/j.enbuild.2010.09.030

29. Luo C., Moghtaderi B., and Page A. W., *Effect of Ground Boundry and Initial Conditions on the Thermal Performance of Buildings*, Applied Thermal Engineering, 30 (2010), pp. 2602-2609

30. Luo C., Moghtaderi B., and Page A. W., *Modelling of Wall Heat Transfer Using Modified Conduction Transfer Function, Finite Volume and Complex Fourier Analysis Methods*, Energy and Buildings, 42 (2010), 605-617

31. Luo C., Moghtaderi B., Sugo H., and Page A.W., *A New Stable Finite Volume Method for Predicting Thermal Performance of a Whole Building*, Building and Environment, 43 (2008), 37 – 43.

32. Luo C., Moghtaderi B., Sugo. and Page A.W., *The Verification of Finite Volume Based Thermal Performance Software Using Analytical Solutions and Measurements*, Proc. IBPSA Australasia 2006 Conference, Adelaide, 2006

33. Moffiet T., Hands S., Alterman D., Colyvas K., Page A., d Moghtaderi B., *Statistical analysis of the effects of insulation and thermal mass on the thermal stability of a building space*, unpublished

34. NatHERS - Nationwide House Energy Rating Scheme, http://www.nathers.gov.au/

35. National Greenhouse Accounts (NGA) Factors, Australian Government Department of Climate Change, 2009; http://www.climatechange.gov.au/workbook/index.html

36. Olesen B.W., Brager G.S., *A Better Way to Predict Comfort: the new ASHRAE Standard 55-2004*, ASHARE Journal, pp.20-26, August 2004

37. Page A.W., Hands S. and Moghtaderi B., "*The Thermal Performance of Reverse Brick Veneer in Australian Housing*", 8th Int. Masonry Conference, Dresden, July 2010

38. Page, A.W., Sugo, H.O., Hands, S., & Moghtaderi, B., *A Study of the Influence of R-Value on the Thermal Characteristics of Australian Housing*, in Proc. Building Australia's Future 2009, Australian Building Codes Board, Gold Coast, Sept., 2009

39. SAS Institute, *JMP Statistical Discovery Software: Version 4 - Design of Experiments,* SAS Institute Inc., Cary, NC, USA (2000).

40. SAS Institute, *JMP Statistical Discovery Software: Version 4 - Introductory Guide,* SAS Institute Inc., Cary, NC, USA (2000).

41. SAS Institute, *JMP Statistical Discovery Software: Version 4 - User's Guide,* SAS Institute Inc., Cary, NC, USA (2000).

42. SAS Institute. JMPer Cable, Newsletter for JMP Users (Issue 3, Fall 1996), http://www.jmp.com/about/newsletters/jmpercable/pdf/03_fall_1996.pdf

43. Seem, J.E., *Modeling of heat transfer in buildings*, in Department of Mechanical Engineering, University of Wisconsin-Madison, 1987

44. Sugeno M. and Kang G. T., *Structure Identification of Fuzzy Model. Fuzzy Sets and Systems*; 28(1), 1988, pp. 15-33.

45. Sugo H., Page A.W., Inglis C., *Thermal Performance Studies at the University of Newcastle*, Proc. ANZES Solar 07, Alice Springs, Oct 2007

46. Sugo H.O., Hands S.A., Page A.W., *Thermal Performance of Australian Masonry Housing- Heating/ Cooling Demands Under Spring Conditions*, in Proc. 14IBMAC, Sydney, Feb., 2008

47. Sugo H.O., Moghtaderi B and Page A.W., *The Study of Heat Flows in Masonry Walls in a Thermal Test Building*, in Proc. 10th Canadian Masonry Symposium, Banff, June 2005, pp 191 – 201

48. Sugo H.O., Page A.W. & Moghatderi B., *The Influence of Wall Properties on the Thermal Performance of Australia Housing*, 11th Canadian Masonry Symposium, 2009

49. Sugo H.O., Page A.W.,Moghtaderi B., *The Thermal Performance of Cavity Brick and Brick Veneer Thermal Test Modules Containing a Window*, Proc. 10th NAMC, St Louis, June, 2007, pp 165-177

50. Sugo, H.O., Page, A.W., Moghtaderi, B, *A Comparative Study of the Thermal Performance of Cavity and Brick Veneer Construction*, Proc. 13th IBMAC, Amsterdam, July 2004, pp 767-776

51. Sugo, H.O., Page, A.W., Moghtaderi, B, *Experimental Study of the Thermal Performance of Australian Masonry Housing – an Overview*, in Proc. 7AMC, Newcastle, July, 2004, pp 192-203

52. Sugo. H.O., Page, A.W. and Moghtaderi, B. 'A Comparative Study of the Thermal Performance of Cavity and BrickVeneer Construction' Proc. 13th IBMAC, Amsterdam, University of Eindhoven, 2004, pp. 767-776.

53. Think Brick Australia, 8 Star House. 2007, http://thinkbrick.com.au/showcase/showcase_home_content.cfm?obj_uuid=BE6FE49F-FB53-7FC1-CB11-E44362422C25.

54. Walsh P.J. and Delsante A.E., *Calculation of the thermal behaviour of multi-zone buildings*, Energy and Buildings, 5(4), 1983, pp. 231-242.

APPENDIX

A. APPENDIX 1 – ADDITIONAL DETAILS OF STATISTICAL MODEL

The basic statistical summary of the statistical model described in Section 5.6 is presented in Tables A.1 and Table A.2. This section has been prepared by Dr Trevor Moffiet and will be published as a separate paper shortly (Moffiet et al.).

Table A.1 Summary of model fit

RSquare	0.86787
RSquare Adj	0.866023
Root Mean Square Error	1.322479
Mean of Response	21.66563
Observations (or Sum Wgts)	6962

Table A.2 Effects tests of model variables

Source	Nparm	DF	Sum of Squares	F Ratio	Prob > F
Mean(External Air Temperature)	1	1	12940.914	7399.242	0.0000*
Season	3	3	1644.225	313.3735	<.0001*
Q Day	3	3	396.376	75.5454	<.0001*
BasicConfig	5	5	59.353	6.7873	<.0001*
BasicConfig*Season	15	15	299.715	11.4245	<.0001*
BasicConfig*Q Day	15	15	247.469	9.4330	<.0001*
Season*Q Day	9	9	333.999	21.2190	<.0001*
BasicConfig*Season*Q Day	45	45	54.172	0.6883	0.9443

The minor departures in assumptions suggested that some care should be taken with making precise interpretations of p-values and confidence intervals, but the model was still considered to be very suitable for making general inferences on the separate and combined effects of insulation and thermal mass on internal module temperatures.

Examinations of residual plots and checks on modelling assumptions indicated a slight departure from normality of the residuals, a slight increase in error variance with increase in external temperature and the presence of outlying observations particularly when external temperatures were high at night.

The three-way interaction was indicated to be not significant while the other two-way interaction terms and main effects in the model were statistically significant. As an example of interpretation of a significant interaction, the two-way interaction term ‘BasicConfiguration*Season’ may be interpreted as “at least one of the combinations of building configuration and season has a mean air temperature effect that is significantly different to the mean effect for all combinations of building configuration and season(s)”. Similar interpretations can be made for the other significant interaction terms. The results are presented numerically in Table A.3.

Table A.3 Summary of estimated interior air temperatures for given external temperatures by season

Season & Period of Day	Seasonally averaged External Air Temperature (ºC)	95% Confidence intervals for mean internal air temperatures T_{int}± D (ºC)					
		BV	InsBV	CB	InsCB	InsLW	InsRBV
Autumn_N1	14.4	21.09 ±0.59	21.36 ±0.30	21.4 ±0.23	22.07 ±0.30	20.69 ±0.49	22.07 ±0.42
Autumn_D1	18.2	22.62 ±0.59	22.8 ±0.30	22.3 ±0.23	22.99 ±0.30	22.64 ±0.49	23.19 ±0.42
Autumn_D2	22.1	26.92 ±0.58	26.73 ±0.29	24.63 ±0.22	25.45 ±0.29	26.79 ±0.47	25.62 ±0.41
Autumn_N2	17.2	23.58 ±0.59	23.59 ±0.30	22.7 ±0.22	23.32 ±0.3	22.87 ±0.47	23.28 ±0.42
Winter_N1	9.7	16.61 ±0.33	16.54 ±0.33	15.56 ±0.18	16.56 ±0.31	16.13 ±0.34	17.44 ±0.61
Winter_D1	12.7	18.28 ±0.33	18.19 ±0.33	16.66 ±0.19	17.62 ±0.31	17.81 ±0.34	18.72 ±0.61
Winter_D2	16.8	22.19 ±0.33	21.81 ±0.33	18.92 ±0.18	20.01 ±0.31	22.15 ±0.34	21.33 ±0.61
Winter_N2	12.1	18.72 ±0.33	18.64 ±0.34	16.84 ±0.18	17.88 ±0.32	18.38 ±0.34	18.81 ±0.63
Spring_N1	14.9	19.48 ±0.26	19.9 ±0.53	20.13 ±0.18	21.07 ±0.28	19.34 ±0.27	20.11 ±0.63
Spring_D1	19.5	20.48 ±0.26	20.69 ±0.53	20.53 ±0.18	21.77 ±0.28	21.02 ±0.27	20.97 ±0.63
Spring_D2	22.5	23.95 ±0.26	23.68 ±0.51	22.53 ±0.18	23.57 ±0.27	24.43 ±0.27	22.71 ±0.59
Spring_N2	17.7	21.52 ±0.26	21.74 ±0.52	21.4 ±0.18	22.12 ±0.28	21.17 ±0.27	21.17 ±0.61
Summer_N1	20.3	24.89 ±0.51	23.81 ±0.41	24.64 ±0.2	23.9 ±0.39	23.2 ±0.37	23.87 ±0.42
Summer_D1	24.3	25.01 ±0.49	23.89 ±0.41	24.56 ±0.20	24.32 ±0.39	24.5 ±0.38	24.12 ±0.42
Summer_D2	26.8	28.39 ±0.5	26.76 ±0.4	26.53 ±0.2	26.17 ±0.39	28.26 ±0.36	25.62 ±0.42
Summer_N2	22.2	26.22 ±0.51	25.28 ±0.42	25.67 ±0.20	25.01 ±0.4	25.13 ±0.38	24.56 ±0.43

(Note: the confidence intervals were obtained using the Generalised Linear Mixed Model procedure in SAS software. Output for each row in the table is based on least squares means for the seasonally averaged external temperatures provided in each row of the table).

B. APPENDIX 2 – NUMBERS

B.1. Numerical modelling theory

The main purpose of the software was to predict the energy consumption for air-conditioned buildings and the zone air temperature for free-floating buildings. Fundamental sub-models in the building energy simulation program include the following models:

B.1.1. Weather model

The purpose of the weather model was to predict: the net beam and diffuse irradiation on the outer surfaces based on the direct irradiation on a plane normal to the solar beam, the global solar irradiation and diffuse irradiation on a horizontal surface; and the convective heat transfer coefficient based on the geometry of the building and the wind speed and direction. The net heat flux on the outer surface of a wall reads:

$$q_{ow} = \alpha_s (I_{sb} + I_{sd}) + \varepsilon_2 \sigma (T_2^4 - T_{sky}^4) + H_1 (T_2 - T_a) \quad (1)$$

In which q_{ow} is the net heat flux, α_s is the solar absorbance, ε_2 is the emissivity, H_1 is the convective heat transfer coefficient, I_{sb} and I_{sd} are the beam and diffusive solar irradiation on the surface, T_2, T_a and T_{sky} are the outer surface temperature, outside air temperature and the sky temperature respectively.

The beam solar irradiation is given by:

$$I_{sb} = (I_{hG} - I_{hd}) \cos\theta / \sin\alpha \quad (2)$$

Several models are available for users to choose for calculating the diffuse solar irradiation with the default model by Hay and Davies (Hay and Davies, 1980), being

$$\frac{I_{sd}}{I_{hd}} = \left[(I_{hG} - I_{hd})/I_E\right](\cos\theta/\sin\theta_Z) + \left[1 - (I_{hG} - I_{hd})/I_E\right]\left(\cos^2\frac{\Sigma}{2}\right) \quad (3)$$

The convective heat transfer coefficient can be determined from several models also with the default model by Jayamaha et al. (Jayamaha et al., 1996):

$$H_1 = 4.955 + 1.444 V_w \quad (4)$$

B.1.2. Wall thermal conduction models

B.1.2.1. Finite volume method (FVM)

The basic concept of the finite volume method is to divide any material layer into three sections with two inner nodes and two surface nodes, and to use some algebra to remove the variables at the inner nodes as shown in Luo et al. (Luo et al., 2010). The advantage of this method is that for most building materials the resulting discretised equations do not involve any inner nodes. The resulting equations correlating heat flux and temperature at both inner and outer surfaces are:

$$\frac{1}{162k}L^2{}_t\rho_b Cp_b\left[\left(57T_{s0}+24T_{s1}-\frac{9L_t}{k}q''_{s0}+\frac{6L_t}{k}q''_{s1}\right)^n-\left(57T_{s0}+24T_{s1}-\frac{9L_t}{k}q''_{s0}+\frac{6L_t}{k}q''_{s1}\right)^{n-1}\right]$$
$$=\frac{\Delta t}{2}\left[\left(-T_{s0}+T_{s1}+\frac{L_t}{k}q''_{s0}\right)^n+\left(-T_{s0}+T_{s1}+\frac{L_t}{k}q''_{s0}\right)^{n-1}\right] \quad (5)$$

$$\frac{1}{162k}L^2{}_t\rho_b Cp_b\left[\left(24T_{s0}+57T_{s1}-\frac{6L_t}{k}q''_{s0}+\frac{9L_t}{k}q''_{s1}\right)^n-\left(24T_{s0}+57T_{s1}-\frac{6L_t}{k}q''_{s0}+\frac{9L_t}{k}q''_{s1}\right)^{n-1}\right]$$
$$=\frac{\Delta t}{2}\left[\left(T_{s0}-T_{s1}-\frac{L_t}{k}q''_{s1}\right)^n+\left(T_{s0}-T_{s1}-\frac{L_t}{k}q''_{s1}\right)^{n-1}\right] \quad (6)$$

In which k is the thermal conductivity of the material layer, L_t is the thickness, ρ_b and Cp_b are the density and specific capacity respectively, T and q'' represent temperature and heat flux, subscripts s0 and s1 represent the outer and inner surface respectively, superscripts n and n-1 denote the current time and previous time instant, and Δt is the time step. For schemes with a higher order of temporal discretisation, refer to Luo et al. (Luo et al., 2010).

An air-gap is treated as a special construction layer in NUMBERS. To treat the air-gap in a wall, it is assumed that no heat source or sink is introduced into the air-gap and the change of the air temperature of the air gap contributes negligible heat to the total heat balance of the air-gap. Accordingly, the equations correlating the heat flux and temperature at the both ends of the air-gap are:

$$q''_{s0}=q''_{s1} \quad (7)$$

$$q''_{s0}=\frac{h_{s0}h_{s1}}{h_{s0}+h_{s1}}(T_{s0}-T_{s1})+\frac{\varepsilon_{s0}\varepsilon_{s1}\sigma({T_{s0}}^4-{T_{s1}}^4)}{\varepsilon_{s0}+\varepsilon_{s1}-\varepsilon_{s0}\varepsilon_{s1}} \quad (8)$$

In which h is the convective heat transfer coefficient, and ε the thermal radiation absorbivity. Note that Eqs. (3) and (4) are valid at any time (n - 1, n, n + 1).

For a wall with L construction layers (the air gap is also counted as a layer), there will be 2L governing equations with 2L + 2 unknowns (at any surface, heat flux and temperature are defined as the unknowns). Therefore, for any walls, given any two supplementary equations defining the heat flux or temperature at either end of the wall, the entire solution for the wall will be obtained which would provide the heat flux and temperature at any layer surface in the wall.

B.1.2.2. Conduction transfer function method (CTF)

The basic idea of the CTF method is to define the inner and outer wall surface heat flux at the current time $n\Delta t$ as a function of the inner or outer surface temperature at times $n\Delta t$, (n-1)Δt, (n-2)Δt, (n-3)Δt ...and the surface heat flux at the previous times (n-1)Δt, (n-2)Δt, (n-3)Δt .... It reads:

$$\begin{pmatrix} q''_{s0,n} \\ q''_{s1,n} \end{pmatrix}=\sum_{j=0}^{nz}\mathbf{M}_j\begin{pmatrix} T_{s0,n-j} \\ T_{s1,n-j} \end{pmatrix}+\sum_{j=1}^{nq}\mathbf{\Phi}_j\begin{pmatrix} q''_{s0,n-j} \\ q''_{s1,n-j} \end{pmatrix} \quad (9)$$

With

$$\mathbf{M}_j = \begin{pmatrix} X_j & -Y_j \\ Y_j & -Z_j \end{pmatrix}, \quad \mathbf{\Phi}_j = \begin{pmatrix} \phi_j & 0 \\ 0 & \phi_j \end{pmatrix} \tag{10}$$

In which X_j, Y_j and Z_j are outside, cross and inside CTF coefficients, ϕ_j is the heat flux CTF coefficient, nz and nq represent the cut-off terms of the temperature and flux CTF series respectively.

$$\mathbf{M_0} = \left(\mathbf{C\Gamma}_2 + \mathbf{D}\right) \tag{11}$$

$$\phi_1 = Trace(\mathbf{Y_0} e^{\mathbf{A}\Delta t}),\ \mathbf{M_1} = \mathbf{CY_0}\left(\mathbf{\Gamma}_1 - \mathbf{\Gamma}_2\right) + \mathbf{CY}_1\mathbf{\Gamma}_2 - Trace(\mathbf{Y}_0 e^{\mathbf{A}\Delta t})\mathbf{D} \tag{12}$$

$$\phi_2 = \frac{1}{2} Trace(\mathbf{Y_1} e^{\mathbf{A}\Delta t}),\ \mathbf{M}_2 = \mathbf{CY_1}\left(\mathbf{\Gamma}_1 - \mathbf{\Gamma}_2\right) + \mathbf{CY_2}\mathbf{\Gamma}_2 - Trace(\mathbf{Y_1} e^{\mathbf{A}\Delta t})\mathbf{D} \tag{13}$$

$$\phi_j = \frac{1}{j} Trace(\mathbf{Y_j} e^{\mathbf{A}\Delta t}),\ \mathbf{M}_j = \mathbf{CY_{j-1}}\left(\mathbf{\Gamma}_1 - \mathbf{\Gamma}_2\right) + \mathbf{CY_j}\mathbf{\Gamma}_2 - Trace(\mathbf{Y_{j-1}} e^{\mathbf{A}\Delta t})\mathbf{D} \tag{14}$$

In which $\mathbf{\Gamma}_1 = \mathbf{A}^{-1}(e^{\mathbf{A}\Delta t} - \mathbf{I})\mathbf{B}$, $\mathbf{\Gamma}_2 = \mathbf{A}^{-1}\left[\mathbf{\Gamma}_1 / \Delta t - \mathbf{B}\right]$, and

$$\mathbf{Y}_0 = \mathbf{I} \tag{15}$$

$$\mathbf{Y_j} = \mathbf{Y_{j-1}} e^{\mathbf{A}\Delta t} - \frac{1}{j} Trace\left\{\mathbf{Y_{j-1}} e^{\mathbf{A}\Delta t}\right\}\mathbf{I} \tag{16}$$

In which **I** is a unit matrix, and matrices **B**, **C** and **D** as well as the coefficient matrix **A** are defined in the paper (Seem J.E., 1987). The covergence criteria for calculating the CTF coefficients is the same as Seem (Seem J.E., 1987), ie., $\left|\phi_j / \phi_1\right| < \text{ConvrgLim}$, in which ConvrgLim is the convergence limit and is taken as 1.0×10^{-13} for all cases in this paper.

It should be noticed that $M_{12} = -M_{21}$ according to Eq. (10). However, for multi-layer building walls, the **M** matrices calculated from Eqs. (11-14) do not always satisfy this limitation. This will be discussed in the following section. In Seem's dissertation, the following Taylor expansion to calculate the exponential matrix $e^{\mathbf{A}\Delta t}$ was used:

$$e^{\mathbf{A}\Delta t} = \mathbf{I} + \mathbf{A} + \frac{\mathbf{AA}}{2!} + \frac{\mathbf{AAA}}{3!} + \frac{\mathbf{AAAA}}{4!} + \ldots\ldots \tag{17}$$

In this paper, for any multi-layer building wall, the coefficient matrix **A** is a tri-diagonal matrix with negative diagonal elements and positive non-diagonal elements. For a single layer building wall, the matrix **A** is symmetrical, hinting that the matrix has all real eigenvalues. For multi-layer building walls, **A** is not symmetrical, because **A** has positive non-diagonal elements ($A_{ij}>0$, $i \neq j$), **A** still has all real eigenvalues,

$$\mathbf{A}=\mathbf{P\Lambda P}^{-1} \tag{18}$$

$$e^{\mathbf{A}\Delta t} = \mathbf{P} e^{\mathbf{\Lambda}\Delta t} \mathbf{P}^{-1} \tag{19}$$

$$e^{\mathbf{\Lambda}\Delta t} = \begin{pmatrix} e^{\lambda_1 \Delta t} & 0 & 0 & 0 & 0 & 0 \\ 0 & e^{\lambda_2 \Delta t} & 0 & 0 & 0 & 0 \\ 0 & 0 & e^{\lambda_{j-1} \Delta t} & 0 & 0 & 0 \\ 0 & 0 & 0 & e^{\lambda_j \Delta t} & 0 & 0 \\ 0 & 0 & 0 & 0 & e^{\lambda_{n-1} \Delta t} & 0 \\ 0 & 0 & 0 & 0 & 0 & e^{\lambda_n \Delta t} \end{pmatrix} \tag{20}$$

In which $\mathbf{\Lambda}$ and $\mathbf{P}$ are the eigenvalue matrix, eigenvector matrix for $\mathbf{A}$ respectively, λ_j is the eigenvalue and $\mathbf{P}^{-1}$ is the reverse of eigenvector matrix $\mathbf{P}$.

Using the central finite difference scheme to discretize the thermal conductivity term, matrix $\mathbf{A}$ as discussed in paper [4] for a single layer construction with six internal nodes reads:

$$\mathbf{A} = \frac{\alpha}{\Delta x^2} \begin{pmatrix} -2 & 1 & 0 & 0 & 0 & 0 \\ 1 & -2 & 1 & 0 & 0 & 0 \\ 0 & 1 & -2 & 1 & 0 & 0 \\ 0 & 0 & 1 & -2 & 1 & 0 \\ 0 & 0 & 0 & 1 & -2 & 1 \\ 0 & 0 & 0 & 0 & 1 & -2 \end{pmatrix}, \quad \mathbf{B} = \frac{\alpha}{\Delta x^2} \begin{pmatrix} 1 & 0 \\ 0 & 0 \\ 0 & 0 \\ 0 & 0 \\ 0 & 0 \\ 0 & 1 \end{pmatrix} \tag{21}$$

The order accuracy for the surface heat flux representation to 4th order accuracy are expanded, the matrix $\mathbf{C}$ and $\mathbf{D}$ are for multi-layer building walls,

$$\mathbf{C} = \begin{pmatrix} \frac{-96k_0}{24\Delta x_0} & \frac{72k_0}{24\Delta x_0} & \frac{-32k_0}{24\Delta x_0} & \frac{6k_0}{24\Delta x_0} & 0 & 0 \\ 0 & 0 & \frac{-6k_1}{24\Delta x_1} & \frac{32k_1}{24\Delta x_1} & \frac{-72k_1}{24\Delta x_1} & \frac{96k_1}{24\Delta x_1} \end{pmatrix} \tag{22}$$

$$\mathbf{D} = \begin{pmatrix} \frac{50k_0}{24\Delta x_0} & 0 \\ 0 & -\frac{50k_1}{24\Delta x_1} \end{pmatrix} \tag{23}$$

With the original 1st order accuracy

$$\mathbf{C} = \begin{pmatrix} -\frac{k_0}{\Delta x_0} & 0 & 0 & 0 & 0 & 0 \\ 0 & 0 & 0 & 0 & 0 & \frac{k_1}{\Delta x_1} \end{pmatrix} \qquad \mathbf{D} = \begin{pmatrix} \frac{k_0}{\Delta x_0} & 0 \\ 0 & -\frac{k_1}{\Delta x_1} \end{pmatrix} \tag{24}$$

In which k_0, Δx_0 are the thermal conductivity and spatial step for the outer construction layer, k_1, Δx_1 are the thermal conductivity and spatial step for the inner construction layer.

For multi-layer walls with varying spatial steps, the details for the matrix **A** are modified with consideration of

$$\left(\frac{\rho_1 C_{p1}\Delta x_1}{2}+\frac{\rho_2 C_{p2}\Delta x_2}{2}\right)\left.\frac{\partial T}{\partial t}\right|_{x0}=-k_1\frac{T_{x0}-T_{x0-\Delta x1}}{\Delta x_1}+k_2\frac{T_{x0+\Delta x2}-T_{x0}}{\Delta x_2} \tag{25}$$

Rearranging (25) leads to:

$$\left.\frac{\partial T}{\partial t}\right|_{x0}=\left(\frac{\rho_1 C_{p1}\Delta x_1}{2}+\frac{\rho_2 C_{p2}\Delta x_2}{2}\right)^{-1}\left[\frac{k_1}{\Delta x_1}T_{x0-\Delta x1}-\left(\frac{k_1}{\Delta x_1}+\frac{k_2}{\Delta x_2}\right)T_{x0}+\frac{k_2}{\Delta x_2}T_{x0+\Delta x2}\right] \tag{26}$$

Using Eq (26), refining the spatial step at the interface between different construction layers to 1/100 of the original step will mitigate the effect of the multilayer on the discretised accuracy order.

For an air-gap, according to Eq. (8), its overall coefficient of heat transfer is defined as:

$$U_{airgap}=\frac{h_{s0}h_{s1}}{h_{s0}+h_{s1}}+\frac{\varepsilon_{s0}\varepsilon_{s1}\sigma(T_{s0}{}^2+T_{s1}{}^2)(T_{s0}+T_{s1})}{\varepsilon_{s0}+\varepsilon_{s1}-\varepsilon_{s0}\varepsilon_{s1}} \tag{27}$$

And accordingly, the thickness of the air gap is determined by:

$$l_{airgap}=0.0263/U_{airgap} \tag{28}$$

In which the thermal conductivity of the air is 0.0263 Wm/K.

It should be noted that the CTF method uses the heat flux and temperature at both ends of a wall, not the construction layer surface for the FVM as computational state variables, leading to less governing equations than the FVM. However, for "heavy" wall systems such as a cavity brick system, and the ground floor (if treated as a "wall"), the cutoff terms *nz* and *nq* could be very large and the resulting CTF coefficients are not reliable. NUMBERS provides a hybrid method which combines the advantages of CTF and FVM, in other words, the CTF method is employed for the "light" wall system and FVM for the "heavy" wall system.

B.1.2.3. Analytical complex Fourier expansion method

Starting from a one-dimentional energy balance equation for a homogeneous material, as shown by Luo et al. (Luo et al., 2010), the temperature and heat flux solutions can be expressed as,

$$\begin{aligned}T(x,t)&=A+Bx+\sum_{i=1}^{N}(A_i e^{\sqrt{j\omega_i/\alpha}x}+B_i e^{-\sqrt{j\omega_i/\alpha}x})e^{j\omega_i t}\\&=A+Bx+\sum_{i=1}^{N}T_i(x)e^{j\omega_i t}\end{aligned} \tag{29}$$

$$Q(x,t) = -kB - \sum_{i=1}^{N} k\sqrt{j\omega_i/\alpha}\,(A_i e^{\sqrt{j\omega_i/\alpha}x} - B_i e^{-\sqrt{j\omega_i/\alpha}x})e^{j\omega_i t}$$
$$= -kB + \sum_{i=1}^{N} Q_i(x)e^{j\omega_i t} \tag{30}$$

In which T is the temperature, x the distance from the left wall surface as illustrated in Figure B.1, t the time variable, ω_i the angular frequency, α the thermal diffusivity coefficient ($k/\rho C_p$), Q the heat flux, and A, B, A_i and B_i are arbitrary constants determined by initial/boundary conditions. $T_i(x)$ and $Q_i(x)$ are also the coefficients of the complex Fourier expansions for temperature and heat flux, respectively. T, Q, T_i, Q_i, A, B, A_i and B_i are all complex numbers and j is the unit imaginary part of the complex numbers.

Assuming $H = \sqrt{j\omega_i/\alpha}L$ and $R = L/k$, the relationship between the temperature and heat flux coefficients on the left ($x = 0$) and right wall surfaces ($x = L$) for a homogeneous material layer can be obtained from Walsh and Delsante (Walsh and Delsante, 1983),

$$\begin{pmatrix} T_{s1} \\ Q_{s1} \end{pmatrix} = \begin{pmatrix} \cosh(H) & -R\sinh(H)/H \\ -H\sinh(H)/R & \cosh(H) \end{pmatrix} \begin{pmatrix} T_{s0} \\ Q_{s0} \end{pmatrix} \tag{31}$$

For a multi-layer material, the temperature and heat flux coefficients of the inside surface (the right wall surface) can be related to those of the outside surface using the following expression,

$$\begin{pmatrix} T_{w1} \\ Q_{w1} \end{pmatrix} = A_N A_{N-1} \ldots A_1 \begin{pmatrix} T_0 \\ Q_0 \end{pmatrix} = \begin{pmatrix} a_{11} & a_{12} \\ a_{21} & a_{22} \end{pmatrix} \begin{pmatrix} T_{w0} \\ Q_{w0} \end{pmatrix} \tag{32}$$

Note that the matrix components a_{11}, a_{12}, a_{21} and a_{22} are all complex numbers. And for an air gap which is treated as a construction layer, the matrix is:

$$A_{airgap} = \begin{pmatrix} 1 & -/C_{gap} \\ 0 & 1 \end{pmatrix} \tag{33}$$

In which
$$C_{gap} = \left[\frac{h_{s0}h_{s1}}{h_{s0}+h_{s1}} + \varepsilon_{s0}\varepsilon_{s1}\sigma(\overline{T_{s0}}^2 + \overline{T_{s1}}^2)(\overline{T_{s0}} + \overline{T_{s1}})/(\varepsilon_{s0} + \varepsilon_{s1} - \varepsilon_{s0}\varepsilon_{s1}) \right] \tag{34}$$

where $\overline{T_{s0}}$ and $\overline{T_{s1}}$ are the average of the outside and inner surface temperatures.

Equation (32) provides two equations for correlating the complex Fourier expansion coefficients at both wall surfaces at a specified angular frequency ω_i. For the whole building solution, similar results can be obtained with proper linearization about the convective heat transfer coefficients of the outer wall surfaces exposed to atmosphere. This will be addressed in the model for the complete building.

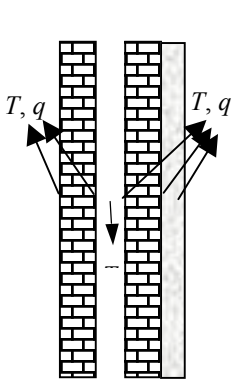

Total 11 primitive variables;
6 FV Equations;
1 zone equation for the air gap;
2 equations defining heat flux at the surfaces of the air gap;
1 supplementary equation defining heat flux at outside surface;
1 supplementary equation defining heat flux at inside

Figure B.1 Primitive variables for a typical wall: temperatures and heat fluxes at the homogeneous constructing layers, air temperature at the air gap.

B.1.3. Ground floor model

As shown in Figure B.2, the ground floor is assumed to be a "wall" comprising several layers of construction, with an air gap and 10 layers of soil each with a thickness of 0.1 m. The heat flux at the lower surface of the deepest layer is assumed zero.

Figure B.2 Boundary conditions at a typical floor.

B.1.4. Window model

The window model takes into account the amount of the solar radiation through a window as well as an impact of sunshine on the internal areas of a module such as floor, opposite and neighbouring walls. The model also depends on the location of a window, the geometry of a room, the solar elevation and the solar azimuth.

As an example, the software predictions for the Newcastle brick veneer test module incorporating a window in the northern wall are shown in Figure A.3. It can be seen that no sunshine from the window is projected onto the southern internal wall (the wall directly opposite the northern wall containing the window). A very small amount of sunshine was projected onto the western internal wall. It can also be seen that the peak ground area on 31 December is lower and the starting time is also later.

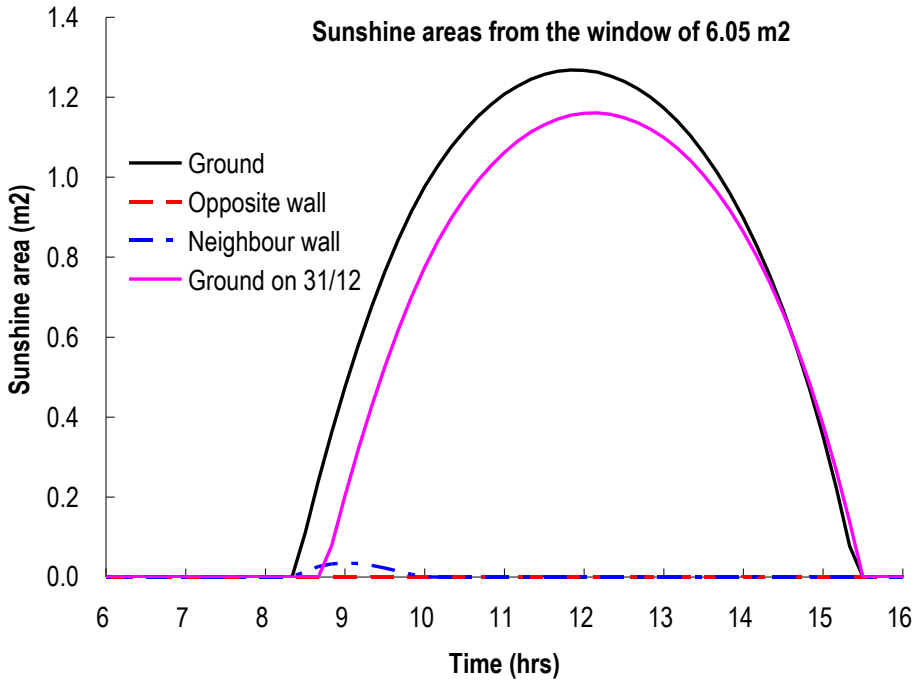

Figure B.3 Calculated sunshine areas of the Newcastle brick veneer module on 01/12/2004.

B.1.5. Energy balance equations for zones

For any zone, the zone air temperature is defined as a new primitive variable. The energy balance equation applied to this zone can be obtained by the following:

$$V_r \rho_a Cp_a \frac{\partial T_r}{\partial t} = \sum_{i=1}^{N_r} A_i h_{ri} (T_{ri} - T_r) + Cp_a \dot{m}_{\inf} (T_{env} - T_r) + \dot{q}_{in} \qquad (35)$$

in which $\dot{m}_{\inf}$ is the mass flowing rate (kg/s) of the infiltration from environments (including other zones or the atmosphere), T_{env} represents the temperature of the environmental air, V_{r} the volume of the zone, ρ_{a}, Cp_{a} and T_{r} represent the density, thermal capacity and the temperature of the zone air respectively, A_{i}, h_{ri}, and T_{ri} are the area, convective heat transfer coefficient and surface temperature of the surrounding wall i respectively, and $\dot{q}_{in}$ (J/s) is the energy input from the heating/cooling equipment (HVAC). If the zone is air conditioned and the zone air temperature is set by the thermostat, the $\dot{q}_{in}$ is chosen as the primitive variable to replace the zone air temperature, leading to the energy consumption of the zone becoming the output parameter. As shown in Figure A.4, in the zone equation constructor, the equations defining the zone wall surface heat fluxes are established, and these can be modified depending on the HVAC equipment. If necessary, new variables or new equations defining the HVAC equipment can also be inserted.

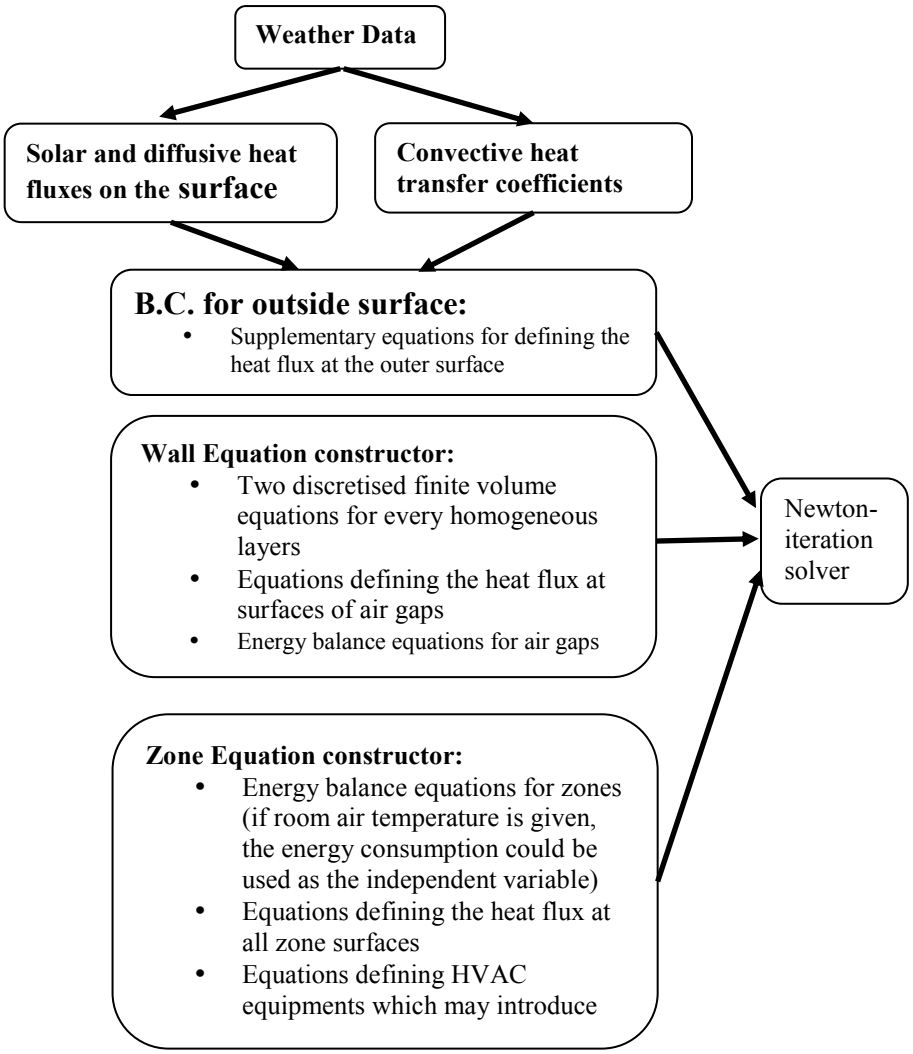

Figure B.4 Flow chart of the building energy simulation programs using the special finite volume method.

B.1.6. Software input and output parameters

Weather data are used to calculate the heat flux and the convective heat transfer coefficients on the outer wall/roof surfaces. At the same time, relative humidity (RH) in the atmosphere can be used to determine the indoor RH based on the air exchange between the building zones and outside atmosphere. The contents of the weather data depend on the format of the weather data. The following are the major components provided by the weather data:

- dry air temperature
- wind speed
- wind direction
- beam solar radiation on a horizontal plane
- diffuse solar radiation on a horizontal plane
- relative humidity
- cloud index

For the construction materials, the required thermal properties are:

- thermal conductivity
- thermal capacitance which equals the product of density (ρ) and specific heat capacity (C_p)

For phase changing materials, except for the thermal properties stated above, the following extra thermal properties are required:

- melting temperature
- heat of fusion
- density
- ρC_p at the liquid phase

For windows, the following parameters depend on the beam incidence angle:

- solar heat gain coefficient (SHGC)
- glass front solar radiation reflectance
- glass back solar radiation reflectance
- solar transmittance
- solar absorptive coefficients for all glass layers (Layer 1, Layer 2 and Layer 3)

And the following thermal properties which do not depend on the beam incidence angle are also demanded:

- thermal conductivities for all glass layers
- thermal capacitances for all glass layers
- thickness for all layers
- thermal emissivity for all layer surfaces
- CHTC for all layer surfaces

For building walls, solid construction layers are selected from the construction database, and the air gap is defined by the following thermal properties:

- Thermal emissivity at the surrounding surfaces
- CHTC at both surrounding wall surfaces

For building zones, building walls are selected from the wall database, and the following information is needed for any wall selected:

- neighbor zone name
- azimuth angle with respect to south orientation (0 for south, 90 degrees for east, 180 degrees for north, 270 degrees for west)
- tilt angle with respect to horizontal plane (90 degrees for a vertical wall)
- corresponding wall name in the neighbor zone name
- thermal emissivity for the outer wall surface
- thermal emissivity for the inner wall surface
- CHTC for the outer wall surface
- CHTC for the inner wall surface
- solar absorptive coefficient for the inner wall surface
- air conditioned (yes or no)
- zone volume
- air change per hour (ACH)

- floor solar absorptive coefficient
- start heating temperature
- start cooling temperature
- heating set temperature
- cooling set temperature

For a building wall exposed to the atmosphere, a shadow factor is needed as an extra parameter.

B.2. ASHRAE BESTTEST Standard

The following data was used in assessing the performance of NUMBERS using the ASHRAE BESTEST standard.

Table B.1 Material specifications lightweight case, (Ashrae Standard, 2007)

Element	k, W/(m·K)	Thickness, m	U, W/(m²·K)	R, (m²·K)/W	Density, kg/m³	C_p, J/(kg·K)
Lightweight Case: Exterior Wall (inside to outside)						
Int Surf Coef			8.290	0.121		
Plasterboard	0.160	0.012	13.333	0.075	950.000	840.000
Fiberglass quilt	0.040	0.066	0.606	1.650	12.000	840.000
Wood Siding	0.140	0.009	15.556	0.064	530.000	900.000
Ext Surf Coef			29.300	0.034		
Total air—air			**0.514**	**1.944**		
Total air—surf			**0.559**	**1.789**		
Lightweight Case: Floor (inside to outside)						
Int Surf Coef [a]			8.290	0.121		
Timber flooring	0.140	0.025	5.600	0.179	650.000	1200.000
Insulation	0.040	1.003	0.040	25.075	(see Note b)	(see Note b)
Total air—air			**0.039**	**25.374**		
Total air—surf			**0.040**	**25.254**		
Lightweight Case: Roof (inside to outside)						
Int Surf Coef [a]			8.290	0.121		
Plasterboard	0.160	0.010	16.000	0.063	950.000	840.000
Fiberglass quilt	0.040	0.1118	0.358	2.794	12.000	840.000
Roofdeck	0.140	0.019	7.368	0.136	530.000	900.000
Ext. Surf Coef			29.300	0.034		
Total air—air			**0.318**	**3.147**		
Total air—surf			**0.334**	**2.992**		

Summary: Lightweight Case

Component	Area, m²	UA, W/K
Wall	63.600	32.715
Floor	48.000	1.892
Roof	48.000	15.253
S Window	12.000	36.000
Infiltration		18.440[c]
Total *UA* (with S Glass)		**104.300**
Total *UA* (without S Glass)		**68.300**

ach	Volume, m³	Altitude, m
0.500	129.600	1609.000

[a]The interior film coefficient for floors and ceilings is a compromise between upward and downward heat flow for summer and winter.
[b]Underfloor insulation shall have the minimum density and specific heat the program being tested will allow, but not < 0.
[c]UA corresponding to infiltration based on: ach × volume × (specific heat of air) × (density of air at specified altitude).

Table B.2 Infiltration rates depending on the presence of automatic altitude adjustment, (Ashrae Standard, 2007)

Altitude Adjustment Algorithm	Input Air Changes per Hour (ach)	Adjustment Factor
Programs with automatic altitude adjustment; set altitude to 1609 m above sea level	0.5	1.0
Programs with fixed assumption that site is at sea level (no automatic adjustment)	0.41	0.822[a]

[a](Specified Rate) × 0.822 = (altitude adjusted rate)

Table B.3 Opaque surface radiative properties, case 600, (Ashrae Standard, 2007)

	Interior Surface	Exterior Surface
Solar absorptance	0.6	0.6
Infrared emittance	0.9	0.9

Table B.4 Exterior combined surface coefficient versus surface texture, case 600, (Ashrae Standard, 2007)

Surface Texture	Exterior Combined Surface Coefficient
Brick or rough plaster (all walls and roofs)	29.3 W/(m^2·K)
Glass (window)	21.0 W/(m^2·K)

Note: All values in table based on a mean annual wind speed of 4.02 m/s.

Table B.5 Interior combined surface coefficient versus surface orientation, (Ashrae Standard, 2007)

Orientation of Surface and Heat Flow	Interior Combined Surface Coefficient
Horizontal heat transfer on vertical surfaces	8.29 W/(m^2·K)
Upward heat transfer on horizontal surfaces	9.26 W/(m^2·K)
Downward heat transfer on horizontal surfaces	6.13 W/(m^2·K)

Table B.6 Window properties, (Ashrae Standard, 2007)

Property	Value
Extinction coefficient	0.0196/mm
Number of panes	2
Pane thickness (standard 1/8 in. glass under the inch-pound [I-P] system)	3.175 mm
Air gap thickness	13 mm
Index of refraction	1.526
Normal direct-beam transmittance through one pane in air	0.86156
Thermal conductivity of glass	1.06 W/(m·K)
Conductance of each glass pane	333 W/(m^2·K) [R-0.003 m^2·K/W]
Combined radiative and convective heat transfer coef of air gap (h_a)	6.297 W/(m^2·K) [R-0.1588 m^2·K/W]
Exterior combined surface coefficient (h_o)	21.00 W/(m^2·K) [R-0.0476 m^2·K/W]
Interior combined surface coefficient (h_i)	8.29 W/(m^2·K) [R-0.1206 m^2·K/W]
U-Value from interior air to ambient air	3.0 W/(m^2·K) [R-0.3333 m^2·K/W]
Hemispherical infrared emittance of ordinary uncoated glass	0.84 (Use 0.9 for simplicity of input. If the program being tested must use 0.84 this is acceptable because the effect on outputs will be less than 0.5%)
Density of glass	2500 kg/m^3
Specific heat of glass	750 J/(kg·K)
Curtains, blinds, frames, spacers, mullions, obstructions inside the window	None
Double-pane shading coefficient (at normal incidence)	0.907
Double-pane solar heat gain coefficient (at normal incidence)	0.789

Table B.7 Angular dependence of optical properties for the double-pane window, (Ashrae Standard, 2007)

Angle of Incidence	Trans	Abs Outer Pane	Abs Inner Pane	Refl	SHGC
0	0.747	0.064	0.052	0.136	0.789
10	0.747	0.065	0.053	0.136	0.789
20	0.745	0.066	0.053	0.136	0.787
30	0.740	0.068	0.055	0.137	0.784
40	0.730	0.071	0.057	0.143	0.775
50	0.707	0.075	0.058	0.160	0.754
60	0.652	0.080	0.059	0.210	0.700
70	0.517	0.086	0.054	0.343	0.563
80	0.263	0.094	0.041	0.602	0.302

*Trans = transmittance, Refl = reflectance, Abs = absorptance, SHGC = solar heat gain coefficient.

Table B.8 Interior solar distribution fractions by surface, case 600, (Ashrae Standard, 2007)

Surface	Floor	Ceiling	East Wall	West Wall	North Wall	South Wall	Solar Lost Through Window
Solar Fraction	0.642	0.168	0.038	0.038	0.053	0.026	0.035

B.3. Software operation overview

The following is a brief overview of the use of the NUMBERS software.

Step 1: Set-up a new project

To set-up a new project click in the file menu "*new project*", and key a name, post code, select a suburb (or latitude, longitude, location name, time zone and state, what update name automatically), next key in elevation and author details and click "*confirm*" button.

For old project, click "*open an old project*" and select the old project file as shown below:

Step 2: Dealing with construction materials Adding new construction materials and establishing possible construction materials for building walls

Construction material can be either selected from the existing database as shown below or modified/added new one. The new materials can be also added to the database by pressing "*save_this_material_to_original_data_base*" button.

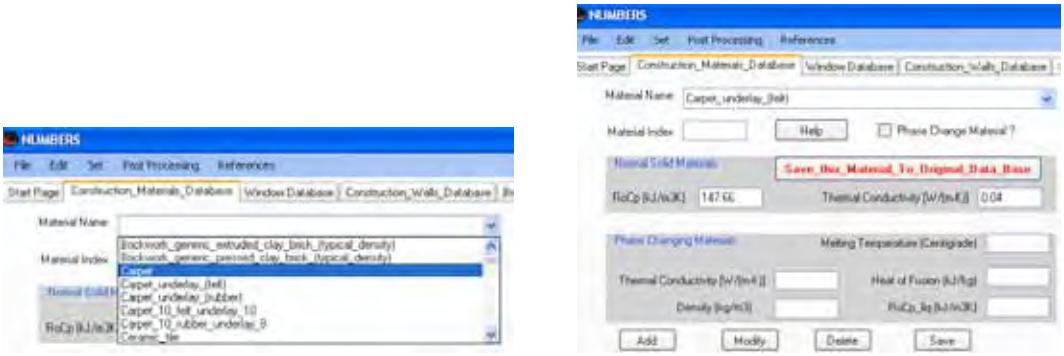

Step 3: Creating wall types of a building (including roofs, doors, grounds)

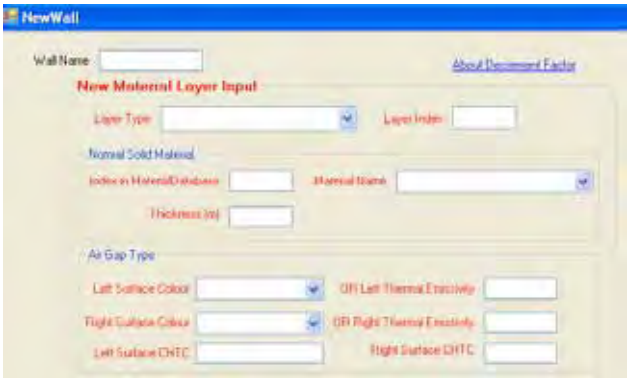

Step 4: Establishing building windows located in the building walls

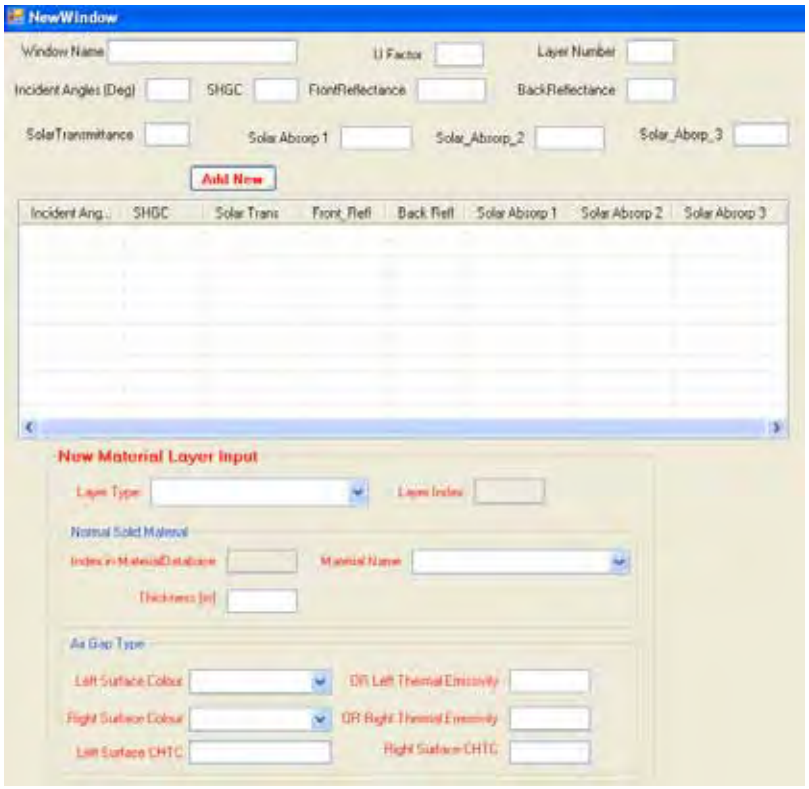

Step 5: Establishing building zones

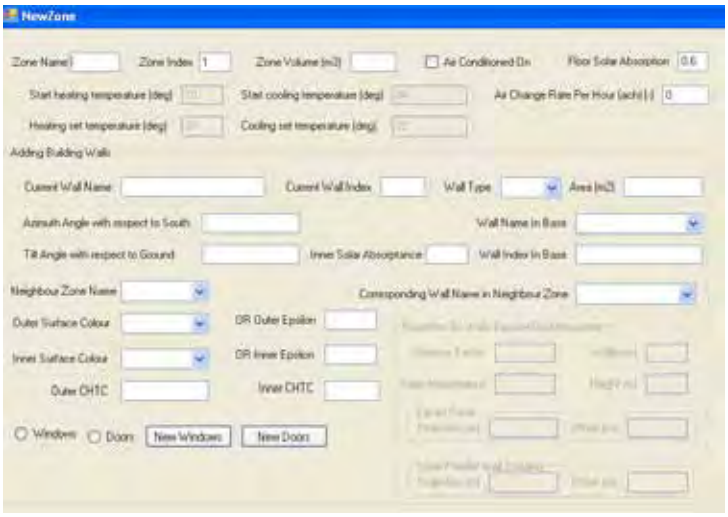

Step 5: Choosing weather data, solar radiation model, outer surface CHTC method, surrounding condition and wall surface condition.

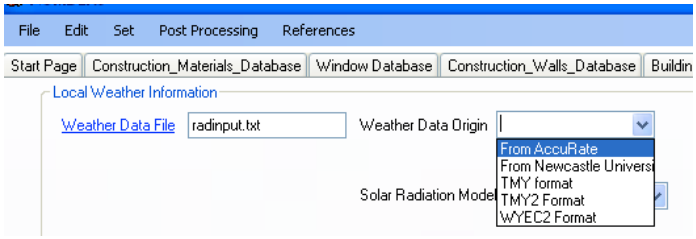

Step 6: Setting the solution parameters.

To start calculation press “save” and next “calculate” button.

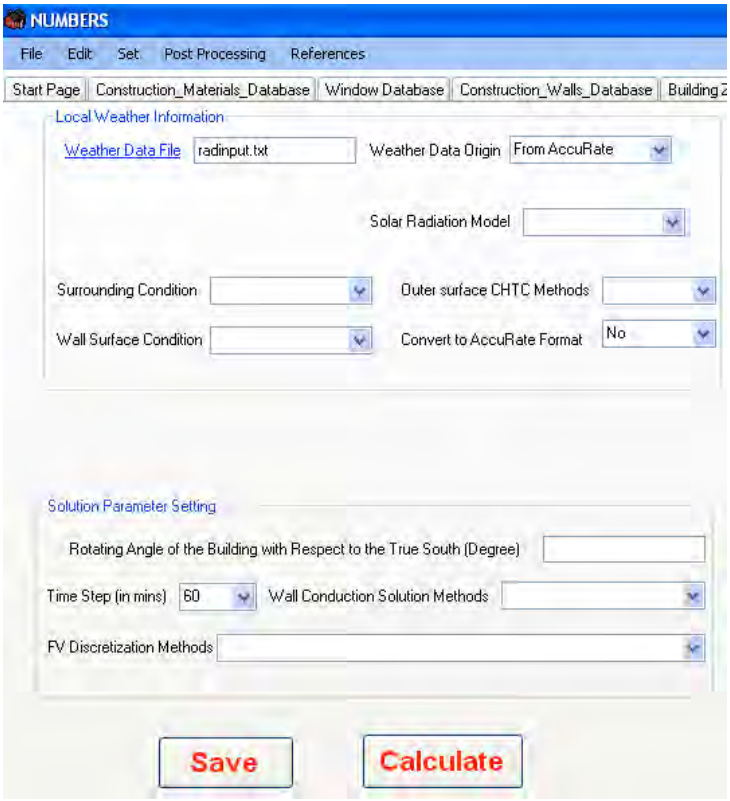

Step 7: Post processing data

For air conditioned zones, the heating/cooling loads (energy consumption) will be displayed on the right panel. There are four output files generated from the solver. And four output files are located at the software installation directory (typically, C:\Program Files\NUMBERS) with following filenames: result_zone_temp.txt, result_surfaces.txt, result_HFsurfaces.txt and energyconsumption.txt. The files include following variables:

(1) for "*result_zone_temp.txt*", which exports the zone temperatures, from the left column:

- time_in_hr,
- wind_direction,
- wind_speed (m/s),
- diffuse_radiation (J/m^2),
- global_radiation (J/m^2),
- zone 1_temperature ($^{\circ}C$),
- zone 1_energy_consumed (J),
- zone 2_temperature ($^{\circ}C$),
- zone 2_energy_consumed (J),
- zone 3_temperature ($^{\circ}C$),
- zone 3_energy_consumed (J)

(2) for "*result_surfaces.txt*", which exports the zone temperatures and the original source code is "write(24, '(1x, 5HThour, 1x, 4HTair, 1x, 50(i3, 1x,i3))') (iaazone(i2), iaawall(i2), i2 = 1, i6) Thour(it), Tair(it), (aat(i2), i2 = 1, i5)", from left column:

- time in hours,
- outside air temperature, outer surface temperature defined by the zone number and wall number (defined by the 1st column),
- inner surface temperature defined by the zone no and wall no (defined by the 1st column)
- outer surface temperature defined by the zone no and wall no (defined by the 1st column)
- inner surface temperature defined by the zone no and wall no (defined by the 1st column)
- outer surface temperature defined by the zone no and wall no (defined by the 1st column)
- inner surface temperature defined by the zone no and wall no (defined by the 1st column)

(3) for "*result_HFsurfaces.txt*", which exports the zone temperatures, the source code is "write(24, '(1x, 5HThour,1x, 4HTair,1x,50(i3, 1x, i3))') (iaazone(i2), iaawall(i2), i2=1, i6)write(25, '(1x, f12.4, 1x, 150(1x, e12.4))') Thour(it), Tair(it), (aahf(i2), i2 = 1, i5)

- time in hours,
- outside air heat flux,
- outer surface heat flux defined by the zone no and wall no (defined by the 1st column)
- inner surface heat flux defined by the zone no and wall no (defined by the 1st column)
- outer surface heat flux defined by the zone no and wall no (defined by the 1st column)

- inner surface heat flux defined by the zone no and wall no (defined by the 1st column)
- outer surface heat flux defined by the zone no and wall no (defined by the 1st column)
- inner surface heat flux defined by the zone no and wall no (defined by the 1st column)

C. APPENDIX 3 - ANFIS APPROACH

The framework implemented in the study is represented by a neuro-fuzzy system which is basically an ANFIS Sugeno-type model (Sugeno M. and Kang G. T., 1988). The ANFIS model is a hybrid framework obtained by combining the concepts of fuzzy logic and neural networking into a unified platform. The model has a fuzzy inference system in the form of an adaptive network for system identification and a predictive tool that maps a given input space to its corresponding output space based on a representative training data set.

The ANFIS inference system relies on both fuzzified human knowledge (human knowledge modelled in the form of fuzzy "*if-then*" rules) and a set of input-output data pairs (patterns) to accomplish the process of input-output mapping.

The ANFIS modelling strategy is widely used in applications or systems that involve uncertainty or imprecision in the definitions of the variables constituting the system's behaviour. That is, it has the ability to qualitatively model and represent human knowledge without the need for precise or quantitative definitions. Moreover, it is capable of modelling and identifying nonlinear systems as well as predicting chaotic time-dependant behaviour.

The most important step in designing an ANFIS system is the so-called input space partitioning, i.e. defining the rule base. The dimension of the input space - and, therefore, the complexity of the rule base - depends on two factors: the number of input variables of the modelled system and the number of membership functions, (*MFs*), assigned to each input variable. The smaller the number of input variables and MFs in the system, the less complexity involved. The relationship between the number of rules and the number of inputs/MFs is exponential and is mathematically expressed as in Equation 36.

$$\#rules = m^n \tag{36}$$

where m is the number of MFs and n is the number of inputs. For instance, a fuzzy system with 6 inputs and 3 MFs on each input would result in $3^6 = 729$ fuzzy "if-then" rules, which is prohibitively large. This problem of exponential explosion in the number of rules is referred to as "**the curse of dimensionality"**. To overcome this a grid partitioning strategy can be used, with only the small number of inputs and MFs for each input. Some other partitioning mechanisms exist and can also be used to alleviate the problem of exponential increase in the number of rules such as **tree partitioning** and **scatter partitioning**; however, they also have their own flaws.

In this study, none of these partitioning methodologies have been used and a very simple ANFIS Sugeno-type architecture has been implemented. This simplified version is manually constructed so that it has five fuzzy "*if-then*" rules governing the operation of processing a set of applied input variables to produce a single predicted output which can then be compared to the corresponding measured (target or desired) output for validation purposes. Each rule contains a completely distinct set of input MFs and a different consequent linear function, i.e. any given input MF can not exist in two different rules and each rule should contain one MF of each input. That is, the number of rules is restricted by and equal to the number of MFs assigned to each input, assuming all inputs have the same number of MFs. The rule base used in the ANFIS model of this study is of the form that appears in Formula 36a, below where the number of inputs to the ANFIS is n, which varies depending on the developed ANFIS sub-model in use (the developed ANFIS sub-models are explained in the next section). Each input variable attracts five parameterised Gaussian-shaped MFs that represent its fuzzy linguistic labels or values (i.e. very low, low, medium, high and very high). Figure C.1 depicts the "initial" MFs (the same for all inputs) which are equally spaced along the

"normalised" range of the prospective input variable.

Rule 1: IF x_1 is $A_{1,1}$ AND x_2 is $A_{2,1}$ AND … AND x_n is $A_{n,1}$
THEN $f_1 = p_{1,1}.x_1 + p_{2,1}.x_2 + \ldots + p_{n,1}.x_n + p_{0,1}$
Rule 2: IF x_1 is $A_{1,2}$ AND x_2 is $A_{2,2}$ AND … AND x_n is $A_{n,2}$
THEN $f_2 = p_{1,2}.x_1 + p_{2,2}.x_2 + \ldots + p_{n,2}.x_n + p_{0,2}$
Rule 3: IF x_1 is $A_{1,3}$ AND x_2 is $A_{2,3}$ AND … AND x_n is $A_{n,3}$
THEN $f_3 = p_{1,3}.x_1 + p_{2,3}.x_2 + \ldots + p_{n,3}.x_n + p_{0,3}$
Rule 4: IF x_1 is $A_{1,4}$ AND x_2 is $A_{2,4}$ AND … AND x_n is $A_{n,4}$
THEN $f_4 = p_{1,4}.x_1 + p_{2,4}.x_2 + \ldots + p_{n,4}.x_n + p_{0,4}$
Rule 5: IF x_1 is $A_{1,5}$ AND x_2 is $A_{2,5}$ AND … AND x_n is $A_{n,5}$
THEN $f_5 = p_{1,5}.x_1 + p_{2,5}.x_2 + \ldots + p_{n,5}.x_n + p_{0,5}$ (36a)

In the above formula 36a, x_i is the ith input ($i=1,\ldots,n$) and f_j is the jth output function of the jth fuzzy rule ($j=1,\ldots,5$). $A_{i,j}$ ($i=1,\ldots,n$ and $j=1,\ldots,5$) is the jth MF assigned to the ith input variable. The collective set of the individual parameters of all MFs constitutes the set of "antecedent" or "nonlinear" parameters. $p_{i,j}$ ($i=0,\ldots,n$ and $j=1,\ldots,5$) is the ith coefficient of the jth linear polynomial, f_j, in the jth rule. The collective set of the individual coefficients of all polynomials constitute the set of "consequent" or "linear" parameters. Each Gaussian MF possesses and is characterised by two nonlinear parameters defined in Equation 37.

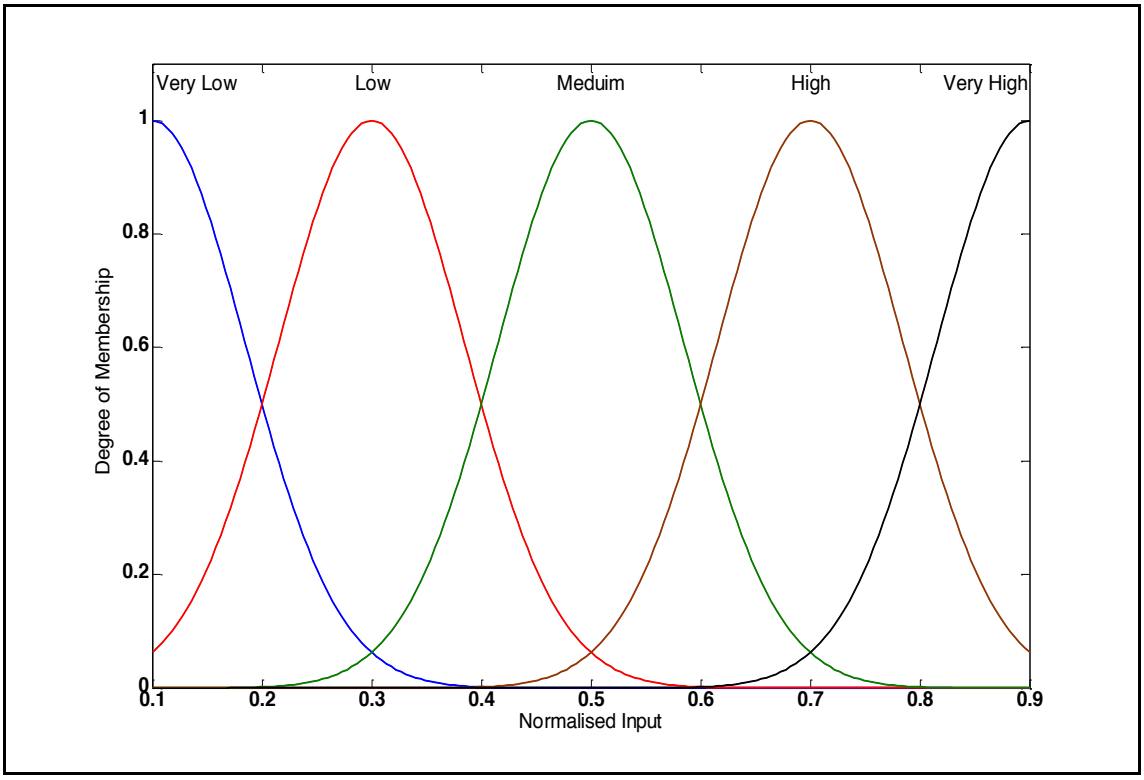

Figure C.1 The initial five Gaussian MFs along the normalised input range.

$$gauss(x,c,\sigma) = e^{-\frac{1}{2}(\frac{x-c}{\sigma})^2} \quad (37)$$

Where:

c and σ are the centre and width of the Gaussian MF, respectively.

The resultant output of each fuzzy "*if-then*" rule is calculated by performing a linear combination of all inputs in the corresponding premise part as illustrated in Formula 36a. Finally, the overall (or aggregated) predicted output is evaluated by performing a weighted average process on all crisp output functions of the individual rules using Equation 38.

$$f = \frac{\sum_{j=1}^{5}(w_j f_j)}{\sum_{j=1}^{5} w_j} \quad (38)$$

Where w_j is the firing strength of the jth rule obtained by 'multiplying' all membership grades of all inputs in that rule. The algebraic multiplication is probably the most common operator used to implement the "AND" connector in the fuzzy rules and is adopted in this study. In fact any other T-norm operator can be utilised to perform this task.

Normalisation of the input and output numerical data was performed prior to ANFIS training to ensure that no specific factor was dominant over the others during the training phase. The normalisation process is carried out using a "linear" scaling function which maintains the original properties of the raw data and "linearly" maps the data from its original range into a predefined range usually between [0, 1] or [-1, 1]. The linear scaling function used for this purpose scales the actual data range down to the compact range [0.1, 0.9] to prevent the occurrence of 0's and 1's and is given by Equation 39. Note that the scaling function is found to be an effective mechanism for eliminating the possibility of the domination of a specific factor during the training process and is used in the literature.

$$Z_i = \frac{z_i - z_{\min}}{z_{\max} - z_{\min}} \times 0.8 + 0.1 \quad , \text{ for i=1,2,3,…,k} \quad (39)$$

where Z_i is a scaled data point of the z_i value and k is the number of data points collected for a given variable (z can be either input or output variable).

The ANFIS model uses either a backpropagation or a hybrid learning approach. The latter method implies that the Least Squares Error (LSE) principle is used to identify the consequent parameters of each rule, and the error rates are back-propagated in order to update the premise parameters by means of gradient descent computational tool. The hybrid learning method was used throughout this study to ensure optimal results.

Implementation of the ANFIS Sugeno-type model employed in this study was achieved using a simple-to-use ANFIS Editor Graphical User Interface (GUI) in the MATLAB environment rather than a self-developed code to avoid complexity and save on time. The ANFIS Editor GUI is shown in Figure C.2 which can be invoked by typing "*anfisedit*" at the MATLAB command line. As Figure C.2 shows, the ANFIS GUI consists of six distinct sections each of which is used to perform a specific task of the entire modelling process. These sections appear in the lower part of the GUI

Editor window and they are:

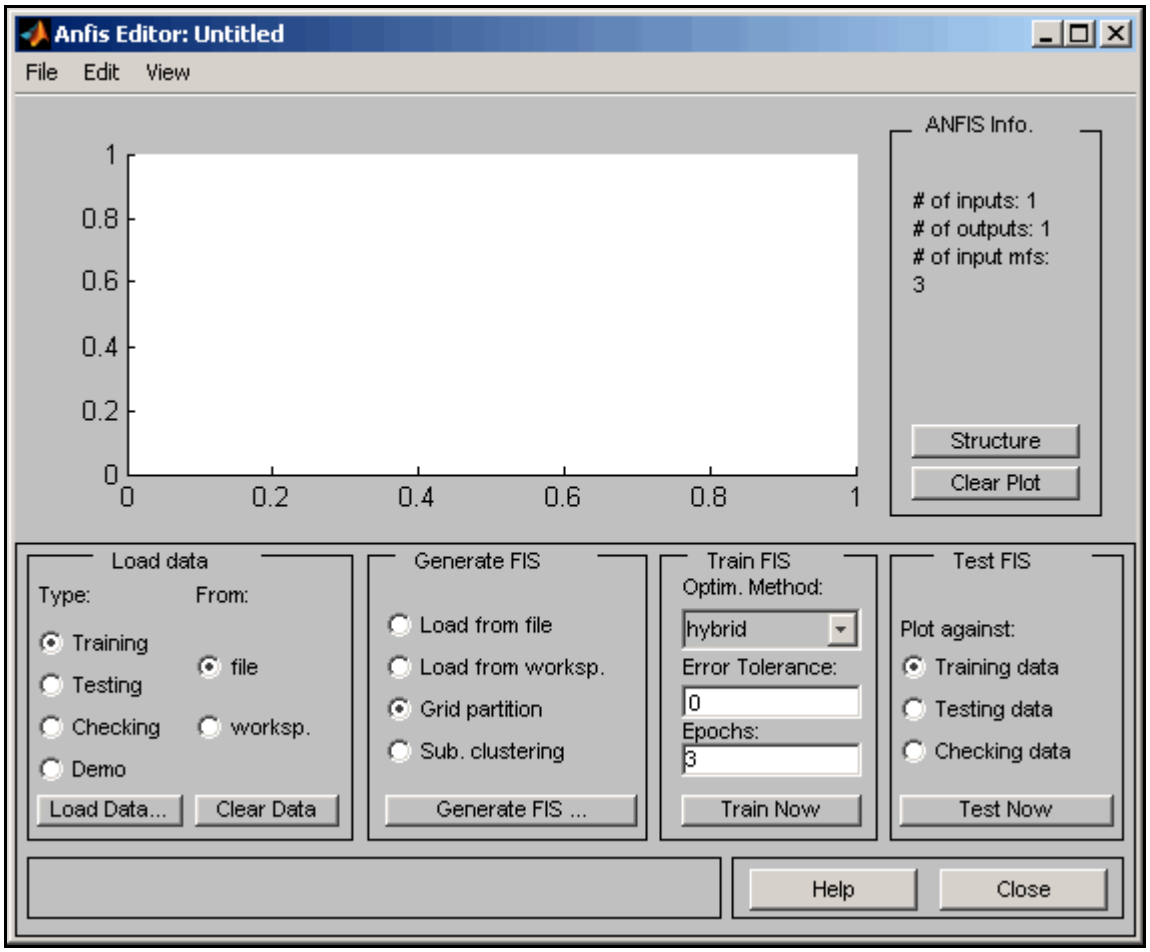

Figure C.2 The GUI Editor window of the Sugeno-type ANFIS model showing its components.

"Load Data" section: allow specialization of the data type (i.e. training, testing or checking data), load it from an existing file or the MATLAB workspace and clear it. Loading the "training data" set is the first and most important step in preparation for the ANFIS training process. Data files (regardless of their type) contain the input/output data of the system to be modelled and should be arranged in column vectors with the final column representing the desired output variable (room temperature in our case).

"Generate FIS" section: this function lets you specify an initial ANFIS model structure prior to starting the training session. This can be achieved using one of the following options:

Loading a previously constructed and saved Sugeno-type ANFIS structure from an existing file or the MATLAB workspace.

Generating the initial ANFIS model using one of two automatic partitioning techniques to define the rule base of the system, namely: **grid partition** or **subtractive clustering**.

As explained earlier, the rule base of the ANFIS model utilised in this study was constructed manually using five simple fuzzy "if-then" rules; therefore, none of the aforementioned automatic partitioning techniques were used.

"Train FIS" section: once the loading of the training data and the generation of the initial ANFIS structure are completed, the training of the ANFIS can be started by clicking the **Train Now** button.

This portion of the GUI allows the determination of three training parameters:

Optimisation Method: A choice between **backpropagation** or **hybrid** can be made. ANFIS optimisation implies training (adjusting) the membership function parameters to emulate the training data. As indicated earlier, the "hybrid" optimisation approach uses a combination of the least-squares and backpropagation gradient descent methods to adjust the parameters of all membership functions and is used in the development of the ANFIS system throughout this study.

Error Tolerance and **Epochs** to set the stopping criteria for the training process. This means that training stops whenever the maximum epoch number is reached or the training error goal is achieved, whichever occurs first. The default values are **0** and **3** respectively.

"Test FIS" section: upon completion of the ANFIS training, this part allows the testing or validation of the performance of the trained ANFIS using **Testing** or **Checking** data which is loaded beforehand and different to the training data. It also allows the examination of the training phase outcomes by comparing the actual training data output to the corresponding ANFIS training output.

Plotting area: this is the white area into which different types of plots are shown. It allows the user to visualise the loaded Training/Testing/Checking data output (either alone or against its corresponding ANFIS output) as well as the training error curve.

"ANFIS Info.": this portion displays some information about the ANFIS model such as the number of inputs, the number of outputs (which is always 1) and the number of MFs associated to each input variable. In this section, you can also clear the current plot and view the structure or architecture of the developed ANFIS system.

Note that the use of "checking data" is optional, yet highly recommended to cross-validate the training and to detect any possible model overfitting during the training process especially when the number of input variables (and hence the number of weights) is large with respect to the number of training data pairs or examples. Model overfitting is determined when the checking error (the difference between checking data output and ANFIS checking error) starts to increase after reaching a minimum value. If it exists, overfitting may result in the loss of generalisation leading to predictions that are far beyond the range of the training data as well as the fitting noise signals. In other words, the ANFIS model will generally have poor predictive performance and will not be able to generate accurate predictions for cases that are not in the training data set as it can exaggerate minor fluctuations in the data.

In this study, the "checking" option was not employed simply because the training data sets were extremely large in size compared to the number of inputs; thus, the risk of "overfitting" was very unlikely to occur. This was verified by the excellent ANFIS predictions obtained.

The internal architecture of the ANFIS model used in this study is shown in Figure C.3.

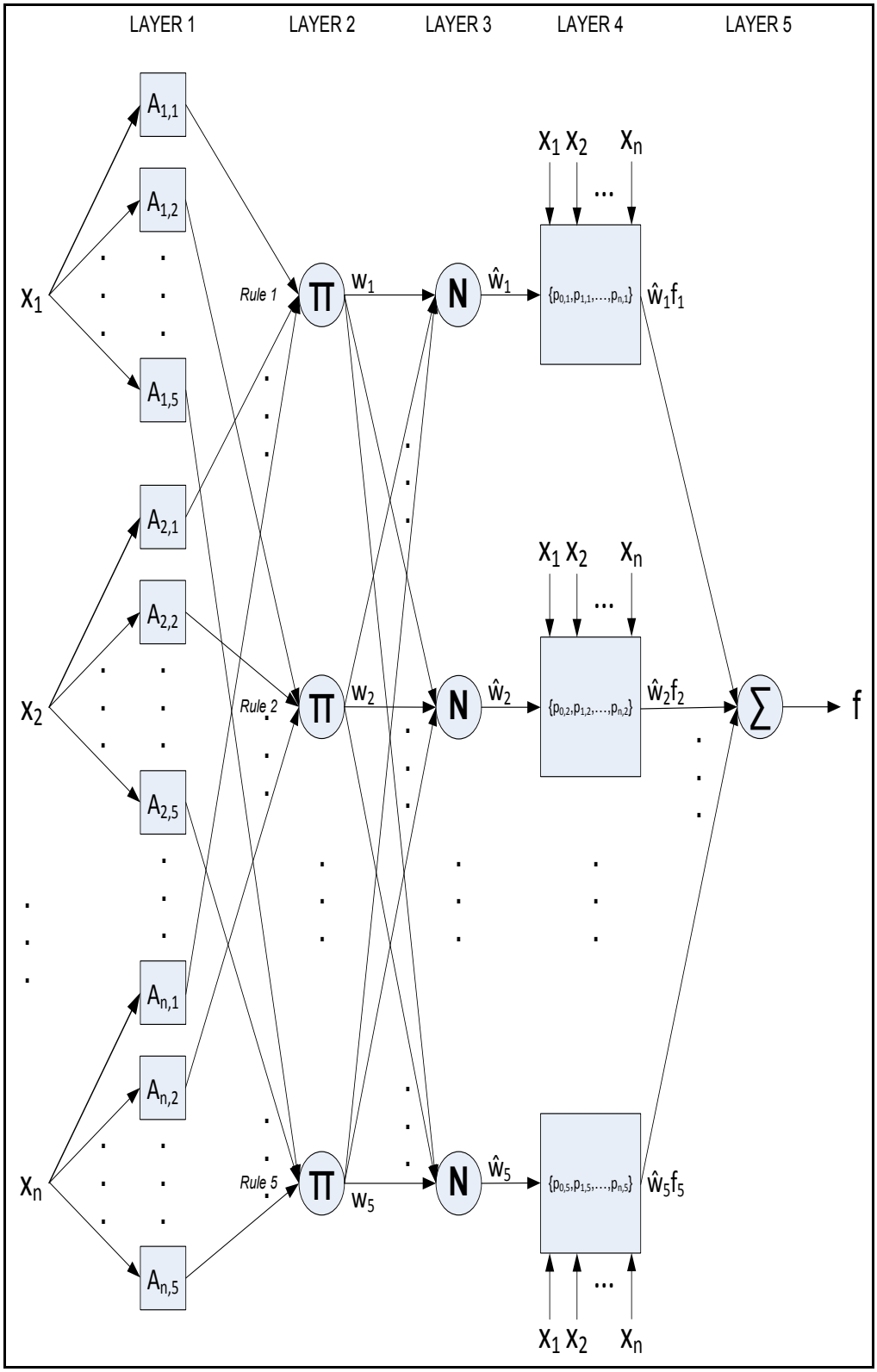

Figure C.3: Generic architecture of the underlying ANFIS system used in the four developed models where only the number of inputs (n) varies from model to model.

D. APPENDIX 4 - GLOSSARY

Solar Radiation – Total frequency spectrum as emitted by sun. Measured data from modules is filtered through atmosphere and includes infrared radiation as emitted from atmosphere.

Direct Solar Radiation – Unobstructed solar radiation direct from source incident on a material.

Diffuse Solar Radiation – Non-direct radiation such as reflected from surfaces or blocked by cloud cover incident on a material.

Thermocouple – Measurement device for temperatures. Consists of a junction of two differing metals to produce a voltage, temperature is determined by cold-junction compensation.

Heat Flux – Flow of heat per unit area per time. Measured as W/m^2.

Total Heat Flux Sensor – Thin thermopile measuring wavelength from X to X, Output proportional to heat flow.

Radiant Heat Flux Sensor – Measures radiant heat transfer from 2µm to 20µm

Standard Deviation – Measurement of the variability of data from a mean. Larger standard deviations indicate a larger spread of data. Expressed in same units as data.

Range – Interval between maximum and minimum values.

Diurnal Swing – Daily variation in temperature from maximum to minimum.

Solar Altitude – The angular height of the sun measured from the horizon.

Convection – Transfer of heat from one location to another by the movement of liquid or gaseous molecules.

Conduction – Transfer of heat through a substance without the movement of molecules.

Radiation – Emission of electromagnetic radiation due to the temperature of a material.

Thermal Lag – Related to the time required for heat to transfer through a material. A description of the material's thermal mass in terms of time.

Energy Envelope – Integral of heat flux representing the total net energy into and out of a surface over a period of time.

TDMT – Through-day mean temperature profile. Profile of the mean temperatures for each quarter of the day.

p-Value – Probability of obtaining an explanatory variable or interaction term as significant as the observation.

R^2 – Statistical measure of the fit of a regression to real data.

Q-Day – Quarter period of day as defined in statistical model Chapter X.X

Confidence Interval – Estimated interval surrounding a parameter indicating the reliability of the estimate.

Variance – Averaged squared differences from the mean. The square of standard deviation.

Thermal Mass – Describes a material's heat capacity.

Insulation – Material to reduce the magnitude of heat transfer.

R-Value – Measure of thermal resistance (m^2K/W).

NUMBERS – Building thermal performance simulation software produced by the University of Newcastle. Acronym for Newcastle University Modelling and Building Energy Rating Software.

Heat Transfer Coefficient – Proportionality coefficient between the heat flux and the driving force (temperature difference), (W/m^2K).

Relative Humidity – The quantity of water vapour in air to the amount possible when saturated. Expressed as a percentage ratio.

Thermal Capacitance – Property of a material that corresponds to the heat storage capacity.

Thermal Conductivity – Property of a material that reflects the ability to transfer heat.

Thermal Resistance – Property of a material to resist the transfer of heat.